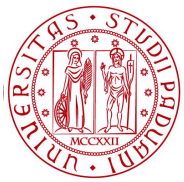

UNIVERSITÀ
DEGLI STUDI
DI PADOVA

Sede Amministrativa: Università degli Studi di Padova

Dipartimento di Biologia

SCUOLA DI DOTTORATO DI RICERCA IN: BIOSCIENZE E BIOTECNOLOGIE
INDIRIZZO: BIOLOGIA CELLULARE
CICLO: XXVII

DEVELOPMENT OF NEW TOOLS TO EXPLORE ORGANELLE CALCIUM DYNAMICS *IN VIVO*: A NEW FRET-BASED CALCIUM SENSOR AND A MITOCHONDRIA TARGETED CHANNELRHODOPSIN

Direttore della Scuola: Ch.mo Prof. Giuseppe Zanotti
Coordinatore d'indirizzo: Ch.mo Prof. Paolo Bernardi
Supervisore: Ch.mo Prof. Tullio Pozzan
Co-supervisore: Ch.ma Prof.ssa Paola Pizzo

Dottorando: Elisa Greotti

INDEX

Index **1**

Summary **4**

Riassunto **7**

PART-I: DEVELOPMENT OF NEW TOOLS TO EXPLORE ORGANELLE CALCIUM DYNAMICS *IN VIVO*: A NEW FRET-BASED CALCIUM SENSOR AND A MITOCHONDRIA TARGETING CHANNELRHODOPSIN **10**

Introduction **11**

1. Ca^{2+} homeostasis **11**

1.1 Plasma membrane **13**

1.1.1 Ligand Operated Ca^{2+} entry 12

1.1.2 Voltage Operated Ca^{2+} entry 14

1.1.3 Plasma membrane Ca^{2+} ATPases 14

1.2 Nucleus **15**

1.3 Cytosol: Calcium binding-protein **15**

1.4 Intracellular Calcium Store **16**

1.4.1 Endoplasmic Reticulum 16

1.4.2 Golgi Apparatus 19

1.4.3 Acidic compartments 21

1.5 Mitochondria **21**

1.5.1 Mitochondrial Ca^{2+} equipment 23

1.5.2 The functionality of mitochondrial Ca^{2+} homeostasis 29

1.5.3 The ER-mitochondria connection: microdomains hypothesis and Mitochondria Associated Membranes 34

2. Ca^{2+} sensors **35**

2.1 Ca^{2+} measurement in living cells **35**

2.2 Synthetic Ca^{2+} Indicators **36**

2.3 Genetically Encoded Ca^{2+} Indicators **37**

2.3.1 Bioluminescence-based GECIs: Aequorin 37

2.3.2 GFP-based fluorescent GECIs 39

2.4 Delivery systems for GECIs: Adeno-associated viruses **44**

2.5 FLIM **45**

2.5.1 FLIM-FRET 48

3. Optogenetic **49**

3.1 Channelrhodopsin **51**

Aim of the work **54**

Results **55**

1. Generation and characterization of the new cytosolic and mitochondrial Cameleon **55**

1.1 The new generated D3mCerulean3 is a functional and brighter probe compared to the original D3cpV 55

1.2 Fluorescence improvement and mitochondria targeted D3cpV generation 56

1.3 Dynamic Range 58

1.4 Photostability 61

1.5 pH sensitivity 63

1.6 Ca^{2+} affinity 64

2. *In vitro* characterization of new Cameleon probes **65**

3. FLIM **66**

4. *In vivo* delivery of the new probes **71**

5. A new mitochondria targeted Channelrhodopsin **75**

5.1 The targeting to mitochondria 75

5.2 The new mitochondria targeted Channelrhodopsine display the correct topology in the IMM 76

5.3 Mitochondria depolarization 78

5.4 Mitochondrial depolarization results in mitochondrial Ca^{2+} up-take inhibition 79

5.5 The mitochondrial targeted Channelrhodopsine is able to suppress the spontaneous beating of neonatal rat cardiomyocytes 83

Discussion **84**

Materials and methods **90**

1. Generation and characterization of new Cameleon probes 90

2. Channelrhodopsin experiments 98

PART-II: SINGLE ORGANELLE FRET-BASED ANALYSIS OF INTRACELLULAR CALCIUM: EFFECTS OF PRESENILINS CARRYING FAMILIAL ALZHEIMER'S DISEASE MUTATIONS ON CAPACITATIVE CALCIUM ENTRY 101

Introduction 102

4. Alzheimer's disease 102

4.1 The pathology 102

4.2 γ-secretase 104

4.3 Presenilins 106

4.4 The "Amyloid cascade hypothesis" 107

4.5 The hyperphosphorylated tau hypothesis 110

4.6 The "Ca^{2+} hypothesis" 111

5. Capacitative Ca^{2+} entry 114

5.1 STIM 116

5.2 Orai 117

5.3 Presenilins and CCE 117

Aim of the work 119

Results 120

6. Presenilins effect on CCE 120

6.1 SH-SY5Y cells expressing different PSs show a decreased CCE 120

6.2 Human primary fibroblasts from patients carrying the FAD-associated PS1A246E or PS2N141I mutation show a decreased in CCE. 122

6.3 PSs over-expressing SH-SY5Y cells and PS1A246E/PS2N141I human FAD fibroblasts show a decreased STIM1 protein level 125

Discussion 126

Materials and methods 129

Bibliography 131

Acknowledgments 156

Attachments 157

Summary

The first part of this thesis aims to develop new tools to explore mitochondrial Ca^{2+} dynamic *in vivo* by the improvement of a mitochondria targeting Cameleon probes and by creating a mitochondria targeted Channelrhodopsin.

Genetically encoded calcium indicators (GECIs) allow quantitative Ca^{2+} measurements in different experimental models. Organelle-specific targeting signals are fused with the GECI's sequence, achieving selective targeting to a specific organelle or cytoplasmic domain. Moreover, GECI's coding sequences can be placed under the control of tissue specific or inducible promoters, allowing spatial and temporal control of their expression. Different types of GECIs have been created: in our laboratory we use a class of FRET-based Ca^{2+} sensors, called Cameleons. FRET (Förster resonance energy transfer) microscopy detects the direct transfer of energy from a donor to an acceptor fluorescence protein (FP) in a living cell. Cameleon structure consists of two Ca^{2+}-responsive elements that alter the efficiency of FRET between two FPs: a cyan fluorescent protein (CFP), the donor, and a yellow fluorescent protein (cpV), the acceptor. The two Ca^{2+}-responsive elements are Calmodulin (CaM) and the CaM-binding domain of myosin light chain kinase.

As reported in the beginning, the aim of this study is to develop novel molecular sensors and new methodologies to express the probes *in vivo* in intact tissues as well as in organisms in order to explore organelle Ca^{2+} dynamics *in vivo* (in particularly in brain and heart).

One of the limitations of Cameleon probes, especially critical for *in vivo* applications, is the low fluorescence of CFP, reducing the maximal obtainable signal-to-noise ratio, and a multi-exponential lifetime, indicating the presence of multiple excited-state decay pathways. Recently, a brighter and more stable FP, compared to CFP, has been developed: mCerulean3. It has high fluorescence quantum yield and high photostability, making this protein a good donor candidate in Cameleon probes. For this reason, CFP has been replaced with mCerulean3 in two different Cameleons: the cytosolic D3cpv and the mitochondria-targeted probe named 4mtD3cpv. The new probes have been tested in different cell types: HeLa, neonatal rat cardiomyocytes and neonatal mouse neurons. The brightness, the photostability, the pH-sensitivity and the dissociation constant (K_d) of the new probes have also been measured *in situ* and the data show a clear improvement in brightness and in photostability, compared to the original Cameleons, in both cytosolic and mitochondrial probes. The only drawback of the new probes is a reduced amplitude (about 20-30%) in the maximum change in the fluorescence emission ratio due to Ca^{2+} binding (dynamic range). In order to extend the dynamic range different approaches have been used. The addition of 16 glycines between the two Ca^{2+} responsive elements allowed us to generate a new cytosolic probe (D3mCerulean3+16) with an increased dynamic range (+ 20%). Similarly, we have modified the mitochondrial probe, starting from the targeting sequence, each N-terminal sequence of COX-VIII (subunit VIII of human cytochrome C oxidase) was elongated of 5 aminoacids. Indeed, 24 h after transfection a significant mis-localization in the cytosol was observed with the original probe, while the mis-targeting of the modified targeting sequence containing probe was decreased. Moreover, the reduction in the dynamic range due to the mCerulean3 presence was almost fully recovered adding the 16 glycines linker. We than analysed the effect of pH, observing a general stability of all the probe variants in the pH range tested. Finally, we evaluated the Ca^{2+} affinity of all the mitochondrial variants generated so far, obtaining a K_d of 0.06 µM and one of 10.84 µM in 4mtD3cpV, a K_d of 6,5 µM in 4mtD3mCerulean3 and a K_d of 0.03 µM and one of 10.7 µM in 4mtD3mCerulean3+16. To better characterize the new cytosolic and mitochondrial Cameleon probes, we purified the proteins expressed in *E.Coli* in order to measure also *in vitro* all the parameters described above. Up to now only preliminary data have been obtained, however a comparison of *in situ* and *in vitro* data suggests that the DR calculated for cytosolic probes is about 3, while that for a mitochondria like environment is about 2.5. Concerning the Ca^{2+} affinity, just few $[Ca^{2+}]$ concentrations have been tested so far, therefore all the mitochondrial and cytosolic probes display a single K_d. However, further experiments are required to confirm the *in vitro* calculated K_d.

In parallel, we are also assessing another method to measure Ca^{2+} with FRET-GECIs, as an alternative of the classical intensity-based method. We are indeed employing FLIM technique that measures the lifetime of FPs (the time the molecule spend in the exited state), which is totally independent from phenomena such as probe photobleaching, expression level, image shading. Preliminary results in cells expressing all the Camelon probes described so far, suggest the presence of homo-FRET phenomena and mCerulean3-based Ca^{2+} sensors seem to be less affected by them.

Finally, to express the new probes *in vivo* we are testing three strategies: i) adeno-associated virus (serotype 9) with cardiac tropism viral vectors; ii) adeno-associated virus (serotype 9) with neuron-specific promoters (synapsin promoter) for intracranial injection; iii) transgenic mice. These strategies will allow us to perform

in vivo Ca^{2+} measurements in different tissues and subcellular compartments. We have just generated the AAV9 for the expression of the D3mCerulean3 and 4mD3mCerulean3 under the control of CMV promoter. A good expression levels in heart was obtained through intraperiotneal injection of neonatal mice.
In conclusion, the results obtained so far make the mCerulean3-based Cameleons an attractive choice for *in vivo* experiments.
To study the role of mitochondria *in situ* and *in vivo*, we also took advantage of an optogenetic tool: Channel Rhodopsins (ChRs). ChRs represent the only type of ion channels directly gated by light. When excited by light, ChRs open and depolarize the plasma membrane. For activation, opsins require binding of retinal, a vitamin A–related organic cofactor. In collaboration with Prof. Sekler's group (Ben-Gurion University-Israel), we have developed a new mitochondria-targeted ChR, called mitochondrial Stabilized Step Function Opsin (4mt-SSFO). This ChR variant was modified to stabilize the conducting state of the channel: SSFO deactivation occurs in 30 minutes after a brief pulse of activating blue light (460-480 nm). It has also been reported the possibility to terminate the photocurrents with red light. To create a non-functional control, a truncated form Chr2(TR) lacking retinal binding site was generated. The targeting of proteins to the inner mitochondrial membrane (IMM) was obtained fusing four signal sequences, derived from human cytochrome C oxidase subunit VIII sequence, to the N-terminus of ChR. To verify the correct topology of the probe, confocal microscopy, elecrtophisiological recordings and fluorescence quenching experiments were carried out. When 4mtSSFO-YFP is properly inserted in the IMM, its C-terminal YFP tag should face the mitochondrial matrix. Indeed, the application of proteinase K to Digitonin permeabilized cells did not cause a significant reduction of 4mtChR2B-YFP signal, while that of N33D3cpv (a probe in which the YFP is located on the cytoplasmic surface of the OMM) is completely abolished. Trypan blue addition, that is permeable across the OMM, but not the IMM, did not affect the fluorescence of 4mtSSFO-YFP or that of the matrix located Cameleon 4mtD3cpv. The 4mtD3cpv fluorescence however was totally lost after alamethicin application that permeabilizes both mitochondrial membranes and releases all matrix proteins into the medium, while the fluorescence of 4mtSSFO-YFP was not affected by the latter treatment, as expected for a membrane bound protein. Taken together these data are consistent with a proper IMM localization.
The new mitochondrial 4mtSSFO-YFP constructs were then tested *in situ* for their ability to change the mitochondrial membrane potential in response to light, resulting in a significant organelle depolarization in cells expressing 4mtSSFO-YFP, while no effect was induced by blue light in control cells. We then analysed in more details the effects of mitochondrial depolarization on mitochondrial Ca^{2+} uptake using two genetically encoded probes, 4mtD3cpv and mt-aequorin. Both approaches demonstrate that the depolarization of mitochondria triggered by photo-activation of the channel causes, as predicted, a significant reduction in the amplitude of the mitochondrial Ca^{2+} rise observed upon stimulation of HeLa cells with an IP_3-generating agonist. Thus, we generated a tool able to modulate diverse mitochondria activities in a temporary-controlled, reversible (at least in principle) and cell-specific manner, offering an approach to quantitatively investigate mitochondrial role in a large variety of critical cellular processes.

In the second part of the thesis, the investigation was focused on the role of Presenilins in Ca^{2+}dyshomeostasis associated to Alzheimer's Disease (AD) using a single cell analysis approach and focusing on the role of AD Presenilin 1 and Presenilin 2 mutations in the modulation of Capacitative Calcium Entry (CCE).
AD is the most frequent form of dementia. A small percentage of cases is inherited (Familial AD, FAD) and is due to dominant mutations on three genes, coding for Amyloid Precursor Protein (APP), Presenilin-1 (PS1) and Presenilin-2 (PS2). Mutations in these genes cause alterations in the cleavage of APP by a PS1- or PS2- containing enzyme, named γ-secretase complex, thus leading to an increase in the ratio between Aβ42 and Aβ40, the two main peptides eventually derived from APP maturation. This event, in turn, leads to an increased deposition of amyloid plaques, one of the main histopathological feature of AD. To date, the generation of Aβ42 peptides, its oligomers and amyloid plaques is the core of the most widely accepted pathogenic hypothesis for AD, the "Amyloid Cascade Hypothesis". PS1 and PS2 are ubiquitous 9 transmembrane domains homologous proteins localized mainly in intracellular membranes (Endoplasmic Reticulum, ER, Golgi apparatus, and endosomes) and plasma membrane. Despite being the catalytic core of γ-secretase complex, PSs display also some specialized, γ-secretase independent activities. On this line, numerous studies reported a role for FAD-linked PS mutations in cellular Ca^{2+} alterations. Ca^{2+} is a key second messenger in living cells and it regulates a multitude of cell functions; thus, alterations in its signalling cascade can be detrimental for cell fate. Ca^{2+} mishandling has been proposed as a causative

mechanism for different neurodegenerative diseases and in particular for AD. Although supported by several groups for many years, the Ca^{2+} hypothesis for AD pathogenesis has never been undisputedly accepted, since some data were clearly conflicting, especially those considering FAD-PS2 mutations. One of the Ca2+ pathway reported to be modulated by different FAD-PSs mutation is the so called CCE or Store Operated Calcium Entry (SOCE). CCE is the mechanism responsible for Ca^{2+} entry in response to ER Ca^{2+} depletion. The key molecules responsible for this Ca^{2+} entry have been identified only recently: STIM and Orai. Basically, Orai forms the channels located in the PM, while STIM is the protein that can "sense" the [Ca^{2+}] in the ER lumen. Upon store depletion, STIM1 changes its distribution from diffuse to clusterized "puncta" and interacts with plasma membrane-located Orai1. Employing a cytosolic Cameleon probe (D3cpV), the CCE variation in SH-SY5Y cells overexpressing PSs or in human FAD and control fibroblasts was investigated. In particular, measuring the effect of PS1-A246, PS2-T122R (in overexpression) and PS1-A246 and PS2N141I (in fibroblasts) FAD-linked mutations, a decrease in both peak and rate of CCE was observed. This phenomenon could be explained by a decrease in STIM1 protein levels, while Orai1 level was not analysed because no antibody sufficiently specific is available. In the over-expression system of SH-SY5Y cells also wild type forms of PS1 and PS2 cause a decrease in CCE and this could be due to the accumulation of the full-length form of the proteins that is thought to be the mediator of the effect.

Riassunto

La prima parte di questa tesi si propone di sviluppare nuovi strumenti per esplorare l'omeostasi del calcio (Ca^{2+}) mitocondriale *in vivo*, migliorando la sonda Cameleon indirizzata ai mitocondri, già presente in laboratorio, e creando un canale regolato dalla luce (Channelrhodopsin) indirizzato a sua volta ai mitocondri.
Gli indicatori per il Ca^{2+} geneticamente codificati (Genetically encoded calcium indicators, GECIs), consentono di eseguire misure quantitative di Ca^{2+} in diversi modelli sperimentali. Segnali di indirizzamento a specifici organelli possono essere fusi con la sequenza codificante i GECIs, consentendo di misurare variazioni della concentrazione di Ca^{2+} in diversi compartimenti subcellulari. Inoltre, le sequenze codificanti i GECIs possono essere poste sotto il controllo di promotori tessuto-specifici o inducibili, consentendo così il controllo spaziale e temporale della loro espressione. Diversi tipi di GECIs sono stati creati: nel nostro laboratorio usiamo una classe di sensori Ca^{2+} basati su FRET, chiamati Cameleon. La microscopia FRET (trasferimento di energia di risonanza Förster) si basa sul trasferimento diretto di energia da una proteina fluorescente (FP), detta donatore, a un'altra FP, detta accettore, in una cellula vivente. Strutturalmente, la sonda Cameleon, è composta da due elementi responsivi per il Ca^{2+}, che modificano l'efficienza di FRET tra le due FPs. All'interno di questa sonda sono infatti presenti due FPs: una proteina fluorescente di colore ciano (CFP), il donatore, e una proteina fluorescente gialla (cpV), l'accettore. I due elementi che rispondono a variazioni di Ca^{2+} sono la Calmodulina (CaM) e il dominio di legame della calmodulina (M13) della chinasi della catena leggera della miosina.
Come anticipato, lo scopo del mio studio è lo sviluppo di sensori molecolari e di nuove metodologie per esprimere le sonde *in vivo* al fine di esplorare le dinamiche di Ca^{2+} di particolari organelli *in vivo* (in particolare nel cervello e nel cuore).
Un limite delle sonde Cameleon, particolarmente critico per le applicazioni *in vivo*, è il basso grado di fluorescenza della CFP, che causa un basso rapporto segnale-rumore ed è caratterizzato da un tempo di vita multi-esponenziale, che indica la presenza di percorsi multipli di decadimento dallo stato eccitato. Recentemente è stata sviluppata una FP più luminosa e più stabile, rispetto alla CFP: mCerulean3. Quest'ultima ha elevata resa quantica di fluorescenza e alta fotostabilità, rendendo questa proteina un buon candidato alla sostituzione del donatore originale nelle sonde Cameleon. Per questo motivo, la CFP è stata sostituita con mCerulean3 in due differenti sonde Cameleon: la sonda citosolica D3cpv e la sonda mitocondriale 4mtD3cpv. Le nuove sonde sono state testate in diversi tipi cellulari: HeLa, cardiomiociti di ratto neonato e neuroni da topi neonati. Sono quindi stati misurati *in situ* vari parametri indicativi della qualità delle nuove sonde create, quali la luminosità, la fotostabilità, la sensibilità al pH e la costante di dissociazione (K_d), mostrando un netto miglioramento della luminosità e fotostabilità, rispetto alle sonde Cameleon originali. L'unico inconveniente delle nuove sonde è una riduzione del range dinamico, di circa il 20-30%, un parametro molto importante che rende conto della massima variazione del rapporto di fluorescenza emessa alle due lunghezze d'onda in seguito a variazioni di Ca^{2+}. Al fine di sopperire a tale svantaggio, sono stati utilizzati diversi approcci, tra cui l'aggiunta di una sequenza di 16 glicine tra i due elementi responsivi al Ca^{2+} che ha consentito di recuperare il range dinamico della sonda mitocondriale e di aumentare del 20% quello della sonda citosolica, senza modificare i miglioramenti prima descritti, ottenuti con la semplice sostituzione del donatore. Parallelamente, poiché era stata osservata una scarsa localizzazione mitocondriale a 24 ore dalla trasfezione del 4mtD3cpV, anche la sequenza di indirizzamento è stata modificata (allungando ciascuna delle sequenze originali di 5 minoacidi), diminuendo notevolmente la quantità di sonda espressa erroneamente nel citosol. Come anticipato, l'effetto del pH è stato valutato, evidenziando una stabilità generale delle varie delle sonde tra pH 7 e pH 9. Infine, sono state calcolate le costanti di affinità delle varie sonde mitocondriali. Una doppia affinità per il Ca2+ è stata rilevata: la sonda 4mtD3cpV ha una K_d di 0.06 μM e una di 10.84 μM, mentre la sonda 4mtD3mCerulean3+16 ha una K_d di 0.03 μM e una di 10.7 μM. Per caratterizzare meglio le nuove sonde Cameleon, citosolica e mitocondriale, esse sono state prodotte in *E.Coli* e purificate per misurare anche *in vitro* tutti i parametri sopra descritti.
Ad oggi sono stati ottenui solo dati preliminari che evidenziano una riduzione del range dinamico passando dall'ambiente citosolico (DR=3) a quello mitocodnriale (DR=2.5). Per quanto riguarda l'affinità per il Ca^{2+}, solo poche concentrazioni di questo ione sono state testate, dando come risultato una K_d singola sia per la sonda mitocondriale che per quella citosolica. Tale dato dovrà essere confermato da ulteriori esperimenti.
Tipicamente, le variazioni di Ca^{2+} rilevate da sonde basate su FRET vengono effettuate utilizzando metodi basati sull'intensità delle due proteine fluorescenti, tuttavia tecniche alternative basate sul tempo di vita della proteina sembrano dare risultati più accurati e robusti. Stiamo perciò iniziando a valutare biofisicamente le

sonde Cameleon utilizzando la tecnica FLIM, tecnica che misura quanto tempo una molecola fluorescente resta nello stato eccitato. Il FLIM presenta diversi vantaggi in quanto è totalmente indipendente da fenomeni come il photobleaching, i diversi livelli di espressione, i cambi di fuoco. I dati prelimianri raccolti eveidenziano la presenza di fenomeni di homo-FRET nelle sonde testate, fenomeni che sembrano tuttavia essere meno evidenti nelle sonde in cui la CFP è stata sostituita da mCerulean3.
Infine, per esprimere questi due nuove sonde *in vivo* stiamo applicando tre strategie: i) la creazione di un virus adeno-associato (sierotipo 9) con tropismo cardiaco; ii) la generazione di un altro virus adeno-associato (sierotipo 9) dotato di un promotore neurone specifico (sinapsina) per l'iniezione intracranica; iii) la creazione di topi transgenici. Queste strategie ci permetteranno di effettuare misurazioni *in vivo* di Ca^{2+} in diversi tessuti e compartimenti subcellulari. Recentemente, la generazione di un AAV9 per l'espressione del D3mCerulean3 e 4mD3mCerulean3 sotto il controllo di un promotore ubiquitario (CMV) ci ha consentito di osservare un buon livello di espressione nel cuore, iniettando il virus per via intraperitoneale in topi neonati. In conclusione, i risultati finora ottenuti rendono le nuove sonde Cameleon, basate su mCerulean3, una scelta interessante per gli esperimenti *in vivo*.
Come anticipato, al fine di studiare il ruolo dei mitocondri *in situ* e *in vivo*, abbiamo anche approfittato di uno strumento optogenetico, le Channelrhodopsine (ChRs), canali appartenente alla famiglia delle opsine. I ChRs sono l'unico tipo di canali ionici, direttamente controllati dalla luce, in grado di indurre depolarizzazione della membrana plasmatica, se opportunamente illuminati. Per l'attivazione, le opsine richiedono il legame con un cofattore organico della vitamina A, chiamato retinale. In collaborazione con il gruppo del Prof. Sekler (Ben-Gurion University-Israel), abbiamo fuso una variante del classico ChR2, detta SSFO (Step stabilized function Opsin), con una sequenza di localizzazione mitocondriale, al fine di creare una canale controllato dalla luce in grado di depolarizzare i mitocondri in modo reversibile (4mt-SSFO). Infatti, le SSFOs sono varianti di ChR in grado di aprirsi, se eccitate con luce blu, e di chiudersi, dopo circa 30 minuti dall'attivazione. É possibile tuttavia accelerare la chiusura del canale utilizzando della luce rossa. Per creare un controllo non funzionante di questo 4mt-SSFO, è stata creata una forma tronca di ChR2(TR) mancante del sito legante il retinale. La localizzazione di SSFO alla membrana mitocondriale interna (IMM) è stato ottenuta fondendo al N-terminale del ChR quattro sequenze di indirizzamento mitocondriale derivate da quella presente nella subunità VIII della citocromo C ossidasi umana. Per verificare la corretta topologia della sonda, sono stati effettuati esperimenti in microscopia confocale, di elettrofisiologia e di fluorescenza sfruttando la variante del 4mtSSFO fusa ad una YFP. Utilizzando vari "quenchers" di fluorescenza e diverse proteasi (Trypan Blue, Proteinase K, Alamethicin) abbiamo dimostrato che il nuovo canale localizza correttamente in IMM con il C-terminale protetto nella matrice mitocondriale. Il secondo passo è stata la verifica della funzionalità dei nuovi costrutti 4mtSSFO-YFP *in situ*, verificando la loro capacità di modificare il potenziale di membrana mitocondriale in risposta alla luce. Confermata la funzionalità, abbiamo poi analizzato più in dettaglio l'effetto della depolarizzazione mitocondriale sulla capacità del mitocondrio di regolare l'ingresso di Ca^{2+}, utilizzando due sonde geneticamente codificate, il 4mtD3cpv e l'aequorina indirizzata ai mitocondri. Entrambi gli approcci dimostrano che la depolarizzazione dei mitocondri, innescata dalla fotoattivazione del canale, induce, come atteso, una significativa riduzione dell'entrata del Ca^{2+} all'interno del mitocondrio. L'ingresso di Ca^{2+} in questo organello è stato indotto stimolando cellule HeLa con un agonista producente IP_3. Concludendo, i dati ottenuti sino ad ora confermano la generazione di uno strumento molecolare in grado di modulare l'attività dei mitocondri con precisione temporale e in modo reversibile (almeno in linea di principio) e specifico, offrendo così un nuovo approccio per determinare quantitativamente il ruolo mitocondriale in una grande varietà di processi cellulari critici.

Nella seconda parte della mia tesi, mi sono concentrata sullo studio del ruolo delle Preseniline nell'alterazione dell'omeostasi del Ca^{2+} nella malattia di Alzheimer (AD), utilizzando un approccio a singola cellula e concentrandomi sul ruolo delle mutazioni presenti in Presenilina 1 e Presenilina 2 correlate ad AD nella regolazione dell'ingresso capacitativo di calcio (CCE).
AD è la forma più frequente di demenza. Una piccola percentuale di casi è ereditaria (Familial AD, FAD) ed è dovuta a mutazioni dominanti in tre geni, che codificano per la proteina precursore dell'amiloide (APP), Presenilina-1 (PS1) e presenilina-2 (PS2). Mutazioni in questi geni provocano alterazioni nel taglio di APP mediato da un enzima, detto complesso γ-secretasico, che annovera tra i suoi componenti PS1 e PS2, e che è in grado di causare un aumento del rapporto tra Aβ42 e Aβ40, i due peptidi derivati dalla maturazione di APP. La generazione di tali peptidi, a sua volta, aumenterebbe la deposizione di placche amiloidi, una delle caratteristiche istopatologiche principali dell'AD. Ad oggi, la generazione dei peptidi Aβ42, dei suoi

oligomeri e delle placche amiloidi, costituisce il cuore dell'ipotesi patogenetica più accreditata per AD, "l'ipotesi della cascata amiloide". PS1 e PS2 sono proteine omologhe e ubiquitarie formate da 9 domini trans-membrana. Esse sono localizzate prevalentemente nelle membrane interne di reticolo endoplasmatico (ER), apparato di Golgi, endosomi e nella membrana plasmatica (PM). Pur essendo il nucleo catalizzatore della γ-secretasi, le PSs svolgono anche ruoli indipendenti dall'attività di questo enzima, tra cui la regolazione dell'omeostasi del Ca^{2+}. Quest'ultimo fenomeno infatti risulta variamente alterato in presenza di mutazioni FAD nelle PSs. Il Ca^{2+} è un secondo messaggero intracellulare chiave nelle cellule viventi e regola una moltitudine di funzioni cellulari, pertanto alterazioni nelle sue vie di segnale possono essere dannose per il destino della cellula. Alterazioni nell'omeostasi del Ca^{2+} sono state proposte come meccanismo causale per diverse malattie neurodegenerative e in particolare per l'AD. Sebbene supportata da diversi lavori, l'ipotesi del Ca^{2+} per la patogenesi dell'AD è stata a lungo messa in discussione, a causa dello scarso consenso della comunità scientifica sull'effetto di mutazioni in PSs nella regolazione di questo ione. Uno dei meccanismi che sembra essere modulato da diverse mutazioni FAD associate a PSs, è il cosiddetto CCE, o Store Operated Calcium Entry (SOCE). Il CCE è il meccanismo responsabile dell'influsso di Ca^{2+} all'interno della cellula in risposta allo svuotamento dell'ER. Le molecole chiave responsabili del CCE sono state identificate solo di recente: STIM e Orai. Brevemente, Orai1 forma i canali situati in PM, mentre STIM1 è la proteina che "sente" la [Ca^{2+}] nel lume dell'ER. Quando l'ER si svuota, STIM1 cambia la sua distribuzione diffusa, oligomerizza in punte (puncta) discrete che, a questo punto, sono in grado di interagire con Orai1 a livello della PM. Utilizzando una sonda citosolica Cameleon (D3cpV), ho valutato le variazione di CCE in cellule SH-SY5Y sovra-esprimenti PSs e in fibroblasti derivati da pazienti FAD o da controlli sani. In particolare, le mutazioni FAD, PS1-A246 e PS2-T122R (in sovra-espressione) e PS1-A246 e PS2-N141I (in fibroblasti) causano una diminuzione del CCE, sia della sua entità che della sua velocità di attivazione. Questo fenomeno può essere spiegato da un diminuito livello di STIM1 nei campioni FAD rispetto ai controlli, mentre non è stato possibile valutare i livelli proteici di Orai, poiché non è disponibile un anticorpo abbastanza specifico. Negli esperimenti di sovra-espressione, anche la forma wild type di PS1 e PS2 causa una diminuzione del CCE, fenomeno probabilmente dovuto all'accumulo della forma lunga (non tagliata) delle PSs, forma che sembra essere responsabile degli effetti mediati dalle PSs sull'omeostasi del Ca^{2+}.

PART-I

DEVELOPMENT OF NEW TOOLS TO EXPLORE ORGANELLE CALCIUM DYNAMICS *IN VIVO*: A NEW FRET-BASED CALCIUM SENSOR AND A MITOCHONDRIA TARGETED CHANNELRHODOPSIN

Introduction

1. Ca^{2+} homeostasis

The majority of extracellular signals, such as hormones, neurotransmitters and growth factors, cannot enter the cell freely and act by binding to plasma membrane receptors that in turn propagate such signals intracellularly. In order to adapt to changing environments, cells have developed a complex signal system based on messengers whose concentration changes in both time and space. The intracellular signalling depends either on the activation of a cascade of events initiated by the intrinsic enzymatic activity of the receptors (*e.g.*, the tyrosine kinase activity of growth factor receptors) or through the generation of second messengers. In turn, the latter (*e.g.*, cAMP, inositol 1,4,5 trisphosphate) can be synthesized by specific enzymes coupled to the receptors via G-proteins, or, in the case of calcium (Ca^{2+}), they diffuse into the cytoplasm through selective ion channels. The number of second messengers is relatively small and they can be classified in: (I) hydrophobic molecules, such as diacylglycerol and phosphoinositides; (II) hydrophilic molecules, like cyclic adenosine monophosphate (cAMP), cyclic guanosine monophosphate (cGMP), inositol 1,4,5 trisphosphate (IP_3), cyclic adenosine diphosphate - ribose (cADPR), nicotinic acid adenine dinucleotide phosphate (NAADP) and $Ca^{2+;}$ (III) gaseous molecules, such as nitric oxide, carbon monoxide, hydrogen sulphide. The latter share some properties with classical second messengers, but they are produced intracellularly and, unlike second messengers, diffuse at short distance through the membranes. Second messengers are able to trigger and modulate a wide range of cellular functions such as proliferation, differentiation, contraction, migration, survival, apoptosis and gene transcription. As far as Ca^{2+} is concerned, such a broad spectrum of functions is ensured by a fine spatial and temporal regulation of its concentration ($[Ca^{2+}]$). Since Ca^{2+} is a small highly diffusible molecule, it cannot be chemically altered, thus cells develop mechanisms to store this ion in specific subcellular compartments and to release it into the cytosol upon specific stimuli. The complex toolkit that ensures the tight control of Ca^{2+} concentration comprises a variety of channels, antiporters, pumps and Ca^{2+}-binding-proteins that are expressed differentially in the different cell compartments and are subjected to specific regulation of activity and expression level.

Originally, cells began to exclude Ca^{2+} from cytoplasm, in order to prevent its ability to precipitate phosphate; later the energy spent by cells to exclude this ion was used to trigger signal transduction (Clapham 2007). In resting conditions, the cytosolic Ca^{2+} concentration ($[Ca^{2+}]_c$) is maintained at around 100 nM (variability is observed in different cell type), compared to an extracellular millimolar concentration ($[Ca^{2+}]_e$ is around 1.8 mM). Upon different stimuli, $[Ca^{2+}]_c$ can rapidly increase up to 1-3 micromolar, triggering different cellular events ranging from exocytosis to muscle contraction, fertilization and transcription activation. This increase in both excitable and non-excitable cells is due to the release of Ca^{2+} from the intracellular stores (mainly endo/sarcoplasmic reticulum, ER/SR, where $[Ca^{2+}]$ can reach 200-900 μM) and/or the entry of Ca^{2+} from the extracellular space. In the first case, the predominant mechanism in the majority of tissues (but not in muscle cells) is the activation of phospholipase C (PLC) that results in the

production of IP_3 and diacylglycerol (DAG). IP_3 interacts with Ca^{2+} releasing channels located in the ER and Golgi Apparatus (GA), causing their opening and the release of Ca^{2+} into the cytosol. The subsequent Ca^{2+} depletion into the stores often induces also a Ca^{2+} influx through PM channels, triggering a phenomenon called Capacitative Ca^{2+} Entry (CCE) (Figure1) (Wang et al., 2010; Lewis, 2007). cADPR and NAADP similarly cause the release of Ca^{2+} through RyRs (cADPR) or other, still poorly identified, channels (NAADP) possibly located in acidic Ca^{2+} stores. The mechanisms leading to the production, upon receptor activation, of these two messages remain still not completely understood and the target and localization of NAADP are still debated (Ogunbayo et al., 2011).

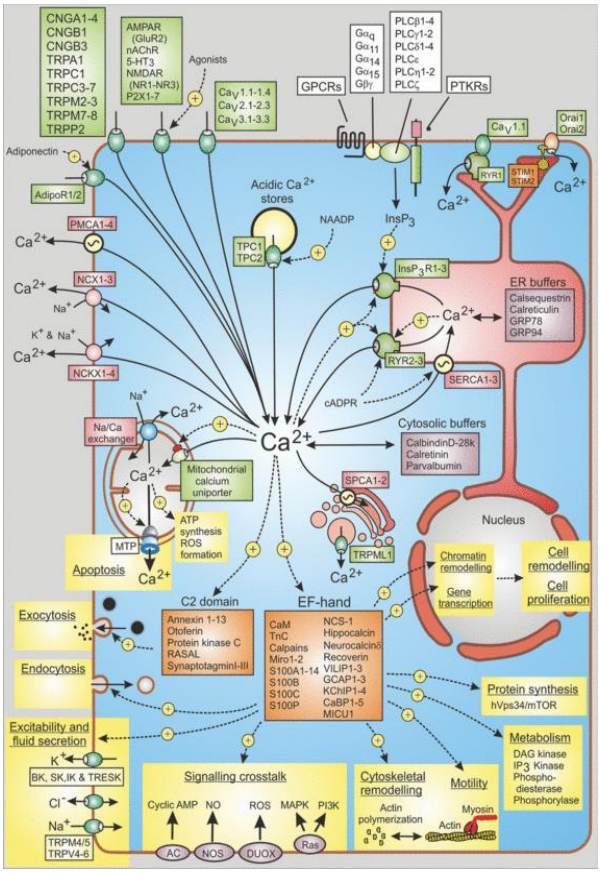

FIGURE 1. The Ca^{2+} signalling toolkit. (Berridge, 2012)

1.1 PLASMA MEMBRANE

The plasma membrane (PM) is the barrier that isolates the intracellular from the extracellular environment, maintaining different features between these two compartments. The PM is able to rapidly transmit signals in the form of ionic movements from the extracellular space into the cell, thanks to a lot of different receptor and channels present on its surface (Rizzuto and Pozzan, 2006). The ionic movements are driven by electrochemical gradients (maintained by the PM itself) and are allowed by the opening of specific channels. Most ion channels are gated, *i.e.* capable of making transitions between conducting and non-conducting conformations. Gating of ion channels depends on different electrical or chemical stimuli (Piertrobon et al., 1990; Fasolato et al., 1994). These channels could be distinguished on the basis of their ionic selectivity and

the mechanism for their activation/opening (Berridge et al., 2003). Basically we can distinguish: ligand-gated Ca^{2+} channels and voltage-operated Ca^{2+} channels (VOCCs).

1.1.1 Ligand-operated Ca^{2+} entry.

Ligand-gated Ca^{2+} channels are characterized by a lower selectivity for Ca^{2+} over other monovalent cations if compared to VOCCs (see below). This family of Ca^{2+} channels is usually divided into four subgroups:

(1) Receptor-operated Ca^{2+} channels (ROCCs or ROCs). This first type of channel possesses a ligand-binding site in the same polypeptide or in the same molecular complex forming the channel itself. The extracellular binding of the ligand, either hormone or neurotransmitter, may trigger channels opening and the further Ca^{2+} entry. Among them, NMDAr and AMPAr are activated by their physiological ligand glutamate and play a fundamental role in neurons, where, depending from their specific subcellular localization (*i.e.*, in the soma or at synapses) and the amount of Ca^{2+} that they allow to enter, could generate different or even opposite signals, such as LTD (long term depression) or LTP (long term potentiation) (Wojda et al., 2008).

(2) G-protein-Operated Ca^{2+} channels. The function of these channels, called G-protein-coupled receptors (GPCRs), is coupled with the action of G-proteins. These proteins exert a fundamental role in several intracellular transduction pathways that are activated by seven transmembrane receptors. G-proteins are heterotrimeric molecules composed of α, β and γ subunits. In the resting state, G-proteins carry guanosine diphosphate (GDP) bound in a pocket of their α subunit, but after stimulation of the receptor, the GDP is released and a guanosine triphosphate (GTP) molecule from the cytoplasm takes its place. The heterotrimeric G-protein then dissociates into two parts, a cytosolic $G\alpha$-GTP and a membrane-bound $G\beta\gamma$ dimer. These subunits are the active forms of the G-protein and are capable of signalling to specific membrane associated effectors such enzymes and ion channels. Typically, GPCRs generate IP_3 through PLC activation, thus triggering Ca^{2+} release (Berridge, 2003).

(3) Second-messenger Operated Ca^{2+} channels (SMOCs). Second-messenger Operated Ca^{2+} channels are activated by second messengers produced or released after activation of G-protein or enzyme-coupled receptors. The most common second messengers are: cAMP, cGMP, IP_3, DAG, arachidonic acid and Ca^{2+} itself (Clapham, 2007).

(4) Store-Operated Ca^{2+} channels (SOCCs or SOCs). These channels are responsible for a Ca^{2+} entry in response to ER (ER) Ca^{2+} depletion. The key molecules accountable for this Ca^{2+} entry have been identified only recently: STIM and Orai. Basically, Orai forms the channels located in the PM (Feske et al., 2006; Yeromin et al., 2006), while STIM is the protein that can "sense" the $[Ca^{2+}]$ into ER lumen. Upon store depletion, STIM1 changes its distribution from diffuse to cluster in "puncta" on ER membrane and interacts with Orai in PM, stimulating Ca^{2+} entry (Roos et al, 2005; Liou et al., 2005). For an extensive description of this mechanism see the PART II.

1.1.2 Voltage Operated Ca^{2+} Channels (VOCCs)

In excitable tissues, such as nervous system and heart, an important role is played by VOCCs, whose opening is regulated by membrane depolarization, which transforms electrical signals into chemical signals. VOCCs are multi-subunit complexes made up of a pore-forming subunit, a voltage-sensing $\alpha 1$ subunit, and several auxiliary subunits, such as 2δ and β subunits and, in some cases, also γ subunits. They constitute a complex family of channels comprising a large number of different subtypes, which have in common a steep voltage dependence of the open probability and a very high selectivity for Ca^{2+} over Na^{+} and K^{+} ions in physiological condition (Catterall 2011). Based on their voltage and inhibitors sensitivity they have been classified in L-, N-, T-, P/Q-, and R- type. For example the N- and P/Q-subtypes are present in synapses and control the Ca^{2+} dependent release of neurotransmitters, while the L-type are present in dendrites and can mediate a Ca^{2+}-dependent gene transcription (Berridge et al., 2003). L-type VOCCs are also reported to be present in skin fibroblast, but their function in these cells is still unknown (Baumgarten et al., 1992). In the nervous system they control a broad array of functions including neurotransmitter release, neurite outgrowth, synaptogenesis, neuronal excitability, differentiation, plasticity, etc... VOCCs are present also in other cell types, such as cardiac and smooth muscle cells, where their activation initiates contraction directly by increasing cytosolic $[Ca^{2+}]$ and indirectly by activating Ca^{2+} induced Ca^{2+} release (CICR) (Catterall, 2011). VOCCs are also present in endocrine cells, where they mediate Ca^{2+} entry that initiates secretion of hormones (Yang and Berggren, 2006).

1.1.3 PM Ca^{2+} ATPases

Ca^{2+} signals must be finely tuned and controlled both spatially and temporally, to ensure the specificity required to control cell function and to avoid excessive and dangerous stimulation. During a typical Ca^{2+} transient, the reactions that cause an increase in $[Ca^{2+}]_i$ ("on" reactions) are counteracted by the reactions aimed at decreasing it ("off" reactions); the "off" reactions depend on various pumps and exchangers that remove Ca^{2+} from cytosol, assuring that $[Ca^{2+}]_i$ at resting is maintained at ~100 nM and that internal stores are kept loaded. Two main mechanisms extrude Ca^{2+} from the cells through PM: the PM Ca^{2+} ATPases (PMCA) and the Na^{+}/Ca^{2+} exchangers (NCX) (Berridge et al., 2003).

The PMCA is a ubiquitous PM protein of about 125-140 KDa that catalyses the active transport of Ca^{2+} out of the cell. The energy required for this reaction is supplied by ATP hydrolysis. The Ca^{2+}:ATP stoichiometry is 1:1. PMCA is classified as a type P pump since its mechanism of Ca^{2+} extrusion is mediated by the formation of a phosphorylated intermediate during the reaction cycle. PMCA has a lower transport rate compared to NCX, but a higher affinity, and thus it functions as a housekeeping protein that controls $[Ca^{2+}]_c$ at resting state. Four different genes codifying for PMCA are present in higher eukaryotes; their different expression pattern, the existence of splice variants and the regulation of PMCA activity by various mechanisms, explain its flexibility in responding to different tissue or cell-specific Ca^{2+} homeostasis demands (Carafoli, 2005). The NCX is an electrogenic antiport located in the PM; it exchanges 3 moles of Na^{+} for 1 mole of Ca^{2+}, either inward or outward, depending on the electrochemical gradient across the membrane. Thanks to its lower affinity for Ca^{2+}, but higher transport rate compared to PMCA, it constitutes

the principal Ca^{2+} extrusion system in excitable cells (Rizzuto and Pozzan, 2006). A closely related family of exchangers, the Na^+/Ca^{2+}-K^+ exchange (NCKX) gene family, has been discovered (Haug-Collet et al., 1999). This family of proteins comprises five members; NCKXs exchange 4 moles of Na^+ for 1 mole of Ca^{2+} and 1 mole of K^+ (Schnetkamp, 2013).

1.2 NUCLEUS

The nucleus is the organelle that separates genomic material from the cytosol. It is formed by an Outer Nuclear Membrane (ONM), exposed to the cytosol, and an Inner Nuclear Membrane (INM), in continuity with the lumen of the ER that face the nucleoplasm and isolate the perinuclear space (PNS). It is organized in different subregions: nucleolus, "chromosome territories", Cajal bodies, promyelocytic leukaemia nuclear bodies and SC35 domains (Rippe, 2007).

The nuclear Ca^{2+} homeostasis is of great interest since Ca^{2+} signal mediates the regulation of nuclear functions, modulating the transcription of several genes (Hardingham et al., 1997). Indeed it has been reported that it is endowed with a Ca^{2+} toolkit similar to those present in ER membranes (*i.e.*, Sarco/Endoplasmatic Reticulum Calcium ATPase or simply SERCA pumps; IP_3Receptors called IP3Rs; Ryanodine Receptor or RyRs, as well as NAADP receptors), in particular in the area occupied by the intra-nuclear branching of the envelope, called nucleoplasmic reticulum (Echevarria et al., 2003). Anyway, large protein pores in the nuclear membrane allow the permeability of molecules smaller than 20 kDa. Consequently, it is well accepted that, in mammalian cells, Ca^{2+} very rapidly diffuses across the nucleus (with a short delay of about 100-200 ms), mirroring cytosolic Ca^{2+} changes (Zampese and Pizzo, 2012).

1.3 CYTOSOL: Ca^{2+} BINDING-PROTEINS

Two are the main mechanisms to terminate a Ca^{2+} signal: extrusion from the cytosol into the extracellular space or re-accumulation into intracellular Ca^{2+} stores (Clapham, 2007). However, in the generation and propagation of cytosolic Ca^{2+} signals, it must be considered also the buffering capacity not only of specific organelles within the cytosol (such as mitochondria and other see below), but also of the cytosol itself. Indeed, the cytosol is endowed with Ca^{2+} binding-proteins involved in chelating Ca^{2+} ions, characterized by a broad spectrum of affinities for Ca^{2+} (that can vary from nM to mM) and also by different Ca^{2+} binding rate. Many Ca^{2+} binding-proteins exist, such as Parvalbumin, S100, Calbindin and Calretinin (Schwaller, 2009). These proteins are characterized by the presence of conserved EF-hands domains specialized in Ca^{2+} binding, containing a "helix-turn-helix peptide, where several negatively charged oxygen atoms can coordinate Ca^{2+} in a 12 amino acids group (turn) between two orthogonal α-helices. One of the best-known proteins able to shape and transduce Ca^{2+} signal is Calmodulin (CaM), a ubiquitous Ca^{2+} sensor. CaM has been highly conserved during evolution, indicating its essential function in all eukaryotes. It is made up of a central α-helix with two EF hand domains at each end of the protein. Upon Ca^{2+} binding, a conformational change causes the exposure of the hydrophobic surface that in turn allows CaM to interact with the amphipatic regions of target proteins, thus modifying their activities (Hoeflich and Ikura, 2002). However, other Ca^{2+}

binding domain exist, such as C2 domain, where the binding of two or three Ca^{2+} ions cause protein's association with a specific region of cellular membranes. This domain is often associated with enzymatic domains and is typical of phosphatases (Donato, 1999).

1.4 INTRACELLULAR CALCIUM STORES

Several subcellular compartments exert a role in Ca^{2+} homeostasis by accumulating or releasing this ion and also by shaping its transients: mitochondria, Golgi apparatus, exocytic vesicles and nucleus. However, the main intracellular Ca^{2+} store is the ER or SR, its muscle equivalent (Pozzan et al., 1994; Rizzuto and Pozzan 2006). Another important Ca^{2+} store is the Golgi Apparatus (GA).

1.4.1 Endoplasmic Reticulum

The ER is a complex and continuous membrane network that extends in the whole cytoplasm, with its luminal space occupying up to 10% of the whole cell volume. It is subdivided into three major regions: the smooth ER, the rough ER (with bound ribosomes on its surface) and the nuclear envelope. A specialized version of ER is the SR, found in the striated muscle cells.

In addition to its fundamental role in protein synthesis/folding/modifications/transport and lipid synthesis, the ER represents also the main intracellular Ca^{2+} store and plays a major role in cell Ca^{2+} homeostasis and signalling (Csala et al, 2006). Indeed this compartment houses several proteins that actively regulate the traffic of molecules from and towards the ER (proteins, ions, etc.). Being endowed with Ca^{2+} toolkit, it contains ATP driven pumps for Ca^{2+} uptake (SERCAs), Ca^{2+} binding-proteins for Ca^{2+} storage within the lumen, and channels for Ca^{2+} release (the IP_3R and the RyR) (Figure 2). In many cell types increases in $[Ca^{2+}]_c$ can be due, at least in part, to the release of Ca^{2+} from the ER. The ER contains a high intra-luminal $[Ca^{2+}]$ that has been measured with different methodologies in different cell types, ranging from 200 μM up to 1mM (Meldolesi and Pozzan 1998).

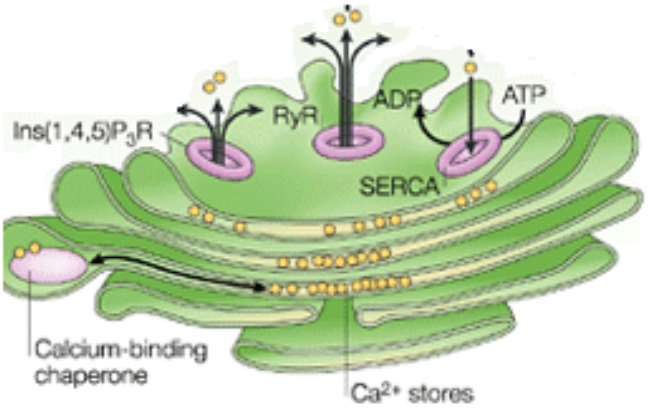

FIGURE 2. The Endoplasmic Reticulum Ca^{2+} toolkit (adapted from Syntichaki et al., 2003)

The ER Ca^{2+} accumulation depends on the activity of SERCAs, a family of transmembrane proteins that can pump actively two Ca^{2+} ions in the ER lumen employing the energy of one molecule of ATP (Wuytack et al., 2002). SERCA has the same membrane topology and mechanism of action of PMCA pump. In mammals

three genes (ATP2A1, ATP2A2, and ATP2A3) are present encoding three SERCA proteins that have also different splicing variants. The different tissue-specific expression pattern of the SERCA variants can also change during development. The SERCA2b, considered the housekeeping isoform, is almost ubiquitous (Brini and Carafoli, 2009). Several drugs are able to inhibit the SERCAs, such as the irreversible inhibitor thapsigargin (Tg) (Thastrup et al, 1990) and the reversible inhibitors: cyclopiazonic acid (CPA) (Seidler et al, 1989) and 2,5-di-(ter-butyl)-1,4-benzohydroquinone (t-BHQ) (Oldershaw and Taylor, 1990).

In the ER lumen different proteins bind Ca^{2+}, acting as Ca^{2+} buffers or chaperones, such as:

(1) calreticulin (CRT), responsible for the binding of almost half of the Ca^{2+} present in the ER (Michalak et al., 2009);

(2) calnexin (CNX), the main Ca^{2+} buffering-protein in the SR, similar to CRT but membrane bound;

(3) calsequestrin (CSQ), located in SR;

(4) glucose-related protein 78 (GRP78 or Bip) and glucose-related protein 94 (GRP94), two ER chaperons also active as buffers (Zampese and Pizzo, 2012).

All these proteins have multiple Ca^{2+} binding sites with low Ca^{2+} affinity (K_d around 1mM). These latter features provide a double advantage: they are able to buffer a large amount of Ca^{2+} and they can free it rapidly within the organelle, allowing its prompt release upon opening of Ca^{2+} releasing channels (Zampese and Pizzo, 2012).

Upon release into the cytosol and consequent store depletion, the SERCA activity and the activation of CCE ensure a rapid reuptake of Ca^{2+} into the ER, reestablishing a new equilibrium.

The ER Ca^{2+} release is tightly controlled by several factors, including Ca^{2+} itself and an expanding group of messengers, such as IP_3, cADP-R, NAADP and sphingosine-1-phosphate that either stimulate or modulate ER Ca^{2+} release channels.

Two distinct channels are responsible for Ca^{2+} release: the IP3R and the RyRs, found primarily, but not exclusively, in excitable cells.

Three IP3Rs isoforms are encoded by three different genes. These three isoforms are differently expressed depending on the cell type, but they have also an overlapping expression pattern, since they are thought to mediate different types of signalling. The IP3R is a ligand-gated ion channel of 310 kDa, with 6 transmembrane (TM) domains. It is controlled by the second messenger IP_3, generated by enzymes of the PLC family that include distinct isoforms differing in their activation mechanism (Foskett et al., 2007). An IP3R molecule contains:

(1) a large cytoplasmic N-terminal domain (~85% of the protein), that includes the IP_3 binding region (Mignery et al., 1990) and a regulatory/coupling domain containing phosphorylation sites and binding sites for nucleotides and proteins;

(2) a central hydrophobic region that forms six membrane-spanning helices that contribute to the ion-conducting pore of the channel;

(3) a relatively short cytoplasmic C-terminus that contains a suppressor domain that can inactivate the channel (Foskett et al, 2007).

The complete IP3R channel is a homo- or hetero-tetramer of four IP3R molecules (Joseph et al., 1997; Patel et al., 1999), in which the 5th and 6th helices of the TM region and the cytosolic C-terminus are critical for creating the basic pore structure (Michikawa et al., 1999; Ramos-Franco et al., 1999). When IP_3 binds the N-terminus of the channel, it induces conformational changes that activate the gate, enabling ions to flow through the channel (Foskett et al., 2007).

Different proteins have been reported to interact with and modulate IP3Rs activity, although one of the most important regulators of its activity is Ca^{2+} itself (Zampese and Pizzo, 2012). Indeed several molecules such as homer, protein phosphatases (PP1, PP2A), RACK1, chromogranin, Na^+/K^+-ATPase, carbonic anhydrase-related protein (CARP) and IRBIT interact with the IP3R and modulate its activity, suggesting that the receptor can form multi-molecular complexes and function as a centre for signalling cascades (Mikoshiba, 2007). Anyway, Ca^{2+} itself is the most important modulator of the IP3R, following a biphasic operation: at low cytosolic [Ca^{2+}] (250-300 nM) the channel is activated, potentiating the IP_3 response, while at a higher concentration (>10 μM), occurring in close proximity of a receptor upon Ca^{2+} release, the channel is blocked (Foskett et al, 2007). This contributes to the so called Ca^{2+}-induced Ca^{2+} release (CICR), a phenomenon capable of coordinating the opening of a single or few channels transforming them into more complex events, such as the propagation of a Ca^{2+} wave, by recruiting neighbouring channels.

The other major Ca^{2+}-releasing channel located on ER membranes is the RyR. RyRs owe their name to the plant alkaloid *Ryanodine*, a high specific antagonist of the channel. RyRs are large conductance channels of 550 kDa, capable of creating rapid transient increases of $[Ca^{2+}]_c$. Four receptor molecules assemble into a homo-tetramer forming the 2 MDa ion channel (Zampese and Pizzo, 2012). Most of the RyR protein, similarly to the IP3R, forms a large cytoplasmic assembly that is connected to the TM region. Indeed the RyR and the IP3R share an overall 17% sequence identity and the identity increases up to 35% within the predicted TM region, forming the ion-conducting pore of the two proteins (Ponting, 2000). Moreover, the two receptors show also similarities in their function and regulation: indeed both permeate Ca^{2+} and are regulated by it in a biphasic manner (Roderick et al., 2003);

The cytoplasmic region has distinctive structural domains and intervening cavities that permit interaction with modulators. The clamp-shaped regions, located at the corners of the cytoplasmic assembly, contain domains for the interdigitation of neighbouring RyRs and for the interaction with some modulators (Hamilton and Serysheva, 2008). The crystallization of RyR proved to be hard to obtain and many open questions about the structure remained. Recently, thanks to advances in crio- electron microscopy, Marks group shed new light on the rabbit RyR1 structure (for details see Zalk et al., 2015).

In mammals three different genes encode for RyR1 (predominantly expressed in skeletal muscle), RyR2 (expressed mainly in the heart, but also in Purkinje cells and in cortical neurons) and RyR3 (ubiquitously expressed at low levels). RyR is responsible for the release of Ca^{2+} from the SR into the cytosol, which sets off a cascade of events resulting in muscle contraction (Lamb, 2000). Indeed, Excitation-Contraction (E-C) coupling refers to the close interaction between dihydropyridine receptors (DHPRs) L-type Ca^{2+} channels and RyRs: in skeletal muscle, depolarization of the PM activates DHPRs and is coupled to opening of RyR1

on SR membrane (Beam and Bannister, 2010). While in skeletal muscle RyR1 opening is primarily (or exclusively) due to the E-C coupling with DHPRs, the major gating mechanism of RyR2 and RyR3, fundamental in cardiac muscle cells, is CICR. In this latter case, the opening of RyRs is stimulated by the local Ca^{2+} increase, occurring in the proximity of PM L-type Ca^{2+} channels (Fill and Copello 2002).

Finally, a basal Ca^{2+} leak from the ER contribute to determine the steady state of $[Ca^{2+}]_{ER}$. However, despite its physiological relevance, the mechanism of ER Ca^{2+} leak remains elusive. Several players have been proposed to take part to this process, including the ribosomal-translocon complex; channels of the transient receptor potential (TRP) family-like, such as polycystin-2 (TRPP2); Presenilins (PSs); members of anti-apoptotic Bcl-2 families; hemichannel-forming-proteins such as pannexins (Zampese and Pizzo, 2012). Also RyRs and IP_3Rs are known to undergo spontaneous activity, maybe contributing to the basal ER Ca^{2+} leak.

1.4.2 Golgi apparatus

The GA is the main sorting and processing site along the secretory pathway, ensuring that lipids and proteins synthesized in the ER are properly modified (*e.g.*, glycosylated, phosphorylated, processed and packaged into carrier vesicles) and eventually directed to their final destination within or outside the cell. Thus, it contains numerous enzymes such as glycosyltransferases, glycosidases, sulphatases, kinases and pro-protein convertases (such as furin) that cleave protein precursors into their mature forms (Schaefer et al., 1995). Morphologically, GA is a highly dynamic structure that consists of multiple membranous cisternae arranged in close apposition forming multiple polarized stacks. GA is composed by three regions: a cis-side associated with a tubular reticular network of membranes (cis-Golgi network, CGN), a medial area of disc-shaped flattened cisternae, and a trans-side associated with another tubular reticular membrane network (trans-Golgi network, TGN). The steady-state structure of Golgi stacks depends on the balance of anterograde and retrograde vesicle trafficking between the various GA cisternae, the ER and other cellular compartments (Pizzo et al., 2011). The polarized morphology of GA parallels specific functionalities: for example, glycosyltransferases act sequentially in consequent compartments and, in general, enzymes that need to act early in glycan biosynthetic pathways are located within cis- and medial- compartments of the GA, whereas enzymes that need to act later tend to reside within the TGN (Breton et al., 2001).

As mentioned before, GA play a key role as intracellular Ca^{2+} store, containing up to 5% of whole cell Ca^{2+} (Chandra et al., 1991, Pezzati et al., 1991). It can be considered an acidic Ca^{2+} store, as its luminal pH ranged from 6.8 to 5.9. Activity of processing enzymes located in the GA show a strong Ca^{2+} dependency. Moreover, retrograde membrane traffic from the Golgi to the ER (Oda, 1992) and selective aggregation of regulated secretory proteins in the TGN is also critically dependant on GA Ca^{2+} content (Chanat and Huttner, 1991). The Golgi complex contains all the essential components of a Ca^{2+}-storage organelle, i.e. pumps for Ca^{2+} uptake, channels for Ca^{2+} release and Ca^{2+} binding-proteins for Ca^{2+} storage (Zampese and Pizzo, 2012). Thus, in the space of a few microns and despite the continuous inter-mixing dynamics, the GA Ca^{2+} toolkit has a precise distribution in different subregions, drawing areas with different Ca^{2+} features and different properties in Ca^{2+} handling.

The use of a specific Cameleon Ca^{2+} sensor targeted to the different GA compartments, allowed our group to directly demonstrate the functional GA heterogeneity in Ca^{2+} homeostasis:

(1) CGN. The cis-side of GA closely resembles the Ca^{2+} homeostatic properties of the ER, being endowed with IP3R, RyR (as efflux Ca^{2+}channels) and SERCA (as influx Ca^{2+} channel). The [Ca^{2+}] in this compartment is around 250 μM (Pizzo et al., 2011; Cifuentes et al., 2001).

(2) Medial-Golgi. This compartment accumulates Ca^{2+} through SERCA pump and through secretory pathway Ca^{2+}-ATPase 1 (SPCA1, see below) and it releases Ca^{2+} through IP3Rs and RyRs. The steady state [Ca^{2+}] is lower than that in the ER, but higher than that in then Trans-Golgi, being around 250-300 μM (Wong et al., 2013).

(3) TGN. Trans-Golgi is IP_3-insensitive and utilizes solely SPCA1 to uptake Ca^{2+}, keeping [Ca^{2+}] around 130 μM (Lissandron et al., 2010) (Figure 3).

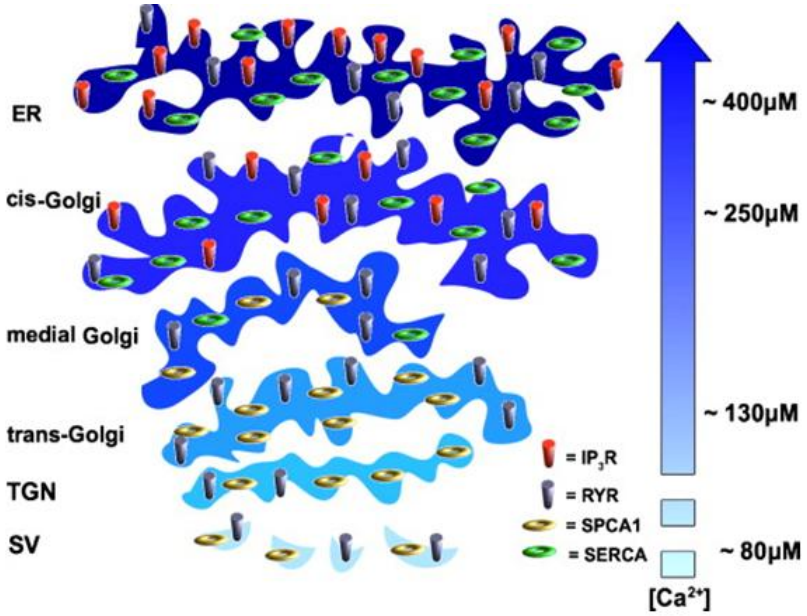

FIGURE 3. Schematic representation of GA Ca^{2+} toolkit and concentrations (Pizzo et al., 2011).

As mentioned before, in addition to SERCA the GA expresses also another ATP-dependent Ca^{2+} pump: the SPCA (Pizzo et al., 2011). In human cells, two different genes encoding for SPCA have been identified: ATP2C1 (expressed in 4 protein variants) and ATP2C2. SPCAs are single subunit integral membrane proteins composed by a large cytosolic head containing an actuator, a nucleotide-binding, and a phosphorylation domain, and a TM domain with 10 hydrophobic helices. Within the TM region, SPCAs contain one high-affinity binding site for Ca^{2+} and Mn^{2+}, providing both cations to the GA. Indeed, Mn^{2+} supply is fundamental for the correct glycosylation of secretory proteins (Kaufman et al., 1994).

The GA is also equipped with luminal Ca^{2+}-binding-proteins: CALNUC is the most abundant and better characterized of the GA Ca^{2+} binding-proteins (Lin et al., 1998); Cab45, a luminal soluble protein important for vesicles sorting (Scherer et al, 1996); p45/NEFA, a luminal protein strongly associated to GA membranes

(Karabinos et al., 1996); Calumenin, a protein present also in the ER and in the secretory pathway, that interacts with SERCA and RyR2 modulating their activity (Jung et al. 2006; Sahoo et al, 2009).

1.4.3 Acidic compartments

Other intercellular Ca^{2+} stores, beside ER and GA, are acidic organelles such as endosomes, lysosomes and secretory granules. The Ca^{2+} content within these organelles is heterogeneous, ranging from 10-40 μM in mast cell and chromaffin cell granules to 100–200 μM in insulin granules, and from 1mM in formed endosomes to ten of mM in secretory granules of many cell types and in the related synaptic vesicles of neurons, underlying the existence of some not well-identified Ca^{2+} buffers. Other acidic compartment rich of Ca^{2+} (around 500 μM) are lysosomes and lysosome-related organelles, such as melanosomes, lytic granules in lymphocyte etc. (Zampese and Pizzo, 2012). Finally, recent results indicate that also peroxisomes are capable of taking up and storing Ca^{2+} within their lumen at concentrations much higher than those found in the cytoplasm (Raychaudhury et al. 2006; Drago et al. 2008). The mechanism of Ca^{2+} uptake and release by acidic organelles is still poorly understood, but evidence suggest that those Ca^{2+} stores take up Ca^{2+} from the cytoplasm using both a SERCA-type Ca^{2+} ATPase and an SPCA-based system, present in dense core secretory vesicles of neuroendocrine cells (Mitchell et al., 2001). Other ATP-dependent Ca^{2+} uptake mechanism not yet identified could also participate to Ca^{2+} influx. However, the idea that the proton gradient is involved in Ca^{2+} homeostasis is well-accepted, since Ca^{2+}/H^{+} exchanger are present (Patel et al., 2010), and also indirect pathways involving Na^{+}/H^{+} and Na^{+}/Ca^{2+} exchangers have been reported (Mahapatra et al., 2004; Krieger-Brauer et al., 1983). Concerning Ca^{2+} release from acidic stores, different stimuli have been reported to act on these organelles: IP_3, cADPR and also a RyR activator, caffeine (Zampese and Pizzo, 2012). Recently, the NAADP has been shown to act as a second messenger, mobilizing intracellular Ca^{2+} stores by activation of two-pore channels (TPCs) in endosomal membranes (Calcraft et al. 2009).

Up to now, many obstacles have been encountered in measuring Ca^{2+} in acidic compartments, since their internal environment is highly acid and rich in protease. Lysosomes and peroxisomes in particular are emerging as crucial organelles involved in cell life, development and human pathology, with some functionalities related to Ca^{2+} homeostasis. Future efforts are thus needed to develop and modify Ca^{2+} sensors able to properly measure Ca^{2+} in these compartments.

1.5 Mitochondria

Mitochondria are known as a factory for energy transduction in eukaryotic cells. They metabolize organic molecules to produce ATP through oxidative phosphorylation, thereby powering cellular activities in animals and other eukaryotes. Mitochondria not only form the cell metabolic hub, but also are crucial players in many cellular pathways, like regulation of Ca^{2+} homeostasis, oxidative stress response, apoptosis and innate immune response, putting the organelle in a central position in controlling cellular function and fate (Contreras et al., 2010; Nunnari and Suomalainen et al., 2012). Mitochondria are dynamic membrane-enclosed cytoplasmic organelles that form an elaborate network in a constant state of change, due to

processes of fission and fusion. Mitochondrial network is organized together with the cytoskeleton and move along the microtubular network aided by the molecular motor proteins dynein and kinesin. Mitochondria are constituted by:

(1) the outer mitochondrial membrane (OMM), characterized by the presence of porins that allow molecules <5 kDa to freely diffuse;

(2) the intermembrane space (IMS), with a concentration of small molecules similar to the cytosol;

(3) the inner membrane (IMM), a highly impermeable membrane in which oxidative phosphorylation takes place;

(4) cristae, generated by infoldings of IMM that expand its surface area and enhance the ability of ATP production;

(5) the mitochondrial matrix, delimited by the IMM, containing the major part of the mitochondrial proteins and involved in pyruvate and fatty acids oxidations and citric acid cycle (Henze et al., 2003).

The endosymbiotic origin of mitochondria explains their unique features such as the presence of mitochondrial DNA, usually organized as a single, circular, double-stranded molecule which encodes for 13 proteins involved in the respiratory chain, 22 tRNAs and 2 rRNAs. The remaining part of mitochondrial proteome is encoded by nuclear genes (Anderson et al., 1981).

The regulation of gene expression and proteins signalling networks in mitochondria, seems to be controlled by Ca^{2+}. Mitochondrial Ca^{2+} homeostasis strongly depends on energy process, in particular Ca^{2+} influx is driven by electrochemical gradient due to the electron transport chain (chemiosmotic hypothesis). Indeed, respiring mitochondria are characterized by a negative membrane potential ($\Delta\psi m$), about -180mV, tightly coupled to a pH gradient (ΔpH) (Pizzo et al., 2012). According with the Nernst equation, $\Delta\psi m$ and ΔpH regulate the three processes controlling Ca^{2+} handling:

(1) Ca^{2+} uptake, mediated by mitochondrial Ca^{2+} uniporter (MCU) (De Stefani et al., 2011);

(2) Ca^{2+} buffering in mitochondrial matrix, mainly due to insoluble xCa^{2+}–xPO4x––xOH– complexes (Nicholls et al., 2005);

(3) Ca^{2+} extrusion in the surrounding, mediated by xNa^{+}/Ca^{2+} exchanger (mNCX) (Gunter et al., 1990) and Ca^{2+} /xH^{+} exchanger (mHCX) (Villa A. et al., 1998) (Figure 4).

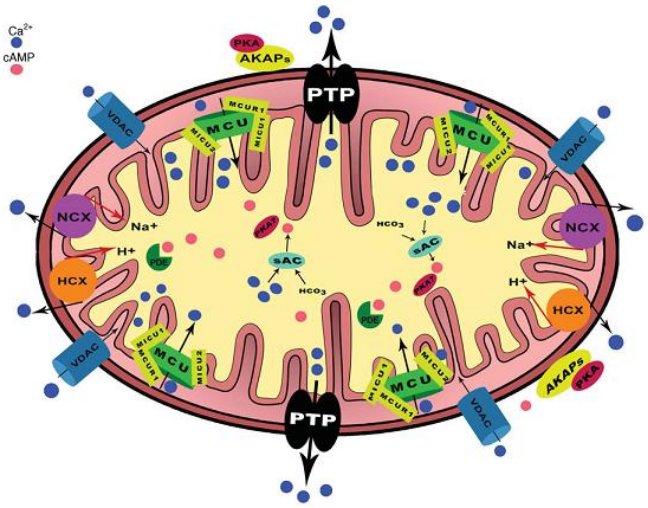

FIGURE 4. Mitochondrial Ca^{2+} toolkit (Di Benedetto et al., 2014)

1.5.1 Mitochondrial Ca^{2+} equipment

Ca^{2+} uptake in mitochondrial matrix depends on the ion capability to cross the OMM and the IMM. Recently, it has become clear that the OMM function as the first Ca^{2+} barrier, indeed changes in membrane conductivity or manipulation of VDAC (Voltage-dependent anion channel) expression levels, can affect the mitochondrial Ca^{2+} concentration ($[Ca^{2+}]_m$) (Rapizzi et al., 2002; Bathori et al., 2006). VDAC is a porin ion channel with a molecular weight of 30 kDa, which forms a β–barrel that spans the OMM. In humans three VDAC genes have been identified. They are modulated by different cytosolic proteins and by mitochondrial lipids composition (Rostovtseva et al., 2008). VDACs show weak anion selectivity and become weak sensitive to cations at $\Delta\psi m$>25mV (Tan et al., 2009). The three proteins display different distribution in OMM and specific interactions with apoptotic regulators (Roy et al., 2009a-b; Cheng et al., 2003). VDAC1 and VDAC2 localized similarly in the OMM, but only VDAC1 is reported to be enriched in mitochondria-associated ER membranes (MAMs) (Szabadkai et al., 2006), while VDAC3 is uniformly distributed over mitochondrial surface (Neumann et al., 2010).

Mitochondria Ca^{2+} influx

Different proteins have been reported to be involved in the mechanism of mitochondrial Ca^{2+} uptake, although several data are controversial and still to confirm. One of that is RyR1 found in IMM of heart mitochondria immune-electron-microscopy and suggested to work in reverse mode, mediating mitochondrial Ca^{2+} uptake (Beutner et al., 2001). Further investigations are needed to confirm this hypothesis.

In another paper, it has been reported that the down-regulation or the overexpression of the uncoupling-proteins 2 and 3 (UCP2/3) reduces or increases the accumulation of Ca^{2+} into mitochondria (Trenker et al., 2007). The same group reported also that UCP2 and 3 are able to modulate the activity of the uniporter, and thus mitochondrial Ca^{2+} uptake, only when cytosolic Ca^{2+} rises, released from the ER (Waldeck-Weiermair et al., 2010). A direct role of UCP2/3 on mitochondrial Ca^{2+} uptake, however, has not been confirmed by others. In particular, mitochondria isolated from UCP2 KO and UCP3 KO mice take up Ca^{2+} normally (Brookes et al., 2008). Moreover, UCP3 has been reported to inhibit SERCA activity by decreasing the

ability of mitochondria to produce ATP (De Marchi et al., 2011). Thus, UCP2/3 effects on mitochondrial Ca^{2+} uptake, if any, could be explained by a general cellular metabolic alteration.

In 2009, the previously believed component of the PM H^+/K^+ exchanger, Letm1, was proposed to be a mitochondrial H^+/Ca^{2+} electrogenic antiport with high Ca^{2+} affinity, distinct from the low affinity MCU (Jiang et al., 2009). Purified Letm1 reconstituted into liposomes was able to mediate a Ruthenium Red sensitive mitochondrial Ca^{2+} uptake. Other groups, however, challenged this idea, showing compelling evidence that Letm1 is probably a H^+/K^+ antiporter, since in MEFs the Letm1 KO phenotype could be rescued by nigericin, a bona fide H^+/K^+ ionophore (for a review see Nowikovsky et al., 2012). For these reasons, the Letm1 role in mitochondria Ca^{2+} uptake is still matter of debate. Anyway, the recent RNA-interference (RNAi) screening, that permitted the identification of MCUR1 (Mallilankaram et al., 2012b), confirmed a role for Letm1 in mitochondrial Ca^{2+} handling, since its silencing induces a decreased Ca^{2+} uptake into the organelles. Again, further investigations will be required to better clarify this issue.

Another mechanisms has been proposed to be involved in mitochondrial Ca^{2+} influx, named rapid mode or RaM, but it still has a debated functional significance. The RaM mechanism has been reported to transfer Ca^{2+} quickly from cytosol to mitochondria during the rising phase of Ca^{2+} pulses (Buntinas et al., 2001).

However, the most accepted mechanism of mitochondrial Ca^{2+} uptake across the IMM is the mitochondrial Ca^{2+} uniporter (MCU). Well before the molecular identification of the protein, its properties as a channel were well-known. The mitochondrial Ca^{2+} uniporter was defined as an highly selective channel, sensitive to Ruthenium Red (RuR) and lanthanide and with low affinity to Ca^{2+} (Bernardi et al., 1984; Mela et al., 1969 and Bragadin et al., 1979). The Vmax of MCU is >1400 nmol Ca^{2+} per mg of protein per min (Bragatin et al., 1979), while its affinity for Ca^{2+} is around 20-30 μM. After many years spent in searching this channel, in 2011 two groups independently reported the identification of this channel. MCU is a 35 kDa protein located at the IMM with two highly conserved TM domains, with N- and C-terminus facing the matrix (Baughman et al., 2011; Martell et al., 2012) and endowed with two EF-hand Ca^{2+} binding domains. In 2 years the general picture has become far more complex than anticipated from functional data: in addition to the MCU pore-forming subunits, other proteins have been described that are capable of modulating the activity, the Ca^{2+} affinity and (probably) the assembly of the channel in the mitochondrial membrane, forming the so called MCUC (Mitochondrial Ca^{2+} Uniporter Complex). The exact stoichiometry of the different subunits forming MCUC and their specific role is still debated but the present picture shows the MCU as one of the most sophisticated ion channel described thus far. Such complexity in subunit composition and regulation, maintained and increased during evolution, suggests an essential role of this mitochondrial function in cell physiology.

Basically MCUC is a super complex with a molecular weight around 480 kDa (Baughman et al., 2011), composed by:

(1) MCU, the pore forming subunit of the channel. Its down-regulation inhibits and overexpression increases Ca^{2+} uptake by mitochondria. Moreover, De Stefani et al. showed that when expressed recombinantly in *E. coli* or in a wheat germ extract cell-free system, purified MCU forms channels

permeable to Ca^{2+} and inhibited by Ruthenium Red. The nuclear MCU gene encodes a 40 kDa protein, while the mature form of MCU is a 35 kDa protein, generating by the cleavage of the N-terminal import domain. MCU is located in IMM and possesses two predicted TM α–helixes domains. The topology model predicts that both its N- and C-terminal domains face the mitochondrial matrix, with the two membrane-spanning domains connected in the IMS by a short loop containing the DIME motif (De Stefani et al., 2011; Baughman et al., 2011). The putative pore region of MCU is defined by eight helices and the negative electrostatic potential needed for cations permeability is due to a cluster of negatively charged aminoacids found in the DIME region, in proximity of the pore (Raffaello et al., 2013). About the functionality of MCU, the first model proposed that MCU is arranged in oligomers, possibly tetramers (Raffaello et al., 2013) that constitute the channel-forming subunits of MCUC.

(2) MCUb. MCUb is a protein structurally similar to MCU, showing an inhibitory role on mitochondrial Ca^{2+} uptake. MCUb is a 35 kDa protein with two TM domains, encoded by a gene located on *Homo sapiens* chromosome 4. Its primary sequence is 50% homologous to that of MCU, but with key mutations in the predicted pore forming region. Its overexpression in intact cells reduces Ca^{2+} uptake of mitochondria in response to cytosolic Ca^{2+} increases, while in lipid bilayers the co-expression of MCU and MCUb dramatically inhibits the Ca^{2+} current due of MCU alone. MCUb expression is quite variable in mouse tissues, and in general lower than that of MCU: MCUb mRNA is abundant in heart and lung, while it is scarce in skeletal muscle (Raffaello et al., 2013). These data on tissue expression, from a functional point of view, relates on Ca^{2+} uptake efficacy, which is greater in skeletal muscle than in heart (Fieni et al., 2012). Structurally, the main differences between MCU and MCUb concern the DIME domain: an E256V substitution makes MCUb less electronegative, affecting the kinetics of Ca^{2+} permeability; aminoacid substitutions R251W and D256V in the putative pore-forming domain inhibit the Ca^{2+} channel activity of MCU. Finally, it has been reported that MCUb can be co-immunoprecipitated with MCU (Sancak et al., 2013).

(3) MICU. Three different isoforms has been identified. The first one, MICU1, discovered about one year before MCU itself (Perocchi et al., 2010), was more recently followed by other two similar protein, MICU2 and MICU3 (Plovanich et al., 2013). They are located on the outer surface of the IMM where they appear to modulate the function of MCU.

a. MICU 1. MICU1 is a 54 kDa membrane protein endowed with two classical EF-hand Ca^{2+} binding domain. The knockout (KO) of MICU1 abolished mitochondrial Ca^{2+} uptake, though overexpression did not result in a major effect on the rate and extent of Ca^{2+} uptake by the organelle (Perocchi et al., 2010). MCU and MICU1 physically interact and have a similar tissue expression pattern (Baughmann et al., 2011). They are both highly conserved during evolution but, while there is general agreement on the fact that MCU represents the pore forming subunit of MCUC, the role of MICU1 is, on the contrary, less clear and contradictory data have been published by different groups. Some groups reported an activator action of MICU1 (Perocchi et al., 2010 and Abell et al., 2011); on the contrary, two other groups suggest a role for MICU1 in establishing a threshold that prevents Ca^{2+} uptake in basal conditions

(Mallilankaraman et al., 2012; Csordas et al., 2013; Hoffman et al., 2013). Very recently, Alvarez and co-workers showed that in HeLa cells silenced for MICU1, the mitochondrial Ca^{2+} uptake is increased at cytosolic Ca^{2+} concentration <2 μM, while it is decreased at cytosolic Ca^{2+} concentration > 4 μM (De La Fuente et al., 2013). No consensus has been reached yet also on the topology of MICU1.

b. MICU2 and MICU3. Mootha's group revealed the expression in most eukaryotic cells of two paralogs of MICU1, MICU2 and MICU3. The authors suggests that these other two genes arose by gene duplication of MICU1, but they exhibit a distinct pattern of tissue expression. MICU2 and 3 share about 25% sequence identity with MICU1 and, similarly to it, possess two EF-hands Ca^{2+} binding sites. MICU2 is a 45 kDa protein ubiquitously expressed in mammalian tissues, exclusively localized in the IMM. MICU3 seems to be mostly expressed in the nervous system and up to now it has not been functionally characterized. On the contrary, an extensive characterization of the role of MICU2 has been done, showing an effect similar to MICU1 on MCU. They proposed a reciprocal regulation of MICU1 and 2 activity that appears to be cell specific and related to reciprocal regulation of MCU, MICU1 and MICU2 proteins expression levels (Plovanich et al., 2013). Anyway, up to now, no general consensus has been obtained about the function of MICU2. Of note, Rizzuto and co-workers recently demonstrated that MICU1 and MICU2 heterodimerize through the formation of a disulphide bond and they interact with MCU through the short DIME loop of MCU. MICU2 seems to exert an inhibitory effect on MCU channel activity in planar lipid bilayers and in intact HeLa cells at low Ca^{2+} level, while MICU1 shows a stimulatory effect on MCU activity during cytosolic Ca^{2+} rise. However, the protein levels of MICU1 and 2 (but not the mRNA) are strongly correlated: the decrease of MICU1 protein expression decreases also the level of MICU2 and results in the absence of gate-keeping on MCU (Patron et al., 2014).

(4) MCUR1. MCUR1 (Mitochondrial Ca^{2+} Uniporter Regulator 1) is another recently discovered member of the complex, whose deletion results in abrogation of mitochondrial Ca^{2+} uptake. It is a 40 kDa protein with two TM domains and one coiled-coil region (Mallilankaraman et al., 2012). The N- and C-terminus face the IMS, while the major part of the protein is exposed to the matrix (Rhee et al., 2013). The striking phenotype of cells deprived of MCUR1 is the lack of any energy dependent Ca^{2+} uptake, without effect on mitochondrial membrane potential. MCUR1 co-precipitates with MCU, but not with MICU1, and its overexpression results in an increase of mitochondrial Ca^{2+} uptake, but only when MCU is co-expressed. MCUR1 appears also to regulate the expression of MCU, as down-regulation of MCUR1 results in a significant increase of both the mRNA and the protein levels of MCU (Mallilankaraman et al., 2012). Although MCUR1 possesses two predicted TM domains, no evidence was obtained in support of its channel forming activity, suggesting that MCUR1 affects either the opening of MCU or the assembly of the complex or both. As for the binding partners of MCUR1, contrasting results have been reported, indicating in one case that MCUR1 did not co-immunoprecipitate with the other MCUC proteins (Sancak et al., 2013) and in another case that it co-immunoprecipitates with MCU (Mallilankaraman et al., 2012).

(5) EMRE (Essential MCU Regulator). EMRE is the last identified member of MCU-associated

proteins. Its KO completely blocks Ca^{2+} uptake by mitochondria, which cannot be rescued by overexpressing MCU. EMRE is a 10 kDa single-pass membrane protein with a highly conserved C-terminus enriched in aspartate. No EMRE homologous exist in plants, fungi or protozoa, suggesting that it most likely arose in the metazoan lineage. As far as EMRE mRNA expression is concerned, it has been found in all mouse tissues analysed and is predicted to be broadly expressed in mammalian tissues. MCUs and MICUs co-immunoprecipitate with EMRE, indicating that it possibly acts as a bridge between MCU and MICUs. Furthermore, EMRE seems to be necessary for the association of MCU with MICU1/2, since, in absence of EMRE MCU cannot co-precipitate with MICU1/2, although it still co-precipitates with MCUb and MICU1 and 2 dimerize (Sancak et al., 2013). EMRE thus appears to be a necessary regulator (or a MCUC assembler), of the MCU transport, rather than a pore-forming unit (Figure 5).

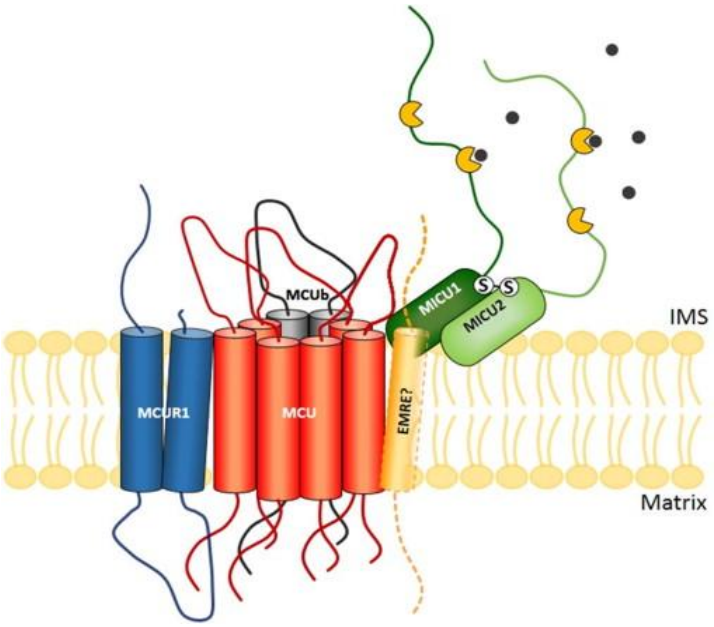

FIGURE 5. Schematic representation, based on our interpretation of published data, of the MCUC organization. IMM: inner mitochondrial membrane, IMS: inter membrane space (Pendin et al., 2014).

Taken together, the data presented so far about MCUC indicate that mitochondria Ca^{2+} import involves an extremely complex molecular machinery, highly conserved in its basic features with regulatory mechanisms that have been probably added during evolution. Together with the enormous set of data indicating the involvement of mitochondrial Ca^{2+} uptake in many key aspect of cell physiology and pathology, it was almost obvious to anticipate that functional KO of MCU would result in an embryonic lethal phenotype. Indeed, a dramatic phenotype was obtained in a study carried out in zebrafish using morpholinos against MCU (Prudent et al., 2013). Anyway a recent paper by Finkel and co-workers show that MCU KO mice, obtained using the gene trap technique, are not only regularly born, but their phenotype is very mild: the animals are slightly smaller than their wild type littermates and they have modest defects in skeletal muscle strength and some alterations of metabolic functions (in particular in the control of pyruvate dehydrogenase).

Furthermore, the same group observed that mitochondria isolated from both skeletal and cardiac muscles of MCU KO mice are totally incapable of accumulating Ca^{2+} in an energy dependent way. In MEFs from the same transgenic mice, Ca^{2+} mobilization from intracellular stores results in no detectable increase in mitochondrial Ca^{2+} levels, but, surprisingly, only a partially reduction of mitochondrial Ca^{2+} content in resting condition was observed in MCU KO compared to that in wild type animals. Moreover, mitochondria from MCU KO mice lack evidence for Ca^{2+}-induced permeability transition pore (PTP) opening, but unexpected this defect does not seem to protect MCU KO cells and tissues from cell death. Furthermore, whereas, as expected, the PTP inhibitor Cyclosporine A (CsA) provided significant protection against ischemia-reperfusion injury to WT hearts, this agent had no demonstrable effect on MCU KO hearts. Thus, in the absence of MCU, alternative PTP- or Ca^{2+}-independent cell death mechanisms could emerge and become predominant. The authors themselves thus hypothesized the existence of alternative Ca^{2+} uptake pathways, capable of catalysing only a slow Ca^{2+} accumulation (Pan et al., 2013). The nature of this (these) pathway(s), if any, remains unknown. On the existence of alternative mitochondrial Ca^{2+} uptake pathways of interest are the recent observations by Graier and co-workers that up to 5 different Ca^{2+} currents can be identified in mitoplasts by electrophysiology (Jean-Quartier et al., 2012). In a more recent study, the same group observed that one of these currents (different from the one generated by MCU) is increased in mitoplast ablated of MCU (Bondarenko et al., 2013). They suggested the existence in mitochondria of at least two different Ca^{2+} channels, one MCU dependent and another, MCU-independent. As much as the existence of multiple mitochondrial Ca^{2+} influx pathways is fascinating (and could explain the mild phenotype of MCU KO mice), it needs stressing that, in MCU KO animals, either in isolated organelles or in living cells, Pan et al. did not found any evidence for energy dependent Ca^{2+} uptake.

Mitochondria Ca^{2+} efflux

The Ca^{2+} extrusion toolkit is composed by mNCX (or NCLX) in excitable cells, and mHCX exchangers in non-excitable cells. mNCX has been extensively studied in isolated mitochondria (Gunter et al., 1990; Bernardi et al., 1999), but only in 2010 Sekler's group, identified this exchanger as a product of the mNCX gene (included in the super-family of NCX genes, comprising NCXs present on ER and PM), located on mitochondria and characterized by a low affinity Ca^{2+} exchange with Na^{+}. The final discovery has originated from a fortuitous manifestation, *i.e.*, the partial mistargeting of the overexpressed mNCX to PM. Indeed, they found that this mistargeted protein was able not only to exchange Na^{+}/Ca^{2+}, but is also to mediate an efficient Li^{+}/Ca^{2+} exchange, a unique feature of the unidentified mitochondrial mNCX, not shared with members of the PM-NCX family. mNCX is also functionally distinct from the other two members of the family because: (i) its inhibition is specifically mediated by a pharmacological compound called CGP-37-157, (ii) its down-regulation or overexpression affects mitochondrial Ca^{2+} release and (iii) fractionation experiments demonstrate that it is enriched in the mitochondrial fraction. mNCX channel is highly similar to the PM ones, thus, the scientific community agrees with the idea that 3 or 4 Na^{+} ions are changed per one Ca^{2+} ion (Patly et al., 2004-2010; Cai et al., 2004). mNCX Vmax ranges from 2.6 to 18 nmol Ca^{2+} per mg of protein per min in different cell types and its dependence on $[Na^{+}]$ has a sigmoidal trend with a Km around 8-10 mM (Cox et

al., 1993).

Less is known about the role on mitochondrial Ca^{2+} efflux played by mHCX, which molecular identity is still debated; indeed no encoding genes have been isolated, but a 66 kDa protein that displays exchanger properties in liposomes has been purified. The ion stoichiometry is still debated also for this exchanger (2/3 H^+ per 1 Ca^{2+}), but it's clear that its functionality depends on membrane potential (Bernardi et al., 1983; Villa et al., 1998). mHCX has a Vmax around 1.2 nmol Ca^{2+} per mg of protein per min and its saturation point is around 25 nmol Ca^{2+} per mg of protein (Wingrove and Gunter, 1986).

Finally, another system utilised by mitochondria to release Ca^{2+} is the permeability transition pore (PTP), a powerful mechanism of rapid and massive cations release associated with Ca^{2+} overload conditions (Bernardi et al., 1999). PTP is a large-size pore, that can undergo transient openings (flickerings), both in isolated mitochondria and in intact cells, thus permitting Ca^{2+} release from mitochondria when the [Ca^{2+}] into the matrix is higher than in the external medium. This phenomenon contributes to organelle Ca^{2+} homeostasis, acting as a rapid, pro-survival Ca^{2+}-induced Ca^{2+} release mechanism without causing catastrophic and irreversible PT (for a review see Rasola and Bernardi, 2011). The molecular nature of PTP is not completely clear. A recent paper, however, provided evidence that dimers of the F0F1-ATP synthase form a channel with features identical to those of the mitochondrial mega channel (MMC), the electrophysiological equivalent of the PTP (Giorgio et al., 2013).

Mitochondrial buffering capacity

Mitochondria have a Ca^{2+} buffering capacity due to the xCa^{2+}–xPO_4– xOH_2^- complex in the mitochondrial matrix, with a molecular stoichiometry similar to that of hydroxyapatite. These Pi function as a compensatory machine to prevent drops in membrane potential and increases in pH due to Ca^{2+} influx (Rossi et al., 1964; Zoccarato et al., 1982). This Ca^{2+} buffering mechanism to prevent Ca^{2+} overload is observed within mitochondria when extracellular [Ca^{2+}] exceeds 400-500 nM or when mitochondrial membrane potential strongly favours Ca^{2+} influx in the organelles. The solubility of Pi strongly depends on matrix pH and, in particular, the formation of Ca^{2+}- Pi precipitates is favoured at matrix alkaline pH (Chalmers et al., 2003; Nicholls et al., 1978-2004).

1.5.2 The functionality of mitochondrial Ca^{2+} homeostasis

Researchers started to study the role of mitochondria in Ca^{2+} homeostasis since 1961. First Deluca, and then Vasington, demonstrated that energized mitochondria from rat kidney were able to accumulate Ca^{2+} (De Luca et al., 1961; Vasington et al., 1962). In 1977 the presence of an extrusion mechanism was demonstrated for the first time and also the existence of a balance between Ca^{2+} influx and efflux. Experimental evidence obtained in the 1980s tended to disprove a role of mitochondria as Ca^{2+} stores (Streb et al, 1983), discovering the ER as the central organelle for Ca^{2+} signaling. Despite biochemical works in the same years demonstrating the role of Ca^{2+} in the regulation of metabolic enzymes inside the mitochondria, their function in Ca^{2+} homeostasis was considered marginal. The demonstration of the existence of an active mechanism of

rapid Ca^{2+} uptake in intact cells stimulated with an IP_3-generating agonist (Rizzuto at al., 1992-1993) reversed this assumptions, and proposed mitochondria as organelles promptly responding to $[Ca^{2+}]_c$ rises.

Mitochondrial Ca^{2+} homeostasis has effects at different levels, since it influences both mitochondrial and cellular functions.

It was clear since 90s that Ca^{2+} was involved in mitochondrial functionality (McCormack et al., 1990). The first evidence that $[Ca^{2+}]_c$ influenced the mitochondrial metabolism was provided by experiments in intact cell performed by Duchen et al., demonstrating that influx of Ca^{2+} from cytosol to mitochondria, could increase ATP production by activating three enzymes: pyruvate dehydrogenase, α-chetoglutarate dehydrogenase and isocitrate dehydrogenase (Duchen et al., 2000). The first one is regulated by a Ca^{2+} dependent phosphatase, while the latest two are regulated by direct binding of Ca^{2+}. The activation of these three enzymes leads to an increase in NADH availability, which results in a flow of electrons down the respiratory chain, finally increasing ATP synthesis (Pralong et al., 1992; Hansford et al., 1994; Jouaville et al., 1999). The amplitude and the kinetics of the $[Ca^{2+}]$ increasing is also sensed by the Ca^{2+}- binding site of the glycerol phosphate dehydrogenase, an enzyme involved in the electron supply of complex II in the respiratory chain. ATP production and metabolite transport is enhanced also by aralar1 and citrin, two aspartate/glutamate exchangers of the IMM, endowed with an EF-hand Ca^{2+} -binding domain exposed in the intermembrane space. Rises in $[Ca^{2+}]_c$ leads to an activation of these two exchangers (Lasorsa et al., 2003; Contreras et al., 2007; Satrustegui et al., 2007).

The tight connection between ATP production and mitochondrial Ca^{2+} uptake was demonstrated in different experiments: Wiederkehr and coworkers showed that the stimulated increase of ATP is inhibited by cytosolic Ca^{2+} chelators and by Ca^{2+} binding proteins targeted to mitochondrial matrix; it has been also observed an increase in NADPH production upon an augment of $[Ca^{2+}]_m$ (Voronina et al.,2002); Foskett and colleagues demonstrated that mitochondrial ATP synthesis is maintained by Ca^{2+} shuttling from ER to mitochondria (Càrdenas et al., 2010).

Ca^{2+} influenced also the shaping of this organelle by activating Drp1 through calcineurin-driven dephosphorylation that occurs after $[Ca^{2+}]_c$ rise (Breckenridge et al., 2003; Cribbs and Strack., 2007). Two other proteins, Miro 1 and Miro 2, involved in mitochondrial fusion, are endowed of EF-hand Ca^{2+} binding domains (Frasson et al., 2006).

Ca^{2+} signalling is also strictly correlated to mitochondrial biogenesis: a reduction in $[Ca^{2+}]_m$ and an increase in mitochondrial volume befall by inducing biogenesis through employing PGC-1α (peroxisome proliferator-activated receptor-gamma (PPARγ) co-activator-1α) (Bianchi et al., 2005; Puigserver et al., 2003).

Mitochondrial Ca^{2+} modulates also many fundamental cellular functions. One of the functional consequences of mitochondrial ability to take up Ca^{2+} is the buffering of bulk $[Ca^{2+}]_c$, indeed $[Ca^{2+}]_c$ waves can be localized at specific cell regions (such as synaptic regions, secretory pole of exocrine cells or immunological synapsis), can diffuse across the cells or they can also oscillate with different frequencies.

The buffering capacity varies in different cells types, depending on mitochondrial number, volume and Ca^{2+} buffering capacity.

Depolarization of excitable cells induces an increase in $[Ca^{2+}]_c$ that leads to an initial rapid recovery phase followed by a slower second phase, owing to $[Ca^{2+}]_m$ redistribution mediated by mNCX (Thayer et al., 1990; David et al, 1998).

Experiments performed *in vivo* in mature skeletal muscles, demonstrated that inhibition of mNCX augments Ca^{2+} buffering capacity of mitochondria, reducing the amplitude of $[Ca^{2+}]_c$ peaks. Similar results are obtained from Maack and co-workers in cardiac myocytes, confirming the important role of mitochondria in modulation of $[Ca^{2+}]_c$ peaks. The red skeletal muscle has high mitochondrial density located in close proximity to Ca^{2+} release sites. By inhibiting mitochondrial Ca^{2+} uptake, there is an alteration in the relaxation rate of skinned red fibers (Franzini-Armstrong et al., 2007; Gillis et al., 1997).

In cardiac muscle, mitochondrial uptake and release of Ca^{2+} seems to follow a "beat-to-beat" model, but this hypothesis is still debated as well as the role of mitochondria. Local $[Ca^{2+}]_c$ sparks are associated by the direct transfer of Ca^{2+} to mitochondria leading to transient increase in $[Ca^{2+}]_m$ (Lukyaneco et al., 2000); Pacher et al., showed that in cardiac cells mitochondrial Ca^{2+} uptake decreases the frequency and the duration of $[Ca^{2+}]_c$ sparks modulating RyR (Pacher et al., 2002). Moreover, mitochondrial Ca^{2+} buffering at the Z-line affects transverse propagation of Ca^{2+} waves (Subramanian et al., 2001). In neonatal cardiac myocytes, the downregulation of MCU increases the cytosolic Ca^{2+} peaks, while the overexpression of MCU decreases Ca^{2+} peak (Drago et al., 2012).

In neurons, there is a powerful example of how mitochondria can shape $[Ca^{2+}]_c$ dynamics by redistributing at Ca^{2+} release area. Indeed they are able to buffering an amount of $[Ca^{2+}]_c$ up to > 10 mmol per kg and they influence neurotransmitter release by buffering $[Ca^{2+}]_c$ at synapses.

In sympathetic neurons (Colegrove et al., 2000) and in adrenal medulla cells (Montero et al., 2000; Montero et al., 2001), mitochondria buffer the massive Ca^{2+} increase due to K^+-dependent depolarization or due to long trains of action potential. Indeed in pre-synaptic terminals, the enhanced synaptic response due to consecutive stimulations, is guaranteed by an elevated $[Ca^{2+}]_c$ baseline due to the re-equilibration of $[Ca^{2+}]_m$ after a cytosolic Ca^{2+} plateau.

Rat astrocytes show a prolonged high $[Ca^{2+}]_m$, perhaps due to a slow activity of the mNCX modulating negatively the propagation of the $[Ca^{2+}]_c$ waves (Boitier et al., 1999).

In pancreatic acinar cells, mitochondrial Ca^{2+} buffering pledge the correct activation of the secretory granules by preventing the spread of $[Ca^{2+}]_c$ from the apical pole to the basal pole. Moreover, the mitochondria at the basal pole seems to be more sensitive to CCE preventing high $[Ca^{2+}]_c$ in this side of the pancreatic acinar cells (Petersen et la, 2006a; Petersen et la, 2006b; Petersen et al., 2012).

T lymphocytes activation by antigens and chemokines seems to be due to a complex interaction between mitochondrial and SOCCs located at PM. Indeed mitochondria seems to regulate Ca^{2+} release-activated Ca^{2+} channel (CRAC) at the immunological synapses, buffering Ca^{2+} influx and modulating the rate of CCE (Hoth et al., 1997).

The mitochondrial ability of shaping $[Ca^{2+}]_c$ waves both spatially end temporally is confirmed by different studies in endothelial and epithelial cells, demonstrating the importance of mitochondria located near the PM and the nucleus in distributing Ca^{2+} not only from ER but also from the extracellular space (Frieden et al., 2004-2005; Varadi et al., 2004; Malli et al., 2003).

Finally, the close connection between ER-mitochondria-plasma membranes, is demonstrated in HeLa cells overexpressing the mitochondrial fission protein hFIS1. Here, the absence of mitochondria near the PM leads to an increase in Ca^{2+} cycling through PMCA and CCE with the consequent bent of Ca^{2+} depletion in the ER under low extracellular $[Ca^{2+}]$ conditions (Frieden et al., 2005; Malli et al., 2005).

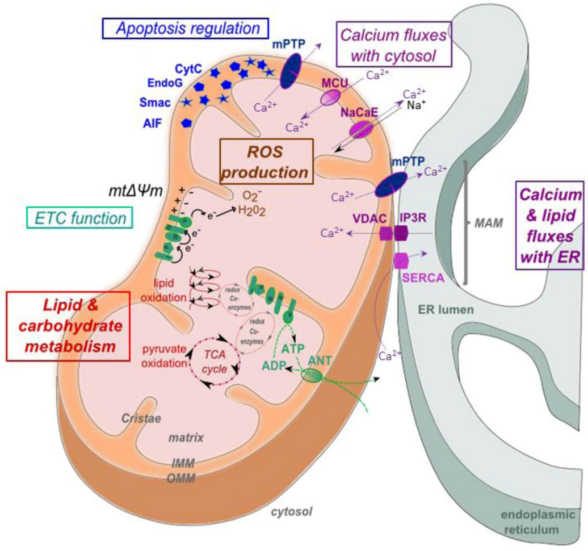

FIGURE 6. Structure and functions of mitochondria (Brault et al., 2013).

As Ca^{2+} plays such a critical and leading role in the regulation of mitochondrial metabolism and cell physiology, it is expected that, on the other side, the derangement of mitochondrial Ca^{2+} homeostasis becomes causal in cell death pathways leading to apoptosis and necrosis (reviewed in Rasola et al., 2011).

Necrosis have long been associated with major increases in $[Ca^{2+}]_c$, as well as with Ca^{2+} overload in mitochondria. Ca^{2+} overload causes the opening of the high-conductance PTP, the rapid collapse of the membrane potential and the swelling of mitochondria, with consequent loss of cytochrome c. The following bioenergetic crisis, characterized by the drop in ATP levels and production of reactive oxygen species (ROS), results in necrotic cell death (reviewed in Rizzuto et al, 2003).

More recently, it became clear that mitochondria also performs a pivotal role in the controlled cell death, in particular along the apoptotic intrinsic pathway. Despite the variety of cellular perturbations that can initiate the pathway, they all end up with the loss of integrity of the mitochondrial membrane, supposed to be mediated by PTP opening triggered by Ca^{2+} overload, which results in the release of pro-apoptotic factors that initiate the caspase cascade (Bernardi, von Stockum, 2012). Of note, in both cases, the causal event that causes PTP opening is mitochondrial Ca^{2+} overload. The outcome appears correlated with the extent of the overload (McConkey and Orrenius, 1996), which affects the duration of the PTP opening, which, in turn,

determines the residual ATP availability (Giorgi et al 2008). As ATP is required for apoptosis to progress, this will ultimately be the key switch between the two types of cell death.

$[Ca^{2+}]_c$ rises have been also shown to induce morphological modifications in mitochondria that correlates with apoptosis: indeed calcineurin-dependent phosphorylation of Drp1 causes its translocation on mitochondrial membrane and triggers mitochondrial fission, which leads to cytochrome c release (Cereghetti, 2008; Frank, 2001; Breckenridge et al., 2003; Cribbs et al., 2007, Friedman et al., 2011).

Numerous experimental evidence led to the formulation of an hypothesis for the role of Ca^{2+} in apoptosis (Baffy et al., 1993; Scorrano et al., 2003; White et al, 2005): an apoptotic stimulus leads to the release of Ca^{2+} from the ER, which triggers Ca^{2+} uptake in mitochondria; an excessive Ca^{2+} accumulation in mitochondria activates the PTP, with consequent release of cytochrome c and other pro-apoptotic factors, leading to the activation of the effector caspases cascade. However, evidence exist that in some cell types or experimental conditions, overexpression of pro-apoptotic proteins does not cause a reduction of $[Ca^{2+}]_{ER}$ (Chen, 2004; Hanson, 2008). An interesting interpretation of this data is that pro- and anti-apoptotic proteins could act modulating specific subtypes of the IP3R, thus determining diverse susceptibility in different cell types.

An important role has been proposed for Ca^{2+} also in the regulation of autophagy. Several evidence suggest that elevations of intracellular $[Ca^{2+}]$ can induce autophagy, by a signal transduction pathway that comprehend the Ca^{2+} mediated phosphorylation of Ca^{2+}/Calmodulin-dependent-kinase-β (CaMKKβ), the activation of AMP-activated protein kinase (AMPK) which produces the inhibition of the mammalian target of rapamycin (mTOR), the central player of the autophagic pathway (Hoyer-Hansen et al., 2007). However, it has also been reported an opposite role for intracellular Ca^{2+}, as an inhibitor of autophagy. It is important to note that the relevance of many of these studies is uncertain, since they often analyse $[Ca^{2+}]$ elevations induced by ionophores for prolonged periods, a situation far from physiological, where Ca^{2+} signals are usually shorter and milder.

Another pathway, independent of mTOR, has been identified, implying Ca^{2+} released from the ER in the regulation of autophagy. In particular, it has been shown that inhibition of phosphatidylinositol signalling (*i.e.* decreasing IP_3, inhibiting IP3R or decreasing IP3R levels) enhances autophagy (Cardenas et al., 2010). Recently, a study reported that upon inhibition of IP3R, autophagy is stimulated in unstressed cells while it is inhibited in starved cells (Decuypere et al., 2011). Based on these observations, it has been hypothesized that in normal feeding conditions the constitutive Ca^{2+} transfer from ER to mitochondria is functional to the maintenance of an efficient mitochondrial respiration and thus prevents autophagy, whereas during starvation cytosolic Ca^{2+} signals have a dominant role in triggering autophagy.

Thus Ca^{2+}, accordingly with its early appearance in evolution as prokaryotic intracellular messenger (Case et al., 2007) and with the endosymbiotic theory of a prokaryotic origin of mitochondria, plays a fundamental role in the internal mitochondrial signalling as well as in signals integrating the organelles in the broader cellular context.

1.5.3 ER-mitochondrial crosstalk: the microdomains hypothesis and Mitochondria Associated Membranes

As mentioned before, the existence of MCU, responsible for Ca^{2+} uptake across the electrochemical gradient was proved. Using mitochondrial Ca^{2+} probes, including fusion proteins carrying the Ca^{2+}-sensitive photoprotein Aequorin, mitochondrial Ca^{2+} uptake was directly monitored in living cells showing that, following stimulation with a $[Ca^{2+}]_c$ raising agonist, the speed and the amplitude of Ca^{2+} accumulation in mitochondria greatly exceed the values that were previously predicted on the basis of MCU properties in isolated mitochondria. Indeed, $[Ca^{2+}]_m$ rises could reach values above 10 μM in response to cytosolic Ca^{2+} elevations rarely higher than 2-3μM . Taken into account the low affinity of the MCU, these observations raised a paradox, which led to formulate the "Ca^{2+} microdomains hypothesis": mitochondria placed in close proximity to the channels that generate rises in $[Ca^{2+}]_c$ (at the ER/SR or PM) are subjected to local $[Ca^{2+}]$ higher than those measured in the cytoplasm, giving rise to high and transient accumulation of Ca^{2+} (Rizzuto and Pozzan, 2006). The hypothesis was largely accepted, and supported by an increasing amount of electron microscopy (Vance, 1990) and fluorescence microscopy data showing regions of close proximity between ER and mitochondrial membranes in different cell types (Csordas et al., 1999; Rizzuto et al., 1998; Hoth et al., 1997 and Gilbert et al., 2000). It was only quite recently that the "Ca^{2+} microdomain" hypothesis has been directly confirmed by our group, using Cameleon probes targeted to the OMM (Giacomello et al., 2010). These experiments have proved the existence of small OMM regions where, upon stimulation of Ca^{2+} release from the ER, $[Ca^{2+}]$ reaches values as high as 15–20 μM. Altogether, these data supports the conclusion that microdomains of high $[Ca^{2+}]_c$ are sensed by mitochondria that are present in close proximity to IP3Rs and RyRs in ER or SR membranes (Giacomello et al., 2010; Korzeniowski et al., 2009), and VOCCs and SOCCs located on the PM (Glitsch et al., 2002; David et al., 1998; Young et al., 2008), generating rapidly dissipating $[Ca^{2+}]_m$ transients. This property allows mitochondria to rapidly sense Ca^{2+} signals and to buffer locally Ca^{2+} rises, thus modulating the frequency of Ca^{2+} oscillations, with important implications in metabolism, secretion, neurotransmission and cell fate.

Recently, the existence of a physical link between mitochondria and ER has been demonstrated (see below). Many proteins with different cellular activities (i.e. involved in the control of lipid biosynthesis, Ca^{2+} signalling and mitochondrial dynamics and division) have been found to be localized in this specialized subdomain, supporting the idea that ER-mitochondria contacts are highly specialized interfaces with an essential physiological role.

The first evidence of the existence of close contacts between ER membranes and the OMM date back to the 1960s (Robertson, 1960; Ruby et al., 1969; Morré et al., 1971), but the multifaceted significance of these appositions has started to be elucidated only more recently. In particular, an ER fraction that is attached to mitochondria can be biochemically isolated as mitochondria-associated membranes (MAMs) and it is reported to be enriched in enzymes that are involved in lipid synthesis, including phosphatidylserine (PS) synthase (Stone and Vance , 2000). This specific subdomains of ER membranes that interact with the OMM were defined as tight associations essential for lipid synthesis and exchange between the two organelles

(Vance, 1990). The distance between the ER and mitochondria in MAMs have been measured to be 10–30 nm. This distance is close enough to suggest that the two organelles are tethered together by proteins located on the apposing membranes. Moreover, ribosomes are excluded from the ER membrane at this level, thus further indicating that contact sites form at specialized ER domains (for a review, see Rowland and Voeltz, 2012). The presence of trypsin-sensitive proteinaceous tethers between the two membranes is now well established (Csordas et al., 2006) and the list of proteins with structural and signalling functions at the ER/mitochondria interfaces is constantly increasing, revealing a previously unexpected complexity (for recent reviews Filadi et al., 2012 and Raturi and Simmen, 2013).

Since 90s, different protein have been suggested to be enriched in these compartment (De Brito and Scorrano, 2010). In yeast, the ERMES complex (ER-mitochondria encounter structure) is a complex of at least four proteins (Mdm10/ Mdm34, which are integral OMM proteins, Mmm1, an integral ER protein and the cytosolic Mdm12) whose assemblying favours lipid/metabolite exchange and zippers ER to mitochondria (Kornmann et al., 2009). In mammals, the proposed ER-mitochondria tether in mammals is Mitofusin-2 (Mfn2). Mfn2 is an OMM protein, but a fraction resides also in the ER, particularly at the level of MAMs. ER resident Mfn2 has been proposed to engage homo- or hetero-typic interactions with respectively Mfn2 or its homologous Mfn1 on OMM, thus mediating a physical tethering between the two organelles that has been shown to affect their Ca^{2+} shuttling (de Brito and Scorrano, 2008). Anyway these latter findings are under debate, since Orci's group demonstrated, using electron microscopy, that MFN2 KO MEFs are characterized by an increase in ER and mitchondria juxtaposition compared to wt MEFs, reversing the model propose by Scorrano's group. Moreover, the presence of residual ER-mitochondria apposition in Mfn2 KO MEFs suggests that additional tethers should exist (Cosson et al., 2011).

Of note, also Presenilin 1 and 2, two proteins involved in Familiar forms of Alzheimer's Disease, have been found to be highly enriched in MAMs (Area-Gomez et al., 2009).

2. Ca^{2+} sensors

2.1 Ca^{2+} measurement in living cells

An adequate measurement of Ca^{2+} dynamics in living cells requires tools with sufficient sensitivity and spatial-temporal accuracy. Indeed, $[Ca^{2+}]$ inside the cell can change quickly, depending from the cell's state (at rest or stimulated) and the specific subcellular compartment analysed. For example, cytoplasmic Ca^{2+} concentration, $[Ca^{2+}]_c$, can increase from ~100 nM (in basal conditions) to peaks of 1-3 μM, reached in just a few tens or hundreds of ms upon cell stimulation. Over the last decades, many classes of indicators, both chemical and protein based, have been developed and can be classified according to their physicochemical characteristics and spectral changes occurring upon Ca^{2+} binding: single wavelength indicators change fluorescence intensity without shifting their excitation or emission wavelengths, while ratiometric indicators change their excitation and/or emission spectra. Single wavelength indicators are generally brighter and facilitate Ca^{2+} detection when more than one fluorophore is used. Ratiometric dyes can be calibrated very

precisely and minimize the most common problems associated with synthetic indicators, including heterogeneous dye loading, photobleaching, dye leakage and changes in focal plane (Paredes et al., 2008).

2.2 Synthetic Ca^{2+} indicators

The first developed family of Ca^{2+} sensors is represented by synthetic dyes. Optical measurements of $[Ca^{2+}]_c$ were performed initially using synthetic molecules that change their fluorescence or absorbance properties upon Ca^{2+} binding. Problems encountered using these indicators included their modest Ca^{2+}/Mg^{2+} selectivity and the variable stoichiometry of cation/dye complexes. The field of Ca^{2+} imaging moved a significant step forward in the 1980s when R.Y. Tsien developed a new class of synthetic fluorescent Ca^{2+} indicators (among them quin2, Fura-2 and Indo-1), combining a fluorophore with the Ca^{2+} chelator EGTA (Grynkiewicz et al., 1985). The structural changes induced by Ca^{2+} binding lead to modifications in the spectral emission and/or excitation properties of the probes, thus allowing a rapid and reliable estimation of $[Ca^{2+}]$ variations. The first rationally-designed fluorescent Ca^{2+} indicator was quin-2 (Tsien, 1980). The substitution of two methylene groups, with two benzene rings, couples the conformational change due to Ca^{2+} binding to a change in the spectral proprieties of the dye. Improvements of the original polycarboxilate indicators were then achieved in the following years in R.Y Tsien laboratory, *e.g.* the synthesis of indicators with different Ca^{2+} affinities and with excitation wavelengths different from the ultraviolet one (characteristic of the first generation of indicators). Key to the success of these indicators was also the discovery of a simple method to load these indicators into living cells, thus avoiding the complex procedure of microinjection. An acetoxymethyl (AM) ester group was added to the dyes, thus improving their hydrophobicity and consequently the permeation through the PM. Indeed, the original dyes had to be microinjected into cells by a time-consuming technique, while AM forms can simply be added to the medium. Once in the cytoplasm, the AM groups are rapidly hydrolysed by cellular esterases, regenerating the water-soluble indicator within the cell and at the same time preventing its release back into the medium.

Over the years, many Ca^{2+} indicators were developed based on the same rationale, with different Ca^{2+} affinities and spectral properties, allowing intracellular Ca^{2+} detection in practically any cell type over a large range of concentrations (from <50 nM to >50 μM). High-affinity indicators are useful to quantify $[Ca^{2+}]_c$ while lower affinity indicators can be in principle optimized for measuring Ca^{2+} within subcellular compartments with higher concentrations (Paredes et al., 2008). The esterases that cleave the AM groups in the fluorescent probes mentioned above are primarily located in the cytosol; accordingly, these indicators cannot be targeted to organelles with adequate selectivity. The only exception is Rhod-2, which accumulates into mitochondrial matrix thanks to its positive charge (Minta et al., 1989). The results obtainable with this dye are far from ideal, and to this end usually genetically encoded Ca^{2+} probes are preferred for mitochondria Ca^{2+} measurement. One way that has been proposed to overcome the limitation of the specific subcellular targeting, is to overexpress esterases in specific subcompartments of the cell (Rehberg et al., 2008). This approach, although interesting, is still poorly exploited.

2.3 Genetically Encoded Ca^{2+} Indicators

The second family of Ca^{2+} indicators comprises proteins, either chemiluminescent (Aequorin) or Green Fluorescent Protein (GFP)-based, both derived from the jellyfish *Aequorea Victoria*. The most important breakthrough in the field of Ca^{2+} imaging at the subcellular level stemmed from the use those two proteins, opening the field of Genetically Encoded Ca^{2+} Indicators (GECIs). Specific targeting signals can be fused to the GECI sequence, achieving selective targeting of the transfected cDNA to organelles or cytoplasmic domains. GECIs targeted to practically all subcellular compartments and for measuring different dynamic parameters (Ca^{2+}, pH, cyclic nucleotides, ATP, O2 radicals, etc) are now available. GECIs display different advantages, since they can be easily modified in their features (such as localization, dynamic range and affinity) by simple molecular biology techniques. They can also be placed under the control of tissue-specific or inducible promoters, allowing spatial and temporal control of their expression. They are also suitable for *in vivo* measurement of Ca^{2+} dynamics in intact tissues as well as in whole organisms, since they can be delivered via transgenesis, viral injection or *in utero* electroporation (Mank et al., 2008). Different classes of GECIs have been created and specific parameters are usually evaluated to characterize each probe, in particular affinity and selectivity for Ca^{2+}, dynamic range and kinetics for Ca^{2+} binding. Usually, the evaluation of these parameters is performed *in vitro* but, since these probes behave differently in subcellular compartments, it is now clear that an *in vivo* evaluation is also necessary to obtain reliable measurements of absolute Ca^{2+} concentrations. Moreover, the cited parameters must be carefully assessed in order to choose the appropriate probe for the designed experiment. Starting from the building blocks Aequorin (Aeq) or GFP, it is possible to divide GECIs in two classes: bioluminescent probes (based on Aeq) and fluorescent probes (based on GFP).

2.3.1 Bioluminescence-based GECIs: Aequorin

Aeq was the first protein-based Ca^{2+} indicator used in biology. In the early 1970s, after purification from jellyfish, it was usually injected into the cells (Llinás et al., 1972), but after the cloning of its cDNA (Inouye et al., 1985) it became the most frequently used probe to measure Ca^{2+} in different organelles. Aeq is a 22 kDa Ca^{2+}-sensitive photoprotein produced by the jellyfish *Aequorea victoria*, with a hydrophobic core that binds the prosthetic group coelenterazine and three EF-hand motifs for Ca^{2+} binding. Upon Ca^{2+} binding, the covalent bond between the prosthetic group and the apoprotein is broken, coelenterazine is oxidized to celenteramide and released with the emission of one photon; this reaction is irreversible (Figure 7). Importantly, the rate of photon emission depends on the $[Ca^{2+}]$, thus allowing the conversion of the speed of emitted light into $[Ca^{2+}]$ through a specific algorithm (Allen et al., 1977; Brini et al., 1995). In particular, there is a relationship between the $[Ca^{2+}]$ and the fractional rate of Aequorin consumption (*i.e.*, L/Lmax, where L is the light intensity at a given time and Lmax is the total amount of light emitted after that point). Since the probe is gradually consumed during an experiment, the $[Ca^{2+}]$ can be obtained only at the end, when all Aequorin is consumed and L/Lmax is back calculated for each experimental point.

The first Aeq variant, called native Aeq or simply Aeq wt, is expressed in the cytosol; the addition of targeting sequences for specific intracellular localization allowed the measurements of $[Ca^{2+}]$ in different

intracellular organelles. In particular, recombinant Aequorin variants have been reported, targeted to: mitochondrial matrix (mt Aeq), mitochondrial intermembrane space (mims Aeq), nucleus (Nu Aeq), ER (er Aeq), SR (sr Aeq), subplasmalemmal space (pm Aeq), Golgi apparatus (go Aeq), peroxisomes (perox Aeq) and secretory vesicles (vamp Aeq) (for a recent review, see Bonora et al., 2013).

Then a second variant of Aeq was created by the generation of a point mutation D119A in the EF2 domain. The low Ca^{2+} affinity mutated version of mtAEQwt (mtAEQmut, with the point mutation D119A in the EF2 domain, see below) was targeted to the mitochondrial matrix and revealed that mitochondrial Ca^{2+} transient, upon stimulation in certain cell type, can rapidly reach the millimolar level. On this line, a recently reported mtAEQmut, with an even lower Ca^{2+} affinity (de la Fuente S. et al., 2012), confirmed the ability of mitochondria to accumulate Ca^{2+} in their matrix up to the millimolar level.

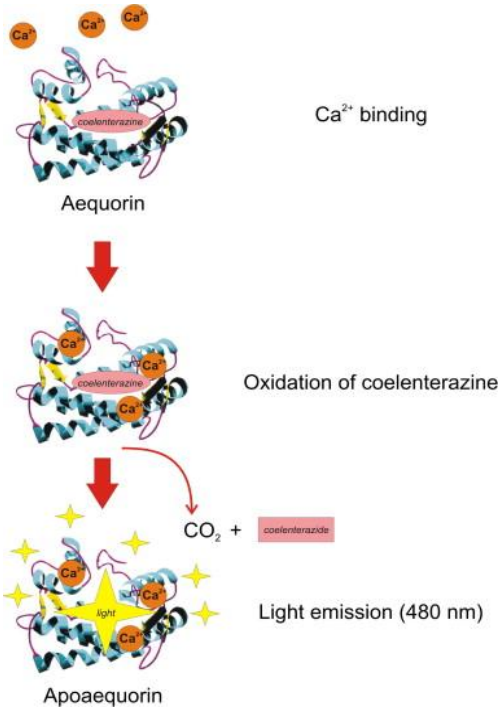

FIGURE 7. Schematic model of the irreversible reaction of Aequorin (Brini, 2008)

The first organelle-targeted GECI was developed in 1992, when the mitochondrial pre-sequence of subunit VIII of cytochrome *c* oxidase (COX) was fused to an HA1-tagged native Aeq (mt Aeq) (Rizzuto et al., 1992). Mt Aeq was particularly important because it was the prototype of the now large family of selectively targeted probes and at the same time because it provided the first direct evidence of fast mitochondrial Ca^{2+} accumulation in living cells in response to a physiological stimulus. Other mitochondrial Aeq-based GECIs were then produced: of particular relevance is the Aeq fused to glycerol phosphate dehydrogenase, a protein of the inner mitochondrial membrane (IMM) with a large C-terminal tail protruding in the mitochondrial IMS. This mims Aeq, provided the first direct evidence of the existence of high [Ca^{2+}] microdomains near the regions of close contact between mitochondria and ER (Rizzuto et al., 1998).

The noteworthy advantages of using recombinant Aeqs are:

(1) their wide dynamic range (from 0.1μM to the low millimolar level), obtained both by modification of the native Aeq and through the use of different coelenterazine derivatives;
(2) the marginal interference with endogenous Ca^{2+} buffering-proteins;
(3) the low sensitivity to pH;
(4) the high signal-to-noise ratio;
(5) in case of co-transfection (as for the other protein-based indicators), the analysis is restricted to the cells expressing the protein of interest, and not to all the cells as with chemical probes;
(6) the equipment required to perform the measurements is relatively simple and cheap.

The use of Aeqs also entails some disadvantages, such as:

(1) the need to transfect the cells or to use stably expressing clones, if compared with chemical probes;
(2) the need to reconstitute the protein with coelenterazine for at least 1h before the experiment, if compared with other protein-based Ca^{2+} indicators;
(3) the low amount of light emitted by the photoprotein, making it difficult to use in single cells;
(4) the irreversibility of the Ca^{2+} triggered reaction makes Aequorin suitable only for relatively short experiment;
(5) not reliable measurements of Ca^{2+} levels in compartments with inhomogeneous behaviour, since the different affinity for Ca^{2+} and the Ca^{2+} binding cooperativity of its three EF-hand domains make Aequorin behaviour steeply dependent from Ca^{2+} concentration;
(6) the photoluminescence measurements are difficult to calibrate in compartments (or in cell populations) with heterogeneous Ca^{2+} levels (Brini et al., 1995; Brini, 2008; and Bonora et al., 2013).

In the last years, other constructs containing Aeq have been generated, such as a dual reporter system comprising of a GFP mutant fused to Aeq (Baubet et al, 2000) and another named GAP, GFP-Aequorin protein (Rodriguez-Garcia et al., 2014). GAP is a fusion of GFP with apoaequorin that does not use the bioluminescence of Aequorin (thus, reconstitution is not necessary), but exploits Ca^{2+} binding to its three EF motifs to induce changes in the excitation/emission properties of GFP. The dual-excitation ratiometric imaging, the high dynamic range, the insensitivity to pH and Mg^{2+}, the stability to photons and the good signal to noise ratio make GAP a promising probe for Ca^{2+} measurements also *in vivo*.

2.3.2 GFP-based fluorescent GECIs

Fluorescent GECIs consist of a fluorescent protein (FP) fused to a Ca^{2+}-binding domain in such a way that Ca^{2+} binding modifies the fluorescence properties of the FP.

The first discovered FP is the Green Fluorescent Protein (GFP). FPs have tens of application in cell biology thanks to their multiple advantages. First of all FPs do not require an external cofactor in order to emit light: in the GFP the brilliant chromophore is formed by amino acids 65 to 67 through a mechanism of cyclization, dehydration and oxidation. Moreover, the chromophore is located into the α-helix running inside a tight structure formed by an 11-stranded β-barrel, and so it is protected against environmental condition's variations, at least in the wild-type form (Tsien, 1998). GFP can be easily modified without affecting its

ability to fluoresce: *e.g.*, with the insertion of other proteins in position 145, and with circular permutation, in which GFP is spliced in two parts and then the amino and carboxyl-termini are interchanged. Moreover, mutations in the amino acids responsible for chromophore formation or located in its proximity allow the generation of FPs with new features, i. e. shifting fluorescence emission wavelength from blue to yellow and obtaining brighter variants or decreased environmental sensitivity (Shaner et al., 2005).

GFP-based Ca^{2+} sensors are useful probes to evaluate Ca^{2+} dynamics in subcellular compartments, since they can be fused with specific targeting sequence, and they seem also to be the most promising for monitoring mitochondrial Ca^{2+} in live animals. Indeed, some examples are now available for *in vivo* Ca^{2+} measurements mainly with cytosolic probes, since they are better characterized and in general are easier to handle. On the contrary, organelle-targeted GECIs require a profound knowledge of both the sensor and the targeted organelle, since probes can be profoundly affected by the environmental conditions of each specific subcellular compartment. Moreover, in the last years a growing colour palette of FPs has been developed and many efforts have been made to red-shift the excitation wavelength of the indicators, reducing phototoxicity, background fluorescence and facilitating deep imaging into the tissues. An interesting challenge is the combination of differently coloured GECIs targeted to distinct organelles, in order to unravel the interconnection of Ca^{2+} signalling across different organelles, both in physiological and pathological animal models. Finally, further efforts should be focused on the amelioration of the signal-to-noise ratio, the reduction of pH and temperature sensitivity of the FPs, the decrease of probe's size, and improvement of the kinetics.

Two strategies have been developed to obtain GFP-based Ca^{2+} indicators: the first employs GECIs containing one fluorescent protein, where binding alters the chromophore environment, inducing a change in the intensity or in the wavelength of the emitted fluorescence. The other, takes advantage of Förster (or fluorescence) resonance energy transfer (FRET) changes that occur between two FPs in molecular constructs where the two proteins are linked through a Ca^{2+}-sensitive peptide.

Single fluorophore GECIs

The development of single fluorophore GECIs started with the discovery that GFP (in its different variants) tolerates the insertion of relatively long peptides at position 145 in their aminoacid sequence. When a Ca^{2+}-binding peptide is inserted, the change in protein structure induced by the binding of the ion affects the protonation of the chromophore, changing its pKa, resulting in an increase or decrease of the chromophore fluorescence when excited at a given wavelength (Baird et al., 1999). The most widely used Ca^{2+}-binding-protein in these type of constructs is Calmodulin (CaM). One molecule of CaM presents four EF-hand domains, each one binding one Ca^{2+} ion cooperatively.

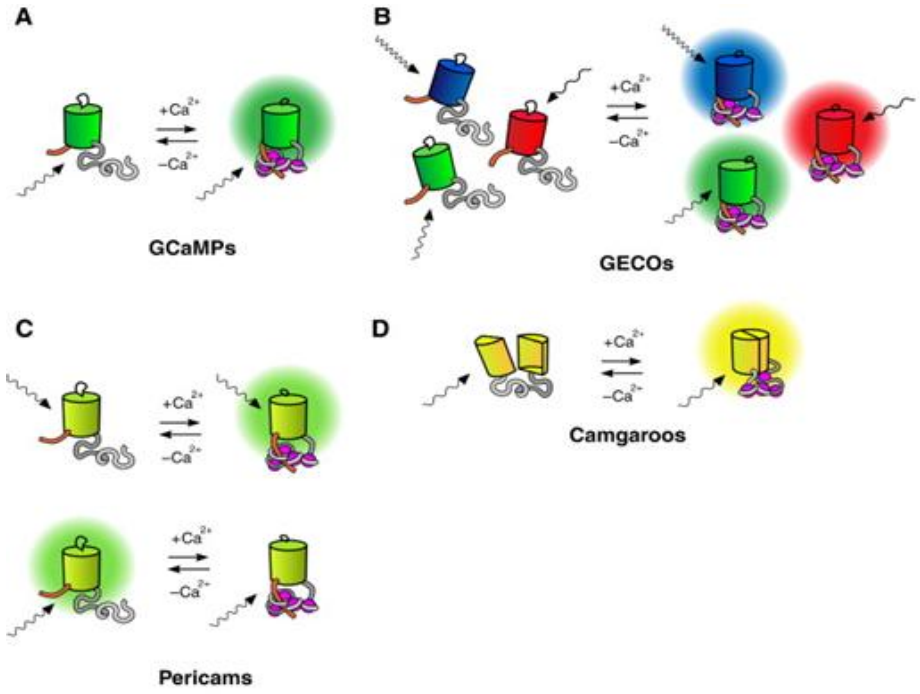

FIGURE 8. Single-fluorescent protein Ca^{2+} indicator families (Koldenkova and Nagai, 2013)

Different type of single fluorophore GECI has been created (Figure 8):

(1) Camgaroo. Camgaroos are a family of Ca^{2+} probes in which the CaM sequence was inserted at position 145 of a yellow fluorescent protein (YFP), and Ca^{2+} binding causes a shift of the absorbance peak of the FP from 400 nm to 490 nm, thus allowing an estimation of [Ca^{2+}]. Given that excitation at 400 nm does not lead to fluorescence emission in YFP, an attempt was made to improve visibility of cells at basal Ca^{2+} concentrations by changing the YFP with another GFP mutant named Citrine, resulting in Camgaroo-2 (Griesbeck et al., 2001).

(2) Pericam. Another important and useful modification of the GFP is the generation of circular permuted YFP (cpYFP). The new sensor Pericam was generated fusing the CaM-binding domain of myosin light chain kinase, the M13 peptide, to the N-term of cpYFP, and CaM to the C-terminal. Upon binding of Ca^{2+}, CaM wraps around the M13 peptide, causing a conformational change in the protein. Point mutagenesis and linker insertions generated variants of Pericam with different properties and affinity for Ca^{2+}. Three different Pericams were generated: flash Pericam, that becomes brighter upon Ca^{2+} binding; inverse Pericam, that on the contrary decreases its fluorescence upon Ca^{2+} binding and ratiometric Pericam. The latter shows a shift in the excitation wavelength upon Ca^{2+} binding, allowing ratiometric measurements. Mitochondrial matrix targeting of ratiometric-Pericam have been obtained by fusing its N-term to the first 12 aminoacids of subunit IV of COX (Nagai et al., 2001) or to one or two copies of the first 36 amino acids of subunit VIII of human COX (Filippin et al., 2005). Another variant, called Inverse Pericam and characterized by the decrease of fluorescence upon Ca^{2+} binding has been fused to subunit VIII of human COX generating the probe Mitycam (Kettlewell, 2009).

(3) G-Camp. A class of sensors that enlarged considerably in the last years was developed starting from G-Camp, an indicator generated fusing M13 peptide and CaM respectively at N- and C-term of a circularly permuted EGFP (Nakai et al., 2001). The first variant showed a suitable affinity for Ca^{2+} and a good dynamic range (4,5 fold change upon Ca^{2+} binding), however it was affected by some disadvantages, such as strong pH sensitivity, low fluorescence at resting state, slow folding and maturation of the fluorophore. Extensive structure-guided optimization has been performed to improve the properties of this sensor, giving birth to a class of sensors with different spectral properties and Ca^{2+} affinity, lastly leading to the generation of the family G-Camp6, characterised by improved brightness, sensitivity, affinity for Ca^{2+}, wider dynamic range and faster kinetics, compared to the previously generated G-Camp5. *In vivo* experiments in neurons proved the sensor G-Camp6f to be the fastest GECI available for measuring cytoplasmic free Ca^{2+} in neurons, with a sensitivity comparable to some commercially available chemical dyes (Chen et al., 2013). GCamPs targeting to mitochondria has been exploited for different sensors. Some attempts have been also made to increase the colour palette of single wavelength GECIs.

(4) CEPIA and GEM-GECO. Recently, new Ca^{2+} sensor based on G-Camp has been generated. Those new probes, called Ca^{2+}-measuring organelle-entrapped protein indicators (CEPIA), are useful to monitor simultaneously Ca^{2+} dynamics in different cellular subcompartments. Indeed CEPIAs with different emission wavelength (green, red or blue/green fluorescence) and targeted to organelles are available, making it possible, for example, to measure mitochondrial, ER and cytosolic [Ca^{2+}] simultaneously (Iino et al., 2014). A ratiometric variant of GEM-GECO called GEM-CEPIA was also generated. It is reported to have grater dynamic range but higher photobleaching and photoconversion (Zhao et al., 2011).

The main drawback of this class of Ca^{2+} sensor is its pH sensitivity (improved in the last generation of G-Camp), and the fact that only a fluorescence intensity change is measured, with the exception of ratiometric Pericam and GEM-CEPIA. The measurement of [Ca^{2+}] variations as changes in fluorescence intensity is prone to errors, since also contractions or shifts in focal plane rise the same effect.

FRET-based GECIs sensing Ca^{2+}

In 1997, Tsien and co-workers (Miyawaki et al., 1997) and independently Romoser's group (Persechini et al., 1997) generated the first class of ratiometric GFP-based Ca^{2+} sensors, named by Tsien "Cameleons". Cameleon probes are ratiometric GFP-based Ca^{2+} sensors initially named YCx, while subsequent computationally redesigned versions have been referred as Dx (x is the number of the variant). The Cameleon structure consists of the two Ca^{2+}-responsive elements CaM and CaM-binding domain of myosin light chain kinase M13 connecting two FPs. The working principle of Cameleons is based on FRET changes: the direct transfer of energy from an excited donor FP (generally, a blue FP) to an acceptor FP (generally, a yellow FP). Ca^{2+} binding to CaM triggers a conformational change in the molecule, forcing the two FPs closer together: this results in an increased FRET efficiency that in turn leads to a decrease in the donor fluorescence intensity and an increase in the acceptor fluorescence intensity. It is thus possible to monitor

changes in [Ca^{2+}] as changes in the ratio (R) between acceptor and donor fluorescence intensity. (Palmer et al., 2006).

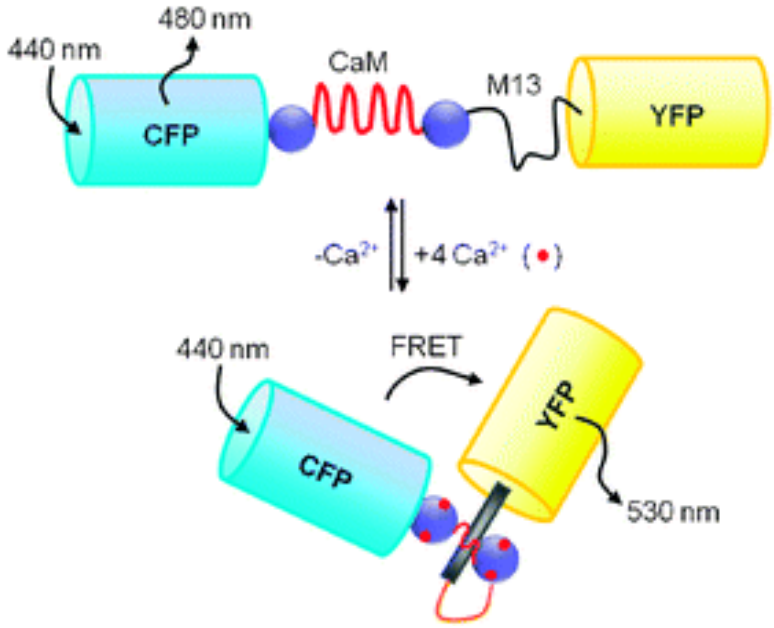

FIGURE 9. Schematic representation of Cameleon probe (Ko et la., 2011)

In the last years, many improvements have been made to the original Cameleons: fluorophores have been replaced or modified to obtain decreased sensitivity to pH and Cl^-, decreased photobleaching, variable Ca^{2+} affinity, improved dynamic range of FRET changes upon Ca^{2+} binding, and reduced interference of the probe with endogenous Calmodulin targets (Miyawaki et al, 1999; Palmer et al., 2006; Griesbeck et al., 2001; Nagai et al., 2004; Horikawa et al., 2010; Evanko et al., 2005; Truong et al., 2001). In particular, one of the issues that have been raised regarding the use of CaM-based GECIs is the possible interference of the probe with endogenous CaM targets. The problem has been overcame by Palmer and colleagues in Cameleon probes by engineering the binding interface between CaM and M13, thus decreasing the interaction between M13 and the endogenous CaM. Another important modification in the perspective of organelle targeting was the mutagenesis of Ca^{2+} binding site and the consequent creation of probes with different Ca^{2+} affinities. As a result of this modification, Cameleon probes with sensitivities that covers a 100 fold range of [Ca^{2+}] (evaluated *in vitro*) are now available (Mank et al. 2006, 2008): D1 (k_d= 0.8, 60 µM), D2 (k_d= 0.03, 3 µM), D3 (k_d=0.6 µM), D4 (k_d= 64 µM). Moreover, different organelle-targeted Cameleons have been generated, directing the probe to the nucleus (Miyawaki et al., 1997), PM (Palmer et al., 2006), peroxisomes (Drago et al., 2008), mitochondria (Filippin et al., 2003; Palmer et al., 2006), ER (Demaurex et al., 2003; Palmer et al., 2004; Kipanyula et al., 2012), cis-medial and trans Golgi apparatus compartments (Lissandron et al., 2010; Wong et al., 2013).

As far as mitochondria are concerned, Cameleons were selectively targeted to the mitochondrial matrix and thus revealed the Ca^{2+} level within the lumen of the organelles. The most used mitochondrial targeted Cameleon probe is the 4mtD3cpV (and 4mtD1cpV), targeted to mitochondrial matrix thanks to the fusion

with 4 sequences of the N-terminal sequence of subunit VIII of human Cytochrome C Oxidase (COX). A unique sensor targeted to the OMM by fusing TOM20 N-terminal tail to D1cpV is also presently available, named N33D1cpV (Giacomello et al., 2010).

4mtD3cpV allows Ca^{2+} dynamics measurement in mitochondrial matrix of different cell types and in different conditions, from physiological phenomena to stimulated mitochondrial Ca^{2+} uptake. 4mtD1cpV shows faster kinetics and double affinity for Ca^{2+}. N33D1cpV allows the evaluation of the amplitude and dynamics of Ca^{2+} hotspots at the OMM generated by the release of Ca^{2+} from the ER or entering the cell through PM channels. Both probes can be easily used *in vitro* and *in vivo* to visualize mitochondrial Ca^{2+} dynamics. A huge number examples of *in vitro* application of the probes can be found, ranging from classical cell lines to primary cultures such as neurons, cardiomyocytes, lymphocytes and so on. *In vivo* applications have been less exploited, but some examples are present in the literature: Ca^{2+} uptake into mitochondria of mouse skeletal muscle during contraction was studied by using 2mt-YC2 (one of the first variant of Cameleon probes) electroporated into hind limb muscles (Rudolf et al., 2004); similarly, mitochondrial Ca^{2+}-handling in fast skeletal muscle fibres was evaluated employing 4mtD3cpv (Scorzeto, 2013); finally, Ivannikov et al., generated a transgenic fly line expressing mitochondrial D4cpV to evaluate mitochondrial Ca^{2+} uptake effects on energy metabolism in motor nerve terminals (Ivannikov and Macleod, 2013). Recently, *Arabidopsis* transgenic plants expressing 4mt-YC3.6 have been used to unravel Ca^{2+} dynamics in the mitochondria of both guard and root cells in plants (Loro et al. 2012-2013) and a transgenic zebrafish expressing mitochondrial targeted YC2.60 was created to analyse embryonic Ca^{2+} waves that occur after fertilization and Ca^{2+} rises induced by contraction in embryonic myocytes.

Another subtype of FRET-based Ca^{2+} sensors is the family of Troponin C (TnC) based indicators, generated to overcome the problems related to the use of CaM and in particular to avoid the interaction with CaM-binding-proteins. To this end, the Ca^{2+}-binding domain of Cameleons was substituted with chicken skeletal muscle Troponin C, TnC or human cardiac TnC, generating the sensors TN-L15 and TN-humTnC, respectively. The resulting sensor was structurally similar to the Cameleon, with the exception that it lacks of a binding peptide (reviewed in Garaschuk et al, 2007). Recently, a new type of FRET TnC-based Ca^{2+} sensor was developed, based on the C-terminal domain of *Opsanus* Troponin C: the so called 'Twitch' sensors. Interestingly, the sensors are endowed with high sensitivity (comparable to that of synthetic Ca^{2+} dyes), high brightness, large dynamic range and linear response properties, proposing them as interesting tools for neuroscience and immunology (Thesturp et al., 2014).

2.4 Delivery systems for GECIs: Adeno-associated viruses

As far as *in vivo* delivery is concerned, a general limitation of chemical dyes is the difficulty to supply the dye to the tissue of interest. On the contrary, GECIs can be delivered by standard approaches such as transgenesis, electroporation *in situ*, and viral infection. Despite these advantages, although some cytosolic GECIs have been exploited *in vivo*, the examples of organelle targeted probes *in vivo* are still scarce. Nonetheless, the *in vivo* models expressing mitochondrial targeted Cameleon probes described above,

ranging from plants to invertebrates to mammals, have contributed to a deeper understanding of Ca^{2+} dynamics *in vivo,* meaning that further effort should be done to improve the promising *in vivo* GECIs application.

The protocols classically used for *in vivo* expression involves principally transgenesis and electroporation *in situ*, two techniques involving time-spending (i.e. for the generation and crossing multiple strains) and laborious tasks. An interesting new *in vivo* delivery technique that permits to overcome the mentioned disadvantages, making it possible to expand the possibilities of *in vivo* GECIs applications, is the viral infection.

They are also useful to improve GECIs expression level, in primary culture resistant to transfection, such as neuron and neonatal cardiomyocytes.

Originally the use of viruses *in vivo* was thought for gene therapy in genetic pathology, but they become soon an interesting approach for more general transgene delivery. Indeed, the possibility to engineering viral genome, allows the insertion of the transgene of interest along with different promoters to achieve cell-specificity, and also the deletion of viral genes to improve safety (Woo et al., 2005). Different type of recombinant viruses have been created, form Lentivirus to Adenoviruses. They are mainly different in terms of operator's safety, immunogenicity, gene transfer duration, organs tropism and cassette's length (the part of the viral genome that host the target transgene). In general Adenovirus, Herpesvirus, and to some extent, Lentivirus are characterized by higher immunogenicity (Wright et al., 2001; Vandendriessche et al., 2007), while Adeno-Associated Viruses (AAV) vectors are considered safer to the operator, since they need a "helper" to infect the host. Moreover AAVs guarantee long-term gene transfer in animal models (Gao et al., 2002; Arruda et al., 2005; Woo et al., 2005). Another advantage of AAVs is the availability of different envelope serotypes conferring distinct organ tropism. Of note is the AAV serotype 9, reported to have a strong cardiac tropism via systemic or local injection (Pacak et al., 2006; Bish et al., 2008) and brain tropism via intracranial injection (Foust et al., 2009). In the latter case, it is also possible to obtain the transgene expression in a specific cell type of the brain, by substituting the classical CMV promoter with a neuronal subtype-specific promoter.

2.5 FLIM

Different methods are available to monitor FRET. The intensity-based approach is one of them and it is the most used. Basically, recording the fluorescence intensity, it is possible to calculate variations in FRET. In the case of Cameleon probes, for example, it is possible to record simultaneously the fluorescence of CFP and of cpV upon CFP excitation. Calculating the fluorescence ratio between the two FPs (cpV/CFP), it is possible to follow the Ca^{2+} dynamics occurring within the sample. Anyway, this approach does not consider the contribution of intermolecular-FRET or homo-FRET (see below) that could occur. When protein-protein interaction is assessed using inter-molecular FRET-based methods (see Sun et al., 2013), one target is labelled with the donor moiety and another one with the acceptor, and thus FRET occurs between two different species. On the contrary, intra-molecular FRET happens between FPs that are part of the same

molecule, as in the Cameleon probe. In both cases, an accurate calibration is required, since there is a contribution from the acceptor molecule that can be directly excited. Moreover, different stoichiometry between donor and acceptor could occur in inter-molecular FRET, raising the possibility of wrong evaluation of FRET efficiency (Becker, 2012). Another critical point is to correct the bleed-through between donor and acceptor fluorescence (Sun et al., 2013).

An alternative and promising method is based on the detection, instead of emission intensity, of the fluorescence lifetime of the probe. In FLIM (Fluorescence Lifetime Imaging Microscopy), measurements of the spatial distribution of probe lifetime is mapped inside living cells. FLIM was developed in the late 1980s (Bugiel and König, 1989) and early 1990s (Lakowicz at al. 1992), but it was widely applied in the late 1990s. This technique measures the average residence time in the excited state of the fluorophore, before it returns to the ground state by emitting a photon. Indeed, when a fluorophore is excited, its molecules are push to an excited and high energy state, where the molecule is unstable. Then, to restore the equilibrium, the molecule comes back to the ground state. This event happens with a certain probability based on the decay rates through a number of different (radiative and/or non-radiative) decay pathways. To observe fluorescence, one of these pathways must be by spontaneous emission of a photon. The emission signal typically follows an exponential decay function described as:

$$I(t) = I_0 e^{(-t/\tau)}$$

Where, t is time, τ is the fluorescence lifetime, I_0 is the initial fluorescence at t=0. The characteristic time constant of this decay in FPs range from a few picoseconds to several nanoseconds (Lakowicz, 2006). FLIM produces images where each pixel represents the probe average lifetime, visualized through a false colours plot. This method allows one to distinguish fluorescent species by means of their fluorescence lifetime, within the same sample area and with overlapped emission spectra. This is particularly useful for the analysis of FRET processes.

FLIM measurements, compared to intensity-based images, have the advantages of being independent of fluorophore concentration, excitation intensity fluctuation, sample thickness, or photobleaching. Indeed, the lifetime is independent of initial intensity and of the emitted light intensity. However, FLIM could be affected by some environmental parameters, such as pH, ion, oxygen concentration and molecular binding.

FLIM is applied for studying a broad number of phenomena:

- In biology, FLIM allows for the separation of multi-colour labelling with similar emission/excitation spectrum, but it is also suitable for detection of molecular interactions, for monitoring conformational changes in structural studies and for environmental sensing experiments;
- In medicine, FLIM is used for tissue characterization by autofluorescence analysis;
- In material science, FLIM is used to characterize and perform quality control on new materials (for further details see Becker et al., 2012).

FLIM can be exploited using two different acquisition modes (Figure 10):

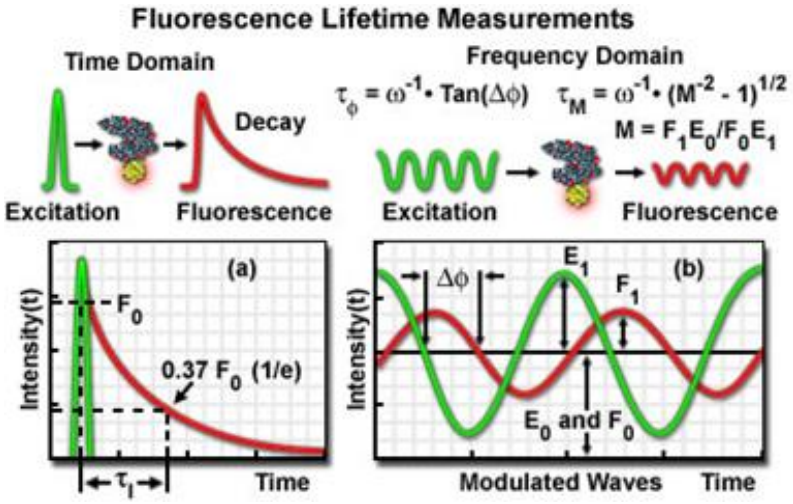

FIGURE 10. Schematic representation of time domain and frequency domain FLIM (from Olympus applications).

(1) Time domain measurements. This methods is performed using a femtoseconds or picoseconds pulsed laser as a source and the lifetime is measured using Time-correlated Single Photon Counting (TCSPC), usually coupled to a laser scanning microscope. TCSPC has a time resolution of sub-ns and it is independent on variations in source intensity and photoelectron amplitudes. TCSPC is usually coupled with different types of detector, such as a photo-multiplier tube (PMT) or an avalanche photo diode (APD), to record the arrival times at which individual photons are detected with respect to the excitation laser pulse. These recordings are repeated until the photons collected are sufficient to build a histogram representing the number of events over time; the histogram will be fit to an exponential function that contains the exponential lifetime decay function of interest (Li et al., 2010). The major disadvantages of this technique is the long-acquisition time. Indeed a critical issue is the number of photons collected, because it influences the accuracy of the lifetime estimations. This is more critical for bi- or tri-exponential decay function, requiring at least 10000 photons recorded per pixel. To shorten the acquisition time, different approaches can be employed, e. g.: lowering the number of recordings, then employing a more rough statistical analysis; using FP with single exponential lifetime, such as mCerulean3 and mTurquise2 instead of CFP; using gating-TCSPC, in which after a brief light pulse the record of photons is done in consecutive time bins (Ebrecht et al., 2014; Sun et al., 2013).

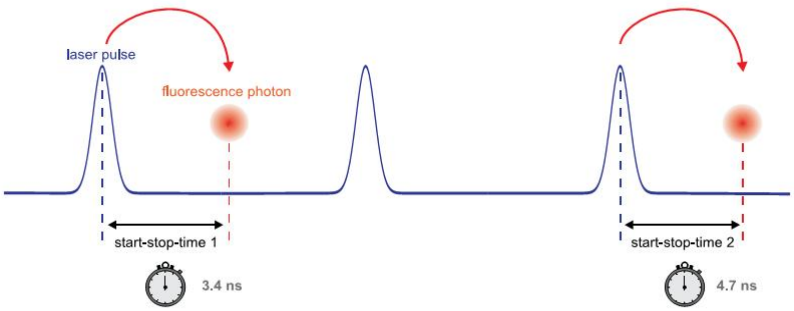

FIGURE 11. Schematic representation of TCSPC method (Picoquant technote).

(2) Frequency domain measurements. This method is carried out by a phase-modulated process, using an excitation light source that is pulsed or modulated at high frequency and a modulated detector such as an intensified camera. The fluorescence lifetime is derived from the decrease in the modulation degree and the phase shift of the fluorescence compared to the excitation features. Indeed, in this case the fluorescence emission mirrors the modulation pattern of the source and the lifetime is determined from the form of the phase shift/delay, since the modulation in the emission signal is generated by the duration of the excited state. An advantage of camera-based frequency domain FLIM is its faster lifetime image acquisition, compared to TCSPC methods, making it suitable for dynamic and kinetic measurements in live cell research (van Munster and Gadella, 2005).

2.5.1 FLIM-FRET

FRET is a process in which a donor direct transfer energy to an acceptor, through a non-radiative process. FRET phenomenon was described in 1948 by Förster and it is defined as a dipole-dipole interaction that occurs between two FPs when a partial overlapping between the donor emission spectrum and the acceptor excitation spectrum is present. Thus, FRET efficiency depends on: distance between donor and acceptor (usually from 1 to 10 nm for FRET to occur), spectral overlap between the two FPs and dipole orientation. Mathematically, the FRET efficiency, E, is described as (Lakowicz, 2006):

$$E= 1/[1+(r/R_0)^6] = 1-I_{DA}/I_D=1-\tau_{DA}/\tau_D$$

Where *r* is the distance between donor and acceptor, while R_0 is the Förster radius that define the distance at which the FRET efficiency is 50%. I_{DA} and τ_{DA} are the donor intensity and fluorescence lifetime in the presence of acceptor, and I_D and τ_D are those in the absence of acceptor.
The rate of FRET efficiency (k) is described as:

$$k= (1/ \tau D)(R_0/r)^6$$

Thus the quenching of the donor by the acceptor is proportional to the FRET efficiency as the fluorescence lifetime is proportional to the fluorescence quantum yield of the fluorophore, meaning that variations in donor brightness are measurable in terms of lifetime (Ebrecht et al., 2014). Thus, the direct transfer of photons between donor and acceptor FPs, produces a decrease in the typical lifetime of the donor only, or it could cause also a rise in the time of the acceptor. The FRET efficiency is calculated comparing the fluorescence lifetime of the donor in presence and in absence of FRET (Becker, 2012). The donor fluorescence is composed by different lifetimes, reflecting the presence of interacting (quenched) and non-interacting (unquenched) molecule. Only the interacting molecules are able to transfer a photon to the acceptor, causing the reduction in the donor lifetime. Usually FRET is described with a double-exponential

model, in which the slow lifetime component comes from the non-interacting, while the fast component comes from the interacting donor molecules; each lifetime is characterized by an amplitude, which mirrors the frequency distribution of each lifetime. From these parameters one can derive: the true FRET efficiency for the interacting proteins and the Förster radius, and the ratio of the relative numbers of interacting and non-interacting donor molecules (Sun et al., 2011; Becker, 2012; Lakowicz, 2006). It is also possible to evaluate the rise time of the acceptor fluorescence in the acceptor channel, allowing the measurement of lifetime only on the molecules involved in FRET. Indeed, the rise feature is a consequence of the delay of acceptor fluorescence following the energy transfer from donor to acceptor (Borst et al., 2008). Hence, FLIM-FRET analysis allows one to distinguish between real FRET (which occurs thanks to the transfer of photons between donor and acceptor) and homo-FRET (which occurs between two donors or two acceptors (Gautier et al., 2001)) and also between intra- and inter-molecular FRET. All this useful information cannot be obtained using most of the intensity-based FRET methods, making the FLIM-FRET analysis a powerful approach to study FRET processes.

3. Optogenetic

Optogenetic is an increasingly used technique to manipulate the depolarization state of polarized cells, used mainly in brain and to a lesser extent also in heart (reviewed on Entcheva, 2013). It represents a powerful tool to modulate ion's concentration inside the cell, both directly and indirectly (*i.e.* as consequence of unbalance of other ions). Optogenetic is a term coined in 2006 by Deisseroth at el., to indicate the combination of optics, genetics and bioengineering used to dissect neural activities. In 2002 Miesenböck's group described the first photoreceptor, called rhodopsin, exploitable to directly stimulate a subset of neurons in *Drosophila*, employing a simply and non-toxic method: the light (Zemelman et al., 2002). This discovery opened a new field: it became possible to use light to read out and even control neuronal activity. Nature chose this powerful technique as "Method of the Year" in 2010, considered the remarkable advantages of using light as an effector. Indeed, light is non-invasive, it allows spatial and temporal precision and it is possible to employ simultaneously multiple wavelengths and reach different tissue locations at the same time. The possibility of genetically encoded photoreceptors, allow their expression in cells and animal models in a very specific way: it is possible to place these genes under the control of specific promoters, finely controlling their spatial and temporal expression pattern. All these features make optogenetics a powerful tool to explore neuronal activities in the whole brain, in specific neuronal cell types or subcellular compartments, but also in order to exploit behavioural experiments and to study neuropathologies exploring local circuits and intralayer.

The first photoreceptor was described in 1949 by Hill and Keynes, but only subsequently, thanks to the work of Deisseroth's group, this became a widely used approach (Sahel and Roska, 2013; Häusser, 2014). 40 years ago, Stoeckenius and Oesterhelt discovered that bacteriorhodopsin acts as a light-gated ion pump (Oesterhelt and Stoeckenius et al., 1971). Six years after the discovery of the microbial opsins, Matsuno-Yagi and

Mukohata discovered halorhodopsin, a light gated ion channel permeable to chloride, identifying the future most important inhibitory tool in optogenetics (Matsuno-Yagi and Mukohata, 1977). Finally, in 2002 Hegemann, Nagel and colleagues discovered the widely used Channelrhodopsin (Nagel et al., 2002).

Briefly, optogenetic tools comprise:

(1) Channelrhodopsin, a cation channel activated by blue light, thus generating an exciting stimulus;

(2) Halorhodopsin, a chloride permeable channel, activated by yellow light, able to generate an inhibitory stimulus (Deisseroth et al., 2011);

(3) OptoXRs, a chimeric rhodopsin-GPCR (G-protein coupled receptor) obtained by substituting the rhodopsin's intracellular loop with a specific adrenergic receptor sequence, allowing the exploration of biochemical signalling causal impact (Airan et al., 2009). Another type of optoXRs is the recently reported bPAC, a bacterial photoactivated adenylyl cyclase (Stierl et al., 2011).

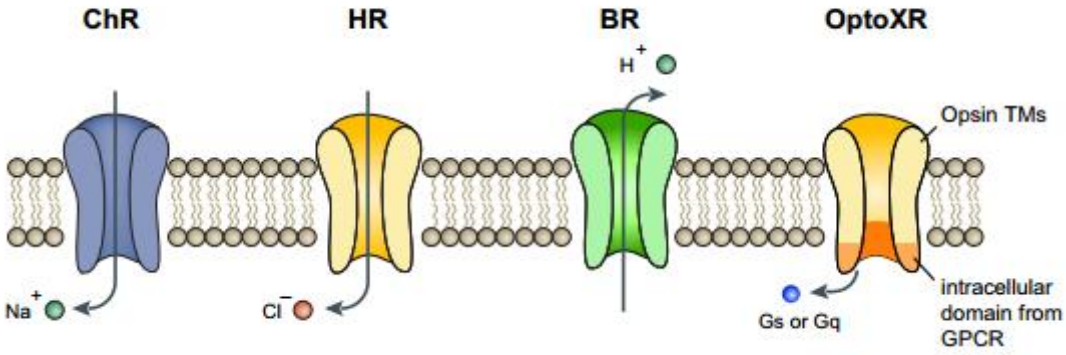

FIGURE 12. Schematic representation of channelrhodopsin-2 (ChR2), halorhodopsin (HR), Bacteriorhodopsin (BR) and OptoXR (Zhang et al., 2012).

Extensive studies about opsins sequence and structure, allow the generation of fast and slow opening kinetic mutants, different light sensitive variants and opsins with bimodal changes in excitability (Deisseroth et al., 2011). Of note, a variant permeable to Ca^{2+} called CatCH has been created: the channel is able to induce Ca^{2+} influx, which in turn activates voltage - Na^{2+} gated channels and causes membrane depolarization (Kleinlogel et al., 2011).

Optogenetics definitely provides a promising tool, however some drawbacks have to be considered when using this tool:

(1) changes in physiologic neural activities are possible, if the spontaneous activity in the target area is not simultaneously recorded during the photoactivation;

(2) the light employed for the photoactivation and the expression level of the channel is heterogeneous, thus the possibility to trigger different degrees of inhibition or activation of the target should be taken into account;

(3) it is possible to induce a non-physiological synchronization of neurons population;

(4) the activation of some axons could lead to uncommon neurotransmitter release;

(5) in the absence of probes able to measure specific parameter (ions concentrations, voltage etc..), the interpretations of optogenetic data may be difficult;
(6) using viral expression systems in animals, it is possible to induce toxicity or adaptation changes in the cellular physiology, since the expression level is not finely controlled (Häusser 2014).

Despite the presented drawbacks, optogenetics impacted on the field of neuroscience since its born, opening new challenges also in other fields of cell biology with the creation of optoXRs. The combination of described optogenetic tools with recently developed fast kinetic GECIs (Chen et al., 2013; Thestrup et al., 2014) or genetically encoded voltage sensors (Hochbaum et al., 2014), is unquestionably pushing forward neuroscience.

3.1 Channelrhodopsin

In general, rhodopsin are photoreceptors composed by opsins, 7 transmembranes-helix proteins. Opsins are linked covalently with the chromophore retinal, a vitamin A-related organic cofactor that undergoes a molecular modification, from cis- to trans- configuration, upon light exposure (Deisseroth et al., 2011).
Two types of opsins have been described:

(1) type I, present in microbes such as archea, eubacteria, fungi and algae. This group is divided in 3 sub-types:
    a. Bacteriorhodopsins (BR), light driven proton pumps (Figure 12);
    b. Halorhodopsins (HR), light-driven chloride pumps with neural inhibitory effect;
    c. Channelrhodopsins (ChRs), light driven ion channels, further subdivided, on the bases of physical properties, in Channelrhodopsin-1 (ChR1) and Channelrhodopsin-2 (ChR2), both derived from *Chlamydomonas reinharditii*. ChR1 has limited usage because of its low conductance at pH 7.
(2) type II, present in animals, including humans, and able to generate ion currents thanks to their coupling with G-proteins (Kato et al., 2012).

ChR2 is a light-gated cation channel derived from algae, which evokes membrane potential depolarization upon photostimulation with blue light in the presence of the chromophore all-trans retinal (Negel et al., 2002). In mammalian neurons, ChR2 generates sufficient photocurrent to depolarize cells, allowing its use to control neuronal activity with very high temporal resolution, thus offering distinct advantages over traditional pharmacological or electrical means of perturbation (Boyden et al., 2005). A number of modified versions of ChR2 exists, differing in channel properties such as channel conductance, ion selectivity, kinetics, desensitization and recovery from desensitized state, light sensitivity, and spectral response (Prakash et al., 2012).
ChR2 is 737 aminoacids protein belonging to the retinylidene photoreceptor family, with the N-terminal functional domain of ~ 300 aminoacids able to generate the photocurrent. It is composed by 7 TM domains, the N-terminal region faces the extracellular space and the C-terminus faces the cytosol. The structure has been recently crystallized. The retinal binding pocket is located on TM7, where the protonate Schiff base

form the site where all-trans retinal binding occurs. The electronegative pore, responsible for the channel permeability, is formed by TM1, 2, 3 and 7, where TM2 seems to be responsible for ion conductance and selectivity (Kato et al., 2012). The wild type ChR2 needs to be stimulated employing high intensity 470 nm-light, and it is characterized by fast opening rate and slow closing kinetic. It properly traffics along the secretory pathway to PM and it shows a mild tendency to aggregate. The main drawback for the use of this channel is the high level of desensitization. To overcome it, different variants have been created by mutagenesis of specific residues in the original sequence (reviewed in Lin, 2010), among them:

(1) H134R: compared to wild type ChR2 shows reduced desensitization, increased light sensitivity, increased photocurrent, but slower opening and closure kinetic.

(2) C128T, C128A, C128S: characterized by increased light sensitivity, but also by reduced kinetic and photocurrent. This represents the first published step-function or bistable opsin, since its closure kinetic can speed up employing orange light. It is used for inducing prolonged sub-threshold depolarization.

(3) D128A: a variant similar to (2), characterized by increased light sensitivity, but also by reduced kinetic and photocurrent.

(4) E123T or ChETA: a variant used for high frequency stimulations, since it shows faster kinetics, but a strong reduction in photocurrent and strongly increased desensitization.

(5) VChR1: a variant of ChR isolated in *Volvox carteri*. A peculiar feature is the red-shift spectrum. However a strong photoactivation is also observed at 400 nm. Moreover, it presents slow kinetics (partially increased introducing E123T mutation), incomplete recovery from the desensitized state and poor membrane trafficking and expression.

(6) ChEF: a chimeric variant obtained by fusing ChR1 and ChR2, characterized by increased steady-state phase response, photocurrent comparable to original ChR2, but also reduction in light sensitivity and partial desensitized state recovery. It shows better trafficking to PM compared to wild type but higher expression levels that could lead to toxicity. A faster kinetic compared to ChEF, but similar to ChR2, was obtained introducing I170V mutation (obtaining a variant called ChIEF). Also in this case the H134R mutation increases the photocurrent.

(7) ChD: another chimeric variant similar to ChEF with improved trafficking and expression.

(8) SSFO (Step stabilized function opsin), has two variants:

   a. mutations C128S/D156A, give rise to prolonged photocurrents far outlasting (around 30 minutes) the initiating pulses of light (Yizhar et al., 2011);

   b. mutations C128A/H134R, is a high-photocurrent SSFO variant, that maintains the prolonged off-kinetic of the previous C128S/D156A variant and opens with a lower amount of light (Prakash et al., 2012).

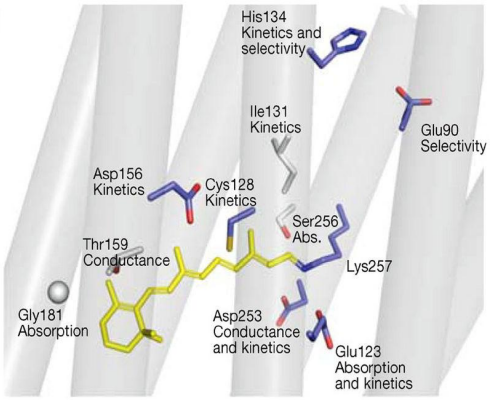

Figure 13. Three-dimensional computer model of ChR2. Mutations of the amino acid residues shown in stick representation are known to substantially influence different ChR properties. Color legend: retinal moiety in yellow, residues conserved in all known ChR in blue (Hegemann and Möglich, 2011).

Aim of the work

Ca^{2+} signalling exerts a plethora of functions in cells, regulating both physiological and pathological conditions. Given its pivotal role, this ion has been widely studied for many years. At the beginning, chemical dyes allowed to monitor Ca^{2+} dynamics only in the cytosol, but thanks to the development of genetically encoded Ca^{2+} indicators (GECIs), the role of subcellular compartments like ER, mitochondria, nucleus and Golgi apparatus in Ca^{2+} handling has been largely unravelled in cells.

Cameleon probes, belonging to GECI's family, have been targeted to different cellular subcompartments and different studies have been carried out *in vitro* and in cell cultures. On the contrary, few examples employing Cameleon probes *in vivo* are available and mainly use the cytosolic version of the probe. Hopefully, the recent development of viral delivery techniques will speed up the application of targeted GECIs *in vivo*, replacing the complicated and expensive transgenesis system.

Cameleon probes have the enormous advantages of being ratiometric Ca^{2+} sensors, a feature fundamental for *in vivo* applications, making the measurement independent of shifts in the focal plane and contraction phenomena that could occur (or be induced) in some tissues during the experiment. However, the low fluorescence quantum yield of donor fluorescent protein CFP and its multi-exponential lifetime prevent some applications, making it difficult to obtain a good signal- to- noise ratio in thick samples and complicating the lifetime analysis. Thus, in the first part of my PhD work, I engineered existing Cameleon probes by substituting CFP with a more brilliant, more photostable, and with a single-exponential lifetime donor, called mCerulean3. This upgrade was performed in cytosolic and mitochondrial Cameleon D3 variants. Further modifications of these probes have been done in order to maximize their biophysical performance, to create an optimized tool for *in vivo* Ca^{2+} measurement.

Another powerful tool has been developed in the last years exploiting Channelrhodopsins, and a plethora of brain cells and tissues features have been explored thanks to the manipulation of neurons membrane potential. In order to expand the high potential of this tool, in collaboration with Prof. Sekler's group (Ben-Gurion University-Israel), we created a new mitochondria targeted Channelrhodopsin. The new tool generated allows to obtain a spatial, temporal and reversible control of mitochondrial membrane potential by simply employing light.

Thus, the first part of my work is aimed at creating two new tools to study mitochondrial physiology, with particular attention to mitochondrial Ca^{2+} handling *in vivo*.

Results

1. Generation and characterization of the new cytosolic and mitochondrial Cameleon probes

1.1 The new generated D3mCerulean3 is a functional and brighter probe compared to the original D3cpV

Cameleon probes have the enormous advantage of being ratiometric Ca^{2+} sensors, a great benefit for *in vivo* applications, making the measurement independent of shifts in the focal plane and contraction phenomena that could occur (or be induced) in tissues during the experiment. The low fluorescence quantum yield of donor fluorescent protein CFP and its multi-exponential lifetime prevent some applications, making it difficult to obtain a good signal-to-noise ratio in thick samples and complicating the lifetime analysis. In 2011 by site-directed mutagenesis, Rizzo's group created a new variant of CFP, called mCerulean3. Basically, the optimization of residues in strands 7 and 8 of the β-barrel combined with T65S mutation in the CFP chromophore improved the quantum yield to 0.87, making this new FP brighter and reducing the fluorescence photoswitching behaviour compared to other CFP variants both *in vitro* and *in situ* in living cells. Another interesting feature of mCerulean3 is the single exponential decay, making mCerulean3 a much better choice for FLIM experiments. Other studies reported also promising results using mCerulean3 as a FRET donor, coupled with mVenus as acceptor (Markwardt et al., 2011). Given these interesting biophysical features of mCerluan3 and considering the described drawbacks of CFP as a FRET donor, we substituted CFP with mCerluean3 in the cytosolic Cameleon probe D3cpV. Figure 14A shows the cloning strategy used to insert mCeruean3 in the place of CFP in D3cpV inserted in the mammalian expression vector pCDNA3 (see materials and methods for details). This construct was used to transfect HeLa cells and the cytosolic localization of the new D3mCerulen3 was confirmed using confocal microscopy. The performance of the new probe was compared to the original one, assessing their ability to detect [Ca^{2+}] changes. HeLa cells expressing D3cpv or D3mCerulean3 were perfused with extracellular-like medium and the cytosolic Ca^{2+} rise was induced employing the IP_3-generating stimulus Histamine. The ionophore Ionomycin was used perfusing extracellular-like medium with 600 μM EGTA, and then perfusing extracellular-like medium with 5 mM Ca^{2+}, a protocol that allows to obtain the minimum and maximum FRET, respectively. The new probe shows similar performance compared to the original one, since both are able to detect the cytosolic Ca^{2+} rise induced by Histamine.

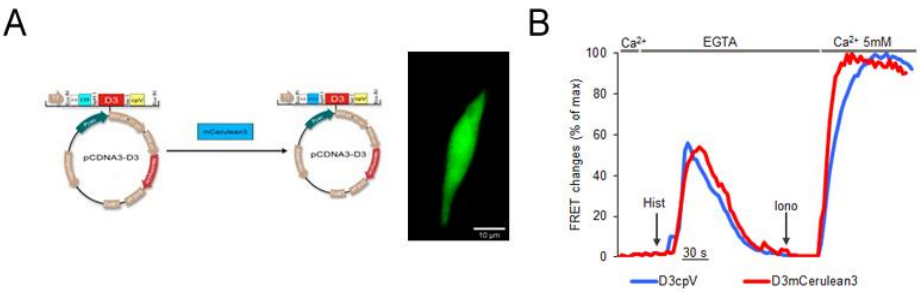

FIGURE 14. The new generated D3mCerulean3 is a functional and brighter probe compared to the original D3cpV. **(A)** *Left:* Schematic representation of the cloning strategy used to substitute CFP with mCerulean3 in D3cpV Cameleon probes. *Right*: Confocal image of the cytosolic D3mCerulean3. **(B)** HeLa cells transiently transfected with D3cpV or D3mCerluean3, were treated with 100 µM Histamine (Hist) and perfused with 600 µM EGTA and then 5mM $CaCl_2$ in presence of 1 µM Ionomycin (Iono), where indicated. Representative kinetics of cytosolic Ca^{2+} uptake in HeLa cells expressing D3cpV (blue) and D3mCerluean3 (red). Data are plotted as FRET changes % of maximum.

1.2 Fluorescence improvement and mitochondria targeted D3cpV generation

One of the main features of mCerulean3 is the brightness improvement. A critical point for *in vivo* application of Ca^{2+} probes, is the signal-to-noise ratio (SNR), which determines the ability of an indicator to properly report Ca^{2+} transients. The SNR depends on the brightness of each FP presents in the probe: the higher is the brightness, the higher is SNR. Moreover, higher brightness provides the possibility of illuminating the sample with a lower amount of light, causing a reduction in phototoxicity. To check whether the brightness improvement of mCerulean3 was maintained in the new probe, mCerulean3 and CFP mean intensity has been measured in D3cpv or D3mCerulean3 expressed in HeLa cells. The fluorescence of cpV, present in both the new generated and the original probe, was chosen to normalize for the protein expression level (see Materials and methods). A significant fluorescence improvement around 50% ($p<0.01$) was obtained with the substitution of CFP (N=27) with mCerulean3 (N=53) in the D3 cytosolic Cameleon variant (Figure 15A).

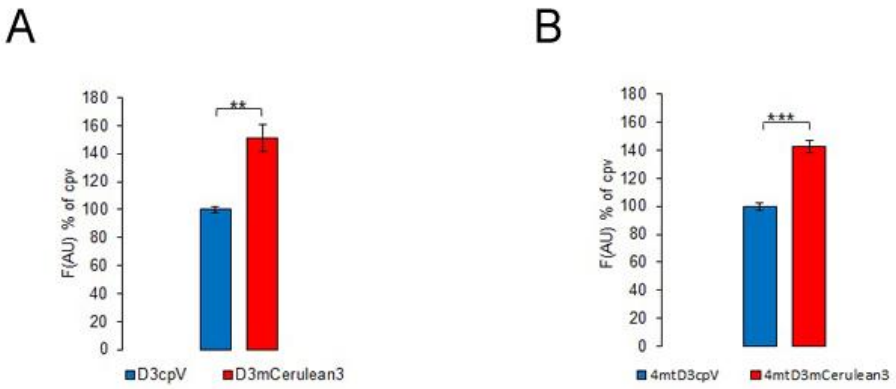

FIGURE 15. Fluorescence improvement in the new generated Cameleon Probes. The histogram represents the mean±SEM of CFP (blue) and mCerulean3 (red) fluorescence, normalize to cpV fluorescence in HeLa cells expressing cytosolic Cameleon probes **(A)** or mitochondrial Cameleon probes **(B)**. N (number of cells) ≥ 27 for each conditions. (* $p<0.05$; ** $p<0.01$; *** $p<0.0001$).

The promising result obtained in terms of brightness was exploited in the perspective of improving available methods to explore mitochondrial Ca^{2+} dynamics *in vivo*, thus also mitochondrial probe has been modified. Figure 16A shows the cloning strategy used to insert mCeruean3 in the place of CFP in 4mtD3cpV in the mammalian expression vector pCDNA3 (see materials and methods for details). At this stage of the work, we decided to optimize also mitochondria localization, acting on the targeting sequence. Indeed, 24 h after transfection of the original D3cpv probe, a significant mislocalization to the cytosol was observed.

Generally the targeting sequence is composed by the first 25 aminoacids of N-terminal signal sequences from subunit VIII of human Cytochrome C Oxidase, but longer variants has been used in other constructs. To improve the targeting to mitochondrial, each of the four targeting sequences present on 4mtD3cpv was elongated adding 5 aminoacids (obtaining sequences of 33 aminoacids) and a Kozak consensus sequence was added before nucleotides coding the starting codon. The probe obtained, named 4mtD3mCerulen3, was expressed in HeLa cells and imaged by confocal microscopy (Figure 16B). Proper localization was confirmed by immunostaining mitochondria using the OMM marker anti-TOM20. The new targeting sequence allows a proper mitochondrial localization in 87.5±9 % of cells (mean±SEM, N=27 number of cells analyzed in six different fields), compared to 38.6±11% (mean±SEM, N=36 number of cells analyzed in six different fields) obtained with the original 4mtD3cpV ($p<0.01$) (Figure 16C).

A critical feature of FP is the protonation state of the chromophore. The protonation state of FP, in turn, is influenced by environmental pH. Thus, since matrix pH is about 8, while the cytosolic is about 7, the brightness improvement of mCerulean3 was tested also in mitochondria targeted Cameleon probes. A significant improvement in fluorescence (around 42.5%, $p<0.0001$) was obtained with the substitution of CFP (N=46) with mCerulean3 (N=39) also in the mitochondria targeted variant of Cameleon (Figure 15B).

The performance of the new probe was compared to the original one, by assessing their ability to detect $[Ca^{2+}]$ changes in response to a physiological stimulus. HeLa cells expressing 4mtD3cpv or 4mtD3mCerulean3 were perfused with extracellular-like medium and the cytosolic Ca^{2+} rise was induced employing the IP_3-generating stimulus Histamine. After Digitonin permeabilization, cells have been then perfused with intracellular-like medium containing 600 μM EGTA, to obtain a condition of absence of Ca^{2+}, and finally with the same medium containing 5 mM Ca^{2+}, to obtain the minimum and maximum FRET, respectively. The new probe was able to detect the Histamine induced mitochondrial Ca^{2+} rise with an efficiency similar to the original one (Figure 16 D).

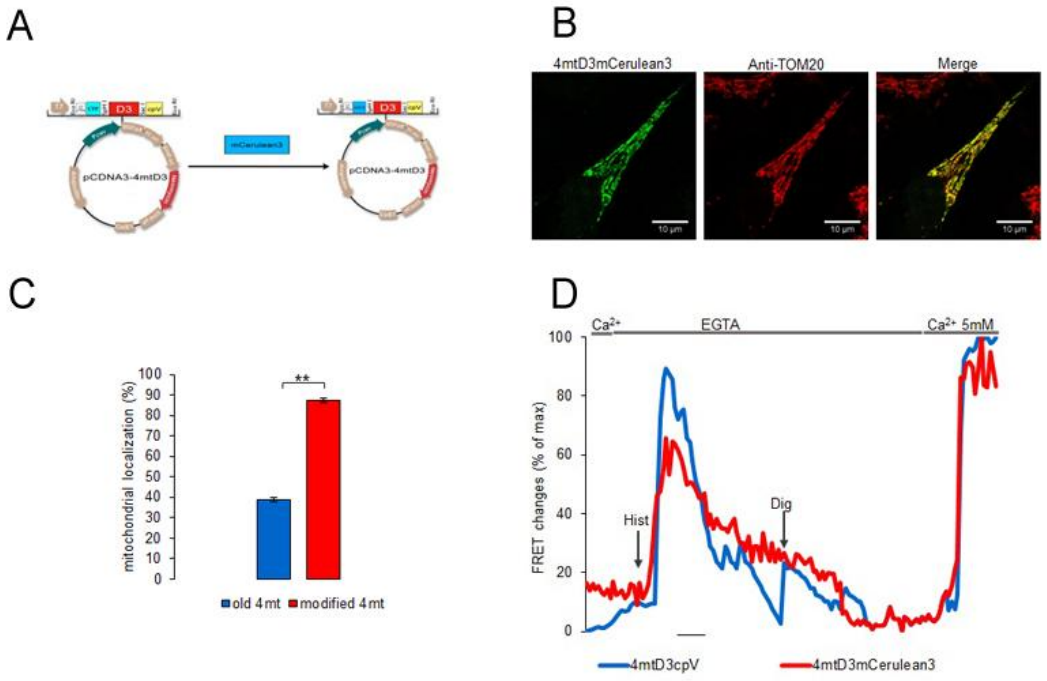

FIGURE 16. The new mitochondria targeted Cameleon probe is improved in localization and is a functional probe. **(A)** Schematic representation of the cloning strategy used to substitute CFP with mCerulean3 in 4mtD3cpV Cameleon probes. **(B)** Confocal images of 4mtD3mCeruean3. The mitochondrial localization of the new probe was checked for the co-localization with a mitochondrial marker, TOM20. Yellow colour indicates co-localization of the mitochondrial maker and 4mtD3mCeruelan3. **(C)** The histogram represents the mean ±SEM of the number of cells showing a proper mitochondrial localization normalized to the number of cells for each field of N ≥ 27 cells for each conditions. **(D)** HeLa cells transiently transfected with 4mtD3cpV or 4mtD3mCerluean3, were treated with 100 µM Histamine (Hist) and perfused with 600 µM EGTA and then 5mM $CaCl_2$ after permeabilization upon 100 µM Digitonin (Dig) treatment, where indicated. Representative kinetics of mitochondrial Ca^{2+} uptake in HeLa cells expressing the original 4mtD3cpV (blue) and 4mtD3mCerluean3 (red). Data are plotted as FRET % of maximum. (* $p<0.05$; ** $p<0.01$; *** $p<0.0001$).

1.3 Dynamic Range

One of the most important parameters that must be evaluated both in the creation/modification of a Ca^{2+} indicator and in choosing the proper Ca^{2+} probe for an experiment, is the dynamic range (DR).

This parameter is differently calculated depending on the type of GECI. In single fluorophore GECIs, the DR indicates how many times brighter is the Ca^{2+}-bound state compared to the Ca^{2+}-free state, and thus it is expressed as

$$DR = I_{max}/I_{min}$$

Where I_{max} is the maximal fluorescence intensity obtained under Ca^{2+} saturated condition, while I_{min} is the fluorescence intensity in the absence of Ca^{2+}.

Similarly, in ratiometric Ca^{2+} GECIs, the DR expresses how many times the maximal FRET ratio is larger than the minimal FRET ratio and thus is calculated as

$DR=R_{max}/R_{min}$

Where R_{max} is the ratio (acceptor/donor) obtained under Ca^{2+} saturated condition, while R_{min} is the ratio in the absence of Ca^{2+} (reviewed in Koldenkova and Nagai, 2013).

This parameter depends on different conditions: in particular, in FRET Ca^{2+} probes, it could be modified by different factors, such as the alteration in the efficiency of photons transfer between donor and acceptor FPs.

To test whether the DR was changed by the substitution of CFP with Cerluean3 in the cytosolic probes, HeLa cells were transfected with D3cpV and D3mCerulean3. Since permeabilization causes the release of the cytosolic probe into the medium, we used the Ca^{2+} ionophore Ionomycin to impose maximal and minimal Ca^{2+} levels in the intact cells. This approach allows a rough estimation of DR, and the data obtained must be confirmed *in vitro*.

DR calculated for D3cpV is 2.53±0.08 (mean±SEM, N=23 number of cells analyzed), while for D3mCerulean3 is 2.11±0.07 (mean±SEM, N=18); the donor substitution thus causes a significant reduction (about 20%, $p<0.01$) of DR (Figure 17B). A similar negative impact has also been recently reported in Twitch sensor, where CFP was substituted with mCerulaen3 or mTuruaise2 (Thestrup et al., 2014).

Different approaches can be employed to improve the DR. One is the acceptor substitution (Nagai et al., 2004). We tested the substitution of cpV with citrin or YPet (two YFP variants), but none of them was able to recover the DR (data not shown).

Another approach reported in literature to modify the DR and the sensitivity of the probes to Ca^{2+} is the elongation of the linker between the two Ca^{2+} responsive elements (Horikawa et al., 2010). Indeed, an interesting feature of Cameleons is the presence of two Ca^{2+} responsive elements, CaM and M13, separated by a short glycines linker. We tried to improve DR in mCerulean3 by adding glycine-based linkers of different length between CaM and M13. The addition of 16 glycines between CaM and M13 in D3mCerulean3 (hereafter called D3mCerulean3+16), allowed not only the recovery but also an improvement of DR (Figure 17B). Indeed D3mCerulean3+16 has a DR of about 3.06±0.07 (mean±SEM, N= 20 number of cells analyzed), significantly higher (around 20%, $p<0.0001$) compared to 2.53 of D3cpV. Again, the performance of the last generated variant has been tested in HeLa cells expressing D3mCerulean3+16, using the same protocol described above (Figure 17C).

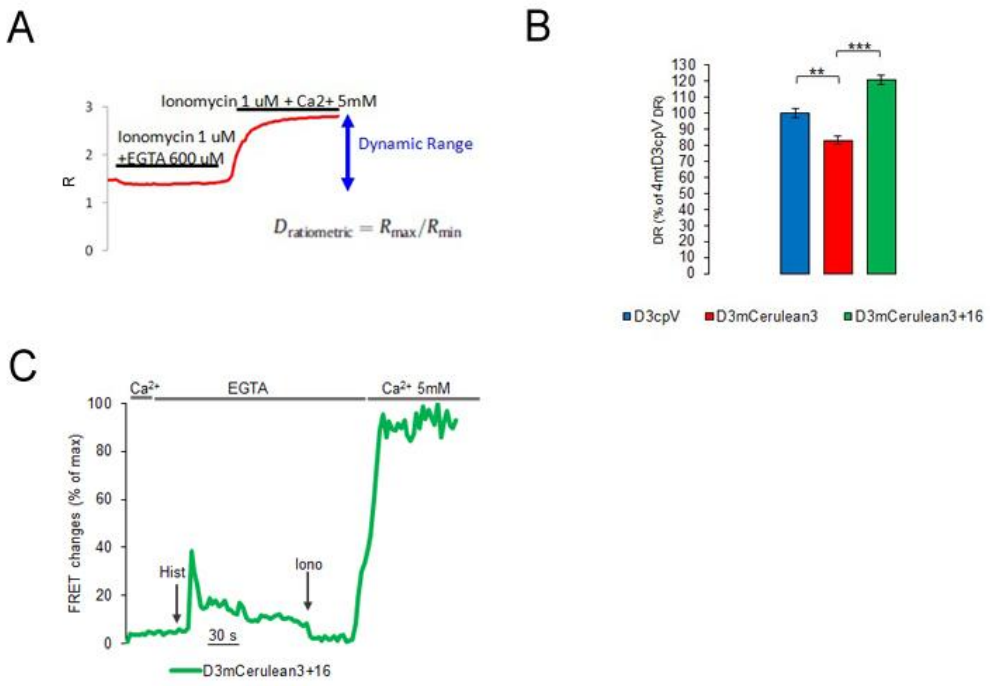

FIGURE 17. Dynamic range evaluation in cytosolic Cameleon probes. **(A)** Protocol for DR evaluation in cytosolic Cameleon probe. HeLa cells expressing the cytosolic probe has been treated with 1 µM Ionomycin (Iono) and perfused with extracellular-like medium containing 600 µM EGTA and then 5mM $CaCl_2$. Data are presented as ratio (R, acceptor/donor). **(B)** The histogram shows the DR mean ±SEM (normalized to control) of N≥18 cells for each conditions. D3cpV is showed in blue, D3mCerulean3 in red and D3mCeruealn3+16 in green. **(C)** Representative kinetics of cytosolic Ca^{2+} uptake in HeLa cells expressing D3mCerluean3+16 employing the same protocol of Figure 14. Data are plotted as FRET % of maximum. (* $p<0.05$; ** $p<0.01$; *** $p<0.0001$).

Since mitochondrial environment differs from that of the cytosol both in term of ions concentration and pH (parameters that can modify Ca^{2+} probes behavior), the DR has been tested also in the mitochondria targeted version 4mtD3mCerulean3. In this case, cells permeabilization ensures the possibility to get a real minimum and maximal FRET. Thus HeLa cells expressing mitochondrial probes were permeabilized and then perfused with intracellular-like medium containing 600 µM EGTA and then with 5 mM Ca^{2+}. Again, the substitution of CFP with mCerulean3 induced a decrease of about 20 % in the DR ($p<0.0001$): 4mtD3cpV displays a DR of 2.44±0.03 (N=53), while 4mtD3mCerulean3 has a DR of 1.94±0.03 (N=24). Employing the same strategy described above for the cytosolic probe, we generated a 4mtD3mCerulean3 version with the addition of 16 glycines in the spacer (hereafter called 4mD3mCerulean3+16). The extension of the linker allowed to recover the probe's DR to 2.37±0.03 (n=38) ($p>0.1$) (Figure 18B). Also in this case the performance of the generated variant has been tested in the intact cells expressing 4mtD3mCerulean3+16 (see the protocol above) (figure 18C).

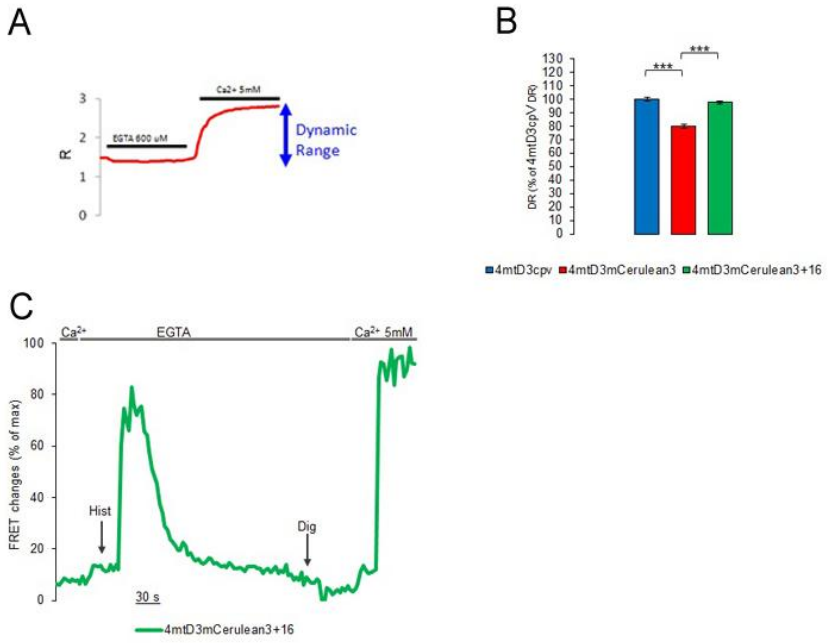

FIGURE 18. Dynamic range evaluation in mitochondrial Cameleon probes. **(A)** Protocol for DR evaluation in mitochondrial Cameleon probe. HeLa cells expressing the mitochondrial probe has been permeabilized with 100 µM Digitonin (Dig) and perfused with intracellular-like medium containing 600 µM EGTA and then 5mM $CaCl_2$. Data are presented as ratio (R) **(B)** The histogram shows the DR mean ±SEM (normalized to control) of N≥24 cells for each conditions. D3cpV is showed in blue, D3mCerulean3 in red and D3mCeruealn3+16 in green. **(C)** Representative kinetics of cytosolic Ca^{2+} uptake in HeLa cells expressing 4mtD3mCerluean3+16 employing the same protocol of Figure 14. Data are plotted as FRET % of maximum. (* $p<0.05$; ** $p<0.01$; *** $p<0.0001$).

1.4 Photostability of the new probes

As mentioned above, it has been reported that mCerulean3 shows an improvement in photostability compared to CFP and its variants. The primary consequence of higher photostability is a smaller decrease in brightness during FP excitation; this makes photostability an important limiting factor in experiments requiring prolonged imaging of cells. To check whether mCerulean3 substitution increased D3 Cameleon photostability, HeLa cells, expressing the original and modified Cameleon probes, were imaged with the same illumination settings (fixed excitation intensity, and exposure time) and acquisition (1 image per second for 20 minutes) under conditions of maximal, minimal and basal FRET. The photostability is quantified indirectly by monitoring the decrease in the ratio (R) (calculated as the difference between R at the beginning of the experiments and R at the end of the experiments). The decrease in the ratio (hereafter simply called ratio bleaching) is the result of multiple factors, *e. g.* single fluorophore bleaching and donor de-quenching. The latter takes place when the donor paradoxically emits more photons (instead of less, as expected in case of bleaching), since the number of acceptors able to receive photons is decreased as a result of their bleaching. Moreover, the linker introduced between CaM and M13 improves the molecule mobility, possibly inducing molecular instability that in turn could affect the efficiency of photon transfers between donor and acceptor, and thus decreases the photostability of the probe. In basal FRET condition, D3cpV

shows a bleaching in ratio of 20±1.9% (mean±SEM, N=24), D3mCerulean3 of 15.4±1.7% (N=32) and D3mCerulean3+16 of 7.5±0.9% (N=23). Thus, in basal FRET condition the D3mCerulean3+16 shows stronger photostability, since it presents a reduction in ratio bleaching over time (around 64% less, $p<0.0001$) compared to D3cpV (Figure 19A). Similarly, in minimal FRET condition, D3cpV shows a bleaching in ratio of 14.7±2.3% (N=17), D3mCerulean3 of 9.8±1.1% (N=29) and D3mCerulean3+16 of 7.4±0.9% (mean±SEM, N=23) (Figure 19B). Again, D3mCerulean3+16 show a significant reduction in ratio bleaching compared to D3cpV (around 50%, $p<0.01$). Also in maximal FRET condition the ratio bleaching of D3mCerulean3+16 is diminished by about 30% compared to the original Cameleon ($p<0.01$). In the last condition, in fact, D3cpV shows a decreased in ratio of 28.3±1.6% (N=22), D3mCerulean3 of 21.8±2% (N=21) and D3mCerulean3+16 of 20±1.19% (N=18) (Figure 19C).

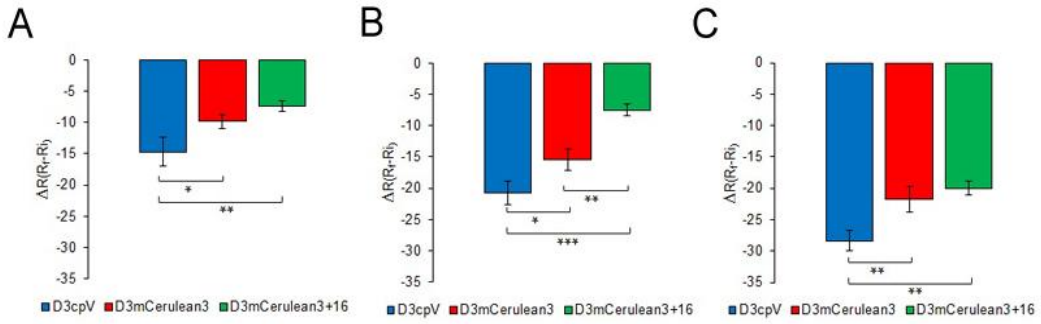

FIGURE 19. The histogram shows the ratio decreased measured by illuminating the sample each seconds for 20 min in HeLa expressing D3cpV (blue), D3mCerulean3 (red) and D3mCerulean3+16 (green) in minimal FRET condition **(A);** basal FRET condition **(B);** in maximal FRET condition **(C)**. Data are represented as mean ±SEM of N≥17 cells for each conditions. (* $p<0.05$; ** $p<0.01$; *** $p<0.0001$).

Also in the case of the mitochondrial targeted Cameleon probes, the photostability was checked in the three different FRET conditions. In basal FRET condition, 4mtD3cpV shows a ratio bleaching of 11.4±0.9% (N=20), 4mtD3mCerulean3 of 7.7±0.9% (N=20) and 4mtD3mCerulean3+16 of 5±0.49% (N=18, -55% compared to 4mtD3cpv, $p<0.0001$) (Figure 20A). Similarly, in minimal FRET condition, D3cpV shows a ratio bleaching of 14.5±1.4% (N=39), 4mtD3mCerulean3 of 8.1±1.15% (N=19) and 4mtD3mCerulean3+16 of 2.8±0.5% (N=15,-80%, $p<0.0001$) (Figure 20B). Similar results were obtained under maximal FRET conditions: 4mtD3cpV shows a ratio bleaching of 33.7±1.26% (N=23), 4mtD3mCerulean3 of 22.3±1.2% (N=30) and 4mtD3mCerulean3+16 of 18.7±0.8% (N=26, -45% $p<0.0001$) (Figure 20C).

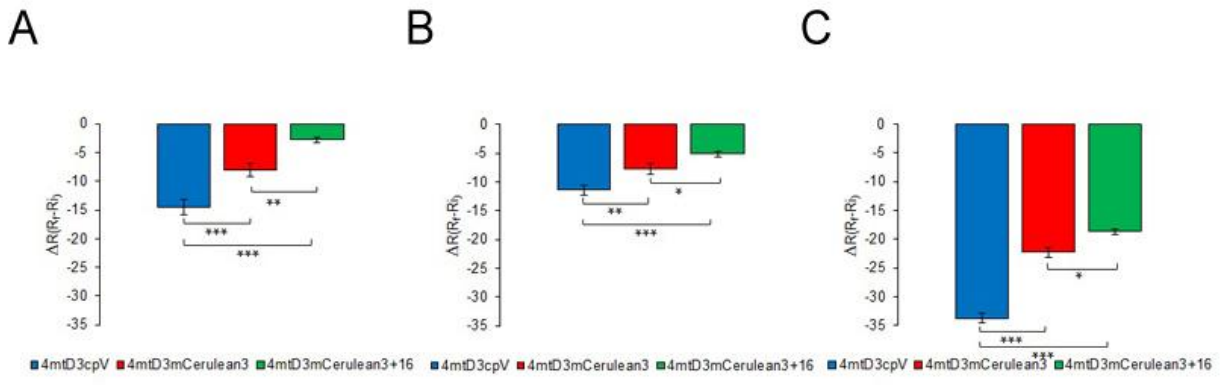

FIGURE 20. The histogram show the ratio decreased measured by illuminating the sample each seconds for 20 min in HeLa expressing 4mtD3cpV (blue), 4mtD3mCerulean3 (red) and 4mtD3mCerulean3+16 (green) in minimal FRET condition **(A)**; basal FRET condition **(B);** in maximal FRET condition **(C)**. Data are represented as mean ±SEM of N≥ 15 cells for each conditions.
(* $p<0.05$; ** $p<0.01$; *** $p<0.0001$).

1.5 pH sensitivity

The proton gradient (ΔpH) across the inner membrane is a key feature of mitochondria, regulating both uptake and efflux of ions and metabolites. Generally, matrix pH ranges from 7 to 9 (reviewed in Poburko and Demaurex, 2012). Variations in pH can affect the affinity of GECIs for Ca^{2+} (reviewed in Koldenkova and Nagai, 2013). Moreover, since each FPs present a specific pKa, the substitution of CFP with mCerulean3 could potentially change the probes pH sensitivity. To check whether mitochondria targeted Cameleon probes are sensitive to pH in the range of pH that mitochondrial could experience, a fixed pH has been imposed within the mitochondrial matrix (protocol described in materials and methods). Figure 21B show the average of the R% absolute value (where R% means ratio normalized to ratio at minimal and maximal FRET) variation at pH 7, 7.5, 8.5, 9 in HeLa cells expressing the three variants of 4mtD3 Cameleon probes. At pH 7, no significant changes were observed (4mtD3cpV, 4±0.2% N=12); 4mtD3mCerulean3, 3.7±0.5% (N=8); 4mtD3mCerulean3+16, 3.1±0.5% (N=11)). The same was obtained at pH 7.5 (4mtD3cpV, 3.9±0.7% (N=14); 4mtD3mCerulean3, 2.30±0.9% (N=3); 4mtD3mCerulean3+16, 1±0.3% (N=12)), at pH 8.5 (4mtD3cpV, 1.95±0.4% (N=24); 4mtD3mCerulean3, 2.1±0.3% (N=11); 4mtD3mCerulean3+16, 0.5±0.1% (N=19)) and at pH 9 (4mtD3cpV, 4.5±0.7% (N=10); 4mtD3mCerulean3, 2.30±0.9% (N=5); 4mtD3mCerulean3+16, 1.4±0.3% (N=14)). All the variants thus appear largely insensitive to pH variations in the range of interest tested (the observed changes in FRET % of maximum are always lower than 5%). Interestingly, 4mtD3mCerulean3+16 proved to be the most stable of the variants assessed. The experiment cannot be carried out for D3 cytosolic Cameleon variants, since permeabilizing the cells would cause the cytosolic probes to diffuse outside the cell.

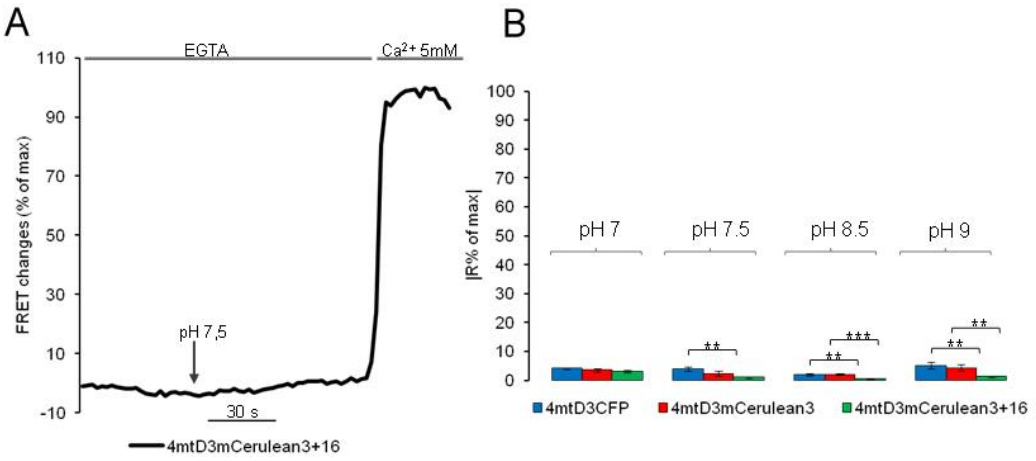

FIGURE 21. Mitochondrial Cameleon probes are insensitive to pH from 7 to 9. **(A)** Representative trace of pH sensitivity experiments. Representative kinetics of the FRET % of maximum in permeabilized HeLa cells transiently transfected with 4mtD3mCerulean3+16. All the experiments are carried out in the presence of 5 µM FCCP and 600 µM EGTA, except when the maximal FRET is induced by adding 5mM Ca_2Cl as indicated by top bars. Where indicated the intracellular medium at pH 8 is substitute with pH 7.5. **(B)** The histogram show the R% absolute values mean±SEM FRET measured in HeLa cells expressing 4mtD3cpV (blue), 4mtD3mCerulean3 (red) and 4mtD3mCerulean3+16 (green) at different pH of N≥3 cells for each conditions. (* $p<0.05$; ** $p<0.01$; *** $p<0.0001$).

1.6 Ca^{2+} affinity

The evaluation of the Ca^{2+} affinity (K_d), provides an idea of the approximate range of Ca^{2+} concentrations in which a GECIs can effectively function as a [Ca^{2+}] indicator (Koldenkova and Nagai, 2013). Moreover, it allows quantitative Ca^{2+} measurement, since it permits to convert values of R in absolute [Ca^{2+}]. *In situ* calibration of the original and new mitochondrial probes was carried out performing passive Ca^{2+} loading experiments. Calibration experiments were carried out in cells permeabilized with Digitonin using an intracellular-like medium supplemented with the uncoupler FCCP and in the absence of energy sources. Under these conditions the [Ca^{2+}] within the matrix should equilibrate with that in the perfusing medium (see materials and methods for details) (Figure 22A). The experimentally calculated K_d are: K_{d1} 0.06 µM and K_{d2} 10.84 µM in 4mtD3cpV; K_{d1} 0.03 µM and K_{d2} 10.7 µM in 4mtD3mCerulean3+16 (Figure 22B-C). The fitting data and the Hill coefficient (n) calculated are summarized in Table 1 (see below).

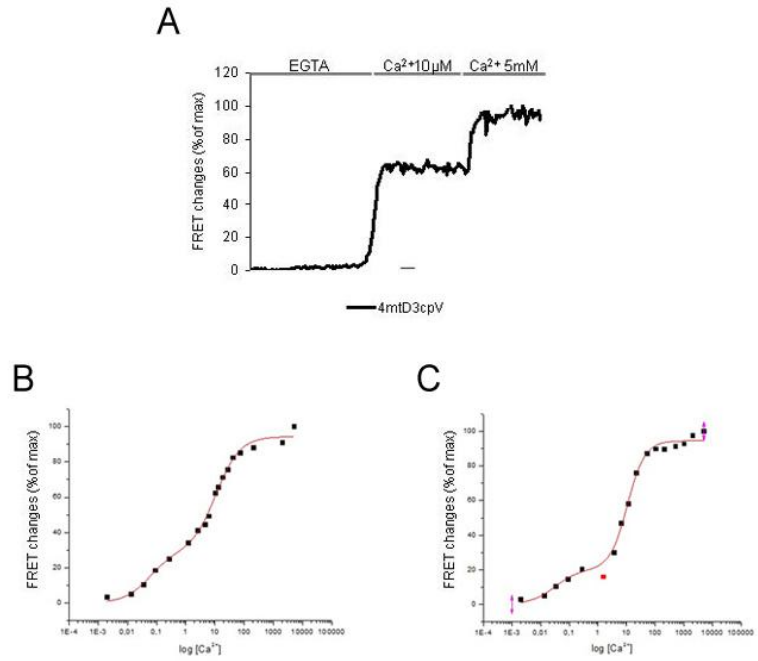

FIGURE 22. (A) Titration protocol. Representative kinetics of FRET % of maximum in permeabilized HeLa cells transiently expressing the 4mtD3mCerulean3+16. Where indicated, Digitonin-permeabilized cells were bathed with an intracellular-like medium without energy source and containing different [Ca^{2+}], in the representative trace is 10 µM $CaCl_2$; 5 mM $CaCl_2$ was finally added to reach the maximum value. *In situ* calcium titration curves of 4mtD3cpV **(B)**, 4mtD3mCerulean3+16 **(C)**, along with corresponding fits of the data. Mean ± SEM. Of N ≥ 3 cells for each [Ca^{2+}].

2. *In vitro* characterization of new Cameleon probes

The data shown above originate from *in situ* evaluations. However, the physiochemical properties of GECIs need to be determined also *in vitro* to allow the comparison of different indicators. Furthermore, the cytosolic probes are difficult to characterize *in situ*, because of the impossibility of permeabilizing cells.

We first verified that the COX VIII mitochondrial targeting sequence (4mt) is properly cleaved after import of the protein in the mitochondrial matrix (Chacinska et al., 2009). Proteins extracted from HeLa cells expressing cytosolic and mitochondrial probes were analysed by Western blot. As expected, if the targeting sequence is properly cleaved, cytosolic and mitochondria targeted probes display the same MW (Figure 23A). Accordingly, only D3cpV and D3mCeruelan3+16 (without the mitochondrial targeting sequence) cDNA was cloned in a bacterial expression vector carrying a Histidine tag fused to their N-terminus. The tag is necessary for the gel agarose binding during the protein purification. These constructs were expressed in *E.coli* and purified with HIS-Select Nickel Affinity Gel (Sigma Aldrich). After proteins purification, the presence of contaminants was verified by SDS-page stained with Comassie Blue (Figure 23B).

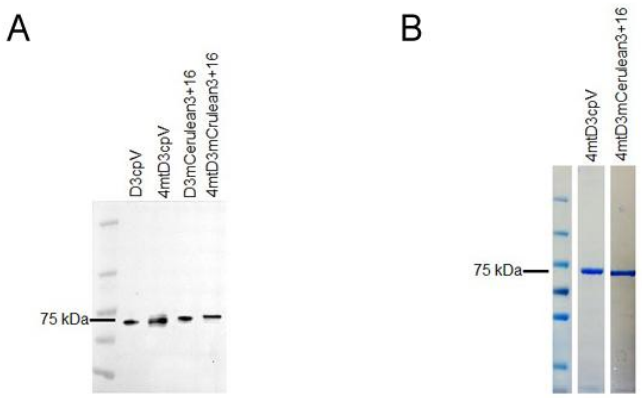

FIGURE 23. (A) HeLa expressing D3cpV, 4mtD3cpV, D3mCerulean3+16 and 4mtD3mCerulean3+16. 24 h after transfection, total proteins were extracted and subjected to Western blot analysis with antibodies anti-GFP. **(B)** Purified D3cpV and D3mCeruelan3 proteins were resolved by SDS-page and stained with Comassie Blue.

The protein bands appeared quite pure with minimal contaminants: The purified proteins was resuspended in intracellular-like medium (see materials and methods) at pH 7, to mimic cytosolic environment, or at pH 8, to mimic the mitochondrial environment and the DR and Ca^{2+} K_d were evaluated. An EnVision® Multilabel Reader PerkinElmer was used to record the fluorescence at different [Ca^{2+}] concentrations, after checking the proper protein concentration required to get sufficient SNR and to avoid protein precipitation. Preliminary data are summarized in Table 1. Of note, just few [Ca^{2+}] concentrations have been tested, hence the evaluation of Ca^{2+} affinity *in vitro* results in a single K_d. However further experiments are required to clarify the discrepancy between *in vitro* and *in situ* data.

	in vitro			*in situ*				
	K_d (µM)	n_1	DR	K_{d1} (µM)	n_1	K_{d2} (µM)	n_2	DR
D3cpV pH7	10,3	0,37±0,03	3,93±0,04	nd	nd	nd	nd	2,53±0,08
D3mCerulean3+16 pH7	5,11	0,42±0,04	3,11±0,12	nd	nd	nd	nd	3,06±0,07
4mD3cpV pH8	6,27	0,35±0,08	2,7±0,04	0,058±0,03	0,97±0,37	10,84±2,35	1,0±0,166	2,44±0,03
4mtD3mCerulean3+16 pH8	5,28	0,41±0,56	2,42±0,05	0,03±0,02	1,02±0,65	10,7±156	1,43±0,2	2,37±0,03

TABLE 1. *In vitro* and *in situ* properties of cytosolic and Cameleon probes. Kd-dissociation constant, n-Hill constant, nd, not-determined. Data are presented as mean ± SEM of N≥2 independent experiments

3. FLIM

As mentioned in the introduction, FLIM measurements, compared to intensity-based images, have the advantages of being independent of fluorophore concentration, excitation intensity fluctuation, sample thickness, or photobleaching. Indeed, the lifetime (τ) is independent of initial intensity and of the emitted light intensity. Moreover FLIM-FRET analysis is a unique technique that allows to distinguish between homo-FRET, intra- and inter-molecular FRET. These experiments are performed in collaboration with Prof. Bozio's group (Department of Chemical science, University of Padua).

Prior to the FLIM analysis of Cameleon sensors, time-resolved fluorescence analysis has been performed in cells expressing donors or acceptor alone. This will be useful for the calibration of further measurements on

Cameleon probes, since in FLIM-FRET analysis is necessary to fix the donor unquenched lifetime in order to get a reliable measure. Thus, HeLa cells transfected with cytosolic or mitochondrial Cameleon variants have been analyzed and data are summarized in Table 2. The last column of the table reports the amplitude-weighted lifetime calculated as:

$$\tau_{AMP} = \sum_{i=1}^{n} A_i \tau_i \Big/ \sum_{i=1}^{n} A_i$$

where A_i is the pre-exponential factor of the i-th component with fluorescence lifetime τ_i. Basically, this value indicates a weighted average of all the lifetimes associated to the fluorophore, simplifying the further analysis. Indeed, since the amplitude-weighted lifetime is proportional to the steady-state intensity, it is useful also for quantitative analysis of FRET process.

Sample	τ_1 (ns)	τ_2 (ns)	τ_{AMP} (ns)
mCerulean3	3,83 ± 0,06		
4mtmCerulean3	3,53 ± 0,04		
CFP	3,02 ± 0,01 (63%)	0,95 ± 0,03 (37%)	2,24 ± 0,01
4mtCFP	3,21 ± 0,09 (67%)	1,02 ± 0,25 (33%)	2,49 ± 0,05
cpV	3,10 ± 0,04 (73%)	1,08 ± 0,10 (27%)	2,55 ± 0,06
4mtcpV	2,94 ± 0,05 (45%)	0,74 ± 0,07 (55%)	1,7 ± 0,3

TABLE 2. Average lifetimes (τ) obtained from the decay fitting of cells expressing the only donor or acceptor of Cameleon probes located in the cytosol or in mitochondria. Values in parenthesis are the relative amplitudes of each decay term. Data are presented as mean ± SEM of N≥5 cells

The following figure reports the lifetime histograms of mCerulean3 and CFP proteins localized in the cytosol or in mitochondria; the insets are the FLIM images, showing the intensity-modulated average lifetime distribution on the cell excluding the nucleus.

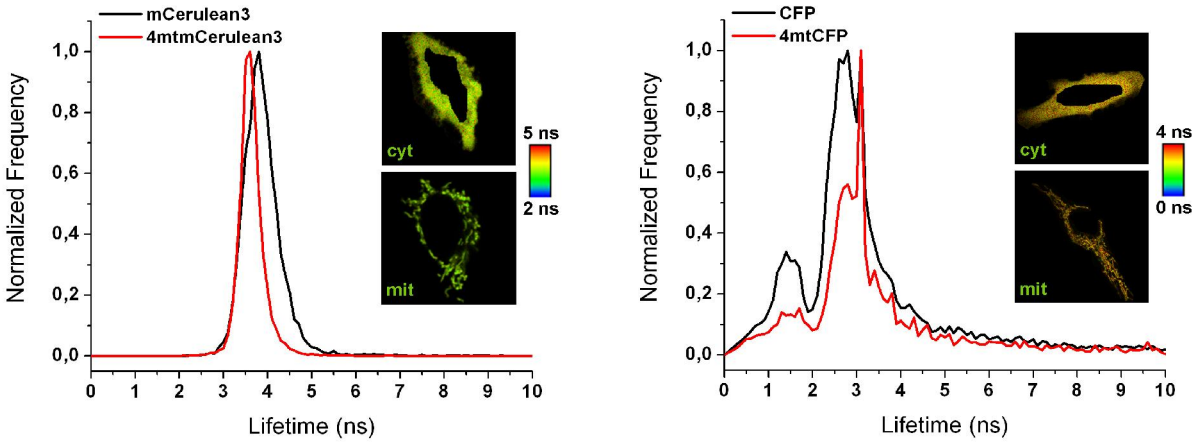

FIGURE 24: Fluorescence lifetime histograms of mCerulean3 (on the *left*) and CFP protein (on the *right*) expressed in HeLa cells and localized in cytosol (black line) or in mitochondria (red line). The insets are the fluorescence lifetime images in a false-color plot with the reported lifetime range.

As demonstrated by the lifetime histograms, which shows the frequency of the lifetimes measured in the sample, the fitting of fluorescence decays of CFP proteins requires a model with two exponential terms, while the mCerulean3 decays are mono-exponential. Also cpV protein shows a two-exponential decay (Figure 25).

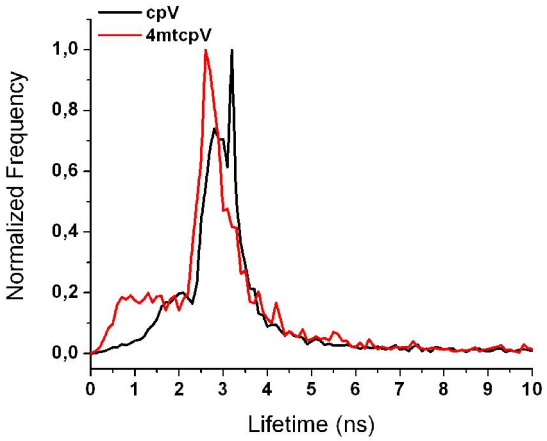

FIGURE 25: Fluorescence lifetime histograms of cpV protein expressed in HeLa cells localized in cytosol (black line) or in mitochondria (red line). The insets are the fluorescence lifetime images in a false-color plot with the reported lifetime range.

As already reported in literature (Millington et al, 2008), CFP is characterized by two lifetime components, attributed to two different conformations of the chromophore in the protein barrel. The longer lifetime of CFP in both cellular environments is shorter than that previously calculated inYC3.60 purified protein (3.57 ns) (Borst et al., 2010), while the relative amplitudes are similar. This could be due to different local features, such as local pH or self-quenching process (homo-FRET). For this reason and because during FRET lifetimes fitting it was impossible to carried out the analysis fixing such a long lifetime, the longer lifetime will be further fixed at 3,57 ns for the fitting of Cameleon sensors data. For cpV it is more difficult to measure the emission decay since its absorption cross-section is low at 400 nm excitation. It is anyway evident the need of a bi-exponential model for the fitting of cpV decay curves.

On the contrary, mCerulean3 protein is characterized by a mono-exponential decay, with fluorescence lifetime similar to that reported by Rizzo's group (Markwardt et al., 2011). In mitochondria, mCerulean3 shows a reduced lifetime, probably caused by the higher probe concentration with respect to the cytosol environment, which could favor homo-FRET phenomena (but also the alkaline mitochondrial pH could affect the lifetime). The mono-exponential decay is an advantage in FLIM-FRET characterization, since the data analysis is less complicated and more accurate.

Preliminary FLIM investigation has been also performed in cells expressing cytosolic and mitochondrial D3 Cameleon probes. For cytosolic probes some attempts have been carried out at physiological [Ca^{2+}] (meaning extracellular-like medium containing 1 mM Ca^{2+}) in order to calculate lifetime by acceptor photobleaching and collating photons from both donor (CH donor) and acceptor channel (CH acceptor) (Figure 26), since usage of saturable ionophore (Ionomycin) prevent the possibility of maintain a fixed Ca^{2+} concentration in

the time-window necessary for FLIM acquisition (over 3 minutes). Data are summarized in Table 3 (see below).

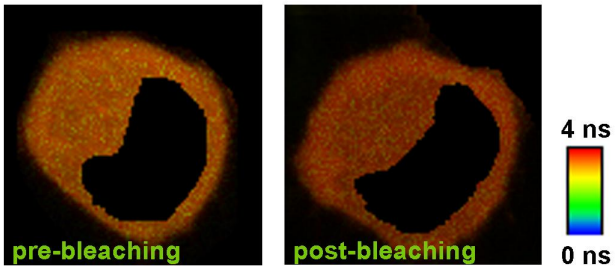

FIGURE 26: FLIM images of D3mCerulean3+16 collected in the donor channel before and after the acceptor photobleaching.

For the mitochondria, we have tested the minimum and maximum FRET condition. The results reported are preliminary data, concerning minimum FRET, and future work will be devoted to the definition of the better methodology for the analysis of FLIM data for FRET efficiency determination.

First of all, in case of 4mtd3mCerulean3+16 sensor at minimal FRET condition, the decay in the channel of donor clearly shows the presence of a second component lifetime, as depicted in figure 27. At the same time, the decay collected in the cpV channel (green line in figure 27) shows a rise on the initial part of the decay, as a consequence of the time-dependent increase in acceptor fluorescence intensity due to energy transfer process from donor to acceptor.

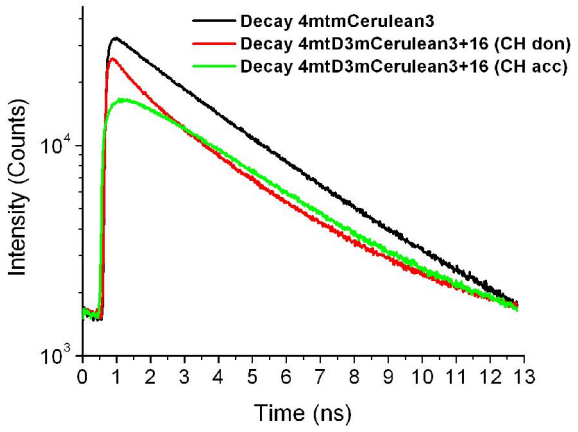

FIGURE 27: Fluorescence decay of 4mtD3mCerulean3+16 (minimum FRET) expressed in HeLa cells. Red and green curves are the emission decay collected in the channel of mCerulean3 and cpV respectively.

In this condition, the probe seemly assumes an "open configuration" (with the two end proteins far away from each other), thus reducing the intra-molecular energy transfer. Other adversary processes are the inter-molecular FRET, involving energy transfer between proteins of different probes, or the homo-FRET, which produce the self-quenching due to the re-absorption of donor moiety emission. To get more information about the processes involved, acceptor photobleaching experiments have also been performed in HeLa cells

expressing the mitochondria targeted Cameleon probes. The lifetimes obtained for the decay fitting of curves collected before and after the 10 minutes irradiation for bleaching are reported in table 4.

D3mCerulean3+16	τ_1 (ns)	τ_2 (ns)	τ_3 (ns)	t_{AMP} (ns)	D3cpV	τ_1 (ns)	τ_2 (ns)	τ_3 (ns)	t_{AMP} (ns)
Pre bleach, CH donor	3,8 (65%)	1,10 (35%)		**2,87**	**Pre bleach, CH donor**	3,57 (13%)	1,85 (50%)	0,64 (37%)	**1,78**
Post bleach, CH donor	3,8 (76%)	0,90 (24%)		**3,11**	**Post bleach, CH donor**	3,57 (35%)	2,00 (36%)	0,79 (29%)	**2,06**
Pre bleach, CH acceptor	3,8 (66%)	3 (14%)	0,4 (-20%)		**Pre bleach, CH acceptor**	3,57 (13%)	3 (57%)	0,48 (-30%)	
Post bleach, CH acceptor	3,8 (76%)	3 (12%)	1,37 (12%)		**Post bleach, CH acceptor**	3,57 (47%)	3 (22%)	1,84 (31%)	

TABLE 3. Average lifetimes (τ) obtained from the decay fitting of cell expressing D3mCerulean3+16 or D3cpV. Values in parenthesis are the relative amplitudes of each decay term. τ_3 indicate the lifetime measured in the acceptor channel.

4mtD3mCerulean3+16	τ_1 (ns)	τ_2 (ns)	τ_3 (ns)	t_{AMP} (ns)	4mtD3cpV	τ_1 (ns)	τ_2 (ns)	τ_3 (ns)	t_{AMP} (ns)
Pre bleach, CH donor	3,53 (74%)	0,99 (26%)		**2,87**	**Pre bleach, CH donor**	3,57 (23%)	1,79 (39%)	0,62 (37%)	**1,78**
Post bleach, CH donor	3,53 (88%)	0,58 (12%)		**3,19**	**Post bleach, CH donor**	3,57 (37%)	1,75 (31%)	0,58 (31%)	**2,06**
Pre bleach, CH acceptor	3,53 (73%)		0,77 (-27%)		**Pre bleach, CH acceptor**	3,57 (32%)	3 (39%)	0,37 (-29%)	
Post bleach, CH acceptor	3,7 (100%)				**Post bleach, CH acceptor**	3,57 (54%)	3 (25%)	1,05 (22%)	

TABLE 4. Average lifetimes (τ) obtained from the decay fitting of cell expressing 4mtD3mCerulean316 or 4mtD3cpV. Values in parenthesis are the relative amplitudes of each decay term. τ_3 indicate the lifetime measured in the acceptor channel.

For fitting of decays in the mCerulean3 channel, τ_1 is fixed at 3.8 ns and 3.53 ns for the probe expressed in cytosol and in mitochondria respectively, as calculated in cells expressing only the donor. In case of CFP based sensors, τ_1 is fixed at 3.57 ns, as calculated in the purified protein (Borst et al., 2010). This lifetime gives a fitting with lower residuals than those using the lifetimes calibrated with CFP alone in our experiments *in situ*. This discrepancy could be related to homo-FRET phenomena of CFP that could occur more frequently in living cells, rather than in purified proteins. For mCerulean3 donor protein this effect is less evident, since it is characterized by smaller overlapping area between the absorption and emission spectra, with respect to the CFP protein (Markwardt et al., 2011).

All other parameters are kept free for the fitting.

Regarding the emission decay collected in the acceptor channel, we consider: the contribution of cpV with main lifetime $\tau_2 = 3$ ns, partial bleed-through of donor emission in the acceptor channel ($\tau_1 = 3.8$ or 3.53 ns) and a third free contribution (τ_3). Before photobleaching, the amplitude of the short lifetime τ_3 is negative for all the experiments, confirming the partial energy transfer process. Since only proteins involved in pure FRET process produce the rise of acceptor fluorescence intensity, it is possible to estimate the FRET efficiency from the rise time, which is equivalent to the donor fluorescence lifetime in the presence of acceptor. Unfortunately, the difficulty in accurately measuring rise times makes complicate a detailed analysis of the data. Future work will be devoted to a precise definition of the IRF (Instrumental Response Function) and accurate models for the fitting of decays in the acceptor channel.

After acceptor photobleaching, the contribution of donor gets larger and, as a consequence, τ_{AMP} increases. Figure 28 shows the comparison of FLIM images of 4mtD3mCerulean3+16 sample before and after cpV bleaching.

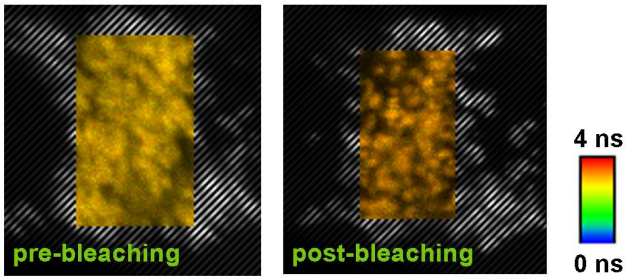

FIGURE 28: FLIM images of 4mtD3mCerulean3+16 collected in the donor channel before and after the acceptor photobleaching.

For all probes, the additional lifetime of donor, necessary to fit the donor decay of the Cameleon sensor, is still present, even if the negative contribution in the acceptor channel seems to disappear. This residual could be the effect of homo-FRET.

4. *In vivo* delivery of the new probes

In vivo expression is usually carried out via transgenesis and electroporation *in situ*, two techniques involving time-spending laborious tasks. An interesting new *in vivo* delivery technique that permits to overcome the mentioned disadvantages is the viral infection. Since our aim is to explore mitochondrial Ca^{2+} dynamics in heart and brain *in vivo*, we took advantage of adeno-associated viral (AAV) injection. In particular, we decided to generate AAV serotype 9, reported to have a strong cardiac tropism via systemic or local injection (Pacak et al., 2006; Bish et al., 2008) and brain tropism via intracranial injection (Foust et al., 2008).

Thus, in collaboration with Dr. Zentilin (International Centre for Genetic Engineering and Biotechnology ICGEB Trieste, Italy) AAV9 containing the transgene of the mitochondrial and the cytosolic variants of Cameleon described so far, has been created. To obtain the probe expression in the heart, a CMV promoter was used, while to get neuronal specific expression, the synapsin promoter was substituted to CMV in the AAV9 vector (generating AAV9syn). Indeed the human synapsin 1 (syn) gene promoter has been shown to provide a neuron specific expression both *in vivo* and *in vitro* (Kügler et al., 2001).

The performance of AAV9 created have been tested in primary cultures. Cortical neurons 72 h after infection with AAV9syn-4mtD3cpV (AAV9syn-D3cpV is still in production) and AAV9syn-D3mCerulean3+16 or AAV9syn-4mtD3mCerulean3+16 have been tasted to check the functionality of the Cameleons. In a typical experiment, we induced mitochondrial Ca^{2+} uptake by inducing neurons depolarization (Figure 29).

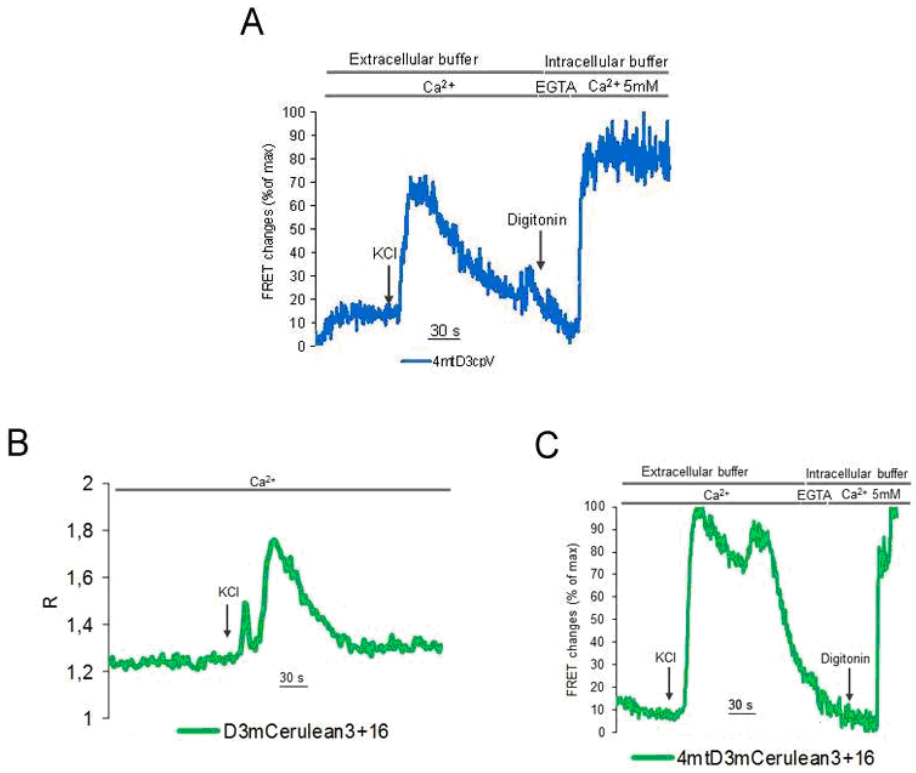

FIGURE 29. Neonatal cortical neurons. Representative traces of cytosolic or mitochondrial Ca^{2+} rise induced by neurons depolarization with 30mM KCl in iso-osmotic extracellular-like medium, where indicated, and expressing AAV9syn-4mtD3cpV **(A)** AAV9syn-D3mCerulean3+16 **(B)**, AAV9syn-4mtD3mCerulean3+16 **(C)**. Data are presented as FRET changes % of maximum or as R as reported.

Similarly, AAV9-D3cpV or AAV9-4mtD3cpV and AAV9-D3mCerulean3+16 or AAV9-4mtD3mCerulean3+16 has been infected in neonatal rat cardiomyocytes. 96 h after transfection, spontaneous mitochondrial Ca^{2+} oscillations has been measured. Figure 30 shows representative traces of the experiments described, demonstrating the correct functionality of the AAV9 created.

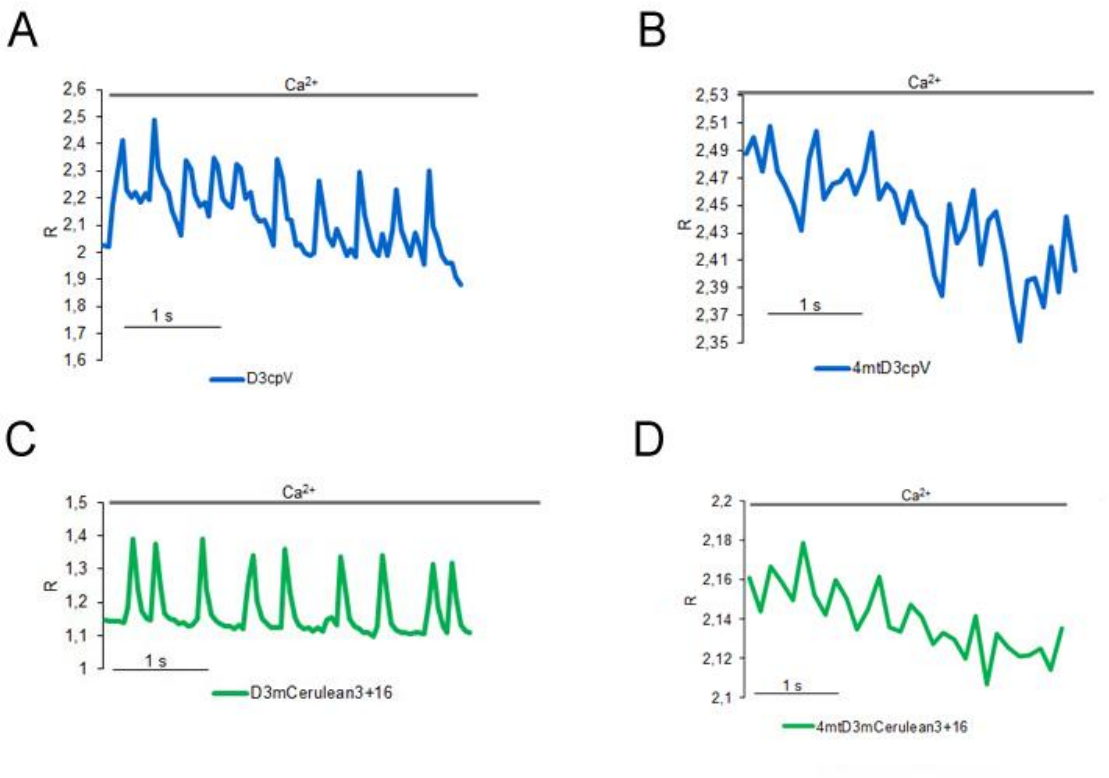

FIGURE 30. Neonatal rat cardiomyocytes. Representative traces of cytosolic or mitochondrial spontaneous Ca^{2+} oscillations expressing **(A)** AAV9-D3cpV, **(B)** AAV9-4mtD3cpV, **(C)** AAV9-D3mCerulean3+16 and **(D)** AAV9-4mtD3mCerulean3+16. Data are presented as R (cpV/CFP or cpV/mCerulean3).

To check if AVV9 are able to induce a sufficient expression level of Cameleon probes for *in vivo*, just one attempt has been done injecting intra-peritoneally 0-1 day newborn mice. Preliminary data obtained in acute heart and brain slices, confirm that intra-peritoneal injection is suitable to obtain Cameleon expression in heart tissue, but is not sufficient to reach expression levels suitable for *in vivo* experiments in live brain (Figure 31). Further attempts to improve brain expression will be carried out, performing intra-cranial injection of AAV9 encoding for Cameleon probes.

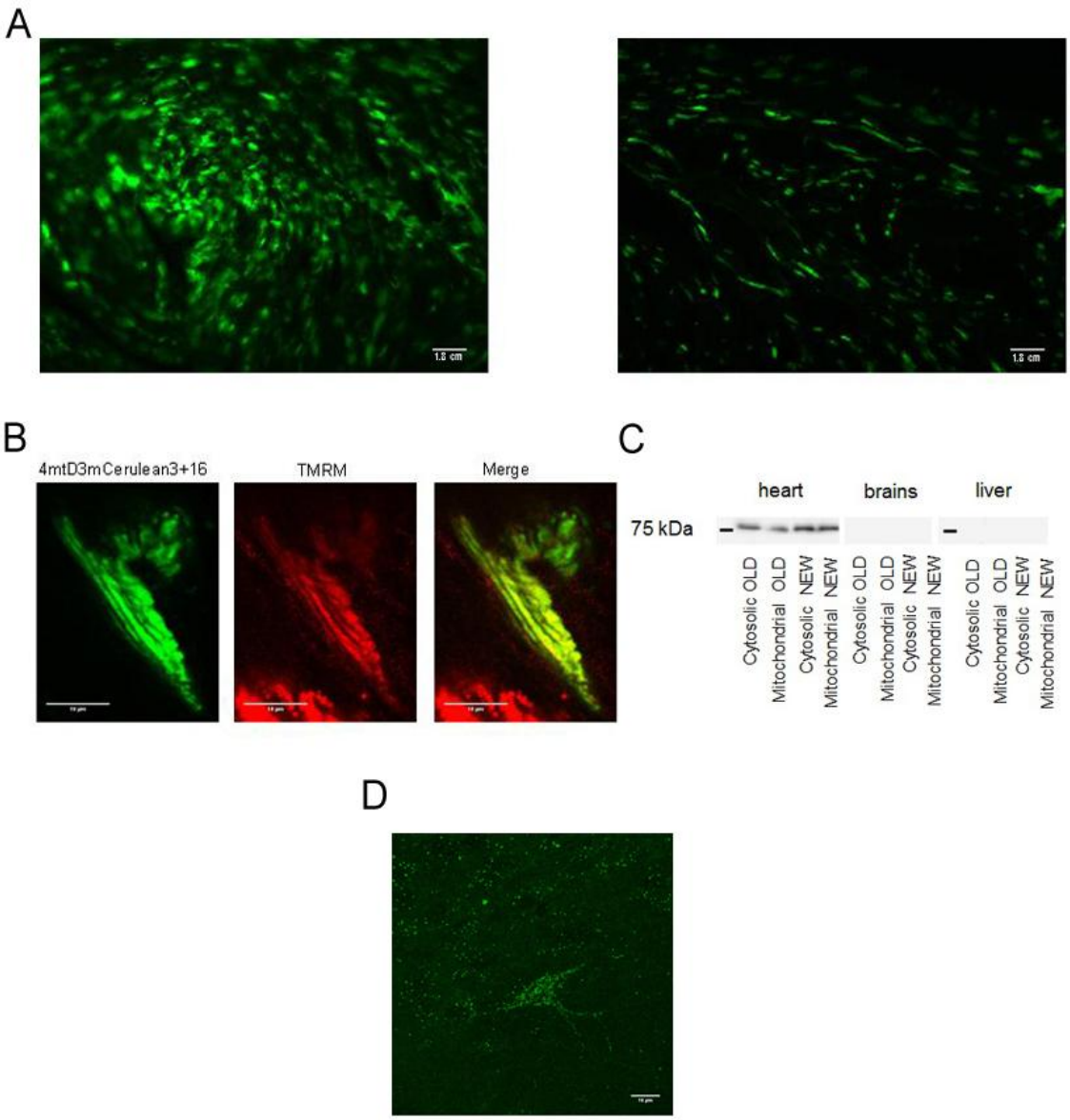

FIGURE 31. (A) Confocal images of acute heart slices of inject mouse with AAV-D3mCerulea3+16 (*left*) and mouse with AAV-4mtD3mCerulea3+16 (*right*). **(B)** Confocal images of single cells from acute heart slices of inject mouse with and mouse with AAV-D3mCerulea3+16 that co-localized with TMRM. **(C)** Western blot form whole heart, brain and liver stained with anti-GFP antibody to detect Cameleon expression**. (D)** Confocal image of acute brain slices of inject mouse with AAV-4mtD3mCerulea3+16

5. A new mitochondria targeted Channelrhodopsin

Since mitochondrial membrane potential can modulate diverse mitochondria activities, like regulation of Ca^{2+} homeostasis, oxidative stress response, apoptosis and innate immune response, putting the organelle in central position in controlling cellular function and fate (Contreras et al., 2010), an interesting tool to manipulate its activity has been exploited.

Channelrhodopsin-2 (ChR2) is a light-gated cation channel, which evokes membrane potential depolarization upon photostimulation with blue light in the presence of all-trans retinal, being able to generate sufficient photocurrent to depolarize cells. In optogenetic, this channel is used to optically stimulate and control neuronal activity with very high temporal resolution, offering distinct advantages over traditional pharmacological or electrical techniques of perturbation (Häusser, 2014). Thus a mitochondria targeted ChR2 has been created and investigate in order to create a method able to induced mitochondrial depolarization in a temporary-controlled, reversible and cell-specific manner.

5.1 The targeting to mitochondria

In order to target ChR2-YFP to the IMM Prof. Sekler's group fused the signaling peptide of the Mitochondrial Calcium Uniporter (MCU) (De Stefani et al., 2011) as well as multiple N-terminal signal sequences from subunit VIII of human Cytochrome C Oxidase (2mt, 4mt) to the N-terminus of Channelrhodopsin, since attaching multiple signal sequences has been shown to improve specific localization of fluorescent probes to the mitochondria (Filippin et al., 2005). Initial experiments with different mitochondria targeting signal showed a poor targeting efficiency for ChR2. Upon transfection into human embryonic kidney (HEK293) cells, all constructs that included full sequence of ChR2 (MCU-ChR2-YFP, 2mtChR2-YFP, 4mtChR2-YFP) were still localized mainly in the PM (Figure 32A) suggesting the presence in the ChR2 protein of a strong internal targeting signal. Indeed, deleting of the initial 24 amino acids from ChR2 N-terminus dramatically changed subcellular localization of the resulting construct. We refer to this shortened form of the channel as ChR2B (Figure 32A). Among tested 2mt, 4mt and MCU signaling sequences 4mtChr2B appeared to be the best construct in terms of mitochondrial localization and the lack of adverse effects. Fluorescence signals of mitoCherry, a mitochondria marker, and 4mtChR2B-YFP merged well in confocal images (Figure 32A). The same mitochondrial localization was obtained in different cell lines (HEK293 and HeLa, Figure 32B) and primary neurons (Figure 32C). To verify the absence of residual 4mtChr2B channels in the neuronal plasma membrane, we recorded neuronal currents during illumination with blue light (Figure 32C). No blue light-sensitive currents were detected during these tests.

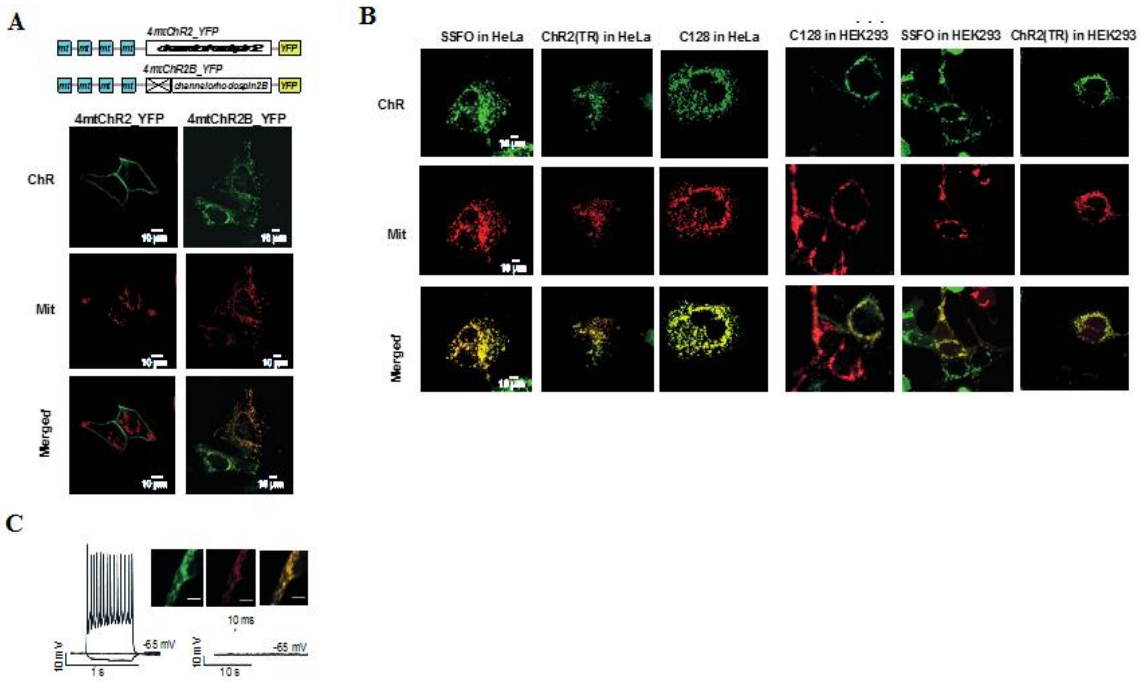

FIGURE 32. 4mtChR2B but not 4mtChR2 is expressed in the IMM. (**A**) Confocal microscope images of 4mtChR2-YFP (*left*, in HEK 293 cells) and 4mtChR2B-YFP (*right*, in human melanoma GA cells) co-expressed with a mitochondria targeted mitoCherry. The structure of constructs is shown on *top.* Yellow color indicates co-localization of the mitochondrial marker and the YFP tagged channel. (**B**) Confocal image examples of HEK293 and HeLa cells expressing several 4mtChR2B-YFP mutated versions. Co-localization of the mitochondria marker with 4mtChR2B-YFP results in a yellow color. (**C**) In neuron, light does not elicit PM depolarization (*right*) indicating no residual 4mtChRB activity in the plasma membrane, while delivering current via the patch pipette to the same neuron causes firing (*left*). Colocalization of 4mtChR2B-YFP with mitoCherry in primary hippocampal neuron (*upper right panel*).

5.2 The new mitochondria targeted Channelrhodopsine display the correct topology in the IMM

Fluorescence quenching experiments were then employed to verify the topology of 4mtChR2B-YFP insertion in the mitochondrial membrane. If 4mtChR2B(SSFO)-YFP (hereafter indicates as SSFO-YFP) is properly inserted in the IMM, the C-terminal YFP tag should face the mitochondrial matrix. Indeed we found that: 1) application of proteinase K to Digitonin permeabilized cells did not cause a significant reduction of SSFO-YFP signal, while it completely abolished that of N33D3cpv (a probe in which the YFP moiety is located on the cytoplasmic surface of the OMM); 2) Trypan blue addition, that is permeable across the OMM, but not the IMM, did not affect the fluorescence of SSFO-YFP or of the matrix located Cameleon 4mtD3cpv (Figure 33B red and blue lines), while completely abolishing that of a YFP-Cytochrome C (not shown and see Giacomello et al., 2010) (Cartoon of quenching protocol in Figure 33A). The 4mtD3cpv fluorescence, however was totally lost after alamethicin application that permeabilizes both mitochondrial membranes (Figure 33C, green line) and releases all matrix proteins into the medium (Hoffman et al., 2013). On the contrary, the fluorescence of SSFO-YFP was not affected by the latter treatment as expected for a membrane bound protein. Taken together these data are consistent with a proper IMM localization of our construct with YFP tag being inaccessible from the cytoplasm or the inter membrane space. Functional experiments below further support the notion that 4mtSSFO-YFP is correctly located in the IMM.

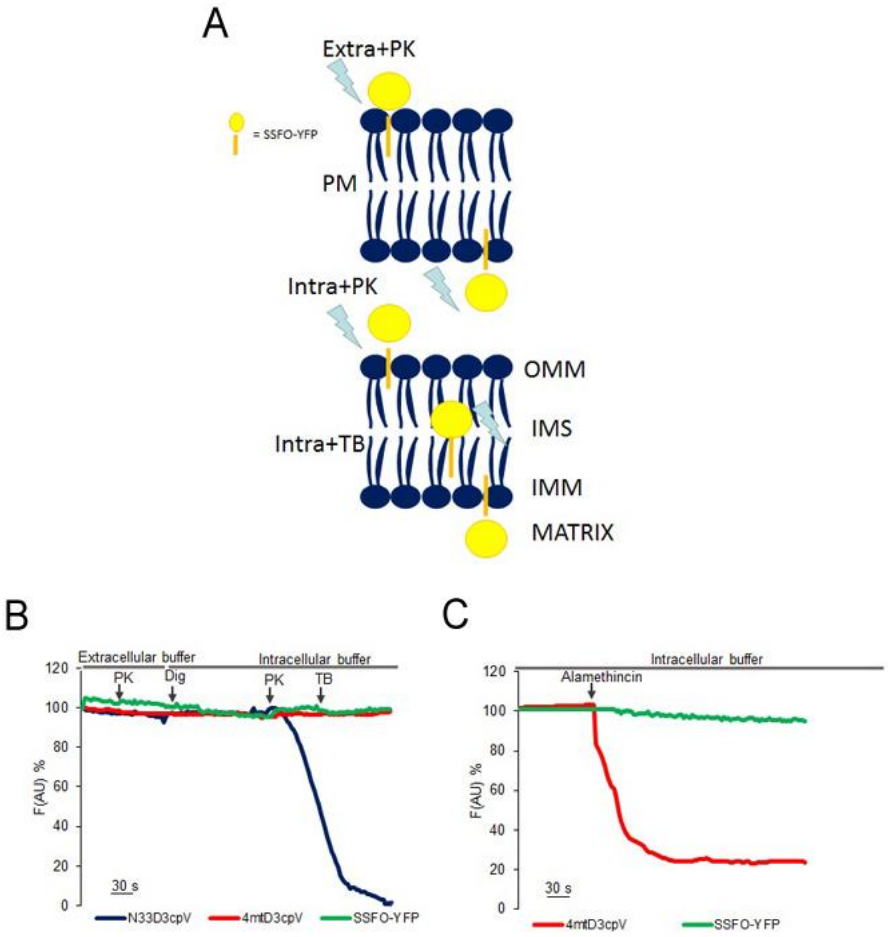

FIGURE 33. (A) Schematic representation of the protocol used to investigate the topology of the expressed channel. HeLa cells were plated and transfected with 0.5 µg of SSFO-YFP cDNA. The experiments were performed after 48 or 72 h and the cells were perfused with different buffers:

(1) Perfusion of extracellular-like Ca^{2+}-free medium with proteinase K 20 µg/uL in order to cut any YFP facing the extracellular space and to check if any ChR2B was located in PM in a wrong conformation.

(2) PM of HeLa cells were pre-permeabilized with 100 µM Digitonin for 1 minute in intracellular-like medium.

(3) Cells were perfused with intracellular-like Ca^{2+} free medium with proteinase K 20 µg/uL, which could cut YFP facing the cytosol, but it's not able to pass through the OMM. In this way we were able to detect if any ChR2B is located in PM or in OMM with the C-terminus facing the cytosol.

(4) Cells were perfused with intracellular-like medium with Trypan blue 0.5 mg/mL, which is able to pass the OMM and quench any YFP facing the inter membrane space allowing us to check if 4mtChR2B-YFP in incorrectly located in OMM, IMS or IMM with the C-terminus facing the IMS.

(B) HeLa cells expressing either SSFO-YFP, N33D3cpv or 4mtD3cpv were first treated with extracellular proteinase K, then, following Digitonin permeabilization, with intracellular proteinase K, and finally with Trypan blue as indicate in top bars and arrows. **(C)** In another experiment cells expressing 4mtChr2B-YFP or 4mtD3cpv were permeabilized with Digitonin in an intracellular-like medium, then treated with alamethicin, which permeabilizes mitochondrial outer and inner membranes. Traces represent YFP fluorescence in arbitrary units (AU) normalized to initial fluorescence.

5.3 Mitochondria depolarization

The new mitochondrial 4mtChR2B constructs were tested *in situ* for their capacity to change the mitochondrial membrane potential in response to light. Sekler's group used several mutated ChR2B forms with different properties and finally we choose the so called stable step-function opsin ChR2 (SSFO). It has been shown that the mutations C128S/D156A, gives rise to prolonged photocurrents far outlasting the initiating pulses of light and ChR2(C128) (Yizhar et al., 2011), mutations C128A/ H134R, is a high-photocurrent SFO variant (Prakash et al., 2012). For the last two ChRs, photocurrents can be precisely initiated and terminated with different colors of light (blue and red respectively, see below), but these currents operate at vastly longer time scales than in conventional ChR. SFOs have inactivation time constants in the order of tens of seconds or more instead of milliseconds. All these constructs are activated by blue (~460 nm) light and then return to a non-conductive state spontaneously; the closing process could be speeded up by red light for ChR2B(SSFO) and ChR2B(C128). To create a nonfunctional control channel we exploited the fact that for activation opsins require binding of retinal, a vitamin A–related organic cofactor. A truncated form ChR2B(TR) lacking the last two helixes and thus not able to bind retinal was constructed.

Since the immediate effect of the opening of a channel inserted into the IMM should be mitochondrial membrane potential ($\Delta\psi m$) collapse, the effects of the blue light on the fluorescence signal of the membrane potential probe TMRM has been tested. TMRM is used in the redistribution mode to assess $\Delta\psi m$, and therefore a reduction in TMRM fluorescence represents $\Delta\psi m$ depolarization. In cells transfected with void vector or ChR2B(TR), as controls, or SSFO-YFP the exposure to blue light caused depolarization only in the last case (measured as a decrease in the TMRM fluorescence, N=17, Figure 34A). No depolarization was induced by blue light in control cells and in cells expressing the truncated version of ChR2B (Figure 34A, N=11 in both controls and ChR2B, $p>0.2$). The rate of depolarization appears, however, quite slow. One explanation of this low kinetics could be that the light used to monitor TMRM signal is able to counteract the channel opening, for example by inducing a partial closure. It could be also possible that the power of light used during TMRM acquisition (which is at the minimum power possible to get good signal-to-noise ratio), is not sufficient to trigger the total closure of all the channels, meaning that the low amount of light used during the experiments starts the closure process, but slowly or partially. To check if 540 nm- light is able to interfere with the opening kinetics we develop another protocol in which after the blue light pulse, the TMRM recording is started with one minute of delay after the blue light flash, avoiding interference of the red light with the opening kinetic. With this protocol the TMRM signal decreased by about 60% after photoactivation only in cells expressing SSFO-YFP (N=57, $p<0.0001$ compared to ChR2B(TR) (N=40) or void vector (N=38)), while in the experiments carried out recording TMRM signal immediately after the blue light pulse, the TMRM signal decreased by about 30% in one minute. Although we did not obtain direct evidence of channel closure following exposure to red light, indirect data indicate that green light interfere with the opening kinetics (Figure 34B).

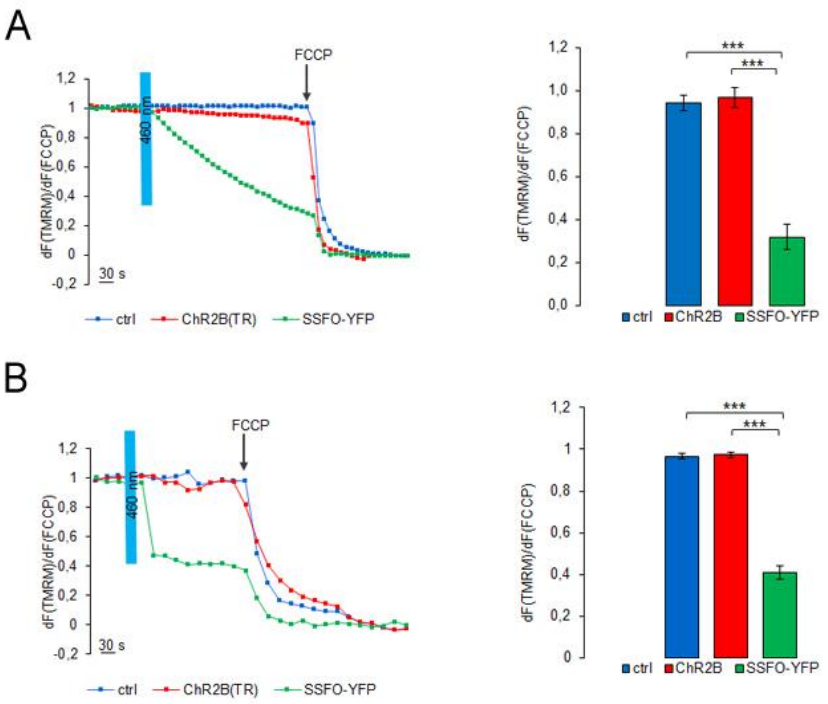

FIGURE 34. Exposure to blue light (460±7.5 nm) induces changes in the mitochondrial membrane potential and mitochondria function in cells expressing 4mtChR2B. (**A**). *Left*: The mitochondrial membrane potential measured as TMRM fluorescence decreased following blue light exposure for 10 seconds (cyan bar) in HeLa cells expressing SSFO-YFP but not in cells expressing void vector and a mitochondrial targeted YFP and in cells expressing ChR2(TR) and a mitochondrial targeted YFP. *Right*: The histogram represents the TMRM signal measured before FCCP addiction normalized to ctrl. Data are represented as mean ±SEM; N (number of cells) ≥ 11 for each conditions. (**B**). *Left*: The mitochondrial membrane potential measured as TMRM fluorescence decreased following blue light exposure for 10 seconds (cyan bar) in HeLa cells expressing SSFO-YFP but not in cells expressing void vector and a mitochondrial targeted YFP and in cells expressing ChR2(TR) and a mitochondrial targeted YFP. In these case the TMRM recording started one min after the photoactivation of the channel. *Right*: The histogram represents the TMRM signal measured before FCCP addition normalized to ctrl. Data are represented as mean ±SEM; N (number of cells) ≥ 38 for each conditions. (* $p<0.05$; ** $p<0.01$; *** $p<0.0001$).

5.4 Mitochondrial depolarization results in mitochondrial Ca^{2+} uptake inhibition

Given that Ca^{2+} uptake in mitochondria is strictly dependent on membrane potential, we analyzed in more detail the Ca^{2+} uptake characteristics in the presence of the mitochondria targeted SSFO, using two genetically encoded probes, 4mtD3cpv and mt-Aeq. Figure 35A shows that in cells co-transfected with SSFO and the matrix located fluorescent Ca^{2+} probe 4mtD3cpv, the amplitude of the mitochondrial Ca^{2+} rise observed upon stimulation of HeLa cells with Histamine was drastically reduced (N=62, $p<0.0001$) by a 460 nm LED pulse, while those of controls (N=40) and of cells expressing the truncated form of the channel (N=43) were indistinguishable ($p>0.2$). The peak of the mitochondrial rise in cells expressing SSFO were similar to those of control cells treated with the classical mitochondrial uncoupler FCCP (N=21, $p>0.2$) (data not shown). The use of a co-transfection protocol insures that at least in 80% of cases the cells expressing the Ca^{2+} probe also expresses the channel.

We also co-transfected SSFO-YFP and SSFO with mitochondrial targeted Aequorin, mt Aeq. In this case, given that Aequorin is a chemiluminescent protein and emits light at 460 nm upon a rise in Ca^{2+} levels, the

prediction is that the light emitted by Aequorin during mitochondrial Ca^{2+} uptake should be sufficient in itself to open (at least in part) the channel and thus to reduce the amplitude of the mitochondrial Ca^{2+} rise. To trigger maximal mitochondrial Ca^{2+} rise and thus maximize Aequorin emission, a mixture of stimuli has been used. Indeed the data of Figure 35B confirm that this is the case: the peak amplitude of the agonist induced Ca^{2+} rise was significantly diminished (about 25-40%) in cells expressing SSFO (N=7) or SSFO–YFP (N=7) compared to controls (ctrl, N=8; ChR2B(TR), N=7) and this effect was strengthened by pre-illuminating the sample with blue-light, resulting in a decrease in Ca^{2+} rise in HeLa cells expressing SSFO (N=6) or SSFO-YFP (N=5) about 40-50% compared to ctrl (N=6) and ChR2b(TR) (N=3) (Figure 35C, $p<0.01$).

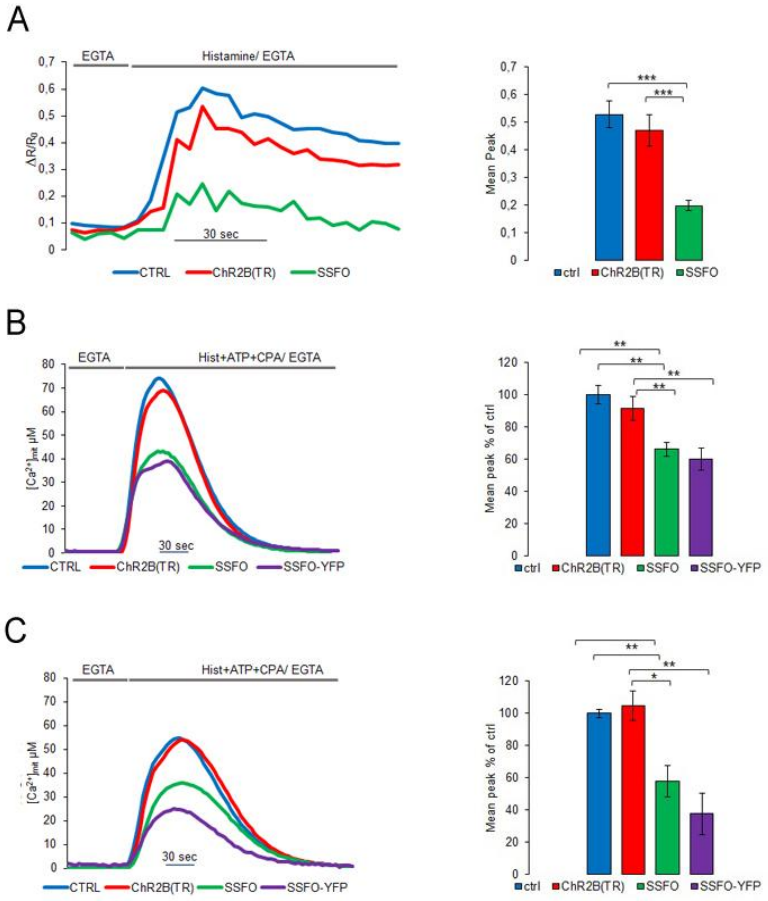

FIGURE 35. Reduction of mitochondrial Ca^{2+} uptake in HeLa cells expressing the new mitochondrial targeted SSFO**. (A)** HeLa cells transiently transfected with void vector, SSFO or ChR2B(TR) and co-transfected with 4mtD3cpV, were treated with 100 µM Histamine where indicated. *Left*: Representative kinetics of mitochondrial Ca^{2+} uptake in control (blue), SSFO (green) and ChR2B(TR)(brown) cells. Data are plotted as $\Delta R/R_0$. *Right*: The histogram represents mean ±SEM $[Ca^{2+}]_m$ increase caused by Histamine treatment of $N \geq 40$ cells for each conditions. **(B)** HeLa cells transiently transfected with empty vector, SSFO, SSFO-YFP or ChR2B(TR), were analysed for $[Ca^{2+}]_m$ changes obtained employing a mix of stimuli by mt-Aeq. *Left*: Representative kinetics of $[Ca^{2+}]_m$ in control (blue), ChR2B(TR)(brown), SSFO (green), and SSFO-YFP (violet) cells. *Right*: The histogram represents mean ±SEM (normalized to ctrl) $[Ca^{2+}]_m$ increase. caused by a mix of stimuli (100 µM Histamine, 100 µM ATP and 20 µM CPA) of $N \geq 7$ experiments for each conditions **(C)** HeLa cells transiently transfected with empty vector, ChR2B(TR), SSFO, and SSFO-YFP, were analysed for $[Ca^{2+}]_m$ changes upon the application of a mix of stimuli by mt-Aeq after a blue light pulse. *Left*: Representative kinetics of $[Ca^{2+}]_m$ after a blue light pulse in control (blue), ChR2B(TR) (brown), SSFO (green), and SSFO-YFP (violet) cells. *Right*: The histogram represents mean ±SEM (normalized to ctrl) $[Ca^{2+}]_m$ increase.caused by a mix of stimuli $N \geq 3$ experiments for each conditions. (* $p<0.05$; ** $p<0.01$; *** $p<0.0001$).

To confirm that the reduction in mitochondrial Ca^{2+} peak is not due to an intrinsic toxicity of the channel, but depends on the depolarization induced by light induced SSFO opening, we induced a much smaller Ca^{2+} rise in mitochondria by activating mitochondrial Ca^{2+} uptake through CCE. Given that Aequorin light emission is not linearly but exponentially related to the Ca^{2+} concentration, a 10 fold reduction in the Ca^{2+} peak (as for CCE compared to IP_3 producing agonists) the reduction in light emitted is over 100 fold (Figure 36A). As expected, thus, in the case of CCE dependent Ca^{2+} influx, the peak amplitude of the mitochondrial Ca^{2+} rise was indistinguishable in SSFO–YFP or SSFO expressing cells compared to controls (Figure 36B, p>0.2).

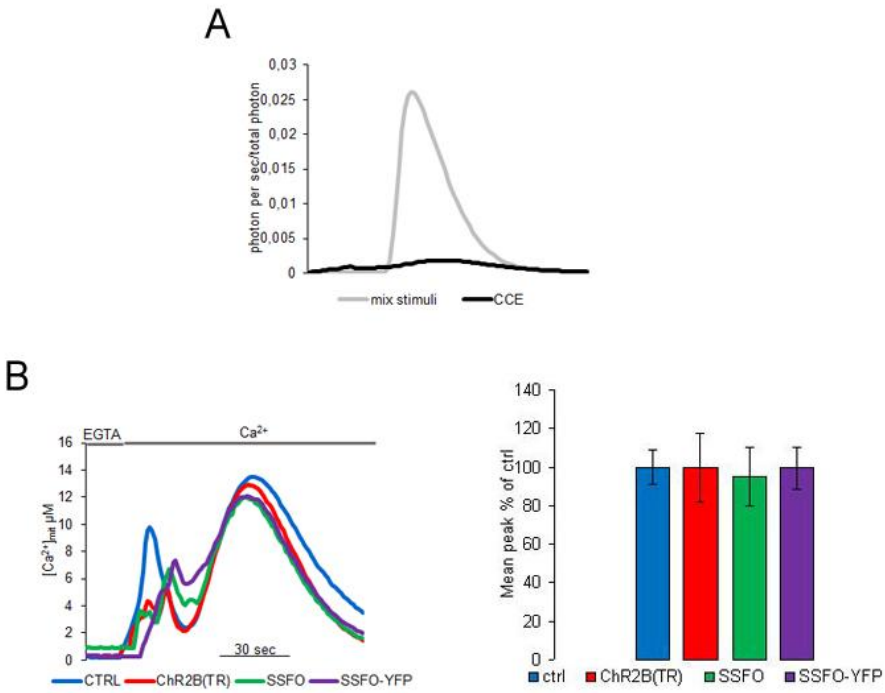

FIGURE 36. Absence of mitochondrial toxicity in HeLa cells expressing mt-Aeq the new mitochondria targeted SSFO**. (A)** HeLa cells transiently expressing void vector, were analysed for mitochondrial Ca^{2+} uptake changes by mt-Aeq in low-light emitting condition. The number of photons emitted per second normalized to the total photon emitted by stimulating a maximal mitochondrial Ca^{2+} uptake is higher than mitochondrial Ca^{2+} uptake induced by a mixture of stimuli (grey) or CCE (black) activation, lowering the SSFO opening probability. The traces represent the photon emitted during mitochondrial Ca^{2+} uptake induced by the application of a mix of stimuli or by inducing CCE. **(B)** HeLa cells transiently transfected with empty vector, SSFO, SSFO-YFP or ChR2B(TR) and mt-Aeq were first treated with 100 nM thapsigargin in Ca^{2+} free EGTA containing medium, to deplete the stores and then perfused with medium containing 2 mM $CaCl_2$ to activate CCE, where indicated. *Left*: Representative kinetics of $[Ca^{2+}]_m$ in control (blue), ChR2B(TR) (brown), SSFO (green) and SSFO-YFP (violet) cells. *Right*: The histogram represents the mean ±SEM (normalized to ctrl) $[Ca^{2+}]_m$ obtained in Aequorin experiments by inducing mitochondrial Ca^{2+} uptake through CCE activation of N ≥ 7 experiments for each conditions.
(* p<0.05; ** p<0.01; *** p<0.0001).

Last, but not least, we also measured the cytosolic Ca^{2+} changes in controls or SSFO (with or without YFP tag) expressing cells using both a mix of stimuli (Figure 37A) or CCE induced Ca^{2+} increases (Figure 37B). No differences between control cells and cells expressing SSFO were observed. Nevertheless, we also assess if the light employed during photoactivation could damage mitochondria by testing their ability to take up

Ca^{2+} in the presence of a mix of stimuli in HeLa cells transfected with mt Aeq and void vector employing or not the pre-illumination. No differences were observed between them (Figure 37C).

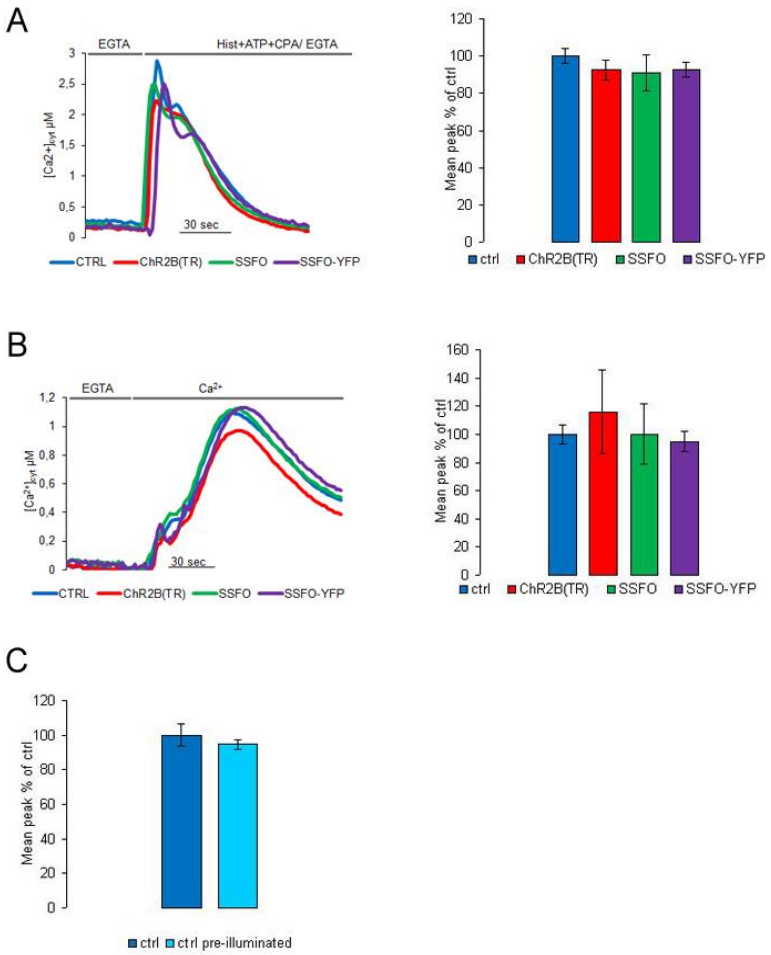

FIGURE 37. Absence of cellular toxicity and photo-toxicity in HeLa cells expressing cyt-Aeq and the mitochondria targeted SSFO**. (A)** HeLa cells transiently transfected with empty vector, SSFO, SSFO-YFP or ChR2B(TR) and cyt-Aeq were treated with a mix of stimuli (100 µM Histamine, 100uM ATP, 20uM CPA). *Left*: Representative kinetics of $[Ca^{2+}]_c$ in control (blue), ChR2B(TR) (brown), SSFO (green) and SSFO-YFP (violet) expressing cells. *Right*: The histogram represents mean ±SEM (normalized to ctrl) $[Ca^{2+}]_c$ increase caused by a mix of stimuli of N ≥ 3 experiments for each conditions. **(B)** HeLa cells transiently transfected with empty vector, SSFO, SSFO-YFP or ChR2B(TR) and cyt-Aeq were first treated with Thapsigargin (100 nM) in Ca^{2+} free, EGTA containing medium, to deplete the stores and then perfused with medium containing 2 mM $CaCl_2$ to activate CCE. *Left*: Representative kinetics of $[Ca^{2+}]_c$ in control (blue), ChR2B(TR) (brown), SSFO (green) and SSFO-YFP (violet) expressing cells. *Right*: The histogram represents mean ±SEM (normalized to ctrl) $[Ca^{2+}]_c$ increase of N≥ 4 experiments for each conditions. **(C)** Control HeLa cells transiently expressing mt Aeq with or without pre-illumination for 10 sec at 470 nm and treated with the mixture of stimuli as in panel A. The histogram represents mean ±SEM (normalized to ctrl) $[Ca^{2+}]_c$ increase. Caused by a mix of stimuli with or without pre-illumination of N ≥ 6 experiments for each conditions. (* $p<0.05$; ** $p<0.01$; *** $p<0.0001$).

5.5 The mitochondria targeted Channelrhodopsin is able to suppress the spontaneous beating in neonatal rat cardiomyocytes

SSFO-YFP was expressed in neonatal rat cardiomyocytes and imaged in bright field. After 10 seconds of blue light pulse, spontaneous beatings were almost immediately blocked only in cardyomyoscytes expressing SSFO-YFP. Contraction was monitored only morphologically in bright field since the co-transfection (SSFO and 4mtD3cpV) efficiency is too low in this cell type. To avoid the possibility that the contraction of neighbor cells could mask the effect in the single transfected cell only isolated and beating cardiomyocytes expressing SSFO were analyzed. As control, cardiomyocytes expressing void vector or ChR2B(TR) were used. SSFO opening resembled quantitatively and kinetically the effect of FCCP (Figure 38).

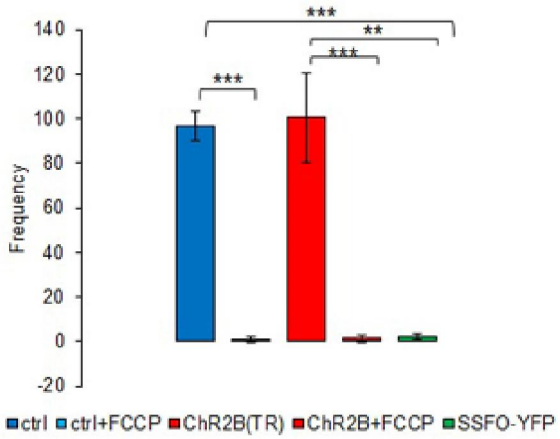

FIGURE 38. The histogram represents the quantification of the beats/second after the blue light pulse employed to photoactivate SSFO, normalized to the frequency of beating measured before the pulse for each condition. The histogram represents mean frequency ±SEM of N=4 number of cells or each conditions. The addition of FCCP in cardiomyocytes expressing void vector or truncated-SSFO again resembled quantitatively and kinetically the effect of SSFO photoactivation.

Discussion

Ca^{2+} exerts many different functions in cells, in both physiological and pathological conditions. Given its pivotal role, this ion has been widely studied for many years. At the beginning, chemical dyes allowed to monitor Ca^{2+} dynamics only in the cytosol, but more recently, thanks to the development of genetically encoded Ca^{2+} indicators (GECIs), the role of subcellular compartments has been largely unravelled.

Cameleon probes have the enormous advantages of being ratiometric Ca^{2+} sensors, thus they are independent of shifts in the focal plane and contraction phenomena that could occur (or be induced) in some tissues during the experiments. This feature is particularly relevant for *in vivo* applications as movement artefacts are unavoidable (blood flux, heart beating, and respiration). In addition the low fluorescence quantum yield of the donor fluorescent protein CFP and its multi-exponential lifetime reduce signal-to-noise ratio in thick samples and complicate lifetime analysis (FLIM).

In 2011 Rizzo's group developed a new variant of CFP, called mCerulean3, characterized by improvements in quantum yield and brightness, a single exponential decay and a reduced fluorescence photoswitching behaviour, compared to other CFP variants (Markwardt et al., 2011). Given these interesting biophysical features of mCerluean3, together with the described drawbacks of CFP as donor, the latter has been substituted with mCerluean3 in the cytosolic D3cpV and mitochondrial 4mtD3cpV Cameleon probes. The new probes created maintained the brightness improvement observed for mCerulean3. Moreover, it showed proper localization and Ca^{2+} changes responsiveness both in the cytosol and in mitochondria. This features lead to an improvement of SNR and lowers the levels of inducible phototoxicity in the sample. Despite these promising results, the donor substitution caused a reduction of about 20% in the dynamic range (DR) of both D3mCerulean3 and 4mtD3mCerulean3. This negative impact has also been reported in Twitch sensor, where CFP was also substituted with mCerulaen3 Thestrup et al., 2014).

To overcome the drawback of DR range reduction different approaches were tested. An advantage of Cameleon probes, compared to Twitch based sensor, is the presence of two Ca^{2+} responsive elements separated by a short linker, meaning the possibility to intervene on the mobility of the two FPs, modifying in turn their ability to sense [Ca^{2+}] changes. Eventually, the extension of the linker between the two Ca^{2+} responsive elements CaM and M13 by addition of 16 glycines, resulted in the recovery of the DR in both cytosolic and mitochondrial-targeted probes. Indeed, the DR was even increased in D3mCerulean3+16, compared to the original Cameleon.

The increase in photostability of the single FP mCerulean3 led also to an improvement in the photostability of the probes D3mCerulean3+16 and 4mtD3mCerulean3+16, evaluated in basal, minimal and maximal FRET conditions. The primary consequence of this improvement is a smaller decrease in FPs brightness during repetitive excitation, which represents an important limiting factor for experiments requiring large numbers of images or the usage of high excitation light intensity.

Another critical point to address was the pH sensitivity of the probes. Since each FPs are characterised by a different pKa, the substitution of CFP with mCerulean3 could change the probes pH sensitivity. Indeed, cpV has a pKa = 6, being the more sensitive to physiological pH, while CFP has a pKa=4.7 (Schaner et al., 2005)

and mCerulean3 a pKa=3.2 (Markwardt et al., 2011); thus we expected mCerulean3 to be less sensitive to pH variations in the range found in the mitochondrial matrix, compared to CFP. Of course the pH can modify the efficiency of photons transfer between donor and acceptor, thus a minor pH sensitivity of the donor could compensate the brightness variation caused by the acceptor pH sensitivity. Moreover, proton gradient within mitochondria can change as a result of modifications in mitochondrial membrane potential and in mitochondrial and cytosolic [Ca^{2+}]. Since pH can affect the affinity of GECIs for Ca^{2+} *in vivo*, the pH sensitivity of mitochondrial variants was tested *in situ*. All the variants are insensitive to pH variations in the range tested and 4mtD3mCerulean3+16 appears the more stable variant.

Finally, the evaluation of the Ca^{2+} affinity (K_d), was carried out *in situ*, resulting in a K_{d1} of 0.06 μM and K_{d2} of 10.84 μM in 4mtD3cpV and a K_{d1} of 0.03 μM and K_{d2} of 10.7 μM in 4mtD3mCerulean3+16.

Since the cytosolic probes can be poorly characterized *in situ* and generally a comparison of GECIs physiochemical features is based on *in vitro* characterization, we analysed the features of purified Cameleon variants *in vitro*. In particular, we calculated DR and K_d values for D3cpV and D3mCerulean3+16 variants, mimicking intracellular environment (intracellular-like medium at pH 7) and mitochondrial matrix environment (intracellular-like medium at pH 8). Since we have demonstrated that the cleavage of 4mtD3cpV and 4mtD3mCerulean3+16 targeting sequences occurs inside mitochondria, we produced these proteins for *in vitro* evaluation without 4mt sequence. Up to now only preliminary data have been obtained, however a comparison of *in situ* and *in vitro* data suggests that the DR calculated for cytosolic probes is around 3, while that for a mitochondria like environment is about 2.5. The major difference between *in situ* and *in vitro* DR values was observed for D3cpV. This discrepancy could have different explanations. First, concerning the cytosolic probes, the imprecise minimum FRET assessment performed *in situ* using the ionophore Ionomycin could account for the discrepancy. Second, intra-molecular FRET or homo-FRET could occur and preliminary FLIM data suggest that this phenomena are predominant in the presence of CFP (see below). Generally, it seems clear that alkaline pH, rather than affecting the ratio (as discussed before), causes a reduction of DR in all the Cameleon variants analysed, since it is decreased at pH 8 compared to the one calculated at pH 7 both *in vitro* and *in situ*.

Concerning the Ca^{2+} affinity, just few [Ca^{2+}] concentrations have been tested so far, therefore all the mitochondrial and cytosolic probes display a single K_d. However, further experiments are required to confirm the *in vitro* calculated K_d. Indeed, given the preliminary nature of the *in vitro* results presented, any other consideration would only be a pure speculation.

One of the reasons that led us to substitute CFP with mCerulean3 is also the single exponential lifetime of the latter. To better characterize biophysically the original and new Cameleon probes, lifetime evaluations have been carried out.

FLIM measurements, compared to intensity-based images, have the advantages of being independent on fluorophore concentration, excitation intensity fluctuations, sample thickness, or photobleaching. Moreover, FLIM-FRET allows to distinguish between different types of FRET: homo-FRET, intra- and inter-molecular FRET. Thus, FLIM-FRET will provide a method to calculate FRET-efficiency and to estimate the presence

and the extension of FRET phenomena that do not participate in the detection of a Ca^{2+} transient, such as homo and inter-molecular FRET. The transfer of energy from donor to acceptor induced the appearance of a shorter lifetime(s), besides the classical longer lifetime of the unquenched donor. This phenomenon is measured in the donor channel.

The lifetime of the donor in the presence of the acceptor (τ_{DA}) and the lifetime of the only donor (τ_D) are required to calculate the FRET-efficiency. Usually to obtained τ_D, acceptor photobleaching is performed to mimic the absence of FRET condition. However, the bleaching phenomenon is still poorly understood and it could generate acceptor's fragments that are still able to quench the donor, preventing the possibility to get a real absence of FRET. In 2008 Borst et al, reported a methodology to measure FRET efficiency with FLIM, which consists in the recording of photons in acceptor channel. In this case only the molecule involved in FRET are measured and FRET is visualize as rise time of acceptor fluorescence. This rise time is a consequence of the time-dependent increase in acceptor fluorescence intensity due to energy transfer process from donor to acceptor (Borst et al., 2008).

Our goal is to evaluate FRET-efficiency in Cameleon probes, comparing different techniques to evaluate the *bona fide* of Ca^{2+} changes measurement obtained employing these Ca^{2+} sensors.

First of all, lifetimes of the single FPs have been measured, since they are required for the calibration of the further measurements on Cameleon probes. Indeed, in FLIM-FRET analysis is necessary to fix the donor unquenched lifetime in order to get a reliable measure.

CFP and cpV show a double exponential decays, while mCerulean3 shows a mono-exponential decay. The mono-exponential decay is an advantage in FLIM-FRET characterization, since the data analysis is less complicated and more accurate. Usually, an average lifetime is required for the analysis of bi-exponential decay. Of note, both CFP and mCerulean3 show shorter lifetime(s) in the mitochondrial environments. This effect could be due to phenomena of homo-FRET or to the differences in pH between cytosol and mitochondria.

Preliminary FLIM investigations have also been performed in cells expressing cytosolic and mitochondrial D3 Cameleon probes. For cytosolic probes some attempts have been carried out at physiological [Ca^{2+}], while for the mitochondrial Cameleon, we have only tested the minimum FRET condition. In both cases the longer lifetime, referred to the unquenched donor, has been fixed based on the lifetimes calculate in cells expressing the single FP, with the only exception of CFP. Indeed, FRET-lifetimes fitting analysis were impossible to perform using the CFP lifetime observed *in situ*, thus the longer lifetime has been fixed at 3.57 ns for the fitting of cytosolic and mitochondrial D3cpV data. This lifetime has been calculated in the purified protein (Borst et al., 2008), suggesting that the lifetime calculated *in situ* could be strongly affected by homo-FRET phenomena. In mCerulean3 donor protein this effect is less evident. This hypothesis is also supported by the fact that mCerulean3 is characterized by smaller overlapping area between the absorption and emission spectra, with respect to the CFP protein (Gautier et al., 2001; Markwardt et al., 2011).

Concerning FLIM experiments on cytosolic Cameleon probes, the presence of a second or third lifetime in D3mCerulen3+16 and D3cpV respectively, recorded in the donor channel, underlines that FRET is occurring

in HeLa expressing both cytosolic probes. This data, further confirmed by the presence of the negative lifetime amplitude recorded in the acceptor channel (related to the rise time of cpV), was expected, since these measurements have been carried out in basal FRET condition. To get minimal FRET we exploit acceptor photobleaching technique, since the usage of saturable ionophore is not compatible with the acquisition time required in FLIM experiments. In both D3mCerulean3+16 and D3cpV a reduction in the amplitudes of the shorter lifetimes (referred to the quenched donor) and a parallel increment of the amplitudes associated to longer lifetime (referred to the unquenched donor) were observed in donor channel recordings. Moreover, the negative component measured in the acceptor channel disappeared, meaning that the absence of FRET was obtained. These preliminary data allow us to conclude that acceptor photobleaching can be a suitable alternative to explore FRET efficiency in cells expressing cytosolic probes.

Similarly, in HeLa cells expressing mitochondria targeted Cameleon probes, the lifetimes of 4mtD3cpV and of 4mtD3mCerulean3+16 in minimal FRET condition have been evaluated in both donor and acceptor channel. Shorter lifetimes in the donor channel and a negative component of the amplitude associate to lifetime measured in the acceptor channel have been observed in both probes, underlining the occurrence of energy transfer. Thus, since the absence of Ca^{2+} was not sufficient to get absence of FRET, acceptor photobleaching has been carried out. After bleaching, the acceptor time rise disappear in both cases, the amplitude related to donor longer lifetime increase and the amplitude related to the shorter lifetime decreased as expected when FRET does not occur. Taken together these preliminary results suggest that in Ca^{2+} free condition, other phenomena besides intra-molecular FRET occur. Furthermore, mCerulean3 substitution seems to be less affected by them, providing more accuracy in $[Ca^{2+}]$ detection. Future experiments will be required to clarify these points and to evaluate FRET efficiency at different $[Ca^{2+}]$. Lifetime measurements will be carried out also with the purified proteins.

In summary, data obtained so far make mCerulean3-based Cameleon variants an interesting and promising choice to exploit mitochondrial Ca^{2+} dynamics *in vivo*, since the new probes are brighter, more photostable, less pH sensitive compared to the original probes. Moreover, based on FLIM data, probes containing mCerulean3 seem to be less prone to homo-FRET, making them more accurate in $[Ca^{2+}]$ evaluation.

Thanks to these positive results, some attempts have been performed to get Cameleon expression *in vivo*.

In vivo expression is usually carried out via transgenesis and electroporation *in situ*, time-spending and laborious tasks. Recently, viral infection has been proposed as an efficient *in vivo* delivery technique that permits to overcome this disadvantages. AAVs serotype 9, characterized by cardiac and brain tropism (Pacak et al., 2006; Bish et al., 2008; Foust et al., 2008), have been generated for the expression of each of the mitochondrial and the cytosolic variants of the Cameleons described. After testing the ability to detect Ca^{2+} changes of both neurons and cardiomyocytes primary cultures with the new viruses, a first attempt was made to obtain *in vivo* expression. Preliminary data obtained in heart and brain acute slices, shows that intra-peritoneal injection is suitable to get Cameleons expression in heart tissue, but it is not sufficient to obtain a good expression in the brain. Indeed the latter seems to require intra-cranial injection of AAVs.

In parallel, we create a tool to modulate mitochondrial activities in collaboration with Professor Sekler's group. The creation of ChR2, a light-gated cation channel, allow the generation of sufficient photocurrent to depolarize cells, providing the possibility to optically stimulate and control neuronal activity with very high temporal resolution and offering distinct advantages over traditional pharmacological or electrical means of perturbation (Häusser, 2014). Since mitochondrial membrane potential can modulate diverse mitochondria activities, a mitochondria targeted ChR2 has been created and investigated. A variant of ChR2 called ChR2B was generated, deleting 24 amino acids from N-terminus of ChR2 and fusing the new N-terminal to four signal sequences from subunit VIII of COX, to target the protein to the inner mitochondrial membrane (IMM). Mitochondrial localization was confirmed with both confocal microscopy in different cell lines (HEK293, HeLa and primary neurons), and with electrophysiological recordings performed in the neuronal plasma membrane, to verify the absence of residual 4mtChr2B channels in PM. The proper IMM localization and topology has been further confirmed in fluorescence quenching experiments employing Trypan blue and proteinase K, two reagents differently permeable through the mitochondrial membranes, and alamethicin, able to create pores in IMM. The new mitochondrial 4mtChR2B constructs were then tested *in situ* for their capacity to change the mitochondrial membrane potential in response to light. Different ChR variants has been tested and the so called stable step-function opsin ChR2(SSFO) has been chosen, because of its ability to give prolonged photocurrents far outlasting the initiating pulses of light at 460 nm. Moreover, in this variant the closing process could be speeded up by red light when expressed in PM (Yizhar et al., 2011; Prakash et al., 2012). Since the opening of a channel in IMM should trigger mitochondrial membrane potential collapse, allowing a massive influx of cations, the effects of the blue light on the fluorescence signal of the mitochondrial potential probe TMRM has been tested, confirming the ability of the mitochondrial targeted SSFO-YFP to induce mitochondrial depolarization, although with a slow kinetic. A different approach, recording TMRM signal with a minute of delay after ChR photoactivation has been employed, demonstrating that 540 nm wavelength interferes with the opening kinetic, maybe causing a partial closure. However, no direct evidence of channel closure following exposure to red light has been obtained so far. For sure further efforts should be done testing different wavelengths in the red light spectra at different light power and with different light pulse duration, in order to clarify if SSFO maintains its reversibility in mitochondrial membrane. Indeed ChRs are highly voltage-sensitive channel, thus it is not excluded the possibility of a change in their biophysical properties due to the higher potential across mitochondrial membrane compared to PM.

Given that Ca^{2+} uptake in mitochondria is strictly dependent on membrane potential, we analyzed in more detail the Ca^{2+} uptake characteristics in the presence of the mitochondria targeted SSFO, using Cameleon probe 4mtD3cpV. The amplitude of the mitochondrial Ca^{2+} rise observed upon stimulation with Histamine of SSFO expressing cells was drastically reduced by a 460 nm light pulse. Similar results were obtained with mt-Aeq and this effect was strengthened by pre-illuminating the sample with blue-light. Of note, a complete abolishment of Ca^{2+} uptake has been never observed. Concerning FRET experiments, this fact could be explained firstly by the usage of a high affinity Ca^{2+} probe. Indeed, also FCCP treatment show a passive

influx of Ca^{2+} in mitochondrial matrix through the MCU (data not shown). Moreover, the co-transfection of Cameleon and SSFO, tested in confocal microscopy, reveals an efficiency of about 80% (data not shown), thus also cells expressing 4mD3cpv but not SSFO are considered in the analysis. Similarly in mt-Aeq experiments, a cell population analysis has been exploited; thus, since the SSFO-YFP is usually expressed in 50% of cells while mt-Aeq has higher efficiency of transfection (confocal microscope analysis, data not shown), the average peak included also cells expressing Aequorin but not SSFO. Furthermore, it is well known that bioluminescence generate a low amount of 460 nm light (Brini, 2008), causing an incomplete channel's photoactivation. Nevertheless, mitochondrial membrane potential collapse strongly depend on the generated photocurrent, which in turns has an amplitude dependent on the number of channel expressed in IMM (that could vary), on the light intensity and on the pulse duration employed during the channel photoactivation.

Aequorin experiments confirmed that the reduction in mitochondrial Ca^{2+} peak was not due to an intrinsic toxicity of the SSFO expression, but depends on the depolarization induced by SSFO photoactivation. In particular, when a much smaller Ca^{2+} rise (and thus less light emitted by aequorin) was induced in mitochondria by activating mitochondrial Ca^{2+} uptake through CCE, no difference was observed between controls and SSFO expressing cells. Also cytosolic Ca^{2+} rises were unaffected by SSFO expression compared to controls. Finally, SSFO-YFP expressed in neonatal rat cardiomyocytes after channel photoactivation, was able to block spontaneous beatings, resembling quantitatively and kinetically the effect of FCCP.

Taken together this data demonstrated that the new generated mitochondria targeted SSFO is functional and non-toxic. The variant is able to mediate mitochondrial membrane potential depolarization and in turn it can modulate diverse mitochondria activities in a temporary-controlled, and cell-specific manner, offering an approach to quantitatively investigate its role in a large variety of critical cellular processes. Although more information on the channel kinetics and on its closure when expressed in the mitochondria membrane is required to achieve better time-resolved control of the mitochondrial membrane potential and functions, this tool offers an entirely new way to test the role of mitochondria in fast processes such as Ca^{2+} ion transport and their influence on excitable cells activity.

Materials and Method

1. Generation and characterization of new Cameleon probes

Constructs generation

mCerulean3 was kindly gifted by Rizzo M. A. (Department of Physiology, University of Maryland School of Medicine, Baltimore, Maryland, United States of America). CFP has been substituted inserting mCerluan3 cDNA between *KpnI* and *SphI* sites in D3cpV-pcDNA3. Restriction sites has been generated by PCR using specific primers: 5'-CGGGGTACCGCCACCATGGTGAGCAAGGGC-3' as forward and 5'-ACATGCATGCGCTTGTAC AGCTCGTCCATGCC -3' as reverse;

The addition of the Kozak consensus sequence (GCCACC) and of the 33 aminoacids N-terminal sequence derived from COX VIII at 5', as well as the insertion of *EcoRI* and *AgeI* sites between CaM and M13 in 4mtD3cpV has been obtained by chemical synthesis (GeneArt Gene Synthesis service from Life Technology). In the mitochondria targeted Cameleon obtained, mCerulean3 has been substituted between *BamHI* and *SpHI* sites, generated by PCR using specific primers: the forward was 5'-GCGGATCCGCCACCATGGTGAGCAAGGGC -3' and the reverse was 5'- ACATGCATGCGCTTGTAC AGCTCGTCCATGCC -3'.

Glycines spacer addition between CaM and M13 was obtained by insertion of annealed oligonucleotides between *EcoRI* and *AgeI* restriction sites.

Oligonucleotides 5'-AATTCGTGCAGATGATGACCGCCAAGGGCGGCGGCGGCGGCGGCGGCGGCG GC GGCGG CGGCGGCGGCGGCGGCGGCAGCAAGAGAAGATGGCAGAAAA-3' (Forward), and 3'-CCGGTTTTCTGCCATCTTCTCTTGCTGCCGCCGCCGCCGCCGCCGCCGCCGCCGCCGCCGCCGCC GCCGCCGCCGCCCTTGGCGGTCATCATCTGCACG-5' (Reverse) has been synthesized by Invitrogen.

For protein purification, D3cpV and D3mCerulean3+16 cDNAs have been cloned in the *E. Coli* expression vector pQE30 (QIAGEN) between *KpnI*/ *HindIII* restriction sites.

For AAV9 generation, D3cpV and 4mtD3cpV cDNAs were cloned in pAAV and AAVs were produced by Vector Biolabs. D3mCerulean3+16 and 4mtD3mCerulean3+16 cDNAs were cloned in pAAV between *BamHI* and *HindIII* sites; 4mtD3cpV, D3mCerulean3+16 and 4mtD3mCerulean3+16 cDNAs were cloned in pAAV-Syn (Plasmid #58880, Addgene) between *HindIII* and K*pnI* restriction sites and AAVs were produced by Dr. L. Zentilin.

4mt-mCerulean3 has been amplified by PCR from 4mtD3mCcerluean3-pcDNA3, using the following primers: forward, 5'-ATGGTACCGCCACCATGAGCGTG-3'; reverse 5'-GGCATGGACGAGCTGTAC AAGTAACTCGAGCA-3'. The PCR product was then cloned in pcDNA3 between *KpnI*/*XhoI* sites.

cpV has been amplified by PCR from 4mtD3mCerluean3, using the following primers: forward, 5'-CGCGGATCCATGGATGGCGGAGTC-3'; reverse 5'-CACAATATCGAGTAACTCGAGCGG-3'. The PCR product was then cloned in pcDNA3 between *BamHI*/*XhoI* sites for cpV, or between *BamHI*/*XhoI* in

4mtD3mCeruelan3-pcDNA3 to get 4mt-cpV.4mt-CFP and CFP in pcDNA3 were already present in the laboratory.

Cell Culture and Transfection

HeLa cells were grown in Dulbecco's Modified Eagles medium containing 10% Fetal Calf Serum, supplemented with L-glutamine (2 mM), penicillin (100 U/ml) and streptomycin (100 µg/ml), in a humidified atmosphere containing 5% CO2. Cells were seeded onto glass coverslips (13-mm diameter for Aequorin experiments, 18-mm diameter for FRET measurements and 24-mm for FLIM) and transfection was performed at 60% confluence using TransIT®-LT1 transfection reagent (Mirus Bio LLC, Bologna, Italy) with 1 µg of DNA in 13-mm and 18-mm coverslips, 2 µg in 24-mm coverslips. FRET or FLIM measurements and confocal imaging were usually performed 24-48 h after transfection.

Neonatal cortical neurons

Primary cortical neurons were obtained from 0-1 day newborn mice (4-6 pups). Cells from mice neonatal cortices were dissociated in trypsin (0.8 mg/ml) for 10 min at 37 °C and digestion was blocked by the trypsin inhibitor (6.3 µg/ml) plus DNAse I (40 µg/ml). Cells were gently suspended in pre-warmed supplemented Minimum Essential Media (MEM; in mM: 20 glucose, 0.5 L-glutamine, 0.0036 biotin, 1 pyruvic acid, also containing 1% N2 supplement, 0.5% B27 supplement, 25 µg/ml penicillin, 25 µg/ml streptomycin, 50 µg/ml neomycin and 10% horse serum). Cells were seeded on poly-L-lysine (100 µg/ml) coated glass coverslips of 15 or 18 mm diameter at a density of 0.5 x 10^6 cells/coverslip. After 24 h, the growth medium was replaced with serum- and antibiotic-free Neurobasal-A medium, containing B27 (2%) and L-glutamine (0.5 mM). Fresh medium (1/5 of total volume) was added every 5th day. At 8 DIV, cells has been infected with 10^{11} GC (genomic content) of AAV9syn-D3cpV, AAV9syn-4mtD3cpV, AAV9syn-D3mCerulean3+16 or AAV9syn-4mD3mCerulean3+16 and Ca^{2+} imaging was performed 96 h after infection. To trigger mitochondrial and cytosolic Ca^{2+} rises, a typical experiment has been performed as follows: after perfusion with extracellular-like medium (see below) containing 1 mM Ca^{2+}, neurons depolarization is triggered with K^+-based medium (see below). Finally neurons are permeabilized for 30 seconds in intracellular-like medium containing 50 µM digitonin and 600 µM EGTA to record minimum FRET. Maximum FRET was reached adding 5 mM $CaCl_2$.

Neonatal cardiomyocytes

Cultures of cardiomyocytes were prepared from ventricles of rats (0–3 days after birth). The heart was removed and rapidly placed in ice-cold HEPES-buffered saline containing in mM: 116 NaCl, 0.8 NaH_2PO_4, 5.3 KCl, 0.4 $MgSO_4$, 5 glucose and 20 HEPES, pH 7.4. Atria were discarded and ventricles were submitted to four subsequent digestions with 0.45 mg/ml collagenase and 5% pancreatin. The first supernatant containing cell debris and blood cells was discarded. Cell suspensions from the three subsequent digestions (20 min each) were centrifuged and the pellet was resuspended in 2 ml of newborn calf serum. Cells were pooled and resuspended in a complete medium DMEM/Medium 199 (4:1) supplemented with 2 mM

glutamine, penicillin (100 U/ml), streptomycin (100 mg/ml), 5% newborn calf serum and 10% horse serum. Cells were then incubated for 1 h at 37°C, allowing a selective attachment of non-myocytes. The unattached cells were plated at a density of 0.6 × 10^6 cell/ml onto 24 mm diameter coverslips coated with laminin (1 μg/cm^2). Immediately after plating, cardiomyocytes have been infected with 10^{11} GC of AAV9-D3cpV, AAV9-4mtD3cpV, AAV9-D3mCerulean3+16 or AAV9-4mD3mCerulean3+16. From DIV1, cells were maintained in DMEM/Medium 199 (4:1) medium containing 5% horse serum and 0.5% newborn calf serum for 3 days. Experiments has been carried out 96 h after infection. Spontaneous Ca^{2+} oscillations have been measured in extracellular-like medium (see below) containing Ca_2Cl 2mM. To evaluate the DR of the probe, cardiomyocytes have been permeabilized for 45 seconds in intracellular-like medium containing 50 μM digitonin and 600 μM EGTA, to record minimum FRET. Maximum FRET was reached adding 5 mM $CaCl_2$.

Immunocytochemistry

Cells were fixed in Phosphate Buffered Saline (PBS) containing 4% paraformaldehyde for 15 min, incubated with 50 mM NH_4Cl for 20 min, permeabilized with 0.1% Triton X-100 in PBS for 3 min and then blocked with 2% BSA and 0.2% gelatine for 30 min; mitochondria were stained using a anti-TOM20 antibody (Santa Cruz Biotechnology, Dallas Texas, USA) (1:100). Alexa Fluor 555 conjugated goat anti-rabbit (Molecular Probes Invitrogen, Eugene) was applied for 1 hour at room temperature. Coverslips were mounted using Mowiol (Sigma-Aldrich Saint Louis, MI). Images were collected at Leica TCS-SP5-II confocal system, equipped with a PlanApo 100×/1.4 numerical aperture objective. For all images, pinhole was set to 1 Airy unit. The Argon laser line (488 nm) was used to excite FPs of the Cameleon sensors and the He/Ne 543 nm laser was used to excite the AlexaFluor555 antibody. Confocal microscopy imaging was performed at 1024×1024 pixels per image, with a 200Hz acquisition rate. Images were elaborated with ImageJ program (Wayne Rasband, Bethesda, USA).

Confocal analysis of mCerulen3 fluorescence and mitochondrial targeting

HeLa cells expressing D3cpV/D3mCerulean3 or 4mtD3cpV/4mtD3mCerulean3 were fixed and then analysed with a Leica SP5 confocal system (DM IRE2) using the Ar/ArKr 458-nm laser line (CFP/mCerulean3) and He/Ne 512-nm laser line (cpV). In order to compare the absolute fluorescence of CFP and of mCerulean3, the measured intensity was normalized to the cpV recorded fluorescence, maintaining the records parameters constant between the acquisitions. Indeed, cpV is present in both probes, thus it was possible to use its fluorescence as a parameter to evaluate the protein expression level in each cell analysed. Confocal microscopy imaging was performed as reported above.

To evaluate the targeting efficiency between old (29 aminoacids) and new (33 aminoacids) optimized mitochondrial targeting sequence, six different fields has been acquired for each condition. The averaged ratio between the number of cells showing the proper mitochondrial localization of the probe and the total number of cells per field expressing the probes has been calculated.

Fluorescence microscope settings for FRET experiments

Live cells expressing the fluorescent probes were analysed using a DM6000 inverted microscope (Leica, Wetzlar, Germany) with a 40X oil objective (HCX Plan Apo, NA 1.25). Excitation light produced by a 410nm LED (Led Engin #LZ1-00UA00 LED) was filtered at the appropriate wavelength (425 nm) through a band pass filter, and the emitted light was collected through a beam splitter (OES s.r.l., Padua, Italy) (emission filters HQ 480/40M (for CFP) and HQ 535/30M (for cpV-YFP); dichroic mirror 515 DCXR). The beam splitter permits the collection of the two emitted wavelengths at the same time, thus preventing artefact due to movement of the organelles. All filters and dichroics were from Chroma Technologies (Bellow Falls, VT, USA). Images were acquired using an IM 1.4C cool camera (Jenoptik Optical Systems) attached to a 12-bit frame grabber. Synchronization of the excitation source and the cool camera was performed through a control unit run by a custom-made software package, Roboscope (developed by Catalin Dacian Ciubotaru at VIMM, Padua, Italy). Exposure time varied from 100 ms to 200 ms, depending on the intensity of the fluorescent signal of the cells analysed. Frequency of image capture depends on the speed of fluorescence changes we were detecting: usually images are acquired every 2-3 seconds, with the only exception of photostability experiments in which 1 image per second is acquired.

During the experiment, cells were mounted into an open-topped chamber and maintained in the proper medium. The extracellular-like medium is composed by modified Krebs-Ringer Buffer, mKRB; in mM: 135 NaCl, 5 KCl, 1 $MgCl_2$, 0.4 KH_2PO_4, 1 $MgSO_4$, 20 HEPES, 11 glucose, pH 7.4 at 37°C (or at 22°c for FLIM experiments), while intracellular-like medium contains in mM: 130 KCl, 10 NaCl, 1 $MgCl_2$, 2 succinic acid and 20 HEPES, 7.0 pH at 37°C. For evaluating pH sensitivity, titration and dynamic range of the probe in mitochondria, a modified intracellular-like medium (called IC) deprived of energy sources has been used: succinic acid was removed. Moreover, HEPES is substituted with 20 mM Tris to get pH 8 at 37°C or 22°C for FLIM experiment.

All media were perfused through a temperature controller (Warner Instruments, TC-324B) to maintain a constant temperature of 37°C in the chamber. Pre-incubations were also performed at 37°C.

Functionality experiments: classical experiments started in extracellular-like medium containing 1 mM $CaCl_2$; after perfusion with 600 μM EGTA, cells were stimulated by perfusion of 100 μM histamine; thereafter:

- in HeLa cells expressing cytosolic probes, the Ca^{2+} ionophore ionomycin (1 μM) was applied in Ca^{2+}-free medium containing 600 μM EGTA to completely empty the stores; then 5mM $CaCl_2$ was applied in extracellular-like medium containing 1 μM ionomycin, to reach high [Ca^{2+}] inside the cell;
- HeLa cells expressing mitochondrial probes were permeabilized using 100 μM digitonin in Ca^{2+}-free intracellular-like medium for 1 minutes; then a saturating $CaCl_2$ concentration (3 mM) was applied.

Data are presented as ratio (R, acceptor/donor) or as FRET changes % of maximum, calculated as:
$R\%= (R-R_{min})/R_{max}-R_{min}) \times 100$.

Dynamic range: minimal and maximal FRET condition has been obtained as described above. DR has been calculated dividing maximal ratio (cpV/CFP or cpV/mCerulean3 fluorescence intensity at saturated $[Ca^{2+}]$) by minimal ratio (cpV/CFP or cpV/mCerulean3 fluorescence intensity in Ca^{2+}-free medium containing 600 µM EGTA).

pH sensitivity: HeLa cells expressing 4mtD3cpV, 4mtD3mCerulean3 or 4mtD3mCerulean3+16 has been permeabilized with 100 µM digitonin in IC Ca^{2+}-free medium containing 600 µM EGTA and the uncoupler 5 µM FCCP (Carbonil cianuro-p-trifluorometossifenil idrazone) for 1 minutes at the physiological mitochondrial pH (pH 8); then cells have been perfused with the intracellular Ca^{2+}-free medium at different fixed pH (7, 7.5, 8.5, 9). Data are presented as FRET % of maximum. Changes in R due to pH has been calculated as the average of absolute values of R in 5 frames normalized to R_{min} and R_{max} at pH 8.

Probes titration: HeLa cells expressing 4mtD3cpV, 4mtD3mCerulean3 or 4mtD3mCerulean3+16 has been pre-permeabilized with 100 µM digitonin in IC Ca^{2+}-free medium containing 600 µM EGTA and the 5 µM FCCP for 1 minutes and then incubated in the same medium without digitonin. Cells were then perfused with IC containing known Ca^{2+} concentrations. At the end of each experiment, saturating $CaCl_2$ concentration (5 mM) was applied. Data are presented as FRET % of maximum. IC supplied with 500 µM BAPTA free acid (Molecular Probes, Life Technology) has been used to achieve $[Ca^{2+}] <1$ µM for K_d evaluation. In solutions with $[Ca^{2+}] >1$ µM, the amount of Ca^{2+} contaminant is calculated with Calcium Green-5N, Hexapotassium Salt (described below).

The data obtained are plotted as $\log_{10}[Ca^{2+}]$ (x-axis) and FRET % of maximum (y-axis) and fitted using Origin 8 SR5 (OriginLab Corporation).

The fitting was made using the following equation (Palmer et al., 2004):

$$R = R_{max1}/(1+(K_{d1}/ [Ca^{2+}])^{n1})+R_{max2}/(1+(K_{d2}/ [Ca^{2+}])^{n2})$$

where R represents the fluorescence intensity ratio cpV/CFP, R_{max} corresponding to the titration end points at 5mM $CaCl_2$, K_d is affinity constant and n is the hill coefficient.

Photostability experiments: HeLa cells expressing the different variants of cytosolic or mitochondrial probes have been illuminated every second using the same laser intensity; images were acquired for 20 minutes in three different FRET conditions. For cytosolic Cameleon probes we analyzed: maximal FRET, obtained in extracellular-like medium supplied with 1 µM ionomycin and 5 mM $CaCl_2$; minimal FRET, obtained in extracellular-like medium containing 5 µM Ca^{2+} chelator BAPTA-AM; basal FRET, obtained in extracellular-like medium supplied with the physiological 1mM $[Ca^{2+}]$.

For mitochondrial cameleon probes, after permeabilization with 100 µM digitonin, we analyzed: minimal FRET, obtained incubating permeabilized cells in intracellular-like Ca^{2+}-free medium containing 600 µM EGTA; maximal FRET, obtained incubating cells in intracellular-like like medium containing 5 mM $CaCl_2$;

basal FRET, obtained incubating cells in extracellular-like medium in the presence of physiological 1 mM $CaCl_2$.

Buffer titration with spectrofluorometer

To evaluate $[Ca^{2+}]$ in IC medium used for the titration experiments, 1 μM of Calcium Green-5N, Hexapotassium Salt (Molecular Probes) was added to the solution and fluorescence was evaluated using a PerkinElmer LS50B spectrofluorometer (excitation and emission wavelengths of 505 and 535 nm, respectively) equipped with magnetic stirring at 37°C.

$[Ca^{2+}]$ concentration is calculated as:

$$[Ca^{2+}]_{free} = 32* [(F-F_{min})/(F_{max}-F)]$$

Where 32 is the dissociation constant (K_d) of Calcium Green-5N calculated in our experimental conditions, F is the fluorescence of the indicator at experimental calcium levels, F_{min} is the fluorescence in the absence of Ca^{2+} and F_{max} is the fluorescence of the calcium-saturated probe .

To measure $[Ca^{2+}]$ in IC Ca^{2+}-free containing BAPTA free acid, 1 μM of Fura2-free acid (Molecular Probes) has been added to the solution and fluorescence is evaluated using either the PerkinElmer LS50B spectrofluorometer equipped with magnetic stirring (display 340 and 380 excitation intensity, 510 nm emission) at 37°C.

$[Ca^{2+}]$ concentration is calculated as:

$$[Ca^{2+}]_{free} = 224* Q [(R-R_{min})/(R_{max}-R)]$$

where 224 nM is the Fura-2 K_d, R represents the fluorescence intensity ratio $F_{\lambda1}/F_{\lambda2}$, in which λ1 (~340 nm) and λ2 (~380 nm) respectively. R corresponding to the titration end points are denoted by the subscripts indicating the minimum and maximum Ca^{2+} concentration. Q is the ratio of F_{min} to F_{max} at λ2 (~380 nm).

Western Blot

HeLa cells expressing D3cpV, 4mtD3cpV, D3mCerulean3+16 or 4mtD3mcerulean3+16 were solubilized in RIPA buffer (50 mM Tris, 150 mM NaCl, 1% Triton X-100, 0.5% deoxycholic acid, 0,1% SDS, protease inhibitor cocktail, pH 7.5) and incubated on ice for 30 min. Insolubilized material was spun down at 4000 x g for 5 min at 4°C. 35 μg of protein were loaded onto polyacrylamide gels (10-12%) and immunoblotted. Proteins were resolved by TruPAGE™ Precast Gels 4-12% (Sigma Aldrich) in TruPAGE™ TEA-Tricine SDS Running Buffer (Sigma Aldrich), blotted onto a nitrocellulose membrane and probed with α-GFP antibody (Rabbit monoclonal; Cell signaling technology, 1:1000).

Protein Purification and imaging

Cameleon probes in pQE30 were transformed in BL21 E. coli (NEB), grown at 37°C. Bacteria were induced with 250uM IPTG (Isopropil-β-D-1-tiogalattopiranoside) over-night at 16°C and lysed in a buffer containing 50 mM sodium phosphate, 0.6 M sodium chloride, triton X-100 0.1%, glycerol 10% and a cocktail of protease inhibitor (EDTA-free, Roche) at pH 8.0. Proteins of interest were selectively bound to HIS-Select Nickel Affinity Gel (Sigma Aldrich) via an N-terminal 6×Histag. The gel with bound proteins was washed with 50 mM sodium phosphate, 0.6 M sodium chloride, 10 mM imidazole, glycerol 10% at pH 8. The protein was eluted in 50 mM sodium phosphate, 0.3 M sodium chloride, and 250 mM imidazole at pH 8. Protein concentration has been determined with Bicinchoninic Protein Assay Kit (Euroclone) and measuring absorbance on the plate reader Infinity M200 (Tecan) at 540 nm. To verify the presence of contaminants and the stability of the protein at 4°C, 5uL of the purified proteins were resolved by TruPAGE™ Precast Gels 4-12% (Sigma Aldrich) in TruPAGE™ TEA-Tricine SDS and stained with Comassie Blue. Fluorescence measurements were conducted on PerkinElmer EnVision plates (excitation filter: 430/24, emission filter: for CFP/mCerulean3 EM=470/24+535/30 for cpV) at 37°C using a protein concentration of 1.2 μM. DR has been calculated in IC containing 600 μM EGTA or 5 mM $CaCl_2$. IC supplied with 500 μM BAPTA free acids has been used to achieve $[Ca^{2+}]$ <1 μM for K_d evaluation. In solutions with $[Ca^{2+}]$ >1 μM, the amount of Ca^{2+} contaminant is calculated with Calcium Green-5N, Hexapotassium Salt (described below).

FLIM

FLIM measurements are carried out using the time-correlated single-photon counting (TCSPC) method. The experimental apparatus is based on a scanning confocal microscope (Olympus IX-71) coupled with a PicoHarp 300 TCSPC electronics (PicoQuant) and two single-photon counting avalanche photodiodes (SPAD, MPD, Italy). Excitation is provided by a frequency doubled Ti:Sapphire fs laser system (Coherent, Mira900-F, 400 nm, 76 MHz), focused onto the sample using a 60× water immersion microscope objective. The laser power on the sample is typically around 50-200 μW. The scan area dimension is selected on the microscope software in order to map single cell in each analysis. The acquisition time is set to 3-5 minutes to collect around 10^4 count in the peak channel.

The fluorescence signal is split in two channels by a 40/60% beam-splitter for the detection of donor emission (Semrock, 482/25 bandpass filter) and of mainly acceptor fluorescence (Semrock, 542/25 bandpass filter). The data acquisition is performed in reverse start-stop mode, with each detected photon assigned to one of the 820 channels with 16 ps width. Lifetime decays, extracted from a ROI, are analyzed with the Symphotime software (PicoQuant) using a model with increasing number of exponential terms until it brought no significant improvement of the quality of the fit. For each decay curve, the instrumental response function (IRF) is obtained by the IRF reconstruction script of the Symphotime software. Its FWHM (Full width at half maximum) is typically of 150-200 ps. The FLIM analysis is performed using a pixel-by-pixel tail-fitting procedure.

Acceptor photobleaching experiments are performed using an Argon laser (Melles Griot, IMA101040ALS) at 514 nm, coupled to the second port of the confocal microscope. FLIM analysis is performed before and after each photobleaching exposure (up to 15 minutes for entire cell) in order to test the effectiveness of the acceptor bleaching.
All experiments are conducted at room temperature at 22 °C.

AAV9 *in vivo* expression

Mice used were C57Bl/6 littermates. The mother (singly housed) of each litter to be injected was removed from the cage. The postnatal-day-1 pups were rested on a bed of ice for anesthetization and then intraperitoneal injections has been performed. Vector solution was drawn into a 3/10 cc 30 gauge insulin syringe. Virus injections were in a total volume of 10 µl of PBS and a total of 10^{11} GC of AAV9-Cameleon probes were injected. After the injection, pups were returned to their cage and the mother was then reintroduced to the cage. Neonatal mice were euthanized 30 days post-injection, hearts and brains were extracted, rinsed in PBS, and then immersion fixed in a 4% paraformaldehyde solution.
All experimental procedures were authorized by the Italian Ministry of Health; all efforts were made to minimize the number of animal used and their suffering. Coronal cortical-hippocampal slices were obtained as previously described (Luvisetto et al., 2004). Briefly, brain was removed and put into ice-cold cutting solution containing (in mM): 120 NaCl, 3.2 KCl, 1 KH_2PO_4, 26 $NaHCO_3$, 2 $MgCl_2$, 1 $CaCl_2$, 10 glucose, 2 Na-pyruvate, and 0.6 ascorbic acid at pH 7.4 (with 5% CO_2/95% O_2).
Briefly, heart was removed and put into ice-cold cutting solution containing (in mM): 118.5 NaCl, 25.0 NaHCO3, 4.7 KCl, 1.2 MgSO4, 1.2 KH2PO4, 1.8, 11 glucose, 11.2 BDM (2,3Butanedione Monoxime).
Slices were obtained by cutting with a Leica Vibratome VT1000S (Mannheim, Germany) 100-150 µ thickness for brain slices and 300 µ for heart slices and imaged in Confocal SP5 as described above after loading with 200 µM TMRM.

Western Blot

Proteins from whole heart tissue has been extracted in lysis buffer containing in mM: 50Tris pH 7,5; 150 NaCl; 10 MgCl2; 0,5 DTT; 1 EDTA; Glycerol 10 %; SDS 2 %; Triton-X 1 %; protease inhibitor Complete mini EDTA-free (Roche). Protein has been quantified. 40 µg of protein per lane. α-GFP (Cell Signalling) 1:500. Secondary antibody .α-rabbit HRP (Biorad)

Materials

Restriction and modification enzymes were purchased from Fermentas Thermo Scientific. FCCP and digitonin were purchased from Sigma-Aldrich; ionomycin were purchased from Calbiochem; Neurobasal-A medium, MEM, N2, B27 supplement, trypsin, L-glutamine, penicillin, streptomycin and neomycin, BATPA-Free Acid, Ca^{2+}-green 5N and Fura-2/AM were purchased from Invitrogen (Carlsbad, CA, USA). All other materials were analytical or of the highest available grade.

Statistical analysis

Off-line analysis of FRET experiments was performed with ImageJ software (National Institutes of Health). cpV and CFP/mCerulean3 images were subtracted of background signals and distinctly analyzed after selecting proper regions of interest (ROIs) on each cell; subsequently, a ratio between cpV and CFP (or mCerulean3) emissions was calculated (R=F530/F430).

Data are presented as a normalized $\Delta R/R_0$ %, where R_0 is the R value at the beginning of the experiment (t_0) and ΔR is the R value at each time (t) of the experiment minus R_0, or as FRET changes % of maximum.

All data are representative of at least three different experiments. Unless otherwise stated, numerical values presented throughout the text refer to mean ± SEM (n=number of independent experiments or cells; ∗ = $p<0.05$, ∗∗=$p<0.01$, ∗∗∗ = $p<0.001$, unpaired Student's t test)

2. Channelrhodopsin experiments

Cell Culture and Transfection

HeLa cells were grown and transfected as mentioned before. Aequorin and FRET measurements were usually performed 48-72 h after transfection. Co-transfection with cDNA of 4mtChR2B(SSFO)/void vector/ChR2B(TR) and Ca^{2+}-probes (Aequorin or Cameleon) was performed in molar ratio 5:1. 2 μM All Trans Retinal (ATR, Sigma) was, routinely, added overnight.

Topology experiments

HeLa cells expressing 4mtChR2B(SSFO)-YFP or 4mtD3cpV (localized in the mitochondrial matrix) or N33D3cpV (localized on OMM) were analyzed using a DM6000 inverted microscope (Leica, Wetzlar, Germany) with a 40X oil objective (HCX Plan Apo, NA 1.25). Excitation light produced by a 460 nm LED (Led Engin LZ1-10DB05 LED) was filtered at the appropriate wavelength (470 nm) through an excitation filter ET470/24, and the emitted light was collected through a long pass filter 515 nm and a dichroic mirror 510 DCXR. All filters and dichroics were from Chroma Technologies (Bellow Falls, VT, USA). Images were acquired using an IM 1.4C cool camera (Jenoptik Optical Systems) attached to a 12-bit frame grabber. Synchronization of the excitation source and cool camera was performed through a control unit ran by a custom-made software package, Roboscope. Images were collected with 0.2 or 0.3 Hz frequency and with 200-ms exposure per image.

Cells were mounted in an open-topped chamber thermostated at 37°C and maintained in an extracellular-like Ca^{2+}-free medium. To cut any YFP facing the extracellular space, cells were perfused with extracellular Ca^{2+}-free medium in the presence of Proteinase K 20 μg/μL (Sigma). Plasma membranes permeabilization was performed with 100 μM Digitonin (Sigma) in an intracellular-like medium. Afterwards, to cut YFP facing the cytosol, cells were perfused with intracellular Ca^{2+} free medium added with proteinase K 20 μg/uL and finally, to quench any YFP facing the inter membrane space, HeLa cells were perfused with intracellular medium added with Trypan Blue 0.5 mg/mL (Sigma).

For alamethicin experiments, plasma membranes of HeLa cells were pre-permeabilized with digitonin (as described above). Alamethicin (20 μg/ml, Sigma) was added in intracellular-like medium to trigger OMM and IMM permeabilization.

Off-line analysis of topology experiments was performed with ImageJ (Wayne Rasband, Bethesda, USA). The YFP fluorescence intensity (subtracted of background signal) was analyzed after selecting proper ROIs on each cell; the intensity was expressed as % of the initial YFP fluorescence. These experiments are carried out without adding ATR, since it has an overlapped spectrum with YFP. A representative scheme of the protocol is presented in Figure 33.

Mitochondrial Transmembrane Potential Measurements (TMRM Assay)

Mitochondrial membrane potential was determined by tetramethyl rhodamine methyl ester (TMRM) fluorescent dye. Cells were loaded for 15-30 minutes, at room temperature, with 20 nm of TMRM in MEM without phenol red (GIBCO, life technology). TMRM fluorescence was viewed using an inverted microscope (Zeiss Axiovert 100) with a ×40 oil objective (Fluar, NA 1.30). Excitation light at 540±7.5 nm was produced by a monochromator (polychrome V; TILL Photonics) and passed through a Zeiss TRITC filter (Emission 573-613 nm) and a dichroic mirror (565 DCXR). Images were acquired using a cooled CCD camera (SensicamQE PCO, Kelheim, Germany). All filters and dichroics were from Chroma Technologies (Bellow Falls, VT, USA).

Images were acquired each 10 seconds (50 ms exposure). For blue light exposure a 460±15 nm produced by a monochromator (polychrome V; TILL Photonics) has been used. Obtained images data were exported for analysis in ImageJ (Wayne Rasband, Bethesda, USA). ATR (2μg/ml final concentration) was added into the culture medium 12hr before experiments.

Fluorescence Ca^{2+} Imaging

HeLa cells expressing the mitochondrial Cameleon probe (4mtD3cpv) co-transfected with SSFO or void vector or ChR2B(TR) were analyzed using a DM6000 inverted microscope (Leica, Wetzlar, Germany) (see above).

Cells were mounted into an open-topped chamber thermostated at 37°C and maintained in an extracellular medium. Classical experiments started in 1 mM $CaCl_2$; after perfusion with 600 μM EGTA, cells were stimulated by applying 100 μM histamine. Cells were pre-illuminated to trigger SSFO opening by employing 460 nm LED (Led Engin LZ1-10DB05 LED) for 10 seconds and the FRET measurements start 1 minute after the illumination.

For off line analysis of FRET experiments see above. Data are presented as a $\Delta R/R_0$ values (where ΔR is the change of the cpV/CFP emission intensity ratio at any time, R0 is the fluorescence emission ratio at the time 0). Numerical values presented throughout the text refer to mean±SEM (N=number of cells; ∗ = $p<0.05$, ∗∗=$p<0.01$, ∗∗∗ = $p<0.001$, unpaired Student's t test).

Aequorin Ca^{2+} Measurements

HeLa cells (0.5×10^5) plated on coverslips (13 mm diameter), after 24 h were transfected and then used for Ca^{2+} measurements 48-72 h after transfection. Cells were incubated at 37°C with coelenterazine (5 μM) for 1 h in extracellular medium and then transferred to the perfusion chamber. All the luminescence measurements were carried out in extracellular medium at 37°C. The experiments were terminated by cell permeabilization with digitonin (100 μM) in a hypotonic Ca^{2+}-rich solution (10 mM $CaCl_2$ in H2O) to discharge the remaining unused Aequorin pool. The light signal was collected as previously described (Brini, et al. 1995).

For mitochondrial Ca^{2+} uptake induced by employing a mix of stimuli, the protocol used is the following. Experiments start in extracellular-like medium containing 1mM $CaCl_2$, after perfusion of 2 minutes with 600 μM EGTA, cells were stimulated by applying a mix of stimuli: histamine (100 μM), CPA (20 μM) and ATP (100 μM). In the indicated cases, cells were pre-illuminated to trigger SSFO opening by employing 460 nm LED (Led Engin LZ1-10DB05 LED) for 10 seconds; the aequorin measurements started 1 minute after illumination.

For CCE activation, cells were pre-treated with the irreversible SERCA inhibitor thapsigargin (100 nM) for 6 minutes in a Ca^{2+}-free, EGTA (600 μM)-containing medium; cells were then perfused with the same medium without the inhibitor and challenged with $CaCl_2$ (0.75 mM).

Statistical analysis

All data are representative of at least three independent experiments. Data were analysed using Origin 7.5 SR5 (OriginLab Corporation) and ImageJ (National Institutes of Health). Unless otherwise stated, numerical values presented throughout the text refer to mean±SEM (N=number of independent experiments or cells; * = $p<0.05$, **=$p<0.01$, *** = $p<0.001$, unpaired Student's t test)

Materials

Restriction and modification enzymes were purchased from Fermentas Thermo Scientific. Histamine, ATP and digitonin were purchased from Sigma-Aldrich, while CPA from Calbiochem. All other materials were analytical or of the highest available grade.

PART-II

SINGLE ORGANELLE FRET-BASED ANALYSIS OF INTRACELLULAR CALCIUM: EFFECTS OF PRESENILINS CARRYING FAMILIAL ALZHEIMER'S DISEASE MUTATIONS ON CAPACITATIVE CALCIUM ENTRY

Introduction

4. Alzheimer's disease

Alzheimer's disease (AD) was first described more than 100 years ago and it represents the most common cause of dementia with an estimated prevalence of 30 million people worldwide, a number that is expected to quadruple in 40 years (Holtzman et al., 2011). Old age is closely linked to AD, but environmental factors and enrichment, diet and hyperlipidemia has been proposed to have an additional role in the onset of the pathology (Förstl and Kurz, 1999).

Although many efforts have been carried out to unravel the causes of this pathology, currently no effective treatments are available and palliative treatments are used to partially slow down the progression of dementia symptoms (Holtzman et al., 2011).

4.1 The pathology

Dementia is an acquired syndrome characterized by a loss or decline in memory and other cognitive disabilities. Around 70% of dementia's cases are classified as AD (Barker et al., 2002), an irreversible neurodegenerative disorder of the central nervous system clinically characterized by the following features:

(1) in the early stage of the pathology: mild impairment in cognitive function, behavioural alterations and slight short-term memory deficits;

(2) in the late stage of the pathology: personality disorders, severe recent memory impairment, learning deficits, language dysfunction, visuo-spatial difficulty, loss of insight (Holtzman et al., 2011);

(3) in the final stage of the pathology (after 5-10 years from the first symptoms): impairment of long-term memory, loss of the ability to recognize familial faces, hallucinations, aggressive behaviour, ambulatory regression, aphasia and impairment of daily living (*e.g.*, dressing, bathing, grooming) (Förstl and Kurz, 1999).

Two forms of AD are defined:

(1) the most common "late onset" (LOAD) form, that affects people > 65 years old;

(2) "early onset" (EOAD) form, which arises in 30-60 years old patients, represents around 5% of total AD cases. Among them, around 15% are hereditary cases (FAD), thus less than 1% of total AD cases, and are caused by autosomal, dominantly inherited mutations in amyloid precursor protein (APP) (Levy et al., 1990), presenilin-1 (PS1) (Levy-Lahad et al., 1995) or presenilin-2 (PS2) (Sherrington et al., 1995). PS1 mutations are associated with a more severe phenotype compared to those in PS2.

Morphologically, AD has a peculiar signature: brain specimens from AD patients show a modest degree of cerebral cortical atrophy, especially at the level of the fronto-temporal cortex and the parietal lobe, and a more significant atrophy of the hippocampus. The loss of brain tissue is generally associated to a dilation of the lateral ventricles. Studies performed using new neuroimaging techniques (such as 18F-FDG PET able to reveal regional brain hypometabolism of glucose) and fluid biomarkers, suggest that AD could be detected pre-clinically, although up to now there is not yet consensus on their diagnostic use (Perrin et al., 2009).

Alois Alzheimer first pointed out in 1907 that the disease, which would later bear his name, has distinct and recognizable neuropathological features (Figure 39):

(1) Senile plaques or Amyloid plaques. These plaques are extracellular accumulations of molecules in the brain, mainly due to the aggregation in fibrils and oligomers of hydrophobic products of APP, called amyloid-β peptides (Aβ, see below) (Kayed et al., 2003). The plaques are often surrounded by dystrophic neurites, microglia and reactive astrocytes (cells involved in the inflammatory response). Two theories have been formulated about the role of the inflammatory response in AD: one proposes that inflammation contributes to brain injury, the other suggests *viceversa* that glial cells play a protective role (Lucin and Wyss-Coray, 2009). Other proteins have been reported to be present in these plaques, such as heparan sulfate glycoproteins, apolipoprotein E, complement proteins, and alpha-1-antichymotrypsin (Perl, 2010).

(2) Neurofibrillary tangles (NFTs). NFTs are intracellular structures localized in neuronal cell bodies. Ultrastructurally, they are composed by a geometrical structure of abnormal fibrils measuring 10 nm in diameter that occur in pairs and are wound in a helical fashion with a regular periodicity of 80 nm (Perl, 2010). They are composed predominantly of aggregated forms of the microtubule binding-protein (tau) hyperphosphorylated. Tau is synthesized and produced in neurons and in glia, where is deputed to bind tubulin and stabilize microtubules. In AD, tau hyperphosphorylation causes its dissociation from microtubules and its tendency to self-aggregate. Data strongly suggest that neurofibrillary pathology contributes to neuronal dysfunction and correlates with the clinical progression of AD (Holtzman et al., 2011). Also in this case, a number of other proteins have been found to be associated with tangles, such as ubiquitin, cholinesterases, and beta-amyloid (Braak H. and Braak E., 1997).

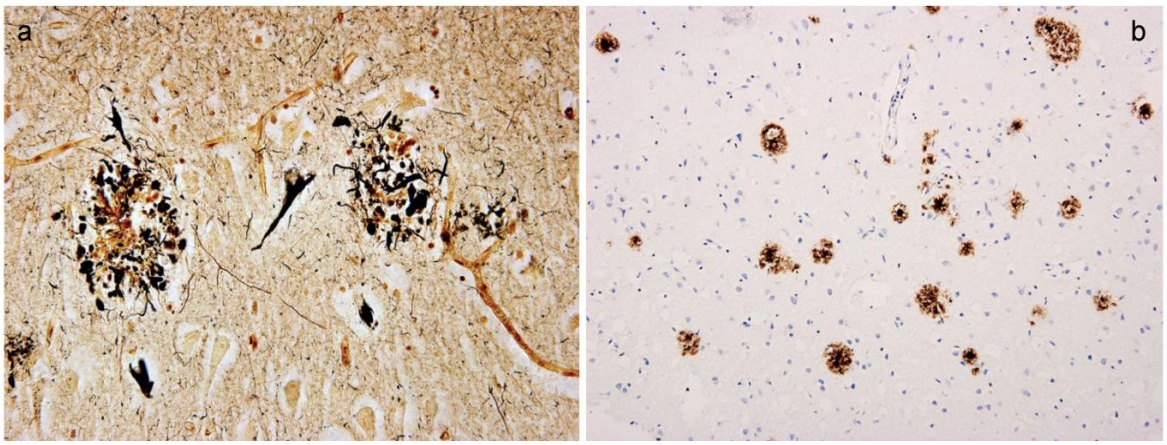

FIGURE 39: a) Two amyloid plaques surrounded by dystrophic neurites and a neurofibrillary tangle between them in the cortex of an AD patient; b) Immuno-histochemical techniques allow to visualize amyloid plaques (modified from Perl, 2010).

4.2 γ-secretase

γ-secretase, is a large enzymatic complex composed of four different integral membrane proteins, responsible for the generation of Aβ from the C-terminal fragment of APP. γ-secretase is an aspartyl-protease that cleaves a number of different substrates, with low specificity (Tolia and De Strooper, 2009). Among them there are APP, Notch, Delta1, E- and N-cadherins, CD44, Nectina-1α, ErbB4 and the β2 subunit of the voltage dependent Na^+ channel (McCarthy et al., 2009). The γ–secretase complex has the peculiar ability of mediating intra-membrane protein cleavage, ability shared with only few other enzymes, called intramembrane-cleaving proteases (I-CLiPs).

Four γ–secretase components have been identified, and they form a complex with a stoichiometry that seems to be 1:1:1:1 (Figure 40). These components are:

(1) Presenilin (either PS1 or PS2), that constitutes the catalytic core of the enzyme (see below for further details) (Tolia and De Strooper, 2009).

(2) Nicastrin (NCT), an 80-130 kDa (depending on the glycosylation state) type I glycoprotein, with the TM domain that interacts with other components of the γ–secretase complex, Aph-1 and PSs (Yu et al., 2000). NCT undergoes a glycosylation/maturation process that causes a conformational change in its ectodomain. This domain is crucial for the incorporation into the γ–secretase complex and contains a DAP (*D*YIGS and peptidase homologous region) domain thought to be critical for the initial binding of the enzyme to substrates. Mature NCT can bind to the ectodomain of APP C-terminal fragment derived from the α-/β-secretase cleavage (see below) and may act as a substrate receptor of γ-secretase (Shirotani et al. 2003).

(3) Antherior Pharynx-defective 1 (Aph-1), is a 7 TM domains protein of 30 kDa with its N-terminus protruding in the lumen and a cytosolic C-terminus. In humans there are two genes coding for Aph-1: Aph-1a and Aph-1b. These variants, together with the two forms of PS, make the composition of the γ–secretase complex highly variable, since different isoforms can participate to its configuration. The GxxxG motif located in its TM4, is necessary for the interaction with Pen-2 and PS. Aph1 interacts with immature NCT and PS to form a relatively stable pre-complex which is then translocated from the ER/cis-Golgi to the Trans-Golgi, for further maturation. Its role is not completely understood, but it seems to work as an initial scaffold for the proper assembly of the entire complex (Lee et al., 2002).

(4) Presenilin Enhancer-2 (Pen-2), is a small hairpin-like protein of about 101 aminoacids with two TM domains and both the N- and C-termini toward the ER luminal side, facing the cytosol. The N-terminus is important for the interaction with PS, while the C-terminus and the TM1 domain are necessary for the endoproteolysis and the following activation of PS, although the mechanism is not clear (Luo et al., 2003).

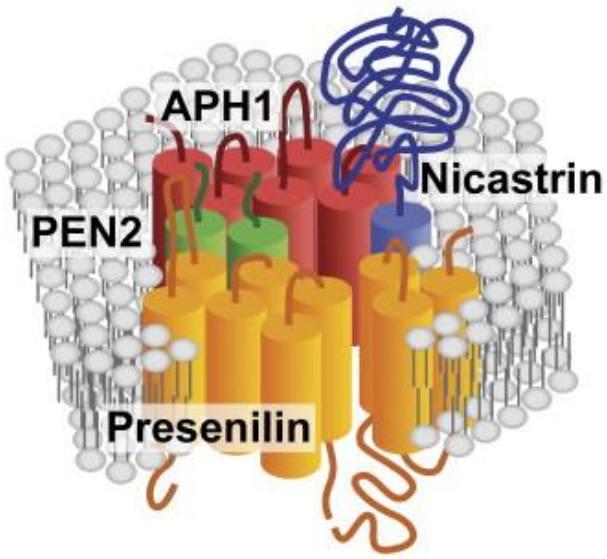

FIGURE 40. Schematic representation of γ–secretase complex (Parks et al., 2007)

Additional proteins might be involved in the regulation of the activity or in the subcellular localization of the complex, and great efforts have been made to determine the precise γ–secretase structure. Despite this, being a membrane-embedded protein complex harbouring at least 19 membrane-spanning domains, crystallization of the purified γ–secretase complex has not been obtained yet (De Strooper et al., 2012).

About the assembly of the complex, different steps are involved in the mature tetramer formation:

(1) NCT and Aph-1 form an initial sub-complex within the ER membrane (De Strooper et al., 2012).

(2) NCT then interacts with PS and Pen-2 sub-complex, which results in the maturation/proteolytic cleavage of PS1 or PS2, to generate its active structure (Kim et al., 2007).

(3) A large amount of these complexes cycles between the ER and Golgi apparatus, but only a small percentage (probably less than 10% of the total) of γ-secretase complexes seems to be active, and reaches endosomes and PM. The final destination of this complex is reached only after the Golgi-mediated glycosylation of NCT (Kaether et al., 2006a and b; Chyung et al., 2005).

As mentioned, γ-secretase has different substrates and their cleavage occur in specific subcellular compartments: APP is mainly cleaved in the TGN and early endosomal domains, whereas Notch is primarily cleaved at the PM (Tarassishin et al., 2004). Thus a disturbance in the localization of the γ-secretase complex may play a role in abnormal Aβ generation and AD pathogenesis (Zhang et al., 2011).

Since γ-secretase plays an essential role in the pathogenesis of AD, being the producer of the Aβ peptide, many efforts have been done to develop γ-secretase inhibitors. However, most of the inhibitors, despite the effectiveness on APP cleavage, displayed toxicity consequently to a non-substrate-specific enzymatic inhibition, due to the large variety of γ-secretase substrates (De Strooper et al., 2012). The non-specific effect is probably due to an impairment in the signalling pathway of Notch, a well-known transmembrane receptor involved in a plethora of cellular pathways, such as neurogenesis.

4.3 Presenilins

Presenilins (PSs) were identified and cloned in the middle of the 1990s (Levy-Lahad et al., 1995; Sherrington et al., 1995). PS1 and PS2 are homologous membrane proteins of about 50 kDa, located mainly in the ER and GA, while they are less abundant in the PM and endosomes. They are highly expressed in the brain, although their expression is detectable in most adult human tissues (Brunkan and Goate, 2005). PS1 and PS2 share an identity of around 65% and they are considered the catalytic core of the γ-secretase complex, since its enzymatic activity is abolished in MEF knockout (KO) for both PS1 and PS2 (Herreman et al., 2000). Structurally, they are characterized by the presence of 10 hydrophobic domains and 9 TM domains, with the N-terminus facing the cytosol and the C-terminus located in the lumen of the organelle (Figure 41). The two catalytically active parts of PSs in the γ-secretase complex are the N-terminal fragment (NTF) and a C-terminal fragment (CTF). NTF of ~ 30 kDa and CTF of ~ 20 kDa are generated from the immature holo-protein by an autocatalytic cleavage within the 7th hydrophobic domain (which is part of a large cytosolic loop) that occurs once PS1 (or PS2) is incorporated into the enzymatic complex forming a dimer. The two aspartate residues critical for the activity of γ-secretase are located into the TM domains 6 and 7; indeed, mutations of these residues lead to the complete inactivation of the enzyme (Kimberly et al., 2000). Despite the cleavage of PS is autocatalytic, PS maturation needs other molecular partners and it is a saturable process. The accumulation of non-mature form of PS, called full length (FL) PS, leads to its proteasomal degradation. Because of this degradation, FL-PSs has a very short half-life, around 1.5 h, compared to half-life of 24 h of the mature form (Kim et al., 1997).

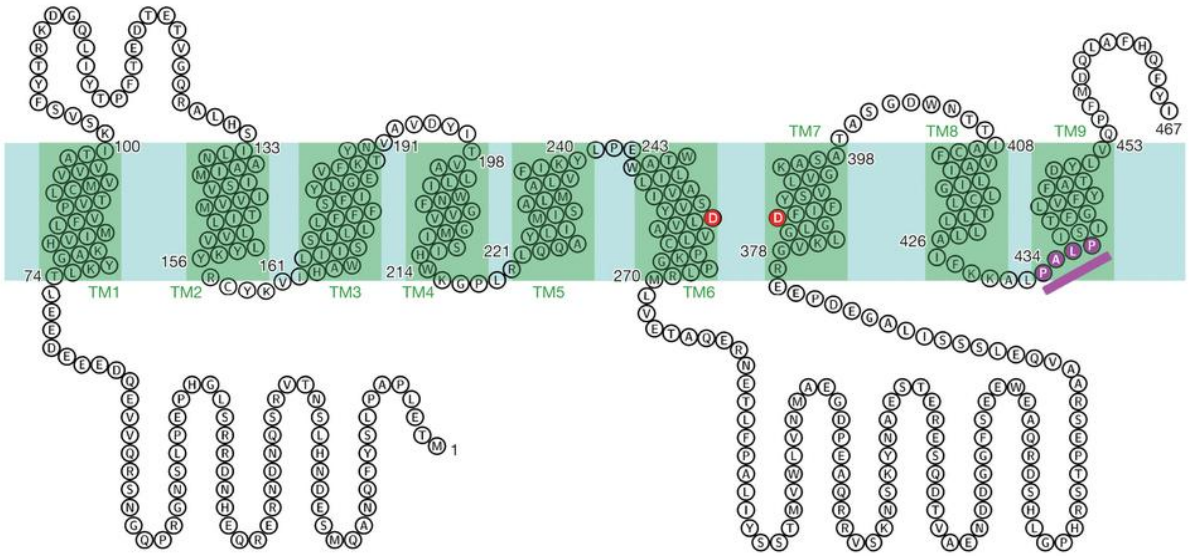

FIGURE 41. Cartoon of the predicted membrane topology of PS1: demarcations for TMs are labelled in green, catalytic aspartates are highlighted in red, substrate recognition sequence PALP is shown in magenta (adapted form Li et al., 2012)

As mentioned before, PSs are the catalytic core of the γ-secretase complex that cleaves APP generating Aβ peptides of different lengths. Among them, the most hydrophobic and, thus, the most prone to aggregate is Aβ42. To date, 185 mutations in PS1 and 13 in PS2 have been associated to the onset of FAD

(http://www.molgen.ua.ac.be). Initially, in different cell models and in transgenic mice carrying FAD-PS mutations, an increased production of Aβ42 associated to an augmentation of the γ-secretase activity it has been reported, suggesting a gain-of-function mechanism of action for FAD-PS mutations (Scheuner et al., 1996; Citron et al., 1997). Recently, however, studies in different experimental AD models have proposed a loss-of function of the γ-secretase activity linked to FAD-PS mutations. Indeed, these studies reported an increase only in the Aβ42/Aβ40 ratio, as a consequence of a drop in the production of Aβ40, suggesting an overall decreased activity of the γ-secretase complex (Florean et al., 2008; Walker et al., 2005; Shimojo et al., 2007). This issue is still under debate, however it is a critical point in AD pathogenesis, since Aβ42 is thought to initiate the oligomerization of all the Aβ species.

Despite their well-established role in γ-secretase activity, PSs have also pleiotropic independent functions, ranging from regulation of Ca^{2+} homeostasis (see below), neurite outgrowth, apoptosis, autophagy, synaptic functions and tumorigenesis (reviewed in De Strooper and Annaert, 2010; De Strooper et al., 2012).

4.4 The "amyloid cascade hypothesis"

In the 1980s, AD associated amyloid plaques were first purified, clarifying their identity of multimeric aggregates of Aβ polypeptides containing about 40 aminoacid residues (Glenner and Wong, 1984). By cloning Aβ peptide complementary DNA (cDNA), it was demonstrated that Aβ is derived from APP (Tanzi et al. 1987). The APP encoding gene, localized on the long arm of chromosome 21, consists of 18 exons and undergoes tissue-specific splicing, generating different isoforms ranging from 365 to 770 aminoacids: the APP695 isoform is predominant in neurons (Matsui et al., 2007).

The APP consists of a large extracellular portion, a hydrophobic TM domain and a short C-terminus that designates the APP intracellular domain (AICD). It is a member of the family of type I transmembrane proteins, which in mammals includes APP and the APP-like protein 1 and 2 (APLP1/2). These proteins contain different well conserved domains, particularly the extracellular domains E1 and E2 and the intracellular domain, while APP is the only one containing the Aβ domain. Despite this latter difference, the functions of the three proteins appear redundant, as demonstrated by combined KO studies (Wolfe and Guènette, 2007). Despite the fact that it is not clear which one is the primary function of these proteins, APP and APP-like proteins have been proposed to be involved in different cell processes: brain tropism, cellular adhesion, cell signalling, axonal transport, transcriptional regulation, synapse formation, neuronal plasticity, iron export and cell migration (reviewed in Guo et al., 2012). One explanation for such a heterogeneous set of functions can be found considering the extensive post-translational modifications of APP that lead to the generation of different peptides. Indeed APP can undergo glycosylation, phosphorylation, sialylation, and tyrosine sulfation, as well as many types of proteolytic processing to generate several peptide fragments. APP has been found in different subcellular compartments*, e.g.,* ER, GA, PM, endosomes, autophagosomes and lysosomes and it (or its fragments) can be transported to mitochondria, cytosol, nucleus etc. (Reviewed in Muresan and Muresan, 2015).

APP can undergo two distinct and competitive maturation pathways, one amyloidogenic and the other non-amyloidogenic (Thinakaran and Koo, 2008) (Figure 42). The latter is predominant and is mediated by the α-secretase cleavage in the 17th aminoacid of Aβ peptide, generating:

(1) a soluble N-terminal fragment, released in the extracellular space (sAPPα),

(2) a C-terminal fragment (C83), that remains bound to the membrane, further cleaved by the γ-secretase complex (see below) (Zhang et al., 2012).

The amyloidogenic pathway is responsible for the generation of the toxic Aβ peptide: APP is firstly cleaved by the β-secretase at the 11th residue (so called β' site) of the future Aβ peptide, generating:

(1) a soluble N-terminal fragment released in the extracellular environment (sAPPβ)

(2) a C-terminal domain bound to the membrane (C99) (Cole and Vassar, 2007).

C83 and C99 can be further processed by γ-secretase in the region corresponding to the TM domain of APP, generating:

a. from C83: an extracellular non-pathogenic peptide P3 and an intracellular AICD, that may migrate to the nucleus to regulate transcription

b. from C99: the amyloidogenic Aβ peptide, which is released in the extracellular space, and again an AICD (Thinakaran and Koo, 2008).

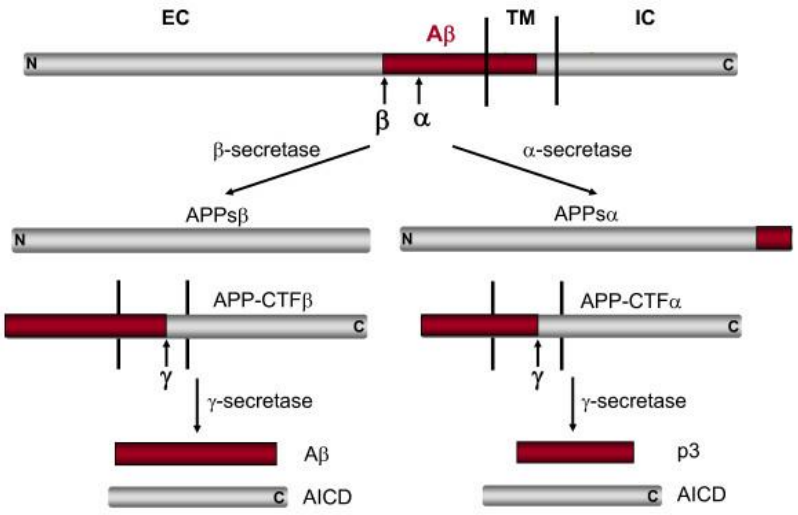

FIGURE 42. Schematic representation of APP processing by secretases (Zheng and Koo, 2011).

Of note, different cleavage sites for γ-secretase are present on APP, thus peptides of different lengths can be generated, ranging from 38 to 49 aminoacids. The most abundant is Aβ40 while about 10% of the total is represented by Aβ42, more hydrophobic and more susceptible to oligomerization.

Three type I integral membrane proteins, called the α-disintegrin and metalloproteinase (ADAM) type 9, 10 and 17, have been proposed to be components of the α-secretase. ADAMs belong to the zinc protease super

family and are implicated in the control of cytokine and growth factor shedding. ADAM10 is widely expressed in the brain and in other tissues and different evidence, both in cells (Kojro et al. 2001) and mice (Postina et al. 2004), shows that its over-expression is able to cause an increase in sAPPα levels, while reducing Aβ generation/plaque formation. Moreover, the expression of a catalytically-inactive form of ADAM10 increases the size and number of amyloid plaques in mouse brains (Postina et al. 2004). Thus, ADAM10 seems to be responsible for constitutive α-cleavage activity. Conversely, ADAM9 and ADAM17 are more likely involved in the regulation of the α -cleavage of APP, since sAPPα generation is not affected in ADAM9/17 knockdown in cells or in ADAM9/17 KO mice, while the over-expression of ADAM9/17 increases the level of sAPPα (Zhang et al, 2012).

The protagonist in Aβ generation is the so called β-site APP cleaving enzyme 1 (BACE1), identified and characterized in 1999 (Sinha et al., 1999). Knocking out BACE1 prevents Aβ generation and completely abolishes Aβ pathology in mice expressing the Swedish mutation of human APP (Cai et al. 2001). BACE1 is a 501 amino acids type I transmembrane aspartyl-protease with its active site located on the luminal side of the membrane. It is predominantly expressed in perinuclear post-Golgi membranes, vesicular structures and PM (Ehehalt et al., 2002).

The amyloid cascade hypothesis (Figure 43) proposes that neurodegeneration observed in AD is due to a series of events generated by the altered processing of APP and subsequent production of the Aβ peptide (Hardy and Selkoe, 2002). Indeed, different studies have demonstrated that Aβ42 is more susceptible to oligomerization and can form the initial nucleus for subsequent Aβ40 deposition, leading to the formation of fibrils found in amyloid plaques (Chen and Glabe, 2006). Moreover, FAD-linked APP, PS1 and PS2 mutations are able to promote the amyloidogenic pathway, favouring the APP processing mediated by β– and γ–secretases. Different mechanisms have been proposed to explain the pathogenic activity of Aβ, among them: alteration of Ca^{2+} homeostasis, mitochondrial and energy metabolism dysfunctions, formation of cationic channels on PM, oxidative stress due to ROS over-production, cytoskeletal and axonal transport alterations, inflammatory processes, increase susceptibility to pro-apoptotic and pro-necrotic stimuli (Parihar and Hemnani, 2004; Fiala, 2007; LaFerla et al., 2007; Gandy, 2005; Querfurth and LaFerla, 2010).

However, since the number of senile plaques does not correlate with AD progression, and they are, indeed, also present in the brain of old healthy subjects, it has been proposed that Aβ soluble oligomers, and not the insoluble fibrils, are the toxic form at the basis of synaptic dysfunctions (Haass and Selkoe, 2007). The latter hypothesis is sustained mainly by the following evidence:

(1) the level of soluble Aβ forms correlates with the degree of cognitive impairment,
(2) one of the best known process involved in memory formation, called long term potentiation (LTP), is inhibited by Aβ soluble oligomers (Walsh et al., 2002), despite no proved mechanistic explanations has been found.

Many possibilities are still open: plaques could represent inert aggregates of Aβ, or they could form a reservoir of smaller, soluble species, or even they could sequester the oligomers, protecting the brain.

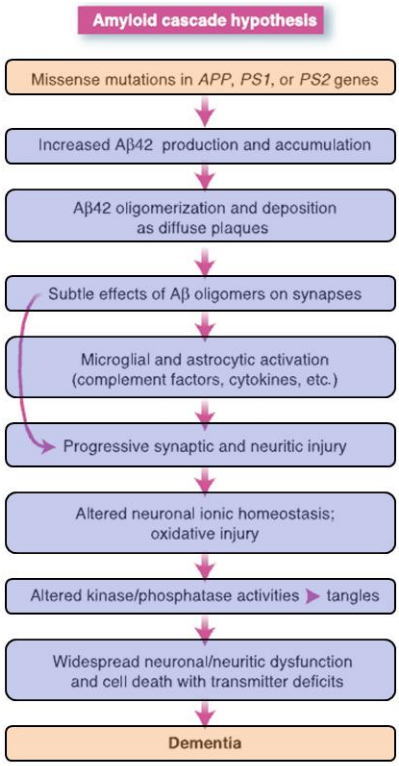

FIGURE 43. The amyloid cascade hypothesis (Hardy and Selkoe, 2002).

4.5 The hyperphosphorylated tau hypothesis

AD belongs to a group of neurodegenerative diseases collectively designated as ‘‘tauopathies’’, characterized by the mechanism of abnormally phosphorylated tau protein aggregation (Martin et al., 2011). Tau protein was identified in 1975 (Weingarten et al., 1975) as a microtubule-associated protein, able to stabilize the cytoskeleton. Exclusively found in higher eukaryotes, it is highly conserved, with a preferential expression pattern in neurons.

Tau protein is characterized by four regions: an acidic region in the N-terminal part, a proline-rich region, a microtubule-binding domain containing “four repeat” domains and a C-terminal region. The phosphorylation site is a serine, located in the conserved consensus motif KXGS of each repeat domain (Ozer and Halpain, 2000). Various kinases and phosphatases regulate tau phosphorylation, with each tau phosphorylation site subjected to the action of one or more protein kinases. This phosphorylation is the basic mechanism by which tau function is regulated. Tau kinases are grouped into three classes: proline-directed protein kinases (PDPKs), protein kinases non-PDPKs and protein kinases specific for tyrosines. The consequence of tau hyperphosphorylation is a decreased affinity for microtubules, which results in the destabilization of the neuronal cytoskeleton (Sengupta et al., 1998). Moreover, phosphorylation specifically promotes tau self-aggregation (Martin et al., 2011).

The “tau hypothesis” considers tau hyperphosphorylation as the initial event that causes tau accumulation as paired helical filaments that in turn aggregate into masses within nerve cell bodies (known as neurofibrillary tangles) and dystrophic neurites associated with amyloid plaques. Moreover cytoskeleton destabilization is well known to impair important cell functions, including axonal growth, vesicle and organelle transport as

well as nervous signal propagation along the nerve network (LaPointe et al., 2009). This hypothesis is supported by the fact that alterations in the expression and/or the activity of tau kinases such as GSK3β, CDK5, DYRK1A, p38 and CK1 have been reported in the brains of AD patients, suggesting that one or several of them could be involved in tau hyperphosphorylation (Chung, 2009).

4.6 The "Ca^{2+} hypothesis"

The pathogenesis of AD is very complex and involves many molecular and cellular events, including the accumulation of β amyloid and the hyperphosphorylation of tau. However, the poor correlation between senile plaques and Aβ levels, together with the observation that plaques and NFTs appear evident only in late stages of the pathology, cast doubts about the validity of the two previously exposed hypotheses. Another mechanism has been proposed, suggesting an early, central role for Ca^{2+} in the pathogenesis of AD, leading to the formulation of the Ca^{2+} hypothesis (Figure 44).

As discussed in the first part of the thesis, Ca^{2+} is one of the most important and versatile intracellular second messenger, particularly relevant at neuronal level, where processes such as excitability, neurotransmitters release, long term synaptic plasticity and gene transcription depend on intracellular [Ca^{2+}] (Berridge, 1998). The Ca^{2+} hypothesis proposes that neurodegeneration observed in AD is due to a sequence of events linked to alterations in intracellular Ca^{2+} handling.

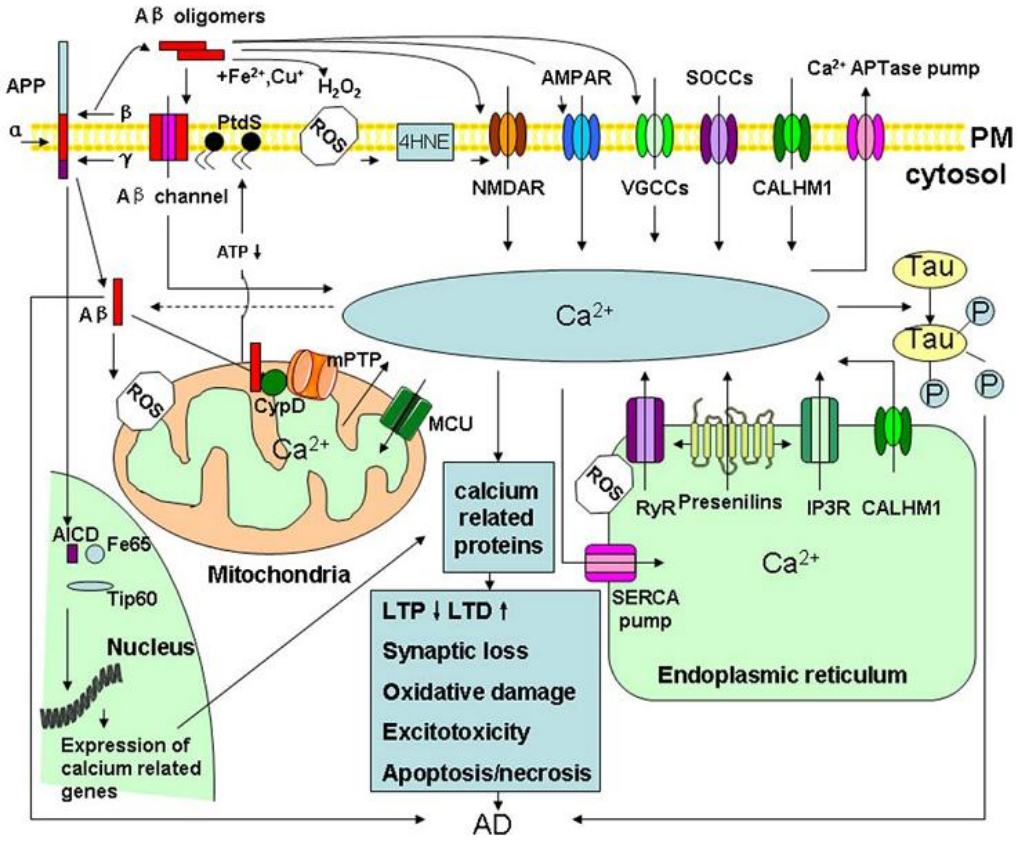

FIGURE 44. Scheme of possible links between Ca^{2+} handling alterations and AD (Yu et al., 2009).

Mutations in PSs have been variably correlated to alterations in Ca^{2+} signalling and different molecular targets have been identified, suggesting a physiological role for these proteins in Ca^{2+} homeostasis. In 1988 Khachaturian firstly proposed sustained alterations in Ca^{2+} homeostasis as responsible for AD degeneration. After few years, evidence supporting this hypothesis was provided: studies in fibroblasts from asyntomathic but FAD-PS expressing patients, reported an increased IP3-mediated Ca^{2+} release from the ER, suggesting alterations in Ca^{2+} homeostasis as an early event in AD pathogenesis (Ito E. et al., 1994; Etcheberrigaray R. et al., 1998). These studies represent the starting points of what will become the "Ca^{2+} overload" hypothesis. This hypothesis sustains the idea that FAD-linked PS mutations, by increasing stored Ca^{2+} content, cause excessive Ca^{2+} release from the ER, increase sensitization to Aβ and produce exocitotoxic stimuli, eventually leading to cell death via Ca^{2+}-dependent mechanisms (Zampese et al., 2009).

Different data (reviewed in Honarnejad and Herms, 2012) support this hypothesis:

(1) different FAD-PS1 cell models, including neurons, and FAD-PS1 transgenic mice present an increased ER Ca^{2+} release upon activation;

(2) FAD-PS1 and FAD-PS2 mutations induce a potentiation of ER Ca^{2+} release from RyRs, probably due to an increased expression level of the RyR itself;

(3) FAD-PS1 and FAD-PS2 mutations increase ER Ca^{2+} release via IP_3;

(4) wt PS holoprotein forms passive Ca^{2+} leak channels on planar lipid bilayers and FAD-PS mutants impaire this leak activity, leading to an increased ER Ca^{2+} content.

Recently, conflicting data against the Ca^{2+} overload hypothesis, together with alternative explanations of old data, emerged, thus opening a new scenario. In particular, new studies prove that:

(1) An increase in the ER Ca^{2+} release is observed also in the absence of ER Ca^{2+} overload, due to the hyperactivity of ER releasing Ca^{2+} channels (Cheung et al., 2008; Green et al., 2008; Cheung et al., 2010).

(2) FAD-linked PS1 mutations lead to an unchanged, or even attenuated, ER Ca^{2+} level (McCombs et al., 2010).

(3) No evidence, in agreement with predictions made by the hypothesis that PS1 holoproteins function as ER Ca^{2+} leak channels, was found (Shilling et al., 2012)

(4) The FAD-linked PS2 mutations M239I and T122R reduce Ca^{2+} release in both fibroblasts from FAD patients and cell lines stably or transiently expressing the PS2 mutants (Zatti et al., 2004; Giacomello et al., 2005).

(5) [Ca^{2+}] measurements in different cell lines expressing FAD-linked PS1 mutations do not show an increase in the Ca^{2+} level in the ER and GA (Zatti et al., 2006); on the contrary, expression of FAD-linked PS2 mutations causes a reduction in [Ca^{2+}] within the stores, due to the inhibition of the SERCA pump (Zatti et al., 2006; Brunello et al., 2009). Recently in our laboratory, it has also been demonstrated that neurons from FAD-PS2 transgenic mice present a reduced Ca2+ response to IP3-generating stimuli, but an increased one to the RyR activator caffeine (Kipanyula et al., 2012);

Although the impairment in store Ca^{2+} handling seems a common effect of a heterogeneous group of FAD-linked PS mutations, the absence of an ER Ca^{2+} overload suggests that the enhanced Ca^{2+} release, reported before upon expression of various FAD-linked PSs, might depend on different mechanisms, not linked to an increased amount of Ca^{2+} within the stores (Zampese et al., 2009).

Moreover, PSs have been reported to physically interact with SERCA2b, IP3Rs and RyRs (reviewed in Honarnejad and Herms, 2012), thus revealing a complex and multifaced role of PSs in the modulation of Ca^{2+} homeostasis. Some attempts to clarify the PSs role in Ca^{2+} homeostasis have been carryied out using MEF cells double KO for both PS1 and PS2. However, inconsistent results have been obtained, describing either attenuated (Kasri et al., 2006) or amplified (Tu H. et al., 2006) Ca^{2+} release from the ER.

Furthermore, an enrichment of PSs at Mitochondria-Associated Membrane (MAM) level has been recently reported (Area-Gomez et al., 2009). Since mitochondria are often called into question as involved in AD pathogenesis, our group has investigated the role of PSs in mitochondria-ER Ca^{2+} connection. We showed that over-expression of PS2, but not PS1, is able to increase the mitochondrial Ca^{2+} transfer from the ER, while PS2 knockdown reduces it. Indeed, when PS2 is over-expressed, an increase in mitochondrial-ER contacts occurs, which in turn could exacerbate neuronal dysfunction, stimulating apoptosis. However, the increase in organelles' contacts could have instead a protective role, mitigating the energetic defect linked to the partial ER Ca^{2+} depletion associated to PS2 over-expression (Zampese et al., 2011).

In addition to the Ca^{2+} handling impairment described so far and the modulation of CCE that will be discussed below, other mechanisms have been implicated in PSs-linked FAD pathogenesis, on the basis of their either physical or functional interaction with proteins involved in cellular Ca^{2+} handling (Zampese et al., 2009), such as sorcin (Pack-Chung et al., 2000), calsenilin (Buxbaum et al., 1998) and calcindin (Guo et al., 1998). Moreover, mRNA levels of several genes involved in the maintenance of Ca^{2+} homeostasis are altered in cerebral tissue from AD patients (Emilsson et al., 2006).

As reported before, amyloid metabolism can influence synaptic plasticity and neuronal apoptosis. According to the Ca^{2+} hypothesis, these cellular events are due to the remodelling of Ca^{2+} signalling through two main pathways:

(1) Aβ oligomers trigger Ca^{2+} entry through different proposed mechanisms: the formation of cationic channels in PM, the direct/indirect activation of PM Ca^{2+} channels, or the peroxidation of membrane lipids that results in the disruption of the membrane integrity (Berridge, 2012).

(2) Aβ oligomers increase Ca^{2+} release from ER, through three proposed mechanisms:
    a. Enhancing the sensitivity and gating of IP3R and RyR channels (Demuro and Parker, 2013; Oules et al., 2012);
    b. Increasing the expression of RyRs (Supnet et al., 2006);
    c. Altering the IP_3/DAG pathway, by destabilizing the phosphatidylinositol-4,5-bisphosphate metabolism (Berman et al., 2008).

Recently, in our lab, using different Ca^{2+} probes to monitor $[Ca^{2+}]_c$ and $[Ca^{2+}]_{ER}$ in cortical neurons, it has been shown that:

- acute application of Aβ42 (monomers or oligomers) at near-physiological levels (0.5-1 μM) does not cause neither Ca^{2+} influx nor Ca^{2+} release;
- incubation of neurons with Aβ42 oligomers (0.5 μM) causes the reduction of Ca^{2+} release mediated by IP_3-generating agonists, while increasing Ca^{2+} release mediated by caffeine (a RyR agonist). Both effects do not depend on alterations of the total store Ca^{2+} content (Lazzari et al., 2014).

Finally, Aβ is reported to affect LTP by interfering with NMDA and AMPA receptors (two ionotropic glutamate receptors) activity (Haass and Selkoe, 2007; Querfurth and LaFerla, 2010).

The data reported suggest the possibility of an interconnection between the "amyloid cascade" and the "Ca^{2+} hypothesis" in AD pathogenesis.

Recently, also a single nucleotide polymorphism in CALHM1 (a newly discovered Ca^{2+} channel) has been reported to modulate the permeability of the channel to Ca^{2+}; CALHM1 polymorphism has been considered a risk factor for sporadic AD (Dreses-Werringloer et al., 2008), although different recent studies argued against this finding (reviewed in Supnet and Bezprozvanny, 2010).

All the described evidence makes the AD Ca^{2+} hypothesis an interesting field to explore, in order to unravel the cellular alterations taking place in the initial stages of the pathology. Indeed, despite many efforts have been done to clarify these processes, a huge debate is still open, requiring further deeper investigations.

5. Capacitative Ca^{2+} entry

As extensively discussed in the introduction of PART-I, two are the main mechanisms causing $[Ca^{2+}]_c$ rises: the release of Ca^{2+} from intracellular Ca^{2+} stores and the influx of Ca^{2+} from the extracellular space. The latter mechanism represents, in non-excitable cells, the so called Capacitative Ca^{2+} Entry (CCE) or Store-Operated Ca^{2+} Entry (SOCE). Its activation involved different steps (Figure 45):

(1) A stimulus, such as a hormone or neurotransmitter, triggers the release of Ca^{2+} from the ER, through IP3Rs o RyRs. An alternative pathway to empty the store is the inhibition of SERCA pump that prevents ER Ca^{2+} re-entry.

(2) A sensor, called STIM (STromal Interaction Molecule), is able to sense the $[Ca^{2+}]_{ER}$ thanks to its EF-domain. Ca^{2+} release from the ER decreases the concentration of this ion in the organelle, which is sensed by STIM that thus oligomerizes.

(3) STIM, moving along microtubules, reaches the PM, where it forms punctae interacting with Orai (or CRAC channel, where CRAC means Ca^{2+} release-activated Ca^{2+}), a protein located in the PM and able to form a Ca^{2+}-channel. In particular, four Orai1 molecules create the pore-forming subunit of the channel that opens upon stimulation by STIM1, via interaction of the C-terminus of STIM1 with the N-terminus of Orai1 (Lewis, 2007).

(4) Ca^{2+} enters the cell and refills the ER (Clapham, 2007).

Mutations in the main actors of CCE, STIM and Orai, are associated with severe phenotypes in both animals and humans: *e.g.*, Severe Combined ImmunoDeficiency (SCID) syndrome is due to mutation in Orai1 or STIM1 genes (Feske, 2009).

Many regulators (scaffolds, Ca^{2+} binding-proteins and chaperones) has been reported to interact with STIM and Orai, to finely tune their activities (reviewed in Shim et al., 2014). Moreover, CCE is inhibited by an intrinsic negative feedback called CDI (Ca^{2+}-dependent inactivation), whose molecular mechanism is still poorly understood (Muik et al., 2012).

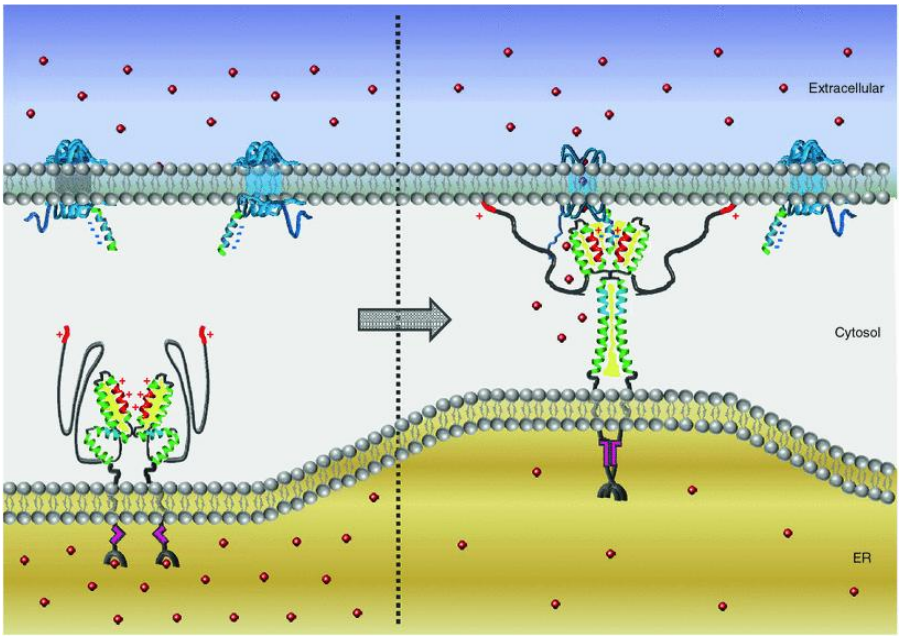

FIGURE 45. Model for STIM1 activation and coupling to Orai1 (Muik. et al., 2012).

Recently, it has also been reported that CCE activation occurs properly only if mitochondrial Ca^{2+} uptake is functional. Indeed, by knocking down MCU and UCP2, it has been shown that mitochondrial ability of shaping IP3-generating Ca^{2+} microdomains is essential to trigger STIM1 oligomerization. Moreover, it has also been reported that the mitochondrial buffering of Ca^{2+} influx is crucial for the maintenance of SERCA-inhibition-induced CCE (Deak et al., 2014).

Furthermore, recently, it has been demonstrated that other Ca^{2+} influx pathways are regulated by ER/SR Ca^{2+} depletion, involving Orai and STIM. Two studies (Park et al., 2010; Wang et al., 2010) reported an interesting role of STIM1 in the regulation of a particular type of VOCCs, called Cav1.2. The latter is an L-type channel expressed in neurons, heart and skeletal muscle, excitable tissues in which CCE is supposed to have a marginal role in the regulation of $[Ca^{2+}]_C$. Both studies reported that over-expression of STIM1 inhibits Cav1.2, while its knockdown enhanced Cav1.2 activity. Whang and colleagues speculate an involvement of Orai1 in this pathway. Recently, also another type of VOOCs, the T-type (essential in cardiomyocytes) is reported to be inhibited by STIM1 (Nguyen et al., 2013). These discoveries underline the possibility that, upon ER/SR depletion, STIM and Orai play different roles in excitable and non-excitable cells, inhibiting VOCCs in the former, while activating CCE in the latter.

5.1 STIM

STIM1 was firstly identified as regulator of CCE in 2005 (Liou et al., 2005; Roos et al., 2005). Two forms of STIM are present in mammals, called STIM1 and STIM2. STIM1 is required for CCE activation, while STIM2 seems to be needed to maintain the correct $[Ca^{2+}]_{ER}$ (Kar et al., 2012). STIM2 derives from an alternative translation of STIM1 and both are ubiquitously expressed in human tissues.

STIM1 is a 77 kDa phosphoprotein, and includes a single TM domain located in the ER in resting cells. Structurally it can be divided in:

(1) an N-terminal part, located in the ER, and formed by a single EF-hand Ca^{2+}-binding motif acting as a luminal ER Ca^{2+} sensor (Liou et al., 2005) and a SAM (Sterile Alpha Motif) domain that regulates STIM oligomerization occurring after $[Ca^{2+}]_{ER}$ depletion (Baba et al., 2006). The EF-hand Ca^{2+} affinity is around 200 μM for STIM1 and around 400 μM for STIM2, making STIM2 more sensitive to changes in ER Ca^{2+} content (Brandman et al., 2007). Moreover, STIM2 EF-domain has slower unfolding and aggregation kinetics, making this protein less efficient in triggering CCE (Zheng et al., 2008; Stathopulos et al., 2009).

(2) A single pass TM motif, which is one of the most conserved part between the two STIM isoforms (Williams et al., 2001), which separates the N-terminal from the C-terminal part.

(3) The C-terminal part organized in different modules:

   a. A domain of the cytosolic loop (located at the C-terminus) of STIM1, also called CAD (CRAC activation domain) or coiled-coil domain, responsible for Orai1 binding and activation. CAD is a dimer that comprises two regions, called CC2 and CC3. One recent model suggests that CC2 domain interacts with Orai1, triggering CAD dimerization and a STIM1 structural modification in order to accommodate Orai1 (Stathopulos et al., 2008).

   b. Another domain located near the CAD, called CC1, reported to play an inhibitory role in STIM1 activation. A model proposes that, upon ER Ca^{2+} depletion, CC1, normally not self-associated, dimerizes, triggering the release of CAD from CC1, and allowing CAD to interact with Orai1 (Zhou et al., 2013).

   The C- terminus of the protein is crucial for CCE activation, since it mediates the interaction with Orai1 and the PM thanks to its enrichment in polybasic residues. This part of the molecule is highly divergent between STIM1 and STIM2, since the latter contains a strong ER retention signal and less affinity for Orai1 binding, underlying the functional difference between the two proteins (Shim et al., 2015).

In resting cells, STIM1 is a dimer uniformly distributed within the ER membrane, and binds to the microtubule-plus-end-tracking-protein EB1, at whose sites microtubule ends contact the ER (Grigoriev et al, 2008). The decrease in $[Ca^{2+}]_{ER}$ causes a conformational change in STIM1 that oligomerizes, forming clusters, called punctae, nearby the PM (Liou et al., 2007). The proper composition and molecular identity of the ER domains associated to PM is still poorly understood, while it is known that the domain responsible for STIM localization at those site are polybasic sequences present in the C-terminus of both STIM1 and STIM2

(Zhou et al., 2013). STIM1 is temperature-sensitive: above 37°C, STIM1 moves into the ER-PM junction, activating CCE, while over 37°C, STIM1 forms clusters, inhibiting CCE activation. Other factors regulate STIM1 activation: S-glutathionylation of a cysteine in position 56 (close to the EF-hand domain) causes CCE activation independently from ER/SR depletion; hypoxia, with the consequent cytosolic acidification, induces the uncoupling of STIM1 and Orai (Muik et al., 2012).

5.2 Orai

In 2006 another molecular component of CCE was discovered: Orai1 (Feske et al., 2006; Vig et al., 2006; Zhang et al., 2006). Indeed, it is the direct molecular interactor of STIM1 (Cahalan, 2009). Orai1 is the pore forming subunit of the CRAC channel and consists of 4 TM domains and N- and C-termini able to interact with STIM1. The TM1 and in particular the aminoacid E106, forms the central part of the pore (McNally et al., 2009; Zhou et al, 2010). The functional CRAC channel is a tetramer of Orai1, while in resting conditions it is organized in six subunits, in which TM domains are located concentrically around the TM1 pore. TM2 and TM3 has been proposed to surround TM1, while TM4 seems to be the lipid exposed segment. Further structural investigations reveal that the middle region of Orai1 host the idrophobic region and the gating site, while the cytoplasmic membrane proximal N-terminus contains several basic residues as well as the CAD-binding site of STIM1 (McNally et al., 2009). These basic residues have been proposed to coordinate anions in order to keep the channel close at resting conditions (Hou et al., 2012).

The C-terminus of Orai1 has been reported to interact with STIM via coiled-coil packing (Stathopulos et al., 2010), while less is known about the interaction site of STIM1 with the Orai1 N-terminus, which seems to be involved in the channel gating since it is enrich in positive charges (Li et al., 2007).

Three forms of Orai are known, called Orai1, Orai2, and Orai3. Less is known about the latter two, but it seems they can also form a STIM-responsive CRAC channel. However, overexpression of both STIM1 and Orai3 is not linked to an increase in CCE activation (phenomenon that happened with the co-overexpression of STIM1 and Orai1 or Orai2), but it can rescue the CCE decrease due to Orai1 knockdown (Mercer et al., 2006). Orai1 is inhibited by 2-APB (2-amonoethyldi-phenyl borate), but Orai2 and Orai3 show different sensitivity to this compound. Also different sensitivities to the inhibitory mechanism CDI (that seems to be mediated by the second cytosolic loop of Orai) are reported: Orai 3 is rapidly inactivated by CDI, while Orai2 and Orai1 are less sensitive, in this order, to this mechanism (Muik et al., 2012). Finally, Orai channels show permeability to other cations (as Ba^{2+} and Na^{2+}) and differences in permeability has been found between the three isoforms (see Lis et al., 2007).

5.3 Presenilins and CCE

Different FAD-linked PS1 mutations have been reported to alter CCE:

(1) M146L mutation was demonstrated to decrease CCE in MEFs (Yoo et al., 2000) and HeLa cells overexpressing the mutant PS1 and in human FAD fibroblasts carrying the mutation (Zatti et al., 2006);

(2) M146V is associated to a CCE reduction in knock-in transgenic mice (Leissering et al., 2000); A246E is ineffective in SH-SY5Y overexpressing cells, while it decreases CCE in HeLa cells (Zatti et al., 2006) and also in M146V transgenic mice (Hermes et al., 2003);
(3) HeLa cells overexpressing the L286V mutation show decreased CCE (Zatti et al., 2006);
(4) delta E9 PS1 expression in SH-SY5Y causes a diminished CCE (Smith et al., 2002);
(5) Human P117L-FAD fibroblasts show no alteration in CCE, but the overexpression of the PS1 mutant exerts an inhibitory effect in HeLa cells (Zatti e al., 2006);
(6) MEFs overexpressing the loss of function D257E and D385A mutations show increased CCE (Yoo et al., 2000).

PS2-FAD mutants as well have been reported to modify CCE:

(1) T122R expression is reported to cause a CCE reduction in HeLa (Zatti et al., 2006), HEK293 cells and human FAD fibroblasts (Giacomello et al., 2005), but not in SH-SY5Y cells (Zatti et al., 2006);
(2) in MEF cells (Yoo et al., 2000) and in HeLa cells (Zatti et al., 2006), the expression of the N141I mutation induces a decrease in CCE;
(3) M239I expression causes a decreased CCE when overexpressed in HeLa cells (Zatti et al., 2006) but it is without effect in human FAD fibroblasts (Zatti et al., 2004);
(4) The loss of function D366A mutation expression causes a decrease in CCE in HeLa overexpressing cells. Since this mutant form of PS2 lacks a key aspartate residue, preventing the endoproteolysis of PS2 (meaning its impossibility to become part of γ-secretase complex), this PS2 effect on CCE is likely independent from γ-secretase activity (Zatti et al., 2004).

Moreover, Ca^{2+} imaging in SH-SY5Y cells and primary neurons reveals that CCE is attenuated upon expression of FAD-linked PS1 and PS2 mutations, while it is potentiated as a result of PS KO or deficiency (Yoo et al., 2000; Herms et al., 2003). Finally, Bojarski et al. found increased expression levels of STIM1 and decreased level of STIM2 in PS-DKO MEFs and patient-derived B-lymphocytes expressing FAD-PS mutations (Bojarski et al., 2009).

Altogether, the results reported so far, with just few exceptions, are consistent with the idea that PSs are negative modulator of CCE. Further investigations are needed to better understand the molecular mechanisms at the basis of this phenomenon, and also to address the pathophysiological role of such alterations in neurons. The recently reported inhibitory effect of STIM1 on VOCCs is an interesting open perspective that could shed new light on the role of PSs on CCE.

Aim of the work

Alzheimer's disease (AD) is the most frequent form of dementia. A small percentage of cases is inherited (Familial AD, FAD) and is due to dominant mutations on three genes, encoding for Amyloid Precursor Protein (APP), Presenilin-1 (PS1) and Presenilin-2 (PS2). PS1 and 2 are the catalytic core of the γ–secretase complex, an enzyme involved in the process of amyloid plaques generation, but they are also involved in other γ–secretase-independent processes, such as Ca^{2+} homeostasis, protein trafficking, cell adhesion and autophagy. Beside the amyloid and tau hyperphosphorylated hypothesis, different studies reported a role for FAD-linked PS mutations in cellular Ca^{2+} alterations, often independently from γ–secretase activity. Ca^{2+} is a key second messenger in living cells that regulates a multitude of cell functions, and alterations in its signalling cascade can be detrimental for cell fate. Despite many efforts have been done in the last years, the role of PSs in Ca^{2+} homeostasis is still debated among the scientific community. To contribute on this topic, the second part of the thesis presents data on the characterization of the role played by PSs in AD Ca^{2+} dyshomeostasis. To address this issue we used a single cell analyses approach, employing different organelle-targeted Cameleon probes. In particular, a cytosolic FRET-based probe, Cameleon D3cpV, was used to perform a single cell analysis evaluating how CCE is influenced by wild type or mutated PSs overexpression in SH-SY5Y neuroblastoma cell line. Moreover, alterations in CCE in human fibroblasts derived from PS-FAD patients, compared to healthy controls, have been investigated.

Results

6. Presenilins effect on CCE

6.1 SH-SY5Y cells expressing different PSs show a decreased CCE

Different FAD-linked PS1 and PS2 mutations has been reported to alter (generally decrease) CCE in different cell types; on the contrary, CCE is potentiated as a result of PSs KO or deficiency (Yoo et al., 2000; Herms et al., 2003). These results were obtained by using chemical Ca^{2+} probes or they were carried out in cell population, employing Aequorin.

The aim of the present investigation was to define whether CCE is altered in a neuroblastoma cell line expressing FAD-linked PSs, employed a single-cell analysis. To this end, we transfected SH-SY5Y cells with the FAD-linked PS1A246E, or PS1wt, and with the PS2T122R mutation, or PS2wt, or a void vector, as a control. Changes in $[Ca^{2+}]_c$ were monitored using the FRET-based genetically encoded Cameleon probe D3cpV. To investigate the influence of the PSs, wt or FAD mutated, on CCE, ER Ca^{2+} depletion was induced by pre-incubating cells for 7 minutes in extracellular buffer, without Ca^{2+} and supplied with a Ca^{2+} chelator (EGTA, 600 μM), and an irreversible SERCA-pump inhibitor (thapsigargin, 100 nM). The induced ER Ca^{2+} depletion is able to trigger STIM1 redistribution into ER puncta close to the PM, where it activates Orai1. Upon 1.5 mM $CaCl_2$ addition, CCE was detected as a large $[Ca^{2+}]_i$ increase.

Figure 45A shows $[Ca^{2+}]_c$ changes as a ratio of the fluorescence intensity of the acceptor (cpV) and the donor (CFP), normalized to baseline ($\Delta R/R_0$), in representative experiments carried out in SH-SY5Y cells overexpressing either PSs wt or FAD-linked PS1A246E/PS2T122R. The CCE average peak height was 0.91 ± 0.06 in controls (mean±SEM, N=16 number of cells analyzed), 0.59±0.04 in PS1 wt overexpressing cells (N=21), showing a reduction of 35% compared to controls ($p<0.01$); 0.60±0.08 in cells expressing PS1A246E (N=16, -33%, $p<0.01$); 0.65±0.045 in PS2wt (N=27,-28%, $p<0.01$) and 0.579±0.08 in PS2T122R (N=14, -36%, $p<0.01$) (Figure 46B). In addition to the CCE peak, also the rate influx has been evaluated and calculated, as maximal derivative of the peak. Similarly, a decrease in the CCE rate has been observed upon PSs expression: 0.086 ± 0.009 in controls (N=16), 0.056 ± 0.005 in PS1wt overexpressing cells (N=21), corresponding to a reduction of 34% compared to controls ($p<0.01$); 0.06 ± 0.007 in cells expressing PS1A246E (N=16, -30%, $p<0.05$); 0.062 ± 0.007 in PS2wt (N=27, -28%, $p<0.05$), and 0.045 ± 0.009 in PS2T122R (N=14, -48%, $p<0.01$) (Figure 46C).

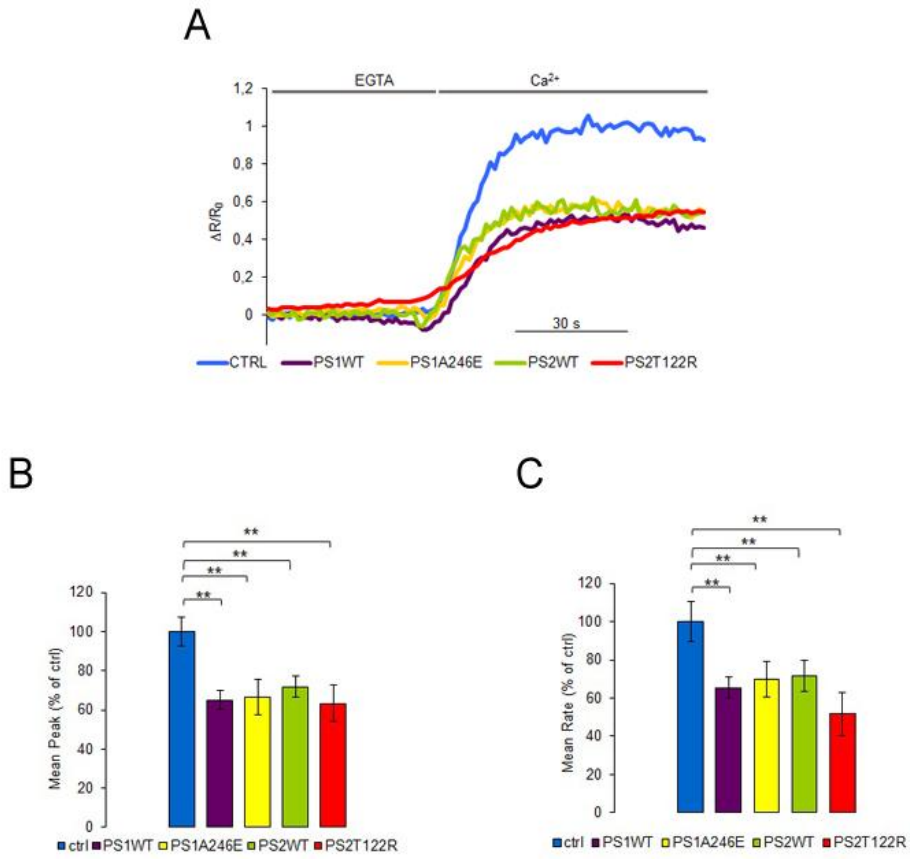

FIGURE 46. PSs overexpression in SH-SY5Y cells induces a reduction in CCE. **(A)** Representative traces of a typical experiment performed in SH-SY5Y cells transfected with void vector (blue), PS1wt (violet), PS1A246E (yellow), PS2wt (green) and PS2T122R (red). Cells expressing the D3cpV Ca^{2+} probe were first treated with thapsigargin (100 nM) in Ca^{2+}-free, EGTA-containing medium, to deplete the stores, and then perfused with a medium containing 1.5 mM $CaCl_2$, to visualize CCE, as indicated by top bars. Data are plotted as $\Delta R/R_0$. **(B)** The histogram shows the average of ΔCCE peak (measured as difference between peak and basal level) for each condition. **(C)** The histogram shows the average of CCE rate for each condition (* $p<0.05$; ** $p<0.01$; *** $p<0.0001$). Data are presented as mean±SEM of N≥14 cells.

It is well known that differences in PM potential strongly affect the rate and extent of CCE by altering the driving force for Ca^{2+} entry (Penner et al., 1993). To nullify differences in membrane potential that could be present in cells differentially transfected, CCE experiments have been carried out using the same protocol described in Figure 45 but with cells perfused with a medium where NaCl was iso-osmotically substituted by KCl (K^+-based medium). Under these conditions, the membrane potential collapsed and differences among cells mostly abridged. Since in this condition the driving force for Ca^{2+} is decreased, the [Ca^{2+}] used to visualize CCE was doubled respect to the previous experiment (from 1.5 to 3 mM). The CCE average peak height and rate were then measured in SH-SY5Y cells transfected with the indicated constructs. Also in this condition, the two parameters are reduced upon PSs expression: CCE peaks height was 0.71±0.03 in controls (N=16), 0.48±0.06 in PS1wt overexpressing cells (N=16, -32%, $p<0.01$); 0.53±0.04 in cells expressing PS1A246E (N=17, -25%, $p<0.01$); 0.45±0.08 in PS2wt (N=9, -36%, $p<0.01$) and 0.42±0.04 in PS2T122R (N=11, -41%,$p<0.0001$) (Figure 47B). Similarly, a decrease in the CCE rate has been observed: a rate of 0.06±0.01 in controls (N=16), 0.03±0.004 in PS1wt overexpressing cells (N=16, -52%, $p<0.01$); 0.04±0.003

in cells expressing PS1A246E (N=17, -40%, $p<0.05$); 0.03±0.005 in PS2wt (N=9, -50%, $p<0.05$) and 0.03±0.007 in PS2T122R (N=11, -46% compared to controls, $p<0.05$) (Figure 47C).

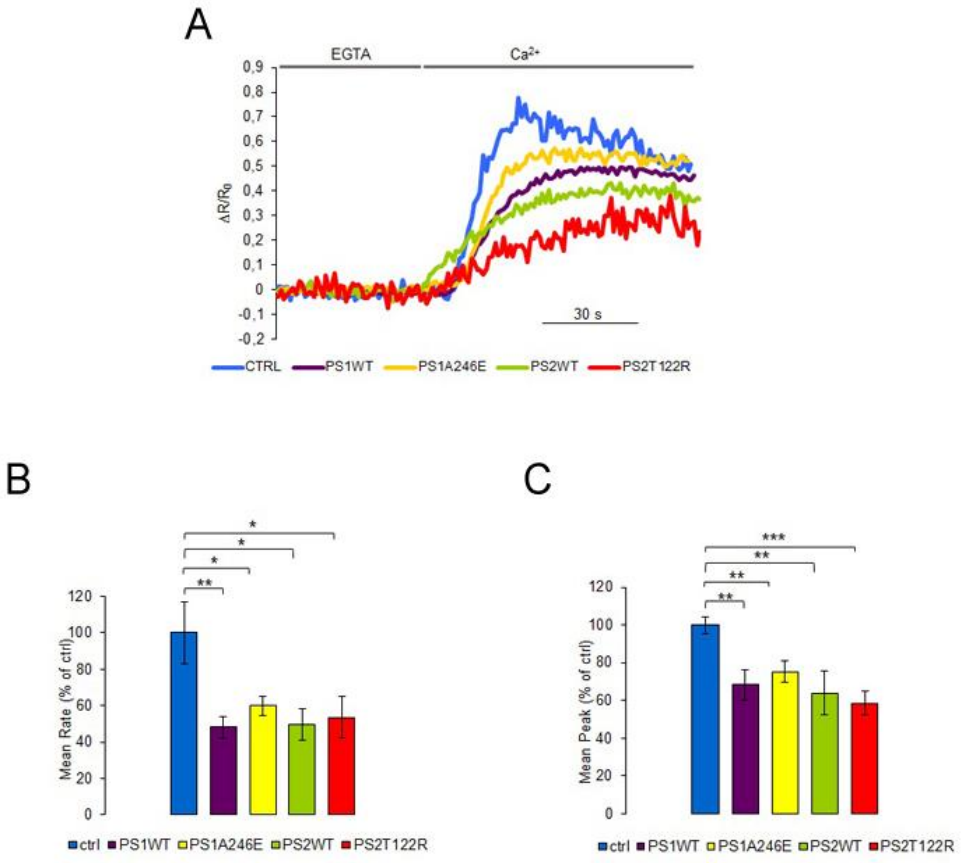

FIGURE 47. PSs overexpression in SH-SY5Y cells induces a reduction in CCE in a K^+-based medium. **(A)** Representative traces of a typical experiment performed in SH-SY5Y cells transfected with void vector (blue) PS1wt (violet), PS1A246E (yellow), PS2wt (green) and PS2T122R (red). Cells expressing the D3cpV Ca^{2+} probe were first treated with thapsigargin (100 nM) in Ca^{2+}-free, EGTA-containing K^+-based medium, to deplete the stores, and then perfused with a medium containing 3 mM $CaCl_2$, to visualize CCE, as indicated by top bars. Data are plotted as $\Delta R/R_0$. **(B)** The histogram shows the average of ΔCCE peak for each condition. **(C)** The histogram shows the average of CCE rate for each condition (* $p<0.05$; ** $p<0.01$; *** $p<0.0001$). Data are presented as mean±SEM of N≥9 cells.

6.2 Human primary fibroblasts from patients carrying the FAD-associated PS1A246E or PS2N141I mutation show a decreased in CCE.

To validate the results obtained in neuroblastoma cells overexpressing FAD-linked PSs, human skin fibroblasts from patients carrying the PS1A246E or the PS2N141I FAD-linked mutation in heterozygosis, and aged-matched controls form healthy individuals, have been analyzed. Fibroblasts have been electroporated with the cDNA for the cytosolic Cameleon D3cpV and CCE activation was induced using the same protocol employed for the SH-SY5Y cell line.

Figures 47A and 48A show $[Ca^{2+}]_c$ changes, as ratio normalized to baseline ($\Delta R/R_0$), in representative experiments carried out in human fibroblasts from controls and FAD patients. As far as FAD-PS1 mutation is concerned, the CCE average peak height measured was: 0.89±0.09 in controls (N=14) and 0.51±0.06 in PS1A246E fibroblasts (N=14), showing a reduction of 42% compared to controls ($p<0.01$) (Figure 48B). Similarly, a decrease in the CCE rate has been observed: 0.15±0.02 in controls (N=14) and 0.08±0.015 in PS1A146E fibroblasts (N=14), meaning a reduction in rate of 46% ($p<0.05$) (Figure 48C).

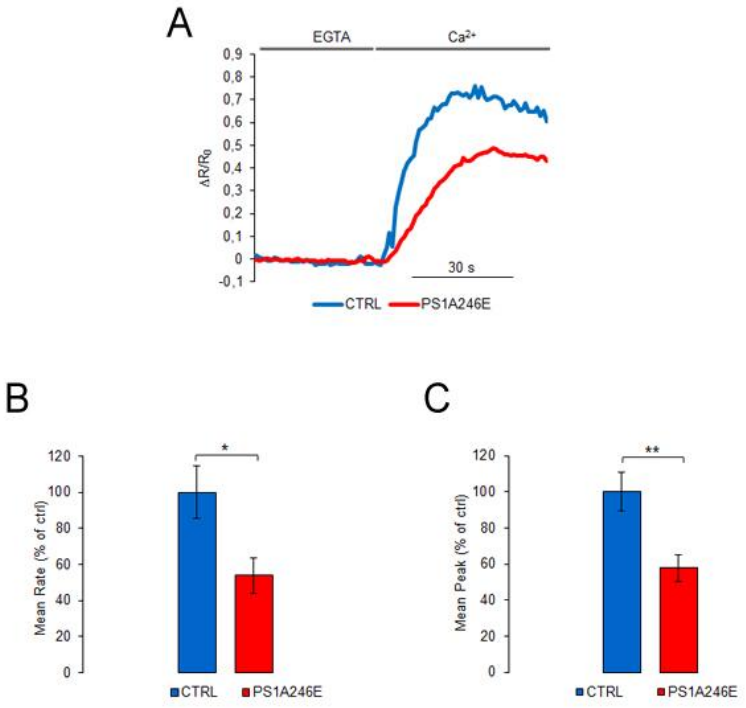

FIGURE 48. Human fibroblasts from a FAD patient carrying the PS1A246E mutation show a reduction in CCE. **(A)** Representative traces of a typical experiment performed in control fibroblasts (blue) and fibroblasts carrying the PS1A246E mutation (red). Cells expressing the D3cpV Ca^{2+} probe were first treated with thapsigargin (100 nM) in Ca^{2+}-free, EGTA-containing medium, to deplete the stores, and then perfused with a medium containing 1.5 mM $CaCl_2$, to visualize CCE, as indicated by top bars. Data are plotted as $\Delta R/R_0$. **(B)** The histogram shows the average of ΔCCE peak for each condition. **(C)** The histogram shows the average of CCE rate for each condition (* $p<0.05$; ** $p<0.01$; *** $p<0.0001$). Data are presented as mean±SEM of N=14 cells.

Then, the analysis was extended to fibroblasts from a FAD patient carrying the PS2N141I mutation, together with fibroblasts from three different age-matched healthy controls, allowing us to take into account also the inter-individual variability in CCE. The measured CCE average peak height was the following: the first control (named ctrl) has a peak of 0.47±0.04 (N=17); the second one (named ctrl bis), 0.44±0.03 (N=17); the third control (named ctrl ter), 0.49±0.05 (N=17); since no significant difference was observed between controls, CCE peaks heights were averaged, giving a mean value of 0.47±0.04 (N=51). CCE average peak height in PS2N141I was 0.33±0.04 (N=15), thus showing a reduction of around 30% compared to averaged controls ($p<0.01$) (Figure 49B). The CCE rate was also calculated: 0.05±0.006 for the first control (N=17); 0.037±0.005 for control bis (N=17); 0.037±0.005 for control ter (N=17). A tendency to a reduction (-25%,

but not statistically significant) is thus observed in fibroblasts control bis and ter, compared to the first control. The mean CCE rate value for controls was 0.04±0.003 (N=51). In PS2N141I fibroblasts the calculated CCE rate was 0.023 ± 0.003 (N=15), showing a reduction of around 44% compared to the averaged value of controls ($p<0.01$) (Figure 49C).

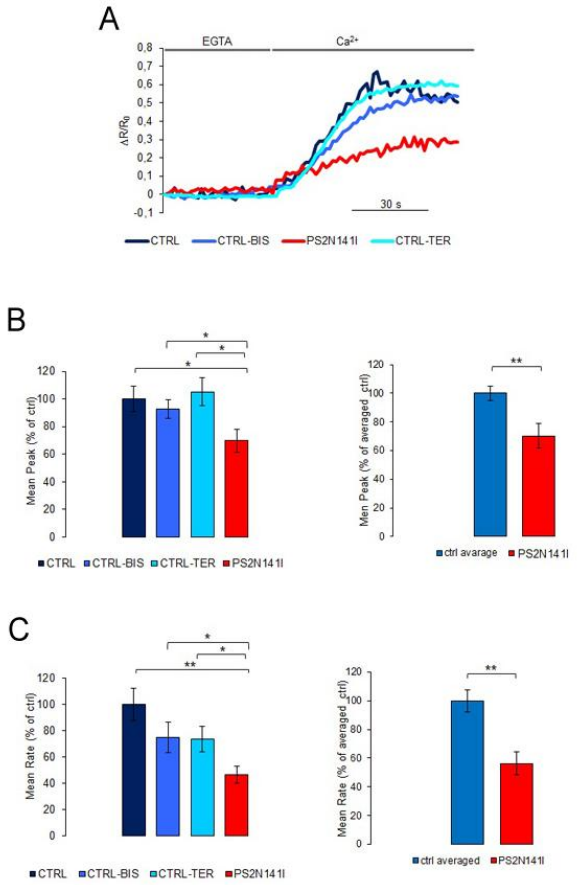

FIGURE 49. Human fibroblasts from a FAD patient carrying the PS2N141I mutation show a reduction in CCE. **(A)** Representative traces of a typical experiment, performed as described in figure 43, in control fibroblasts (dark blue for ctrl, blue for ctrl bis and cyan for ctrl ter) and fibroblasts carrying the PS2N141 mutation (red). **(B)** *Left:* The histogram shows the average of ΔCCE peak for each condition. *Right:* The histogram shows the ΔCCE peak mean value for the different controls (blue) and for PS2N141I fibroblasts (red). **(C)** *Left:* The histogram shows the average of CCE rate for each condition. *Right:* The histogram shows the ΔCCE rate mean value for the different controls (blue) and for PS2N141I fibroblasts (red); (* $p<0.05$; ** $p<0.01$; *** $p<0.0001$). Data are presented as mean±SEM of N≥15 cells.

As for SH-SY5Y cells, a K^+-based medium was employed to ensure that differences observed in CCE peaks/rate in human fibroblasts do not depend on different potential across the PM. However, the presence of L-type VOCCs and the activation of a not well-defined K^+-exchanger in these latter cells (data not shown), prevented the possibility of collapsing membrane potential.

6.3 PSs overexpressing SH-SY5Y cells and PS1A246E/PS2N141I human FAD fibroblasts show a decreased STIM1 protein level

Two proteins have been identified as major players in CCE: STIM1, the ER Ca^{2+} sensor, and Orai1, the pore forming subunit of the CRAC channel in PM. Increased expression levels of STIM1 has been reported in PS-DKO MEFs and FAD-PSs patient-derived B-lymphocytes (Bojarski et al., 2009). To check whether alterations in the expression level of STIM could be involved in the CCE attenuation observed upon PSs expression, STIM1 protein level has been evaluated by Western blot in SH-SY5Y cells expressing the void vector, controls, or different PSs: a significant decrease in the protein level, compared to controls, was observed in all the different conditions: -21% in PS1wt ($p<0.05$), -45% in PS1A245E ($p<0.05$) and around -50% in PS2wt and PS2T122R ($p<0.05$) overexpressing cells (N=4). Similarly, a reduction of around 40% in STIM1 protein level has been measured in PS1A246E-FAD fibroblasts compared to controls ($p<0.05$, N=3) and a reduction of around 43% ($p<0.0001$) was found in PS2N141I fibroblasts compared with averaged controls (N≥5) (Figure 50).

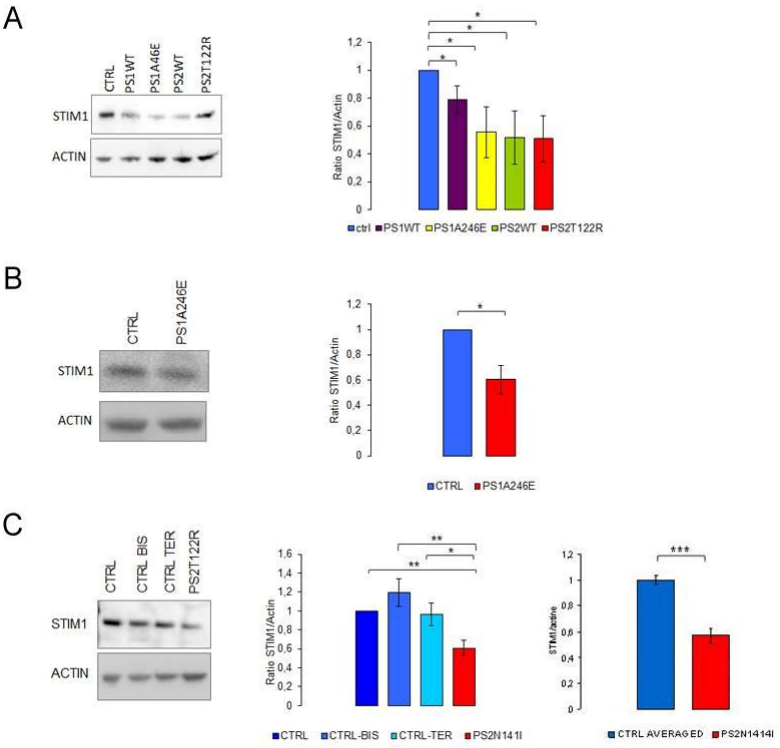

FIGURE 50. SH-SY5Y cells expressing different PSs and human FAD fibroblasts show a reduction in STIM1 protein level. **(A)** SH-SY5Y cells were transfected with the void vector (ctrl), PS1wt, PS1A246E, PS2wt, PS2T122R cDNAs. 24 hrs after transfection, total proteins were extracted and subjected to Western blot with antibodies anti-STIM1, and anti-actin as loading control. *Left:* representative blot. *Right:* Quantification of STIM1 normalized to actin. **(B)** Total proteins from FAD-PS1A246E fibroblasts, and control fibroblasts from an age-matched heathy individual, were extracted and subjected to Western blot as in A. *Left:* representative blot. *Right:* Quantification of STIM1 normalized to actin. **(C)** Total proteins from FAD-PS2N141I fibroblasts, and control fibroblasts from three age-matched heathy individuals, were extracted and subjected to Western blot as in A. *Left:* representative blot. *Middle:* Quantification of STIM1 normalized to actin. *Right:* Quantification of STIM1 normalized to actin and averaging the three controls (* $p<0.05$; ** $p<0.01$; *** $p<0.0001$). Data are presented as mean±SEM of N≥4 independent experiments.

Discussion

The aim of this project is to characterize the role of FAD-linked PSs mutations in the regulation of Ca^{2+} homeostasis. Indeed, beside the amyloid and tau hyperphosphorylated hypothesis, different studies reported that FAD-linked PSs are able to induce cellular Ca^{2+} alterations, independently from γ-secretase activity. Ca^{2+} is a key second messenger in living cells that regulates a multitude of cell functions, particularly essential in neuronal development, synaptic transmission and plasticity, as well as in the regulation of various metabolic pathways at the brain level. In the last decades, abnormalities in Ca^{2+} signaling are emerging as critical features in the pathogenesis of a wide range of neurodegenerative disorders, including AD (review in Mattson et al., 2000). Despite many efforts have been done in the last years, the role of PSs in Ca^{2+} homeostasis is still debated: increased, decreased and unchanged Ca^{2+} responses have been reported in peripheral cells from AD patients, compared to control cells (Honarnejad K. and Herms J., 2012). All the evidence proposes Ca^{2+} dysregulation as a player in the initial stage of the pathology, making Ca^{2+} hypothesis an interesting field to explore to better understand AD onset and progression. Despite opposite effects of PSs on CCE have been published, the majority of the studies reported a decrease in CCE in various cell models expressing FAD-linked PSs mutations. Moreover, CCE potentiation has been described as a consequence of PSs KO or deficiency (Yoo et al., 2000; Herms et al., 2003). These results were obtained by using chemical Ca^{2+} probes or they were carried out in cell population, employing Aequorin. In this study, the impact of FAD-PSs mutations on CCE was unravelled using the cytosolic Cameleon Ca^{2+} probe D3cpV. The use of a GECI presents numerous advantages, *e.g.*: the possibility of monitoring in single cell changes in $[Ca^{2+}]_c$ in real time; the ability of performing ratiometric Ca^{2+} measurements, preventing artefacts due to focal plane shifts; the possibility of restricting analysis only to co-transfected cells.

Firstly, the expression of FAD-linked PS1A246E, or PS1wt, and FAD-linked PS2T122R mutation, or PS2wt, in a neuroblastoma cell line (SH-SY5Y) causes a significant reduction of 30-40% in both CCE peak and rate, compared to controls. Since similar results could be caused by differences in PM potential (Penner et al., 1993), to exclude this possibility the collapse of membrane potential has been induced. Again, SH-SY5Y cells expressing FAD-linked or wt PSs show a reduction of 25-40% in CCE peak and of 40-50% in CCE rate, compared to controls. Taken together, these results confirmed that the observed CCE reduction is not linked to differences in PM potential upon expression of the diverse PS forms. Of note, PS1wt and PS2wt overexpression mimic the effect on CCE of FAD-PS mutations. As previously reported by our laboratory, employing a tetracycline-inducible PS2 expression system in HeLa cells, Ca^{2+} dysregulation correlates with the PS2 protein expression level and higher level of PS2wt, compared to that of the FAD mutant, is required to obtain similar effects on Ca^{2+} handling (Giacomello et al., 2005). Thus, it can be speculated that the effect on CCE is due to an accumulation of PSs holoprotein, a phenotype potentially correlated to FAD-linked mutations (but that is also present upon the experimental overexpression of the wt form of the protein). Indeed, expression of PS2D366A (a mutant form of PS2 that precludes its endoproteolysis, preventing its incorporation in the γ-secretase complex) has been reported to cause a decrease in CCE (Zatti et al., 2004). To surely demonstrate that the effects on CCE are mediated by PS2

holoprotein further investigations are required. A pharmacological approach, inhibiting γ-secretase activity, and a genetic approach, using PS1 mutant "loss of function" for γ-secretase activity, could be employed to address this issue.

In order to investigate CCE impairment in a more pathophysiological system compared to the exploited overexpressing models, CCE was investigated in FAD human fibroblasts carrying the PS1A246E or the PS2N141I mutation in heterozygosis. Fibroblasts carrying the PS2T122R mutation are not available anymore, however it has been previously demonstrated that in these cells the PS2T122R mutant induced a reduction in CCE rate and peak (Giacomello et al., 2005). Moreover, PS2N141I overexpression in MEFs (Yoo et al., 2000) and in HeLa cells (Zatti et al., 2006) has been shown to reduced CCE peak and rate.

Human fibroblasts from a patient bearing the PS1A246E mutation show a reduction of 42% and 46% in CCE peak and rate, respectively, compared to healthy age-matched controls. Similarly, CCE in human fibroblasts from FAD patients carrying the PS2N141I mutation have been analyzed in comparison with fibroblasts from three healthy age-matched controls. In this case, the inter-individual variability is taken into account studying CCE in different healthy-individual fibroblasts. Unfortunately, fibroblasts from other FAD-PS2N141I patients are not available. Since no significant different was observed between controls, CCE peak values were averaged confirming that a reduction of around 30% and 44% in CCE peak and rate, respectively, is present in FAD fibroblasts. The involvement of PM potential in CCE reduction cannot be assessed in these cells, because of the presence of L-type VOCCs (Baumgarten et al., 1992) and the activation of a not well-defined K^+-exchanger.

To provide some molecular hints about the mechanism by which PSs expression alters CCE, STIM1 protein level has been evaluated. Previously, an increased expression level of STIM1 in PS-DKO MEFs and patient-derived B-lymphocytes expressing different FAD-PS mutations has been found (Bojarski et al., 2009). STIM1 protein levels in SH-SY5Y overexpressing PSs are significantly decreased (from -20% to -50%) compared to controls. Similarly, a reduction of around 40% was found in PS1A246E and in PS2N141I human fibroblasts, compared to controls. Thus, these data suggest that CCE reduction observed in fibroblasts is likely independent from changes in PM potential and, instead, correlates with the expression level of STIM1.

Two are the proteins mainly involved in CCE: STIM1, the ER Ca^{2+} sensor and Orai1, the pore forming subunit of CRAC. Despite many attempts have been done, Orai1 protein levels failed to be evaluated by the available antibodies, because of the presence of non-specific bands that prevents the quantification of the expected specific one (at 35 or 50 kDa, depending on the glycosylation state of Orai1). An alternative approach, could be the evaluation of Orai1 and STIM1 mRNA level, in order to clarify if also Orai1 expression is affected by PSs expression and whether the decreased STIM1 protein amount is due to transcriptional or post-transcriptional dysregulation. This is a critical point to address, since alterations in CCE peak and rate could be the result of the same phenomenon, but they could also be differentially mediated by either STIM1 protein level reduction or specific CRAC channel dysfunction, respectively. Moreover, different mechanisms, besides a decreased STIM1 level, could be involved in PS-mediated effects

on CCE. For example, PSs could somehow impairing STIM1 puncta formation, reducing STIM1 ability to activate Orai1. To investigate this point, puncta formation can be monitored employing FRET experiments expressing STIM1 and Orai1 constructs tagged with YFP and CFP, respectively.

Finally, it should be considered that AD is a pathology linked to neuronal dysfunctions. It is still not clear which is the functional role of CCE in neurons, because in these latter cells Ca^{2+} influx from extracellular space is mainly due to VOCCs opening. However, recent studies reported an inhibitory effect of STIM1 on L-type Cav1.2 and T-type VOCCs (Park et al., 2010; Wang et al., 2010; Nguyen et al., 2013), opening the possibility of differential roles played by STIM and Orai in excitable cells. This latter point is surely worth to investigate, considering the observed reduction of STIM1 protein level associated to the expression of FAD-PSs-linked mutations.

Materials and Methods

Cell culture and transfection

SH-SY5Y cells were grown in DMEM containing 10% FCS, supplemented with L-glutamine (2 mM), penicillin (100 U/ml), and streptomycin (100 µg/ml), in a humidified atmosphere containing 5% CO_2.

Human fibroblasts (from Coriell Institute for medical research: FAD-PS2-N141I (AG09908); control fibroblasts (AG08525)) were grown in DMEM containing 20% FCS, supplemented with L-glutamine (2 mM), penicillin (100 U/ml) and streptomycin (100 µg/ml), in a humidified atmosphere containing 5% CO_2. Cells were seeded onto glass coverslips (18 mm diameter) and transfection was performed at 60-70% confluence using Lipofectamine™ 2000 Transfection Reagent (Life Technologies) for SH-SY5Y with 1 µg of DNA (0.25 µg of cameleon codifying cDNAs and 0.75 µg of pcDNA3 or PSs codifying cDNAs); fibroblasts were transfected by electroporation, using the Neon Transfection System (MPK500, Invitrogen). FRET measurements were usually performed 24 h after transfection.

Ca^{2+} measurements

FRET acquisition and analysis have been carried out as reported in PART-I of the Materials and Methods section. Cells, plated on cover slips (18 mm diameter), were mounted into an open-topped chamber thermostated at 37°C and maintained in an extracellular medium, composed by modified Krebs-Ringer Buffer (mKRB) containing in mM: 140 NaCl, 2.8 KCl, 2 $MgCl_2$, 1 $CaCl_2$, 10 HEPES, 11 glucose, pH 7.4, at 37°C. For CCE activation, cells were pre-treated with the irreversible SERCA inhibitor thapsigargin (100 nM) for 7 minutes in a Ca^{2+}-free, EGTA (600 µM)-containing medium; cells were then perfused with the same medium without the inhibitor and challenged with $CaCl_2$ (1.5 mM). Where indicated, extracellular-like medium was substituted with K^+-based medium (in mM: 5 NaCl, 130 KCl, 2 $MgCl_2$, 3 $CaCl_2$, 10 HEPES, 11 glucose, pH 7.4, at 37°C).

Preparation of Protein Extracts and Western Blot Analysis

Human fibroblasts or SH-SY5Y cells overexpressing PSs were solubilised in RIPA buffer (50 mM Tris, 150 mM NaCl, 1% Triton X-100, 0.5% deoxycholic acid, 0,1% SDS, protease inhibitor cocktail, pH 7.5) and incubated on ice for 30 min. Insolubilized material was spun down at 4000 x g for 5 min at 4°C. 35 µg of protein were loaded onto polyacrylamide gels (10-12%) and immunoblotted. Proteins were resolved by TruPAGE™ Precast Gels 4-12% (Sigma Aldrich) in TruPAGE™ TEA-Tricine SDS Running Buffer (Sigma Aldrich) and blotted onto a nitrocellulose membrane and probed with α-STIM1 antibody (BD Transduction Laboratories Purified Mouse 1:250). The proteins are visualized in chemiluminescence using as secondary antibody α-Mouse (Biorad, 1:5000). The intensity of the bands was analysed using ImageJ software.

Materials

Thapsigargin was purchased from Sigma-Aldrich, all other materials were analytical or of the highest available grade.

Statistical analysis

All data are representative of at least three different experiments. Data were analyzed using Origin 7.5 SR5 (OriginLab Corporation) to calculate CCE rates, and ImageJ (National Institutes of Health,) for the off-line analysis of FRET experiments (as reported in PART-I of the Materials and Methods section). Data are presented as a $\Delta R/R_0$ values (where ΔR is the change of the cpV/CFP emission intensity ratio at any time, R_0 is the fluorescence emission ratio at the time 0).

CCE peak values were calculated as difference between peak and baseline values using Microsoft Excel.

Numerical values presented throughout the text are mean±SEM (N=number of independent experiments or cells; $* = p < 0.05$, $**=p<0.01$, $*** = p < 0.001$, unpaired Student's t test).

Bibliography

- Abell E, Ahrends R, Bandara S, Park BO, Teruel MN. Parallel adaptive feedback enhances reliability of the Ca^{2+} signaling system. Proc. Natl. Acad. Sci. U. S. A., 108 (2011), pp. 14485–14490
- Airan RD, Thompson KR, Fenno LE, Bernstein H, Deisseroth K. Temporally precise *in vivo* control of intracellular signalling. Nature. 2009 Apr 23;458(7241):1025-9.
- Akerboom, J., et al., Genetically encoded calcium indicators for multi-color neural activity imaging and combination with optogenetics. Front Mol Neurosci, 2013. 6: p. 2.
- Allen, D.G., J.R. Blinks, and F.G. Prendergast, Aequorin luminescence: relation of light emission to calcium concentration--a calcium-independent component. Science, 1977. 195(4282): p. 996-8.
- Anderson S, Bankier AT, Barrell BG, de-Bruijn MHL, Coulson AR, et al. (1981). "Sequence and organization of the human mitochondrial genome". Nature 290 (5806): 427–465.
- Area-Gomez, E., de Groof, A.J., Boldogh, I., Bird, T.D., Gibson, G.E., Koehler, C.M., Yu, W.H., Duff, K.E., Yaffe, M.P., Pon, L.A. and Schon, E.A. Presenilins are enriched in endoplasmic reticulum membranes associated with mitochondria. Am J Pathol. 175(5):1810-1816 (2009).
- Arruda V.R. Stedman H.H. Nichols T.C. Haskins M.E. Nicholson M. Herzog R.W. Couto L.B. High K.A. Regional intravascular delivery of AAV-2-F.IX to skeletal muscle achieves long-term correction of hemophilia B in a large animal model. Blood. 2005;105:3458–3464.
- Baba Y, Hayashi K, Fujii Y, Mizushima A, Watarai H, Wakamori M, Numaga T, Mori Y, Iino M, Hikida M, Kurosaki T. Coupling of STIM1 to store-operated Ca^{2+} entry through its constitutive and inducible movement in the endoplasmic reticulum. Proc Natl Acad Sci U S A. 2006 Nov 7;103(45):16704-9. Epub 2006 Oct 30
- Baffy G, Miyashita T, Williamson JR, Reed JC. Apoptosis induced by withdrawal of interleukin-3 (IL-3) from an IL-3- dependent hematopoietic cell line is associated with repartitioning of intracellular calcium and is blocked by enforced Bcl-2 oncoprotein production. J Biol Chem 1993; 268: 6511–6519150.
- Baird, G.S., D.A. Zacharias, and R.Y. Tsien, Circular permutation and receptor insertion within green fluorescent proteins. Proc Natl Acad Sci U S A, 1999. 96(20): p. 11241-6
- Bathori G, Csordas G, Garcia-Perez C, Davies E, Hajnoczky G. Ca^{2+}-dependent control of the permeability properties of the mitochondrial outer membrane and voltage-dependent anion-selective channel (VDAC). J Biol Chem 2006;281:17,347–58.
- Baubet, V., et al., Chimeric green fluorescent protein-aequorin as bioluminescent Ca^{2+} reporters at the single-cell level. Proc Natl Acad Sci U S A, 2000. 97(13): p. 7260-5.
- Baughman JM, Perocchi F, Girgis HS, Plovanich M, Belcher-Timme CA, Sancak Y, Bao XR, Strittmatter L, Goldberger O, Bogorad RL, Koteliansky V, Mootha VK (2011). Integrative genomics identifies MCU as an essential component of the mitochondrial calcium uniporter. Nature 476(7360),341-5.
- Baumgarten LB., Toscas K, and Villereal ML. Dihydropyridine-sensitive L-type Ca2' Channels in Human Foreskin Fibroblast Cells (1991) The j0urnal of biological chemistry
- Beam K.G. and Bannister R.A., Looking for answers to EC coupling's persistent questions. J Gen Physiol, Vol.136: 7–12, 2010.
- Becker W. Fluorescence lifetime imaging--techniques and applications. J Microsc. 2012 Aug;247(2):119-36.

- Berman DE, Dall'Armi C, Voronov SV, McIntire LB, Zhang H, Moore AZ, Staniszewski A, Arancio O, Kim TW, Di Paolo G. Oligomeric amyloid-beta peptide disrupts phosphatidylinositol-4,5-bisphosphate metabolism. Nat Neurosci. 2008 May;11(5):547-54.
- Bernardi, P. and Azzone, G.F. Regulation of Ca^{2+} efflux in rat liver mitochondria. Role of membrane potential. Eur J Biochem 134:377–383 (1983).
- Bernardi, P., Paradisi, V., Pozzan, T. & Azzone, G. F. (1984). Pathway for uncoupler-induced Ca^{2+} efflux in rat liver mitochondria: inhibition by ruthenium red. Biochemistry 23, 1645–1651.
- Bernardi, P. Mitochondrial transport of cations: channels, exchangers, and permeability transition. Physiol Rev 79:1127–1155 (1999).
- Bernardi P, von Stockum S. The permeability transition pore as a Ca($^{2+}$) release channel: new answers to an old question. Cell Calcium. 2012 Jul;52(1):22-7.
- Berridge, M.J. Neuronal calcium signalling. Neuron 21: 13-26 (1998).
- Berridge M.J., Bootman M.D. and Roderick H.L., Calcium signalling: dynamics, homeostasis and remodelling. Nat Rev Mol Cell Biol, Vol.4: 517-529, 2003.
- Berridge MJ. Calcium signalling remodelling and disease. Biochem Soc Trans. 2012 Apr;40(2):297-309.
- Beutner, G., Sharma, V.K., Giovannucci, R., Yule, D.I., and Sheu, S.S. Identification of a ryanodine receptor in rat heart mitochondria. J Biol Chem 276:21482–21488 (2001).
- Bianchi K, Vandecasteele G, Carli C, Romagnoli A, Szabadkai G, Rizzuto R. (2005) Regulation of Ca($^{2+}$)signalling and Ca($^{2+}$)-mediated cell death by the transcriptional coactivator PGC-1□. Cell Death Differ 13,586–96.
- Bish LT, Morine K, Sleeper MM, Sanmiguel J, Wu D, Gao G, Wilson JM, Sweeney HL.Adeno-associated virus (AAV) serotype 9 provides global cardiac gene transfer superior to AAV1, AAV6, AAV7, and AAV8 in the mouse and rat. Hum Gene Ther. 2008 Dec;19(12):1359-68.
- Boitier E, Rea R, Duchen MR. Mitochondria exert a negative feedback on the propagation of intracellular Ca^{2+} waves in rat cortical astrocytes. J Cell Biol, 145,795–808 (1999).
- Bojarski L1, Pomorski P, Szybinska A, Drab M, Skibinska-Kijek A, Gruszczynska-Biegala J, Kuznicki J. Presenilin-dependent expression of STIM proteins and dysregulation of capacitative Ca^{2+} entry in familial Alzheimer's disease. Biochim Biophys Acta. 2009 Jun;1793(6):1050-7.
- Bondarenko A.I, Jean-Quartier C., Malli R.,. Graier W.F. Characterization of distinct single-channel properties of Ca(2)(+) inward currents in mitochondria. Pflugers Arch., 465 (2013), pp. 997–1010
- Bonora M, Giorgi C, Bononi A, Marchi S, Patergnani S, Rimessi A, Rizzuto R, Pinton P. Subcellular calcium measurements in mammalian cells using jellyfish photoprotein aequorin-based probes. Nat Protoc. 2013 Nov;8(11):2105-18.
- Borst JW, Laptenok SP, Westphal AH, Kühnemuth R, Hornen H, Visser NV, Kalinin S, Aker J, van Hoek A, Seidel CA, Visser AJ Structural changes of yellow Cameleon domains observed by quantitative FRET analysis and polarized fluorescence correlation spectroscopy. Biophys J. 2008 Dec;95(11):5399-411.
- Boyden ES, Zhang F, Bamberg E, Nagel G, Deisseroth K (September 2005). "Millisecond-timescale, genetically targeted optical control of neural activity". Nat. Neurosci. 8 (9): 1263–8.
- Braak H. and Braak E., Frequency of stages of Alzheimer-related lesions in different age categories. Neurobiol Aging, Vol.18: 351–357, 1997.

- Bragadin, M., Pozzan, T., and Azzone, G.F. Kinetics of Ca^{2+} carriers in rat liver mitochondria. Biochemistry 18, 5972-5978 (1979).
- Brandman O, Liou J, Park WS, Meyer T. STIM2 is a feedback regulator that stabilizes basal cytosolic and endoplasmic reticulum Ca2 + levels. Cell, 131 (2007), pp. 1327–1339
- Brault C, Levy PL, Bartosch B. Hepatitis C virus-induced mitochondrial dysfunctions.Viruses. 2013 Mar 21;5(3):954-80.
- Breckenridge DG, Stojanovic M, Marcellus RC, Shore GC. Caspase cleavage product of BAP31 induces mitochondrial fission through endoplasmic reticulum Ca^{2+} signals, enhancing cytochrome c release to the cytosol. J Cell Biol 160,1115–27. (2003).
- Breton C., Mucha J., Jeanneau C., Structural and functional features of glycosyltransferases. Biochimie, Vol.83: 713–718, 2001.
- Brini, M., Marsault, R., Bastianutto, C., Alvarez, J., Pozzan, T. and Rizzuto, R. Transfected aequorin in the measurement of cytosolic Ca^{2+} concentration ($[Ca^{2+}]c$). A critical evaluation. J Biol Chem.; 270: 9896-9903 (1995).
- Brini, M. Calcium-sensitive photoproteins. Methods 46: 160-166 (2008).
- Brini M. and Carafoli E., Calcium pumps in health and disease. Physiol Rev, Vol.89: 1341-1378, 2009.
- Brookes, P.S., Parker, N., Buckingham, J.A., Vidal-Puig, A., Halestrap, A.P., Gunter, T.E., Nicholls, D.G., Bernardi, P., Lemasters, J.J. and Brand, M.D. UCPs—unlikely calcium porters. Nat Cell Biol 10:1235–1237, author reply 1237–1240 (2008).
- Brunello L., Zampese E., Florean C., Pozzan T., Pizzo P., Fasolato C., Presenilin-2 dampens intracellular Ca^{2+} stores by increasing Ca^{2+} leakage and reducing Ca^{2+} uptake. J Cell Mol Med, Vol.13: 3358-69, 2009.
- Brunkan, A.L. and Goate, A.M. Presenilin function and gamma-secretase activity. Journal of Neurochemistry 93:769–792 (2005).
- Bugiel I,König K,Wabnitz H. 1989. Investigations of cells by fluorescence laser scanning microscopy with subnanosecond time resolution. Laser Life Sci 3: 47–53.
- Buxbaum J.D., Choi E.K., Luo Y., Lilliehook C., Crowley A.C., Merriam D.E., Wasco W., Calsenilin: a calcium-binding protein that interacts with the presenilins and regulates the levels of a presenilin fragment. Nat Med, Vol.4: 1177-81, 1998.
- Cahalan M.D., STIMulating store-operated Ca^{2+} entry. Nat Cell Biol, Vol.11: 669–677, 2009.
- Cai H., Wang Y., McCarthy D., Wen H., Borchelt D.R., Price D.L. and Wong P.C., BACE1 is the major beta-secretase for generation of Abeta peptides by neurons. Nat Neurosci, Vol.4: 233–234, 2001.
- Cai X, Lytton J. Molecular cloning of a sixth member of the K+-dependent mNCXgene family, NCKX6. J Biol Chem 279,5867–5876 (2004).
- Calcraft P.J., Ruas M., Pan Z., Cheng X., Arredouani A., Hao X., Tang J., Rietdorf K., Teboul L., Chuang K.T., Lin P., Xiao R., Wang C., Zhu Y., Lin Y., Wyatt C.N., Parrington J., Ma J., Evans A.M., Galione A., Zhu M.X., NAADP mobilizes calcium from acidic organelles through two-pore channels. Nature, Vol.459: 596–600, 2009.
- Carafoli E., Calcium - a universal carrier of biological signals. FEBS J, Vol.272: 1073-1089, 2005.
- Cardenas, C., Miller, R.A., Smith, I., Bui, T., Molgo, J., Muller, M., Vais, H., Cheung, K.H., Yang, J., Parker, I., Thompson, C.B., Birnbaum, M.J., Hallows, K.R. and Foskett, J.K. Essential regulation of cell bioenergetics by constitutive InsP3 receptor Ca^{2+} transfer to mitochondria. Cell 142:270–283 (2010).

- Case RM, Eisner D, Gurney A, Jones O, Muallem S, Verkhratsky A. Evolution of calcium homeostasis: from birth of the first cell to an omnipresent signalling system. Cell Calcium. 2007 Oct-Nov;42(4-5):345-50. Epub 2007 Jun 14.
- Catterall W.A., Voltage-gated calcium channels, Cold Spring Harb Perspect Biol, Vol.3: 3947-3960, 2011.
- Cereghetti, G. M. et al. Dephosphorylation by calcineurin regulates translocation of Drp1 to mitochondria. Proc. Natl Acad. Sci. USA 105, 15803–15808 (2008).
- Chacinska A, Koehler CM, Milenkovic D, Lithgow T, Pfanner N. Importing mitochondrial proteins: machineries and mechanisms. Cell. 2009 Aug 21;138(4):628-44.
- Chalmers S, Nicholls DG. (2003).The Relationship between Free and Total Ca^{2+} concentrations in the matrix of liver and brain mitochondria. J Biol Chem 278,19,062–70.
- Chanat E. and Huttner W.B., Milieu-induced, selective aggregation of regulated secretory proteins in the trans-Golgi network. J Cell Biol, Vol.115: 1505–1519, 1991.
- Chandra S., Kable E.P., Morrison G.H., Webb W.W., Calcium sequestration in the Golgi apparatus of cultured mammalian cells revealed by laser scanning confocal microscopy and ion microscopy. J Cell Sci, Vol.100: 747–752, 1991.
- Chang, K.T., Niescier, R.F. and Min, K.T. Mitochondrial matrix Ca^{2+} as an intrinsic signal regulating mitochondrial motility in axons. Proc Natl Acad Sci USA 108(37):15456–15461 (2011).
- Chen TW, Wardill TJ, Sun Y, Pulver SR, Renninger SL, Baohan A, Schreiter ER, Kerr RA, Orger MB, Jayaraman V, Looger LL, Svoboda K, Kim DS. Ultrasensitive fluorescent proteins for imaging neuronal activity. Nature. 2013 Jul 18;499(7458):295-300.
- Chen, R. et al. Bcl-2 functionally interacts with inositol 1,4,5-trisphosphate receptors to regulate calcium release from the ER in response to inositol 1,4,5-trisphosphate. J. Cell Biol. 166, 193–203 (2004).
- Chen, Y.R. and Glabe, C.G. Distinct early folding and aggregation properties of Alzheimer amyloid-β peptides Aβ40 and Aβ42: stable trimer or tetramer formation by Aβ42. J. Biol. Chem. 281: 24414–24422 (2006).
- Cheung, K.H., Shineman, D., Muller, M., Cardenas, C., Mei, L., Yang, J., Tomita, T., Iwatsubo, T., Lee, V.M. and Foskett, J.K..et al. Mechanism of Ca^{2+} disruption in Alzheimer's disease by presenilin regulation of InsP3 receptor channel gating. Neuron 58:871–883 (2008).
- Chung S.H., Aberrant phosphorylation in the pathogenesis of Alzheimer's disease. BMB Rep, Vol.42: 467–474, 2009.
- Cheung K.H., Mei L., Mak D.O., Hayashi I., Iwatsubo T., Kang D.E., Foskett J.K., Gain-of-function enhancement of IP3 receptor modal gating by familial Alzheimer's disease-linked presenilin mutants in human cells and mouse neurons. Sci signal, Vol.3, 2010.
- Chouhan AK, Zhang J, Zinsmaier KE, Macleod GT. Presynaptic mitochondria in functionally different motor neurons exhibit similar affinities for Ca^{2+} but exert little influence as Ca^{2+} buffers at nerve firing rates *in situ*. J Neurosci, 2010. 30(5): p. 1869-81.
- Chyung, J.H., Raper, D.M. and Selkoe, D.J. Gamma-secretase exists on the plasma membrane as an intact complex that accepts substrates and effects intramembrane cleavage. J Biol Chem. 280 (6): 4383-4392 (2005).
- Cifuentes F., González C.E., Fiordelisio T., Guerrero G., Lai F.A., Hernández-Cruz A., A ryanodine fluorescent derivative reveals the presence of high-affinity ryanodine binding sites in the Golgi complex of rat sympathetic neurons, with possible functional roles in intracellular Ca^{2+} signaling. Cell Signal, Vol.13: 353–362, 2001.

- Citron, M., Westaway, D., Xia, W., Carlson, G., Diehl, T., Levesque, G., Johnson-Wood, K., Lee, M., Seubert, P., Davis, A., Kholodenko, D., Motter, R., Sherrington, R., Perry, B., Yao, H., Strome, R., Lieberburg, I., Rommens, J., Kim, S., Schenk, D., Fraser, P., St George Hyslop, P. and Selkoe, D.J. Mutant presenilins of Alzheimer's disease increase production of 42-residue amyloid beta-protein in both transfected cells and transgenic mice. Nat Med. 3 (1): 67-72 (1997).
- Clapham, D.E. Calcium signalling. Cell 131 (6): 1047-1058 (2007).
- Cole S.L., Vassar R., The Alzheimer's disease beta-secretase enzyme, BACE1. Mol Neurodegener, Vol.2: 22, 2007.
- Colegrove SL, Albrecht MA, Friel DD (2000). Dissection of mitochondrial Ca^{2+} uptake and release fluxes *in situ* after depolarization-evoked [Ca^{2+}]i elevations in sympathetic neurons. J Gen Physiol 115,351–370
- Contreras, L. et al. Ca^{2+} activation kinetics of the two aspartate-glutamate mitochondrial carriers, aralar and citrin: role in the heart malate-aspartate NADH shuttle. J. Biol. Chem. 282, 7098–7106 (2007).
- Contreras, L., Drago, I., Zampese, E. and Pozzan, T. Mitochondria: the calcium connection. Biochim. Biophys. Acta 1797, 607-618 (2010).
- Cosson P, Marchetti A, Ravazzola M, Orci L.Mitofusin-2 independent juxtaposition of endoplasmic reticulum and mitochondria: an ultrastructural study. PLoS One. 2012;7(9):e46293.
- Cox D.A., Matlib M.A. (1993). Modulation of intramitochondrial free Ca^{2+} concentration by antagonists of Na+–Ca^{2+} exchange, Trends Pharmacol. Sci 14, 408.
- Cribbs JT, Strack S. (2007). Reversible phosphorylation of Drp1 by cyclic AMP-dependent protein kinase and calcineurin regulates mitochondrial fission and cell death. EMBO Rep 8,939–44.
- Csala M., Bánhegyi G., Benedetti A., Endoplasmic reticulum: a metabolic compartment. FEBS Lett, Vol.580: 2160-2165, 2006.
- Csordas, G., Renken, C., Varnai, P., Walter, L., Weaver, D., Buttle, K.F., Balla, T., Mannella, C.A. and Hajnoczky, G. Structural and functional features and significance of the physical linkage between ER and mitochondria. J Cell Biol 174(7): 915–921 (2006).
- Csordás G, Thomas AP, Hajnóczky G.Quasi-synaptic calcium signal transmission between endoplasmic reticulum and mitochondria. EMBO J, 1999. 18(1): p. 96-108.
- Csordas, G., Golenar, T., Seifert, E.L., Kamer, K.J., Sancak, Y., Perocchi, F., Moffat, C., Weaver, D., de la Fuente Perez, S., Bogorad, R., Koteliansky, V., Adijanto, J., Mootha, V.K. and Hajnoczky, G. MICU1 controls both the threshold and cooperative activation of the mitochondrial Ca^{2+} uniporter. Cell Metab 17, 976-987 (2013).
- David, G., Barrett, J. N. & Barrett, E. F. (1998).Evidence that mitochondria buffer physiological Ca^{2+} loads in lizard motor nerve terminals. J. Physiol. 509, 59–65.
- Denton, R.M., Regulation of mitochondrial dehydrogenases by calcium ions. Biochim Biophys Acta, 2009. 1787(11): p. 1309-16.
- de Brito O.M. and Scorrano L., Mitofusin 2 tethers endoplasmic reticulum to mitochondria. Nature, Vol.456: 605–610, 2008.
- de Brito, O.M. and Scorrano, L. An intimate liaison: spatial organization of the endoplasmic reticulum-mitochondria relationship. EMBO J. 29, 2715-2723 (2010).
- de la Fuente S, Fonteriz RI, de la Cruz PJ, Montero M, Alvarez J. Mitochondrial free [Ca($^{2+}$)] dynamics measured with a novel low-Ca($^{2+}$) affinity aequorin probe. Biochem J. 2012 Aug 1;445(3):371-6.

- de la Fuente S, Matesanz-Isabel J, Fonteriz RI, Montero M, Alvarez J.Dynamics of mitochondrial Ca^{2+} uptake in MICU1-knockdown cells. Biochem. J. (2013), pp. 33–40
- De Marchi, U., Castelbou, C. and Demaurex, N. Uncoupling rotein 3 (UCP3) modulates the activity of sarco/endoplasmic reticulum Ca^{2+} -ATPase (SERCA) by decreasing mitochondrial ATP production. J Biol Chem 286:32533–32541(2011).
- De Stefani D., Raffaello A., Teardo E., Szabò I., Rizzuto R., A forty-kilodalton protein of the inner membrane is the mitochondrial calcium uniporter. Nature, Vol.476: 336-340, 2011.
- De Strooper, B. and Annaert, W. Novel Research Horizons for Presenilins and gamma-Secretases in Cell Biology and Disease. Annu Rev Cell Dev Biol. 1-26 (2010).
- De Strooper, B., Iwatsubo, T. and Wolfe, M.S. Presenilins and gamma-secretase: structure, function, and role in Alzheimer disease. Cold Spring Harbor Perspectives in Medicine 2:a006304 (2012).
- Deak AT, Blass S, Khan MJ, Groschner LN, Waldeck-Weiermair M, Hallström S, Graier WF, Malli R. IP3-mediated STIM1 oligomerization requires intact mitochondrial Ca^{2+} uptake. J Cell Sci. 2014 Jul 1;127(Pt 13):2944-55.
- Decuypere JP, Welkenhuyzen K, Luyten T, Ponsaerts R, Dewaele M, Molgó J, Agostinis P, Missiaen L, De Smedt H, Parys JB, Bultynck G. Ins(1,4,5)P3 receptor-mediated Ca^{2+} signaling and autophagy induction are interrelated. Autophagy. 2011 Dec;7(12):1472-89.
- Deisseroth K. Optogenetics. Nature Methods 8,26–29 (2011)
- Deluca, H. F. & Engstrom, G. W. (1961).Ca^{2+} uptake by rat kidney mitochondria. Proc. Natl Acad. Sci. USA 47, 1744–1750.
- Demaurex N, Frieden M. Measurements of the free luminal ER Ca($^{2+}$) concentration with targeted "cameleon" fluorescent proteins. Cell Calcium. 2003 Aug;34(2):109-19. Review.
- Demuro A, Parker I. Cytotoxicity of intracellular aβ42 amyloid oligomers involves Ca^{2+} release from the endoplasmic reticulum by stimulated production of inositol trisphosphate. J Neurosci. 2013
- Di Benedetto G, Pendin D, Greotti E, Pizzo P, Pozzan T. Ca^{2+} and cAMP cross-talk in mitochondria. J Physiol. 2014 Jan 15;592(Pt 2):305-12.
- Donato, R. 1999. Functional roles of S100 proteins, calcium-binding proteins of the EF-hand type. Biochem. Biophys. Acta 1450:191–231.
- Drago I., Giacomello M., Pizzo P., Pozzan T., Calcium dynamics in the peroxisomal lumen of living cells. J Biol Chem, Vol.283: 14384-90, 2008.
- Drago, I., De Stefani, D., Rizzuto, R. and Pozzan, T. Mitochondrial Ca^{2+} uptake contributes to buffering cytoplasmic Ca^{2+} peaks in cardiomyocytes. Proc Natl Acad Sci U S A 109, 12986-12991 (2012).
- Dreses-Werringloer, U., Lambert, J.C., Vingtdeux, V., Zhao, H., Vais, H., Siebert, A., Jain, A., Koppel, J., Rovelet-Lecrux, A., Hannequin, D., Pasquier, F., Galimberti, D., Scarpini, E., Mann, D., Lendon, C., Campion, D., Amouyel, P., Davies, P., Foskett, J.K., Campagne, F. and Marambaud, P. A polymorphism in CALHM1 influences Ca^{2+} homeostasis, Abeta levels, and Alzheimer's disease risk. Cell 133: 1149-1161 (2008).
- Duchen MR. Mitochondria and Ca^{2+}: from cell signalling to cell death. J Physiol 529(Pt 1),57–68. (2000).
- Ebrecht R, Don Paul C, Wouters FS. Fluorescence lifetime imaging microscopy in the medical sciences. Protoplasma. 2014 Mar;251(2):293-305.

- Echevarria W, Leite MF, Guerra MT, Zipfel WR, Nathanson MH (2003) Regulation of calcium signals in the nucleus by a nucleoplasmic reticulum. Nat Cell Biol 5 (5):440-446
- Ehehalt R., Michel B., De Pietri Tonelli D., Zacchetti D., Simons K., Keller P., Splice variants of the beta-site APP-cleaving enzyme BACE1 in human brain and pancreas. Biochem Biophys Res Commun, Vol.293: 30–37, 2002.
- Emilsson, L., Saetre, P. and Jazin, E. Alzheimer's disease: mRNA expression profiles of multiple patients show alterations of genes involved with calcium signaling. Neurobiol Dis. 21: 618-625 (2006).
- Entcheva E. Cardiac optogenetics. Am J Physiol Heart Circ Physiol. 2013 May;304(9):H1179-91.
- Etcheberrigaray, R., Hirashima, N., Nee, L., Prince, J., Govoni, S., Racchi, M., et al. Calcium responses in fibroblasts from asymptomatic members of Alzheimer's disease families. Neurobiology of Disease 5: 37–45 (1998).
- Evanko DS, Haydon PG., Elimination of environmental sensitivity in a cameleon FRET-based calcium sensor via replacement of the acceptor with Venus. Cell Calcium, 2005. 37(4): p. 341-8.
- Fasolato C., Innocenti B., Pozzan T., Receptor-activated Ca^{2+} influx: how many mechanisms for how many channels? Trends Pharmacol Sci, Vol.15: 77-82, 1994.
- Feske S, Gwack Y, Prakriya M, Srikanth S, Puppel SH, Tanasa B, Hogan PG, Lewis RS, Daly M, Rao A.A mutation in Orai1 causes immune deficiency by abrogating CRAC channel function. Nature. 2006 May 11;441(7090):179-85. Epub 2006 Apr 2.
- Feske S. ORAI1 and STIM1 deficiency in human and mice: roles of store-operated Ca^{2+} entry in the immune system and beyond. Immunol Rev. 2009 Sep;231(1):189-209.
- Luvisetto S, Fellin T, Spagnolo M, Hivert B, Brust PF, Harpold MM, Stauderman KA, Williams ME, Pietrobon D. Modal gating of human CaV2.1 (P/Q-type) calcium channels: I. The slow and the fast gating modes and their modulation by beta subunits. J Gen Physiol. 2004 Nov;124(5):445-61.
- Fiala, J.C. Mechanisms of amyloid plaque pathogenesis. Acta Neuropathol. 114: 551-571 (2007).
- Fieni, F., Lee, S.B., Jan, Y.N., Kirichok, Y. Activity of the mitochondrial calcium uniporter varies greatly between tissues. Nat Commun 3:1317 (2012).
- Filadi, R., Zampese, E., Pozzan, T., Pizzo, P. and Fasolato, C. Endoplasmic Reticulum-Mitochondria Connections, Calcium Cross-Talk and Cell Fate: A Closer Inspection. In "Endoplasmic Reticulum Stress in Health and Disease" Agostinis, P. and Samali, A. Springer Edition, Part 1, 75-106 (2012).
- Filippin L, Magalhães PJ, Di Benedetto G, Colella M, Pozzan T. Stable interactions between mitochondria and endoplasmic reticulum allow rapid accumulation of calcium in a subpopulation of mitochondria. J Biol Chem. 2003 Oct 3;278(40):39224-34. Epub 2003 Jul 21.
- Filippin L, Abad MC, Gastaldello S, Magalhães PJ, Sandonà D, Pozzan T. Improved strategies for the delivery of GFP-based Ca^{2+} sensors into the mitochondrial matrix. Cell Calcium. 2005 Feb;37(2):129-36.
- Fill, M. and Copello, J.A. Ryanodine receptor calcium release channels. Physiol Rev 82 (4):893-922 (2002).
- Florean, C., Zampese, E., Zanese, M., Brunello, L., Ichas, F., De Giorgi, F. and Pizzo, P. High content analysis of gamma-secretase activity reveals variable dominance of presenilin mutations linked to familial Alzheimer's disease. Biochim Biophys Acta. 1783 (8):1551-1560 (2008).
- Förstl, H. and Kurz, A. Clinical features of Alzheimer's disease. Eur Arch Psychiatry Clin Neurosci.; 249 (6): 288-290 (1999).

- Foskett J.K., White C., Cheung K., Mak D.O., Inositol triphosphate receptor Ca^{2+} release channels. Physiol Rev, Vol.87: 593-658, 2007.
- Foust KD, Nurre E, Montgomery CL, Hernandez A, Chan CM, Kaspar BK.Intravascular AAV9 preferentially targets neonatal neurons and adult astrocytes. Nat Biotechnol. 2009 Jan;27(1):59-65.
- Frank, S. et al. The role of dynamin-related protein 1, a mediator of mitochondrial fission, in apoptosis. Dev. Cell 1, 515–525 (2001).
- Fransson S, Ruusala A, Aspenstrom P. (2006).The atypical Rho GTPases Miro-1 and Miro-2 have essential roles in mitochondrial trafficking. Biochem Biophys Res Commun 344,500–10.
- Franzini-Armstrong C (2007). ER–mitochondria communication. How privileged? Physiology (Bethesda) 22,261–268
- Frieden M, James D, Castelbou C, Danckaert A, Martinou JC, Demaurex N. Ca(2+) homeostasis during mitochondrial fragmentation and perinuclear clustering induced by hFis1. J Biol Chem 2004;279,22,704–14.
- Frieden M, Arnaudeau S, Castelbou C, Demaurex N. Subplasmalemmal mitochondria modulate the activity of plasma membrane Ca^{2+}-ATPases. J Biol Chem 2005;280,43,198–208.
- Friedman, J.R., Lackner, L.L., West, M., DiBenedetto, J.R., Nunnari, J. and Voeltz, G.K. ER tubules mark sites of mitochondrial division. Science 334, 358-362 (2011).
- Gandy, S. The role of cerebral amyloid beta accumulation in common forms of Alzheimer disease. J Clin Invest. 115: 1121-1129 (2005).
- Gao G.P. Alvira M.R. Wang L. Calcedo R. Johnston J. Wilson J.M. Novel adeno-associated viruses from rhesus monkeys as vectors for human gene therapy. Proc. Natl. Acad. Sci. U.S.A. 2002;99:11854–11859.
- Garaschuk O, Griesbeck O, Konnerth A. Troponin C-based biosensors: a new family of genetically encoded indicators for *in vivo* calcium imaging in the nervous system. Cell Calcium. 2007 Oct-Nov;42(4-5):351-61. Epub 2007 Apr 23. Review.
- Gautier I, Tramier M, Durieux C, Coppey J, Pansu RB, Nicolas JC, Kemnitz K, Coppey-Moisan M. Homo-FRET microscopy in living cells to measure monomer-dimer transition of GFP-tagged proteins. Biophys J 2001;80:3000-3008.
- Giacomello M., Barbiero L., Zatti G., Squitti R., Binetti G., Pozzan T., Fasolato C., Ghidoni R., Pizzo P., Reduction of Ca^{2+} stores and capacitative Ca^{2+} entry is associated with the familial Alzheimer's disease presenilin-2 T122R mutation and anticipates the onset of dementia. Neurobiol Dis, Vol.18: 638-48, 2005.
- Giacomello, M., Drago, I., Bortolozzi, M., Scorzeto, M., Gianelle, A., Pizzo, P. and Pozzan, T. Ca^{2+} hot spots on the mitochondrial surface are generated by Ca^{2+} mobilization from stores, but not by activation of store-operated Ca^{2+} channels. Mol Cell 38(2):280–290 (2010).
- Gilabert, J. A. & Parekh, A. B. Respiring mitochondria determine the pattern of activation and inactivation of the store-operated Ca^{2+} current I(CRAC). EMBO J.19, 6401–6407 (2000).
- Gillis JM (1997) Inhibition of mitochondrial calcium uptake slows down relaxation in mitochondria-rich skeletal muscles. JMuscle Res Cell Motil 18,473–483
- Giorgi C., Romagnoli A., Pinton P., Rizzuto R. Ca^{2+} signaling, mitochondria and cell death. Curr. Mol. Med. 2008;8:119–130.

- Giorgio, V., von Stockum, S., Antoniel, M., Fabbro, A., Fogolari, F., Forte, M., Glick, G.D., Petronilli, V., Zoratti, M., Szabó, I., Lippe, G. and Bernardi, P. Dimers of mitochondrial ATP synthase form the permeability transition pore. Proc Natl Acad Sci U S A 110 (15): 5887-5892 (2013).
- Glenner G.G. and Wong C.W., Alzheimer's disease: initial report of the purification and characterization of a novel cerebrovascular amyloid protein. Biochem Biophys Res Commun, Vol.120: 885–890, 1984.
- Glitsch, M. D., Bakowski, D. & Parekh, A. B. Store-operated Ca^{2+} entry depends on mitochondrial Ca^{2+} uptake. EMBO J. 21, 6744–6754 (2002).
- Green K.N., Demuro A., Akbari Y., Hitt B.D., Smith I.F., Parker I., LaFerla F.M., SERCA pump activity is physiologically regulated by presenilin and regulates amyloid beta production. J Gen Physiol, Vol.132, 2008.
- Griesbeck, O., et al., Reducing the environmental sensitivity of yellow fluorescent protein. Mechanism and applications. J Biol Chem, 2001. 276(31): p. 29188-94.
- Grigoriev I, Gouveia SM, van der Vaart B, Demmers J, Smyth JT, Honnappa S, Splinter D, Steinmetz MO, Putney JW Jr, Hoogenraad CC, Akhmanova A. STIM1 is a MT-plus-end-tracking protein involved in remodeling of the ER. Curr Biol. 2008 Feb 12; 18(3):177-82
- Grynkiewicz, G., M. Poenie, and R.Y. Tsien, A new generation of Ca^{2+} indicators with greatly improved fluorescence properties. J Biol Chem, 1985. 260(6): p. 3440-50.
- Gunter, T. E. & Pfeiffer, D. R. Mechanisms by which mitochondria transport Ca^{2+}.Am. J. Physiol. 258, C755–C786 (1990).
- Guo Q., Christakos S., Robinson N., Mattson M.P., Calbindin D28k blocks the proapoptotic actions of mutant presenilin 1: reduced oxidative stress and preserved mitochondrial function. Proc Natl Acad Sci USA, Vol.95: 3227-32, 1998.
- Guo Q, Wang Z, Li H, Wiese M, Zheng H.APP physiological and pathophysiological functions: insights from animal models.Cell Res. 2012 Jan;22(1):78-89.
- Haass, C. and Selkoe, D.J. Soluble protein oligomers in neurodegeneration: lessons from the Alzheimer's amyloid beta-peptide. Nat Rev Mol Cell Biol. 8:101-112 (2007).
- Hamilton S.L. and Serysheva I.I., Ryanodine receptor structure: progress and challenges. J Biol Chem, Vol.284: 4047-4051, 2008.
- Hansford, R. G. Physiological role of mitochondrial Ca^{2+} transport. J. Bioenerg. Biomembr. 26, 495–508 (1994).
- Hanson, C. J., Bootman, M. D., Distelhorst, C. W., Wojcikiewicz, R. J. & Roderick, H. L. Bcl-2 suppresses Ca^{2+} release through inositol 1,4,5-trisphosphate receptors and inhibits Ca^{2+} uptake by mitochondria without affecting ER calcium store content. Cell Calcium 44, 324–338 (2008).
- Hardingham GE, Chawla S, Johnson CM, Bading H (1997) Distinct functions of nuclear and cytoplasmic calcium in the control of gene expression. Nature 385:260-265
- Hardy, J. and Selkoe, D.J.: The amyloid hypothesis of Alzheimer's disease: progress and problems on the road to therapeutics. Science 297: 353-356 (2002).
- Haug-Collet K1, Pearson B, Webel R, Szerencsei RT, Winkfein RJ, Schnetkamp PP, Colley NJ.Cloning and characterization of a potassium-dependent sodium/calcium exchanger in Drosophila. J Cell Biol. 1999 Nov 1;147(3):659-70.
- Häusser M. Optogenetics: the age of light. Nat Methods. 2014 Oct;11(10)

- Hegemann P, Möglich A. Channelrhodopsin engineering and exploration of new optogenetic tools. Nat Methods. 2011 Jan;8(1):39-42.
- Henze K, Martin W; Martin, William (2003). "Evolutionary biology: essence of mitochondria". Nature 426 (6963), 127–8.
- Herms, J., Schneider, I., Dewachter, I., Caluwaerts, N., Kretzschmar, H. and Van Leuven, F. Capacitive calcium entry is directly attenuated by mutant presenilin-1, independent of the expression of the amyloid precursor protein. J Biol Chem 278: 2484-2489 (2003).
- Herreman, A., Serneels, L., Annaert, W., Collen, D., Schoonjans, L. and De Strooper, B. Total inactivation of gamma-secretase activity in presenilin-deficient embryonic stem cells. Nat Cell Biol. 2: 461-462 (2000).
- Hochbaum DR, Zhao Y, Farhi SL, Klapoetke N, Werley CA, Kapoor V, Zou P, Kralj JM, Maclaurin D, Smedemark-Margulies N, Saulnier JL, Boulting GL, Straub C, Cho YK, Melkonian M, Wong GK, Harrison DJ, Murthy VN, Sabatini BL, Boyden ES, Campbell RE, Cohen AE. All-optical electrophysiology in mammalian neurons using engineered microbial rhodopsins. Nat Methods. 2014 Aug;11(8):825-33.
- Hoeflich KP, Ikura M.Calmodulin in action: diversity in target recognition and activation mechanisms. Cell. 2002 Mar 22;108(6):739-42.
- Hoffman NE, Chandramoorthy HC, Shamugapriya S, Zhang X, Rajan S, Mallilankaraman K, Gandhirajan RK, Vagnozzi RJ, Ferrer LM4 Sreekrishnanilayam K, Natarajaseenivasan K, Vallem S1, Force T, Choi ET6, Cheung JY, Madesh M. MICU1 motifs define mitochondrial calcium uniporter binding and activity. Cell Rep., 5 (2013), pp. 1576–1588
- Holtzman D.M., Morris John C., Goate A., Alzheimer's disease: the challenge of the second century. Sci Transl Med, Vol.6: 77-112, 2011.
- Honarnejad K1, Herms J. Presenilins: role in calcium homeostasis. Int J Biochem Cell Biol. 2012 Nov;44(11):1983-6.
- Horikawa K, Yamada Y, Matsuda T, Kobayashi K, Hashimoto M, Matsu-ura T, Miyawaki A, Michikawa T, Mikoshiba K, Nagai T. Spontaneous network activity visualized by ultrasensitive Ca(2+) indicators, yellow Cameleon-Nano. Nat Methods. 2010 Sep;7(9):729-32.
- Hoth, M., Fanger, C. M. & Lewis, R. S. Mitochondrial regulation of store-operated Ca^{2+} signaling in T lymphocytes. J. Cell Biol. 137, 633–648 (1997).
- Hou X, Pedi L, Diver MM, Long SB.Crystal structure of the calcium release-activated calcium channel Orai. Science. 2012 Dec 7;338(6112):1308-13.
- Høyer-Hansen M, Jäättelä M. Connecting endoplasmic reticulum stress to autophagy by unfolded protein response and calcium. Cell Death Differ. 2007 Sep;14(9):1576-82.
- Inouye S, Noguchi M, Sakaki Y, Takagi Y, Miyata T, Iwanaga S, Miyata T, Tsuji FI. Cloning and sequence analysis of cDNA for the luminescent protein aequorin. Proc Natl Acad Sci U S A. 1985 May;82(10):3154-8.
- Ito, E., Oka, K., Etcheberrigaray, R., Nelson, T.J., McPhie, D.L., Tofel-Grehl, B., et al. Internal Ca^{2+} mobilization is altered in fibroblasts from patients with Alzheimer disease. Proc Natl Acad Sci USA 91:534–853 (1994).
- Ivannikov MV and Macleod GT. Mitochondrial free Ca(2+) levels and their effects on energy metabolism in Drosophila motor nerve terminals. Biophys J, 2013. 104(11): p. 2353-61.
- Jean-Quartier C.,. Bondarenko A.I, Alam M.R., Trenker M., Waldeck-Weiermair M., Malli R, Graier W.F. Studying mitochondrial Ca(2+) uptake – a revisit. Mol. Cell. Endocrinol., 353 (2012), pp. 114–127

- Jiang, D., Zhao, L. and Clapham, D.E. Genome-wide RNAi screen identifies Letm1 as a mitochondrial Ca^{2+}/H + antiporter. Science 326:144–147 (2009).
- Joseph S.K., Boehning D., Pierson S., Nicchitta C.V., Membrane insertion, glycosylation, and oligomerization of inositol trisphosphate receptors in a cell-free translation system. J Biol Chem, Vol.272: 1579–1588, 1997.
- Jouaville LS, Pinton P, Bastianutto C, Rutter GA, Rizzuto R. Regulation of mitochondrial ATP synthesis by Ca^{2+}: evidence for a long-term metabolic priming. Proc Natl Acad Sci USA 1999;96,13,807–12.
- Jung D.H., Mo S.H., Kim D.H., Calumenin, a multiple EF-hands Ca^{2+}-binding protein, interacts with ryanodine receptor-1 in rabbit skeletal sarcoplasmic reticulum, Biochem Biophys Res Commun, Vol.343: 34–42, 2006.
- Kaether, C., Haass, C. and Steiner, H. Assembly, trafficking and function of gamma-secretase. Neurodegener Dis.; 3 (4-5): 275-283 (2006a).
- Kaether, C., Schmitt, S., Willem, M. and Haass, C. Amyloid precursor protein and Notch intracellular domains are generated after transport of their precursors to the cell surface. Traffic. 7 (4): 408-415 (2006b).
- Kar P, Bakowski D, Di Capite J, Nelson C, Parekh AB. Different agonists recruit different stromal interaction molecule proteins to support cytoplasmic Ca^{2+} oscillations and gene expression. Proc Natl Acad Sci U S A. 2012 May 1;109(18):6969-74.
- Karabinos A., Bhattacharya D., Morys-Wortmann C., Kroll K., Hirschfeld G., Kratzin H.D., Barnikol-Watanabe S., Hilschmann N., The divergent domains of the NEFA and nucleobindin proteins are derived from an EF-hand ancestor. Mol Biol Evol, Vol.13: 990–998, 1996.
- Kasri, N.N., Kocks, S.L., Verbert, L., Hébert, S.S., Callewaert, G., Parys, J.B., Missiaen, L. and De Smedt, H. Up-regulation of inositol 1,4,5-trisphosphate receptor type 1 is responsible for a decreased endoplasmic-reticulum Ca^{2+} content in presenilin double knock-out cells. Cell Calcium 40 (1): 41-51 (2006).
- Kato HE, Zhang F, Yizhar O, Ramakrishnan C, Nishizawa T, Hirata K, Ito J, Aita Y, Tsukazaki T, Hayashi S, Hegemann P, Maturana AD, Ishitani R, Deisseroth K, Nureki O. Crystal structure of the channelrhodopsin light-gated cation channel. Nature. 2012 Jan 22;482(7385):369-74.
- Kaufman R.J., Swaroop M., Murtha-Riel P., Depletion of manganese within the secretory pathway inhibits O-linked glycosylation in mammalian cells. Biochemistry, Vol.33: 9813–9819, 1994.
- Kayed R., Head E., Thompson J.L., McIntire T.M., Milton S.C., Cotman C.W., Glabe C.G., Common structure of soluble amyloid oligomers implies common mechanism of pathogenesis. Science, Vol.300: 486–489, 2003.
- Kettlewell, S., et al., Changes of intra-mitochondrial Ca^{2+} in adult ventricular cardiomyocytes examined using a novel fluorescent Ca^{2+} indicator targeted to mitochondria. J Mol Cell Cardiol, 2009. 46(6): p. 891-901.
- Kim, J., Kleizen, B., Choy, R., Thinakaran, G., Sisodia, S.S. and Schekman, R.W. Biogenesis of gamma-secretase early in the secretory pathway. J Cell Biol. 179 (5): 951-963 (2007).
- Kim, T.W., Pettingell, W.H., Hallmark, O.G., Moir, R.D., Wasco, W. and Tanzi, R.E. Endoproteolytic cleavage and proteasomal degradation of presenilin 2 in transfected cells. Journal of Biological Chemistry 272:11006–11010 (1997).
- Kimberly, W.T., Xia, W., Rahmati, T., Wolfe, M.S. and Selkoe, DJ. The transmembrane aspartates in presenilin 1 and 2 are obligatory for gamma-secretase activity and amyloid beta-protein generation. J Biol Chem. 275 (5): 3173-3178 (2000).
- Kipanyula, M.J., Contreras, L., Zampese, E., Lazzari, C., Wong, A.K., Pizzo, P., Fasolato, C. and Pozzan, T. Ca^{2+} dysregulation in neurons from transgenic mice expressing mutant presenilin 2. Aging Cell 11(5): 885-993 (2012).

- Kleinlogel S, Feldbauer K, Dempski RE, Fotis H, Wood PG, Bamann C, Bamberg E. Ultra light-sensitive and fast neuronal activation with the Ca²+-permeable channelrhodopsin CatCh. Nat Neurosci. 2011 Apr;14(4):513-8.
- Ko SK, Chen X, Yoon J, Shin I. Zebrafish as a good vertebrate model for molecular imaging using fluorescent probes. Chem Soc Rev. 2011 May;40(5):2120-30.
- Kojro E., Gimpl G., Lammich S., Marz W., Fahrenholz F., Low cholesterol stimulates the nonamyloidogenic pathway by its effect on the alpha-secretase ADAM 10. Proc Natl Acad Sci USA, Vol.98: 5815–5820, 2001.
- Koldenkova Pérez V, Nagai T. Genetically encoded Ca(2+) indicators: properties and evaluation. Biochim Biophys Acta. 2013 Jul;1833(7):1787-97.
- Kornmann, B., Currie, E., Collins, S.R., Schuldiner, M., Nunnari, J., Weissman, J.S. and Walter, P. An ER-mitochondria tethering complex revealed by a synthetic biology screen. Science 325(5939):477–481 (2009).
- Korzeniowski M.K., Szanda G., Balla T., Spat A. Store-operated Ca^{2+} influx and subplasmalemmal mitochondria. Cell Calcium, 46 (2009), pp. 49–55
- Krieger-Brauer HI, Gratzl M (1983) Effects of monovalent and divalent cations on Ca^{2+} fluxes across chromaffin secretory membrane vesicles. J Neurochem 41 (5):1269-1276
- Kügler S, Meyn L, Holzmüller H, Gerhardt E, Isenmann S, Schulz JB, Bähr M. Neuron-specific expression of therapeutic proteins: evaluation of different cellular promoters in recombinant adenoviral vectors. Mol Cell Neurosci. 2001 Jan;17(1):78-96.
- LaFerla, F.M., Green, K.N. and Oddo, S. Intracellular amyloid-beta in Alzheimer's disease. Nat Rev Neurosci. 8: 499-509 (2007).
- Lakowicz, J.R. (2006) Principles of Fluorescence Spectroscopy, 3rd ed. Springer, Berlin, Heidelberg, New York.
- Lakowicz, Joseph R.; Szmacinski, Henryk; Nowaczyk, Kazimierz; Berndt, Klaus W.; Johnson, Michael (1992). "Fluorescence lifetime imaging". Analytical Biochemistry 202 (2): 316–30.
- Lamb G.D., Excitation–contraction coupling in skeletal muscle: comparisons with cardiac muscle. Clin Exp Pharmacol Physiol, Vol.27: 216–224, 2000.
- LaPointe N.E., Morfini G., Pigino G., Gaisina I.N., Kozikowski A.P., Binder L.I., Brady S.T., The amino terminus of tau inhibits kinesin-dependent axonal transport: implications for filament toxicity. J Neurosci Res, Vol.87: 440–451, 2009.
- Lasorsa, F. M. et al. Recombinant expression of the Ca^{2+}-sensitive aspartate/glutamate carrier increases mitochondrial ATP production in agonist-stimulated Chinese hamster ovary cells. J. Biol. Chem. 278, 38686–38692 (2003).
- Lazzari C, Kipanyula MJ, Agostini M, Pozzan T, Fasolato C. Aβ42 oligomers selectively disrupt neuronal calcium release. Neurobiol Aging. 2014 Oct 20. pii: S0197-4580(14)00678-2.
- Lee S.F., Shah S., Li H., Yu C., Han W., Yu G., Mammalian APH-1 interacts with presenilin and nicastrin and is required for intramembrane proteolysis of amyloid-beta precursor protein and Notch. J Biol Chem, Vol.277: 45013–45019, 2002
- Lehninger, AL, Rossi CS, and Greenawalt JW. Respiration-dependent accumulation of inorganic phosphate and Ca ions by rat liver mitochondria. Biochem Biophys Res Commun, 1963. 10: p. 444-8.
- Leissring MA1, Akbari Y, Fanger CM, Cahalan MD, Mattson MP, LaFerla FM. Capacitative calcium entry deficits and elevated luminal calcium content in mutant presenilin-1 knockin mice. J Cell Biol. 2000 May 15;149(4):793-8.

- Levy E., Carman M.D., Fernandez-Madrid I.J., Power M.D., Lieberburg I., van Duinen S.G., Bots G.T., Luyendijk W., Frangione B., Mutation of the Alzheimer's disease amyloid gene in hereditary cerebral hemorrhage, Dutch type. Science, Vol.248: 1124–1126, 1990.
- Levy-Lahad E., Wasco W., Poorkaj P., Romano D.M., Oshima J., Pettingell W.H., Yu C.E., Jondro P.D., Schmidt S.D., Wang K., et al., Candidate gene for the chromosome 1 familial Alzheimer's disease locus. Science, Vol.269: 973–977, 1995.
- Lewis R.S., The molecular choreography of a store-operated calcium channel. Nature, Vol.446: 284-287, 2007.
- Li Z, Lu J, Xu P, Xie X, Chen L, Xu T. Mapping the interacting domains of STIM1 and Orai1 in Ca^{2+}release-activated Ca^{2+} channel activation. J Biol Chem. 2007;282:29448–29456
- Li, Day-Uei; Arlt, Jochen; Richardson, Justin; Walker, Richard; Buts, Alex; Stoppa, David; Charbon, Edoardo; Henderson, Robert (2010). "Real-time fluorescence lifetime imaging system with a 32 × 32 013μm CMOS low dark-count single-photon avalanche diode array". Optics Express 18 (10): 10257–69.
- Lin JY1, Lin MZ, Steinbach P, Tsien RY. Characterization of engineered channelrhodopsin variants with improved properties and kinetics. Biophys J. 2009 Mar 4;96(5)
- Lin P., Yao Y., Hofmeister R., Tsien R.Y., Farquhar M.G., Overexpression of CALNUC (nucleobindin) increases agonist and thapsigargin releasable Ca^{2+} storage in the Golgi. J Cell Biol, Vol.145: 279–289, 1999.
- Liou J, Fivaz M, Inoue T, Meyer T. Live-cell imaging reveals sequential oligomerization and local plasma membrane targeting of stromal interaction molecule 1 after Ca^{2+} store depletion. Proc Natl Acad Sci U S A. 2007 May 29; 104(22):9301-6.
- Liou J., Kim M.L., Heo W.D., Jones J.T., Myers J.W., Ferrell J.E. Jr, Meyer T., STIM is a Ca^{2+} sensor essential for Ca^{2+}-store-depletion triggered Ca^{2+} influx. Curr Biol, Vol.15: 1235-1241, 2005.
- Lis A, Peinelt C, Beck A, Parvez S, Monteilh-Zoller M, Fleig A, Penner R. CRACM1, CRACM2, and CRACM3 are store-operated Ca^{2+} channels with distinct functional properties. Curr Biol. 2007 May 1;17(9):794-800. Epub 2007 Apr 19.
- Lis A, Zierler S, Peinelt C, Fleig A, Penner R. A single lysine in the N-terminal region of store-operated channels is critical for STIMl-mediated gating. J. Gen. Physiol. 2010;136:673.
- Lissandron V., Podini P., Pizzo P., Pozzan T., Unique characteristics of Ca^{2+} homeostasis of the trans-Golgi compartment. Proc Natl Acad Sci USA, Vol.107: 9198–9203, 2010.
- Llinás R, Blinks JR, Nicholson C. Calcium transient in presynaptic terminal of squid giant synapse: detection with aequorin. Science. 1972 Jun 9;176(4039):1127-9.
- Loro G, Drago I, Pozzan T, Schiavo FL, Zottini M, Costa A. Targeting of Cameleons to various subcellular compartments reveals a strict cytoplasmic/mitochondrial Ca(2+) handling relationship in plant cells. Plant J, 2012. 71(1): p. 1-13.
- Loro G, Ruberti C, Zottini M, Costa A. The D3cpv Cameleon reports Ca(2)(+) dynamics in plant mitochondria with similar kinetics of the YC3.6 Cameleon, but with a lower sensitivity. J Microsc, 2013. 249(1): p. 8-12.
- Lucin K.M. and Wyss-Coray T., Immune activation in brain aging and neurodegeneration: too much or too little? Neuron, Vol.64: 110–122, 2009.
- Lukyanenko V, Gyorke I, Subramanian S, Smirnov A, Wiesner TF, Gyorke S. Inhibition of $Ca^{(2+)}$ sparks by ruthenium red in permeabilized rat ventricular myocytes. Biophys J 2000;79,1273–84.

- Luo W.J., Wang H., Li H., Kim B.S., Shah S., Lee H.J., Thinakaran G., Kim T.W., Yu G. and Xu H., PEN-2 and APH-1 coordinately regulate proteolytic processing of presenilin 1. J Biol Chem, Vol.278: 7850–7854, 2003.
- Mahapatra NR, Mahata M, Hazra PP, McDonough PM, O'Connor DT, Mahata SK A dynamic pool of calcium in catecholamine storage vesicles. Exploration in living cells by a novel vesicle-targeted chromogranin A-aequorin chimeric photoprotein. J Biol Chem 279 (49):51107-51121(2004)
- Malli R, Frieden M, Osibow K, et al. Sustained Ca^{2+} transfer across mitochondria is essential for mitochondrial Ca^{2+} buffering, store-operated Ca^{2+} entry, and Ca^{2+} store refilling. J Biol Chem 2003;278,44,769–79.
- Malli R, Frieden M, Trenker M, Graier WF. The role of mitochondria for Ca^{2+} refilling of the endoplasmic reticulum. J Biol Chem 2005;280,12,114–22.
- Mallilankaraman, K., Doonan, P., Cardenas, C., Chandramoorthy, H.C., Muller, M., Miller, R., Hoffman, N.E., Gandhirajan, R.K., Molgo, J., Birnbaum, M.J., Rothberg, B.S., Mak, D.O., Foskett, J.K. and Madesh, M. MICU1 is an essential gatekeeper for MCU-mediated mitochondrial $Ca(^{2+})$ uptake that regulates cell survival. Cell 151, 630-644 (2012).
- Mallilankaraman, K., Cardenas, C., Doonan, P.J., Chandramoorthy, H.C., Irrinki, K.M., Golenar, T., Csordas, G., Madireddi, P., Yang, J., Muller, M., Miller, R., Kolesar, J.E., Molgo, J., Kaufman, B., Hajnoczky, G., Foskett, J.K. and Madesh, M. MCUR1 is an essential component of mitochondrial Ca^{2+} uptake that regulates cellular metabolism. Nat Cell Biol 14, 1336-1343 (2012b).
- Mank M, Reiff DF, Heim N, Friedrich MW, Borst A, Griesbeck O.A FRET-based calcium biosensor with fast signal kinetics and high fluorescence change. Biophys J. 2006 Mar 1;90(5):1790-6. Epub 2005 Dec 9.
- Mank, M., et al., A genetically encoded calcium indicator for chronic *in vivo* two-photon imaging. Nature Methods, 2008. 5(9): p. 805-811.
- Markwardt ML, Kremers GJ, Kraft CA, Ray K, Cranfill PJ, Wilson KA, Day RN, Wachter RM, Davidson MW, Rizzo MA. An improved cerulean fluorescent protein with enhanced brightness and reduced reversible photoswitching. PLoS One. 2011 Mar 29;6(3):e17896. doi: 10.1371/journal.pone.0017896.
- Martell JD, Deerinck TJ, Sancak Y, Poulos TL, Mootha VK, Sosinsky GE, Ellisman MH, Ting AY, Engineered ascorbate peroxidase as a genetically encoded reporter for electron microscopy. Nat Biotechnol. 2012 Nov;30(11),1143-8.
- Martin L., Latypova X., Terro F., Post-translational modifications of tau protein: implications for Alzheimer's disease. Neurochem Int, Vol.58: 458–471, 2011.
- Matsui T, Ingelsson M, Fukumoto H, Ramasamy K, Kowa H, Frosch MP, Irizarry MC, Hyman BT (August 2007). "Expression of APP pathway mRNAs and proteins in Alzheimer's disease". Brain Res. 1161: 116–23.
- Mattson, M.P., LaFerla, F.M., Chan, S.L., Leissring, M.A., Shepel, P.N., Geiger, D., Calcium signaling in the ER: its role in neuronal plasticity and neurodegenerative disorders. Trends Neurosci, Vol.23: 222 – 229, 2000.
- McCarthy, J.V., Twomey, C. and Wujek, P. "Presenilin-dependent regulated intramembrane proteolysis and gamma-secretase activity". Cell Mol Life Sci. 66 (9):1534-1555 (2009).
- McCombs, J.E., Gibson, E.A. and Palmer, A.E. Using a genetically targeted sensor to investigate the role of presenilin-1 in ER Ca^{2+} levels and dynamics. Molecular Biosystems 6:1640–1649 (2010).
- McConkey DJ, Orrenius S. The role of calcium in the regulation of apoptosis. J Leukoc Biol. 1996 Jun;59(6):775-83. Review.

- McCormack JG, Halestrap AP, Denton RM. Role of Ca^{2+} ions in regulation of mammalian intramitochondrial metabolism. Physiol Rev 1990;70,391–425.
- McNally BA, Yamashita M, Engh A, Prakriya M. Structural determinants of ion permeation in CRAC channels. Proc Natl Acad Sci U S A. 2009;106:22516–22521.
- Mela, L. Inhibition and activation of Ca^{2+} transport in mitochondria. Effect of lanthanides and local anesthetic drugs. Biochemistry 8, 2481–2486 (1969).
- Meldolesi J. and Pozzan T., The endoplasmic reticulum Ca^{2+} store: a view from the lumen. Trends Biochem Sci, Vol.23: 10-14, 1998.
- Mehlmer N, Parvin N, Hurst CH, Knight MR, Teige M, Vothknecht UC.A toolset of aequorin expression vectors for in planta studies of subcellular calcium concentrations in Arabidopsis thaliana. J Exp Bot, 2012. 63(4): p. 1751-61.
- Mercer JC, Dehaven WI, Smyth JT, Wedel B, Boyles RR, Bird GS, Putney JW Jr. Large store-operated calcium selective currents due to co-expression of Orai1 or Orai2 with the intracellular calcium sensor, Stim1. J Biol Chem. 2006 Aug 25; 281(34):24979-90.
- Michikawa T., Hirota J., Kawano S., Hiraoka M., Yamada M., Furuichi T., Mikoshiba K., Calmodulin mediates calcium-dependent inactivation of the cerebellar type 1 inositol 1,4,5-trisphosphate receptor. Neuron, Vol.23: 799–808, 1999.
- Mignery G.A., Newton C.L., Archer B.T. 3rd, Südhof T.C., Structure and expression of the rat inositol 1,4,5-trisphosphate receptor. J Biol Chem, Vol.265: 12679–12685, 1990.
- Mikoshiba K (2007) The IP3 receptor/Ca^{2+} channel and its cellular function. Biochem Soc Symp (74):9-22
- Millington M, Grindlay GJ, Altenbach K, Neely RK, Kolch W, Bencina M, Read ND, Jones AC, Dryden DT, Magennis SW. High-precision FLIM-FRET in fixed and living cells reveals heterogeneity in a simple CFP-YFP fusion protein. Biophys Chem. 2007 May;127(3):155-64.
- Minta A, Kao JP, Tsien RY. Fluorescent indicators for cytosolic calcium based on rhodamine and fluorescein chromophores. J Biol Chem. 1989 May 15;264(14):8171-8.
- Mitchell P and Moyle J. Chemiosmotic hypothesis of oxidative phosphorylation. Nature, 1967. 213(5072): p. 137-9.
- Mitchell K.J., Pinton P., Varadi A., Tacchetti C., Ainscow E.K., Pozzan T., Rizzuto R., Rutter G.A., Dense core secretory vesicles revealed as a dynamic Ca^{2+} store in neuroendocrine cells with a vesicle-associated membrane protein aequorin chimaera. J Cell Biol, Vol.155: 41–51, 2001.
- Miyawaki A, Llopis J, Heim R, McCaffery JM, Adams JA, Ikura M, Tsien RY. Fluorescent indicators for Ca2+ based on green fluorescent proteins and calmodulin. Nature, Vol.388: 882–887, 1997.
- Miyawaki A, Griesbeck O, Heim R, Tsien RY. Dynamic and quantitative Ca2+ measurements using improved cameleons, Proc. Natl. Acad. Sci. U. S. A. 96 (1999) 2135–2140Mizuno, H., et al., Transgenic zebrafish for ratiometric imaging of cytosolic and mitochondrial Ca2+ response in teleost embryo. Cell Calcium, 2013. 54(3): p. 236-45.
- Montero M, Alonso MT, Carnicero E, Cuchillo-Ibáñez I, Albillos A, Garcia AG, García-Sancho J, Alvarez J (2000) Chromaffin cell stimulation triggers fast millimolar mitochondrial Ca^{2+} transients that modulate secretion. Nat Cell Biol 2,57–61

- Montero M, Alonso MT, Albillos A, Cuchillo-Ibanez I, Olivares R, Garcia A, Garcia-Sancho J, Alvarez J (2001) Control of secretion by mitochondria depends on the size of the local [Ca^{2+}] after chromaffin cell stimulation. Eur J Neurosci 13,2247–2254
- Morré, D.J., Merritt, W.D. and Lembi, C.A. Connections between mitochondria and endoplasmic reticulum in rat liver and onion stem. Protoplasma 73(1):43–49 (1971).
- Muik M, Schindl R, Fahrner M, Romanin C. Ca($^{2+}$) release-activated Ca($^{2+}$) (CRAC) current, structure, and function. Cell Mol Life Sci. 2012 Dec;69(24):4163-76.
- Muresan V, Ladescu Muresan Z.Amyloid-β precursor protein: Multiple fragments, numerous transport routes and mechanisms. Exp Cell Res. 2015 Jan 6.
- Nakai, J, Ohkura M, and Imoto K. A high signal-to-noise Ca(2+) probe composed of a single green fluorescent protein. Nat Biotechnol, 2001. 19(2): p. 137-41.
- Nagai T, Yamada S, Tominaga T, Ichikawa M, Miyawaki A. Expanded dynamic range of fluorescent indicators for Ca2+ by circularly permuted yellow fluorescent proteins. Proc Natl Acad Sci USA, Vol.101: 10554–10559, 2004.
- Nagai T, Sawano A, Park ES, Miyawaki A. Circularly permuted green fluorescent proteins engineered to sense Ca^{2+}. Proc Natl Acad Sci U S A, 2001. 98(6): p. 3197-202.
- Nagel G, Ollig D, Fuhrmann M, Kateriya S, Musti AM, Bamberg E, Hegemann P (June 2002). "Channelrhodopsin-1: a light-gated proton channel in green algae"
- Neumann D, Bückers J, Kastrup L, Hell SW, Jakobs S. Two-color STED microscopy reveals different degrees of colocalization between hexokinase-I and the three human VDAC isoforms. PMC Biophys. 2010 Mar 5;3(1):4. doi: 10.1186/1757-5036-3-4.
- Nguyen N, Biet M, Simard E, Béliveau E, Francoeur N, Guillemette G, Dumaine R, Grandbois M, Boulay G. STIM1 participates in the contractile rhythmicity of HL-1 cells by moderating T-type Ca($^{2+}$) channel activity. Biochim Biophys Acta. 2013 Jun; 1833(6):1294-303.
- Nicholls DG. The regulation of extramitochondrial free Ca^{2+} ion concentration by rat liver mitochondria. Biochem J 1978;176,463–74
- Nicholls, D.G. and Crompton, M. Mitochondrial calcium transport. FEBS Lett 111, 261-268 (1980).
- Nicholls, D.G.and Chalmers, S. The integration of mitochondrial calcium transport and storage. J Bioenerg Biomembr 36: 277–281 (2004).
- Nicholls DG. Mitochondria and Ca^{2+} signaling. Cell Ca^{2+} 2005;38,311–17.
- Nowikovsky, K., Pozzan, T., Rizzuto, R., Scorrano, L. and Bernardi, P. Perspectives on: SGP Symposium on Mitochondrial Physiology and Medicine: The pathophysiology of LETM1. J Gen Physiol 139(6):445–454 (2012).
- Nunnari J1, Suomalainen A. Mitochondria: in sickness and in health. Cell. 2012 Mar 16;148(6):1145-59.
- Oda K., Calcium depletion blocks proteolytic cleavages of plasmaprotein precursors which occur at the Golgi and/or trans-Golgi network. Possible involvement of Ca^{2+}-dependent Golgi endoproteases. J Biol Chem, Vol.267: 17465–17471, 1992.
- Oesterhelt D, Stoeckenius W. Rhodopsin-like protein from the purple membrane of Halobacterium halobium. Nat New Biol. 1971 Sep 29;233(39):149-52.
- Oldershaw K.A. and Taylor C.W., 2,5-Di-(tert-butyl)-1,4-benzohydroquinone mobilizes inositol 1,4,5-trisphosphate-sensitive and -insensitive Ca^{2+} stores. FEBS Lett, Vol.274: 214-216, 1990.

- Oluseye A. Ogunbayo, Yingmin Zhu, Daniela Rossi, Vincenzo Sorrentino, Jianjie Ma,‖ Michael X. Zhu, and A. Mark Evans.Cyclic Adenosine Diphosphate Ribose Activates Ryanodine Receptors, whereas NAADP Activates Two-pore Domain Channels Biol Chem. Mar 18, 2011; 286(11): 9136–9140.
- Oulès B, Del Prete D, Greco B, Zhang X, Lauritzen I, Sevalle J, Moreno S, Paterlini-Bréchot P, Trebak M, Checler F, Benfenati F, Chami M. Ryanodine receptor blockade reduces amyloid-β load and memory impairments in Tg2576 mouse model of Alzheimer disease. J Neurosci. 2012 Aug 22;32(34):11820-34.
- Ozer R.S. and Halpain S., Phosphorylation-dependent localization of microtubule- associated protein MAP2c to the actin cytoskeleton. Mol Biol Cell, Vol.11: 3573–3587, 2000.
- Pacak C.A. Mah C.S. Thattaliyath B.D. Conlon T.J. Lewis M.A. Cloutier D.E. Zolotukhin I. Tarantal A.F. Byrne B.J. Recombinant adeno-associated virus serotype 9 leads to preferential cardiac transduction *in vivo*. Circ. Res. 2006;99:e3–e9.
- Pack-Chung E., Meyers M.B., Pettingell W.P., Moir R.D., Brownawell A.M., Cheng I., Tanzi R.E., Kim T.W., Presenilin 2 interacts with sorcin, a modulator of the ryanodine receptor. J Biol Chem, Vol.275: 14440-5, 2000.
- Palmer A.E., Jin C., Reed J.C. and Tsien R.Y., Bcl-2-mediated alterations in endoplasmic reticulum Ca^{2+} analyzed with an improved genetically encoded fluorescent sensor. Proc Natl Acad Sci USA, Vol.101: 17404–17409, 2004.
- Palmer A.E., Giacomello M., Kortemme T., Hires S.A., Lev-Ram V.,Baker D., Tsien R.Y., Ca^{2+} indicators based on computationally redesigned calmodulin-peptide pairs. Chem Biol, Vol.13: 521–530, 2006.
- Palty, R., Ohana, E., Hershfinkel, M., Volokita, M., Elgazar, V., Beharier, O., Silverman, W.F., Argaman, M. and Sekler, I. Lithium-calcium exchange is mediated by a distinct potassium-independent sodium-calcium exchanger. J Biol Chem 279: 25234–25240 (2004).
- Palty, R., Silverman, W.F., Hershfinkel, M., Caporale, T., Sensi, S.L., Parnis, J., Nolte, C., Fishman, D., Shoshan-Barmatz, V., Herrmann, S., Khananshvili, D. and Sekler, I. NCLX is an essential component of mitochondrial Na+/Ca^{2+} exchange. Proc Natl Acad Sci USA 107: 436–441 (2010).
- Pan, X., Liu, J., Nguyen, T., Liu, C., Sun, J., Teng, Y., Fergusson, M.M., Rovira, I.I., Allen, M., Springer, D.A., Aponte, A.M., Gucek, M., Balaban, R.S., Murphy, E. and Finkel, T. The physiological role of mitochondrial calcium revealed by mice lacking the mitochondrial calcium uniporter. Nat Cell Biol 15, 1464-1472 (2013).
- Paredes, R.M., Etzler, J.C., Watts, L.T., Zheng, W. and Lechleiter, J.D. Chemical calcium indicators. Methods 46(3):143-151 (2008).
- Parihar, M.S. and Hemnani, T. Alzheimer's disease pathogenesis and therapeutic interventions. J Clin Neurosci. 11(5): 456-467 (2004).
- Park CY, Hoover PJ, Mullins FM, Bachhawat P, Covington ED, Raunser S, Walz T, Garcia KC, Dolmetsch RE, Lewis RS. STIM1 clusters and activates CRAC channels via direct binding of a cytosolic domain to Orai1. Cell. 2009 Mar 6;136(5):876-90.
- Parks AL, Curtis D. Presenilin diversifies its portfolio. Trends Genet. 2007 Mar;23(3):140-50. Epub 2007 Feb 5. Review.
- Patel S., Joseph S.K., Thomas A.P., Molecular properties of inositol 1,4,5-trisphosphate receptors. Cell Calcium, Vol.25: 247–264, 1999.
- Patel S, Docampo R (2010) Acidic calcium stores open for business: expanding the potential for intracellular Ca^{2+} signaling. Trends Cell Biol 20 (5):277-286

- Patron M, Checchetto V, Raffaello A, Teardo E, Vecellio Reane D, Mantoan M, Granatiero V, Szabò I, De Stefani D, Rizzuto R. MICU1 and MICU2 finely tune the mitochondrial Ca^{2+} uniporter by exerting opposite effects on MCU activity. Mol Cell. 2014 Mar 6;53(5):726-37
- Pendin D, Greotti E, Pozzan T.The elusive importance of being a mitochondrial Ca($^{2+}$) uniporter. Cell Calcium. 2014 Mar;55(3):139-45.
- Penner R, Fasolato C, Hoth M. Calcium influx and its control by calcium release. Curr Opin Neurobiol. 1993 Jun;3(3):368-74.
- Perl, P.D. Neuropathology of Alzheimer's disease. Mt Sinai J Med. 77: 32-42 (2010).
- Perocchi, F., Gohil, V.M., Girgis, H.S., Bao, X.R., McCombs, J.E., Palmer, A.E.and Mootha, V.K. MICU1 encodes a mitochondrial EF hand protein required for Ca($^{2+}$) uptake. Nature 467, 291-296 (2010).
- Perrin, R.J., Fagan, A.M. and Holtzman, D.M. Multimodal techniques for diagnosis and prognosis of Alzheimer's disease. Nature 461: 916-922 (2009).
- Petersen OH, Sutton R (2006) Ca^{2+} signalling and pancreatitis: effects of alcohol, bile and coffee. Trends Pharmacol Sci 27,113–120
- Persechini A, Lynch JA and Romoser VA. Novel fluorescent indicator proteins for monitoring free intracellular Ca2+. Cell Calcium, 1997. 22(3): p. 209-16.
- Petersen OH (2012) Specific mitochondrial functions in separate subcellular domains of pancreatic acinar cells. Pflugers Arch. doi,10.1007/s00424-012-1099-6
- Pezzati R., Bossi M. , Podini P., Meldolesi J., Grohovaz F., High-resolution calcium mapping of the endoplasmic reticulum-Golgi-exocytic membrane system. Electron energy loss imaging analysis of quick frozen-freeze dried PC12 cells. Mol Biol Cell, Vol.8: 1501–1512, 1991.
- Pietrobon D., Di Virgilio F., Pozzan T., Structural and functional aspects of calcium homeostasis in eukaryotic cells. Eur J Biochem, Vol.193: 599-622, 1990.
- Pinton P, Giorgi C, Siviero R, Zecchini E, Rizzuto R. Calcium and apoptosis: ER-mitochondria Ca2+ transfer in the control of apoptosis. Oncogene, 2008. 27(50): p. 6407-18.
- Pizzo P., Lissandron V., Capitanio P., Pozzan T., Ca^{2+} signalling in the Golgi apparatus. Cell Calcium, Vol.50: 184-92, 2011.
- Pizzo P, Drago I, Filadi R and Pozzan T., Mitochondrial Ca^{2+} homeostasis: mechanism, role, and tissue specificities. Pflügers Arch, Vol.464: 3-17, 2012.
- Plovanich, M., Bogorad, R.L., Sancak, Y., Kamer, K.J., Strittmatter, L., Li, A.A., Girgis, H.S., Kuchimanchi, S., De Groot, J., Speciner, L., Taneja, N., Oshea, J., Koteliansky, V., and Mootha, V.K. MICU2, a paralog of MICU1, resides within the mitochondrial uniporter complex to regulate calcium handling. PLoS One 8, e55785 (2013).
- Ponting C.P., Novel repeats in ryanodine and IP3 receptors and protein O-mannosyltransferases. Trends Biochem Sci, Vol.25: 48–50, 2000.
- Postina R., Schroeder A., Dewachter I., Bohl J., Schmitt U., Kojro E., Prinzen C., Endres K., Hiemke C., Blessing M., Flamez P., Dequenne A., Godaux E., van Leuven F., Fahrenholz F., A disintegrin-metalloproteinase prevents amyloid plaque formation and hippocampal defects in an Alzheimer disease mouse model. J Clin Invest, Vol.113: 1456–1464, 2004.
- Pozzan T., Rizzuto R., Volpe P., Meldolesi J., Molecular and cellular physiology of intracellular calcium stores. Physiol Rev, Vol.74: 595-636, 1994.

- Prakash R, Yizhar O, Grewe B, Ramakrishnan C, Wang N, Goshen I, Packer AM, Peterka DS, Yuste R, Schnitzer MJ, Deisseroth K. Two-photon optogenetic toolbox for fast inhibition, excitation and bistable modulation. Nat Methods. 2012 Dec;9(12):1171-9.
- Pralong WF, Hunyady L, Varnai P, Wollheim CB, Spat A. Pyridine nucleotide redox state parallels production of aldosterone in potassium-stimulated adrenal glomerulosa cells. Proc Natl Acad Sci USA 1992;89,132–6.
- Prudent J., Popgeorgiev N., Bonneau B., Thibaut J., Gadet R., Lopez J., Gonzalo P., Rimokh R., Manon S.,. Houart C, Herbomel P., Aouacheria A., Gillet G.. Bcl-wav and the mitochondrial calcium uniporter drive gastrula morphogenesis in zebrafish. Nat. Commun., 4 (2013), p. 2330
- Puigserver P, Spiegelman BM. Peroxisome proliferator-activated receptor-gamma coactivator 1 □ (PGC-1□): transcriptional coactivator and metabolic regulator. Endocr Rev 2003;24,78–90.
- Querfurth, H.W. and LaFerla, F.M. Alzheimer's disease. N Engl J Med. 362: 329-344 (2010).
- Raffaello, A., De Stefani, D., Sabbadin, D., Teardo, E., Merli, G., Picard, A., Checchetto, V., Moro, S., Szabo, I., and Rizzuto, R. The mitochondrial calcium uniporter is a multimer that can include a dominant-negative pore-forming subunit. EMBO J 32, 2362-2376 (2013).
- Ramos-Franco J., Galvan D., Mignery G.A., Fill M., Location of the permeation pathway in the recombinant type 1 inositol 1,4,5-trisphosphate receptor. J Gen Physiol, Vol.114: 243–250, 1999.
- Rapizzi, E., Pinton, P., Szabadkai, G., Wieckowski, M.R., Vandecasteele, G., Baird, G., Tuft, R.A., Fogarty, K.E., and Rizzuto, R. Recombinant expression of the voltage-dependent anion channel enhances the transfer of Ca^{2+} microdomains to mitochondria. J Cell Biol 159: 613–624 (2002).
- Rasola, A. and Bernardi, P. Mitochondrial permeability transition in Ca^{2+}-dependent apoptosis and necrosis. Cell Calcium 50: 222– 233 (2011).
- Raturi, A. and Simmen T. Where the endoplasmic reticulum and the mitochondrion tie the knot: the mitochondria-associated membrane (MAM). Biochim Biophys Acta. 1833(1):213-224 (2013).
- Raychaudhury B., Gupta S., Banerjee S., Datta S.C., Peroxisome is a reservoir of intracellular calcium. Biochim Biophys Acta, Vol.1760: 989–992, 2006.
- Rehberg, M., et al., A new non-disruptive strategy to target calcium indicator dyes to the endoplasmic reticulum. Cell Calcium, 2008. 44(4): p. 386-99
- Rhee, H.-W., Zou, P., Udeshi, N.D., Martell, J.D., Mootha, V.K., Carr, S.A., and Ting, A.Y. (2013). Proteomic mapping of mitochondria in living cells via spatially restricted enzymatic tagging. Science 339, 1328–1331.
- Rippe K (2007) Dynamic organization of the cell nucleus. Curr Opin Genet Dev 17 (5):373-380
- Rizzuto R., Simpson A.W., Brini M., Pozzan T., Rapid changes of mitochondrial Ca^{2+} revealed by specifically targeted recombinant aequorin. Nature, Vol.358: 325–327, 1992.
- Rizzuto, R., Brini, M., Murgia, M. & Pozzan, T. Microdomains with high Ca^{2+} close to IP3-sensitive channels that are sensed by neighboring mitochondria. Science 262, 744–747 (1993).
- Rizzuto, R., Pinton, P., Carrington, W., Fay, F. S., Fogarty, K. E., Lifshitz, L. M., Tuft, R. A., and Pozzan, T. Close contacts with the endoplasmic reticulum as determinants of mitochondrial Ca^{2+} responses. Science 280, 1763–1766 (1998).
- Rizzuto, R. and Pozzan, T. Microdomains of intracellular Ca^{2+}: molecular determinants and functional consequences. Physiol Rev. 86 (1): 369-408 (2006).

- Robertson, J.D. The molecular structure and contact relationships of cell membranes. Prog Biophys Mol Biol 10:343–418 (1960).
- Roderick H.L., Berridge M.J., Bootman M.D. Calcium-induced calcium release. Curr Biol, Vol.13: R425, 2003.
- Rodriguez-Garcia, A., et al., GAP, an aequorin-based fluorescent indicator for imaging Ca^{2+} in organelles. Proc Natl Acad Sci U S A, 2014. 111(7): p. 2584-9.
- Rogers KL, Picaud S, Roncali E, Boisgard R, Colasante C, Stinnakre J, Tavitian B, Brûlet P.., Non-invasive *in vivo* imaging of calcium signaling in mice. PLoS One, 2007. 2(10): p. e974.
- Roos J, DiGregorio PJ, Yeromin AV, Ohlsen K, Lioudyno M, Zhang S, Safrina O, Kozak JA, Wagner SL, Cahalan MD, Veliçelebi G, Stauderman KA. STIM1, an essential and conserved component of store-operated Ca^{2+} channel function.J Cell Biol. 2005 May 9;169(3):435-45. Epub 2005 May 2.
- Rossi CS, Lehninger AL. Stoichiometry of respiratory stimulation, accumulation of Ca++ and phosphate, and oxidative phosphorylation in rat liver mitochondria. J Biol Chem 1964;239,3971–80.
- Rostovtseva, T. K. & Bezrukov, S. M. VDAC regulation: role of cytosolic proteins and mitochondrial lipids. J. Bioenerg. Biomembr. 40, 163–170 (2008).
- Rowland, A.A. and Voeltz, G.K. Endoplasmic reticulum-mitochondria contacts: function of the junction. Nat Rev Mol Cell Biol. 13(10):607-265 (2012).
- Roy, S. S. et al. Bad targets the permeability transition pore independent of Bax or Bak to switch between Ca^{2+}-dependent cell survival and death. Mol. Cell 33, 377–388 (2009).
- Roy, S. S., Ehrlich, A. M., Craigen, W. J. & Hajnoczky, G. VDAC2 is required for truncated BID-induced mitochondrial apoptosis by recruiting BAK to the mitochondria. EMBO Rep. 10, 1341–1347 (2009).
- Ruby, J.R., Dyer, R.F. and Skalko, R.G. Continuities between mitochondria and endoplasmic reticulum in the mammalian ovary. Z Zellforsch Mikrosk Anat 97(1):30–37 (1969).
- Rudolf R, Mongillo M, Magalhães PJ, Pozzan T.*In vivo* monitoring of Ca(2+) uptake into mitochondria of mouse skeletal muscle during contraction. J Cell Biol, 2004. 166(4): p. 527-36.
- Sahel JA, Roska B. Gene therapy for blindness. Annu Rev Neurosci. 2013 Jul 8;36:467-88.
- Sahoo S.K., Kim T., Kang G.B., Lee J.G., Eom S.H., Kim do H., Characterization of calumenin-SERCA2 interaction in mouse cardiac sarcoplasmic reticulum. J Biol Chem, Vol.284: 31109–31121, 2009.
- Sancak, Y., Markhard, A.L., Kitami, T., Kovacs-Bogdan, E., Kamer, K.J., Udeshi, N.D., Carr, S.A., Chaudhuri, D., Clapham, D.E., Li, A.A., Calvo, S.E., Goldberger, O. and Mootha, V.K. EMRE Is an Essential Component of the Mitochondrial Calcium Uniporter Complex. Science 342, 1379-1382 (2013).
- Satrustegui, J., Pardo, B. & Del Arco, A. Mitochondrial transporters as novel targets for intracellular Ca^{2+} signaling. Physiol. Rev. 87, 29–67 (2007).
- Schäfer W., Stroh A., Berghöfer S., Seiler J., Vey M., Kruse M.L., Kern H.F., Klenk H.D., Garten W., Two independent targeting signals in the cytoplasmic domain determine trans-Golgi network localization and endosomal trafficking of the proprotein convertase furin. EMBO J, Vol.14: 2424–2435, 1995.
- Shaner NC, Steinbach PA, Tsien RY.A guide to choosing fluorescent proteins. Nat Methods. 2005 Dec;2(12):905-9. Review.
- Scherer P.E., Lederkremer G.Z., Williams S., Fogliano M., Baldini G., Lodish H.F., Cab45, a novel Ca^{2+}-binding protein localized to the Golgi lumen. J Cell Biol, Vol.133: 257–268, 1996.

- Scheuner, D., Eckman, C., Jensen, M., Song, X., Citron, M., Suzuki, N., Bird, T.D., Hardy, J., Hutton, M., Kukull, W., Larson, E., Levy-Lahad, E., Viitanen, M., Peskind, E., Poorkaj, P., Schellenberg, G., Tanzi, R., Wasco, W., Lannfelt, L., Selkoe, D., and Younkin, S. Secreted amyloid beta-protein similar to that in the senile plaques of Alzheimer's disease is increased *in vivo* by the presenilin 1 and 2 and APP mutations linked to familial Alzheimer's disease. Nat Med. 2 (8): 864-870 (1996).
- Schnetkamp PP. The SLC24 gene family of Na^+/Ca^{2+}-K^+ exchangers: from sight and smell to memory consolidation and skin pigmentation. Mol Aspects Med. 2013 Apr-Jun;34(2-3):455-64.
- Schwaller, B. The continuing disappearance of "pure" Ca^{2+} buffers. Cell Mol Life Sci. 66 (2): 275-300 (2009).
- Scorrano L, Oakes SA, Opferman JT, Cheng EH, Sorcinelli MD, Pozzan T et al. BAX and BAK regulation of endoplasmic reticulum Ca^{2+}: a control point for apoptosis. Science 2003; 300: 135–139.
- Scorzeto M, Giacomello M, Toniolo L, Canato M, Blaauw B, Paolini C, Protasi F, Reggiani C, Stienen GJ. Mitochondrial Ca2+-handling in fast skeletal muscle fibers from wild type and calsequestrin-null mice. PLoS One, 2013. 8(10): p. e74919.
- Sengupta A., Kabat J., Novak M., Wu Q., Grundke-Iqbal I., Iqbal K., Phosphorylation of tau at both Thr 231 and Ser 262 is required for maximal inhibition of its binding to microtubules. Arch Biochem Biophys, Vol.357: 299–309, 1998.
- Shaner, N., Patterson, G.H. and Davidson, M.W. (2007). Advances in fluorescent protein technology. J Cell Sci. 120, 4247- 4260.
- Sherrington R., Rogaev E.I., Liang Y., Rogaeva E.A., Levesque G., Ikeda M., Chi H., Lin C., Li G., Holman K., Tsuda T., Mar L., Foncin J.F., Bruni A.C., Montesi M.P., Sorbi S., Rainero I., Pinessi L., Nee L., Chumakov I., Pollen D., Brookes A., Sanseau P., Polinsky R.J., Wasco W., Da Silva H.A., Haines J.L., Perkicak-Vance M.A., Tanzi R.E., Roses A.D., Fraser P.E., Rommens J.M., St George-Hyslop P.H., Cloning a gene bearing missense mutations in early-onset familial Alzheimer's disease. Nature, Vol.375: 754–760, 1995.
- Shilling, D., Mak, D.O., Kang, D.E. and Foskett, J.K. Lack of evidence for presenilins as endoplasmic reticulum Ca^{2+} leak channels. J Biol Chem. 287(14):10933-10944 (2012).
- Shim AH, Tirado-Lee L, Prakriya M. Structural and Functional Mechanisms of CRAC Channel Regulation. J Mol Biol. 2015 Jan 16;427(1):77-93.
- Shimojo, M., Sahara, N., Murayama, M., Ichinose, H. and Takashima, A. Decreased Abeta secretion by cells expressing familial Alzheimer's disease-linked mutant presenilin 1. Neurosci Res. Mar; 57 (3): 446-53 (2007).
- Shirotani K., Edbauer D., Capell A., Schmitz J., Steiner H., Haass C., Gamma-Secretase activity is associated with a conformational change of nicastrin. J Biol Chem, Vol.278: 16474, 2003.
- Sinha S., Anderson J.P., Barbour R., Basi G.S., Caccavello R., Davis D., Doan M., Dovey H.F., Frigon N., Hong J., Jacobson-Croak K., Jewett N., Keim P., Knops J., Lieberburg I., Power M., Tan H., Tatsuno G., Tung J., Schenk D., Seubert P., Suomensaari S.M., Wang S., Walker D., Zhao J., McConlogue L., John V., Purification and cloning of amyloid precursor protein beta-secretase from human brain. Nature, Vol.402: 537–540, 1999.
- Smith, I.F., Boyle, J.P., Vaughan, P.F.T., Pearson, H.A., Cowburn, R.F., Peers, C.S., 2002. Ca^{2+} stores and capacitative Ca^{2+} entry in human neuroblastoma (SH-SY5Y) cells expressing a familial Alzheimer's disease presenilin-1 mutation. Brain Res. 949, 105 – 111
- Stathopulos PB1, Zheng L, Ikura M. Stromal interaction molecule (STIM) 1 and STIM2 calcium sensing regions exhibit distinct unfolding and oligomerization kinetics. J Biol Chem. 2009 Jan 9;284(2):728-32.

- Stierl M1, Stumpf P, Udwari D, Gueta R, Hagedorn R, Losi A, Gärtner W, Petereit L, Efetova M, Schwarzel M, Oertner TG, Nagel G, Hegemann P. Light modulation of cellular cAMP by a small bacterial photoactivated adenylyl cyclase, bPAC, of the soil bacterium Beggiatoa. J Biol Chem. 2011 Jan 14;286(2):1181-8.
- Stone, S. J. and Vance, J. E. Phosphatidylserine synthase-1 and -2 are localized to mitochondria-associated membranes. J. Biol. Chem. 275, 34534–34540 (2000).
- Streb, H., Irvine, R. F., Berridge, M. J. & Schulz, I. Release of Ca^{2+} from a nonmitochondrial intracellular store in pancreatic acinar cells by inositol-1,4,5-trisphosphate. Nature 306, 67–69 (1983).
- Sun Y, Rombola C, Jyothikumar V, Periasamy A.Förster resonance energy transfer microscopy and spectroscopy for localizing protein-protein interactions in living cells. Cytometry A. 2013 Sep;83(9):780-93.
- Supnet C, Grant J, Kong H, Westaway D, Mayne M.Amyloid-beta-(1-42) increases ryanodine receptor-3 expression and function in neurons of TgCRND8 mice. J Biol Chem. 2006 Dec 15;281(50):38440-7.
- Supnet, C. and Bezprozvanny, I. The dysregulation of intracellular calcium in Alzheimer disease. Cell Calcium 47: 183-189 (2010).
- Syntichaki P, Tavernarakis N. The biochemistry of neuronal necrosis: rogue biology? Nat Rev Neurosci. 2003 Aug;4(8):672-84.
- Szabadkai G, Bianchi K, Várnai P, De Stefani D, Wieckowski MR, Cavagna D, Nagy AI, Balla T, Rizzuto R. Chaperone-mediated coupling of endoplasmic reticulum and mitochondrial Ca^{2+} channels. J Cell Biol. 2006 Dec 18;175(6):901-11.
- Tan, W. & Colombini, M. VDAC closure increases calcium ion flux. Biochim. Biophys. Acta 1768, 2510–2515 (2007)
- Tanzi R.E., Gusella J.F., Watkins P.C., Bruns G.A., St George-Hyslop P., Van Keuren M.L., Patterson D., Pagan S., Kurnit D.M., Neve R.L., Amyloid beta protein gene: cDNA, mRNA distribution, and genetic linkage near the Alzheimer locus. Science, Vol.235: 880–884, 1987.
- Thastrup O., Cullen P.J., Drøbak B.K., Hanley M.R., Dawson A.P., Thapsigargin, a tumor promoter, discharges intracellular Ca^{2+} stores by specific inhibition of the endoplasmic reticulum Ca^{2+}-ATPase. Proc Natl Acad Sci USA, Vol.87:2466-2470, 1990.
- Thayer SA, Miller RJ. Regulation of the intracellular free Ca^{2+} concentration in single rat dorsal root ganglion neurones *in vitro*. J Physiol 1990;425,85–8115.
- Thestrup T, Litzlbauer J, Bartholomäus I, Mues M, Russo L, Dana H, Kovalchuk Y, Liang Y, Kalamakis G, Laukat Y, Becker S, Witte G, Geiger A, Allen T, Rome LC, Chen TW, Kim DS, Garaschuk O, Griesinger C, Griesbeck O. Optimized ratiometric calcium sensors for functional *in vivo* imaging of neurons and T lymphocytes. Nat Methods. 2014 Feb;11(2):175-82.
- Thinakaran, G. and Koo, E.H. Amyloid precursor protein trafficking, processing, and function. J Biol Chem. 283: 29615-29619 (2008).
- Tinel H, Cancela JM, Mogami H, Gerasimenko JV, Gerasimenko OV, Tepikin AV, Petersen OH.Active mitochondria surrounding the pancreatic acinar granule region prevent spreading of inositol trisphosphate-evoked local cytosolic Ca(2+) signals. EMBO J, 1999. 18(18): p. 4999-5008.
- Tolia, A. and De Strooper, B. Structure and function of gamma-secretase. Semin Cell Dev Biol. 20: 211-218 (2009).

- Trenker, M., Malli, R., Fertschai, I., Levak-Frank, S. and Graier, W.F. Uncoupling proteins 2 and 3 are fundamental for mitochondrial Ca^{2+} uniport. Nat Cell Biol 9:445–452 (2007).
- Truong K, Sawano A, Mizuno H, Hama H, Tong KI, Mal TK, Miyawaki A, Ikura M. FRET-based *in vivo* Ca^{2+} imaging by a new calmodulin-GFP fusion molecule. Nat Struct Biol, 2001. 8(12): p. 1069-73.
- Tsien, R.Y. 1998. The Green Fluorescent Protein. Annu. Rev. Biochemistry 67: 509-544.
- Tsien, R.Y. New calcium indicators and buffers with high selectivity against magnesium and protons: design, synthesis, and properties of prototype structures. Biochemistry. 19 (11): 2396-404 (1980).
- Tu, H., Nelson, O., Bezprozvanny, A., Wang, Z., Lee, S.F., Hao, Y.H., et al. Presenilins form ER Ca^{2+} leak channels a function disrupted by familial Alzheimer's disease-linked mutations. Cell 126: 981–993 (2006).
- van Munster EB, Gadella TWJ (2005) Fluorescence lifetime imaging microscopy (FLIM). In: Rietdorf J (ed) Microscopy Techniques. Springer, Berlin, pp 143–175
- Vance, J.E. Phospholipid synthesis in a membrane fraction associated with mitochondria. J Biol Chem 265(13):7248–7256 (1990).
- Vandendriessche T. Thorrez L. Acosta-Sanchez A. Petrus I. Wang L. Ma L., L. De Waele L. Iwasaki Y. Gillijns V. Wilson J.M. Collen D. Chuah M.K. Efficacy and safety of adeno-associated viral vectors based on serotype 8 and 9 vs. lentiviral vectors for hemophilia B gene therapy. J. Thromb. Haemost. 2007;5:16–24.
- Varadi A, Johnson-Cadwell LI, Cirulli V, Yoon Y, Allan VJ, Rutter GA. Cytoplasmic dynein regulates the subcellular distribution of mitochondria by controlling the recruitment of the fission factor dynamin-related protein-1. J Cell Sci 2004;117,4389–400.
- Vasington, F. D. and Murphy, J. V. Ca ion uptake by rat kidney mitochondria and its dependence on respiration and phosphorylation. J. Biol. Chem. 237, 2670–2677 (1962).
- Vig M, et al. Defective mast cell effector functions in mice lacking the CRACM1 pore subunit of store-operated calcium release-activated calcium channels. Nat Immunol. 2008;9:89–96
- Villa A, Garcia-Simon MI, Blanco P, Sese B, Bogonez E, Satrustegui J (1998) Affinity chromatography purification of mitochondrial inner membrane proteins with calcium transport activity. Biochim Biophys Acta 1373,347–359
- Voronina, S. et al. Correlation of NADH and Ca^{2+} signals in mouse pancreatic acinar cells. J. Physiol. 539, 41–52 (2002).
- Waldeck-Weiermair, M., Malli, R., Naghdi, S., Trenker, M., Kahn, M.J. and Graier, W.F. The contribution of UCP2 and UCP3 to mitochondrial $Ca(^{2+})$ uptake is differentially determined by the source of supplied $Ca(^{2+})$. Cell Calcium 47:433–440 (2010).
- Walker, E.S., Martinez, M., Brunkan, A.L. and Goate, A. Presenilin 2 familial Alzheimer's disease mutations result in partial loss of function and dramatic changes in Abeta 42/40 ratios. J Neurochem. 92 (2): 294-301 (2005).
- Walsh, D.M., Klyubin, I., Fadeeva, J.V., Cullen, W.K., Anwyl, R., Wolfe, M.S., Rowan, M.J. and Selkoe, D.J. Naturally secreted oligomers of amyloid beta protein potently inhibit hippocampal long-term potentiation *in vivo*. Nature 416: 535-539 (2002).
- Wang, Y., Deng, X. and Gill, D.L. Calcium signaling by STIM and Orai: intimate coupling details revealed. Sci Signal 3 (148): pe42 (2010).
- Weingarten M.D., Lockwood A.H., Hwo S.Y., Kirschner M.W., A protein factor essential for microtubule assembly. Proc Natl Acad Sci USA, Vol.72: 1858–1862, 1975.

- Whitaker M. Genetically encoded probes for measurement of intracellular calcium. Methods Cell Biol, 2010. 99: p. 153-82.
- White C White C1, Li C, Yang J, Petrenko NB, Madesh M, Thompson CB, Foskett JK., Li C, Yang J, Petrenko NB, Madesh M, Thompson CB, Foskett JK.The endoplasmic reticulum gateway to apoptosis by Bcl-XL modulation of the InsP3R. Nature Cell Biol. 7, 1021–1028 (2005).
- Williams RT, Manji SS, Parker NJ, Hancock MS, Van Stekelenburg L, Eid JP, Senior PV, Kazenwadel JS, Shandala T, Saint R, Smith PJ, Dziadek MA. Identification and characterization of the STIM (stromal interaction molecule) gene family: coding for a novel class of transmembrane proteins. Biochem J. 2001 Aug 1; 357(Pt 3):673-85.
- Wingrove D.E., Gunter T.E., Kinetics of mitochondrial calcium transport. II. A kinetic description of the sodium-dependent calcium efflux mechanism of liver
- Wojda, U., Salinska, E. and Kuznicki, J. Calcium ions in neuronal degeneration. IUBMB Life 60: 575-590 (2008).
- Wolfe, M.S. and Guénette, S.Y. APP at a glance. J Cell Sci. 120: 3157-3161 (2007).
- Wong, A.K., Capitanio, P., Lissandron, V., Bortolozzi, M., Pozzan, T. and Pizzo, P. Heterogeneity of Ca^{2+} handling among and within Golgi compartments. J Mol Cell Biol. 5(4):266-276 (2013).
- Woo Y.J. Zhang J.C. Taylor M.D. Cohen J.E. Hsu V.M. Sweeney H.L. One year transgene expression with adeno-associated virus cardiac gene transfer. Int. J. Cardiol. 2005;100:421–426
- Wright MJ, Wightman LM, Lilley C, de Alwis M, Hart SL, Miller A, Coffin RS, Thrasher A, Latchman DS, Marber MS. *In vivo* myocardial gene transfer: optimization, evaluation and direct comparison of gene transfer vectors. Basic Res Cardiol. 2001 May-Jun; 96(3):227-36.
- Wuytack F., Raeymaekers L., Missiaen L., Molecular physiology of the SERCA and SPCA pumps. Cell Calcium, Vol.32: 279-305, 2002.
- Xiaochun Li, Shangyu Dang, Chuangye Yan, Xinqi Gong, Jiawei Wang & Yigong Shi. Structure of a presenilin family intramembrane aspartate protease.Nature 493,56–61(2013)
- Yang S.N. and Berggren P.O., The role of voltage-gated calcium channels in pancreatic beta-cell physiology and pathophysiology. Endocr Rev, Vol.27: 621–676, 2006.
- Yeromin AV, Zhang SL, Jiang W, Yu Y, Safrina O, Cahalan MD. Molecular identification of the CRAC channel by altered ion selectivity in a mutant of Orai. Nature. 2006 Sep 14;443(7108):226-9. Epub 2006 Aug 20.
- Yizhar O, Fenno LE, Prigge M, Schneider F, Davidson TJ, O'Shea DJ, Sohal VS, Goshen I, Finkelstein J, Paz JT, Stehfest K, Fudim R, Ramakrishnan C, Huguenard JR, Hegemann P, Deisseroth K. Neocortical excitation/inhibition balance in information processing and social dysfunction. Nature. 2011 Jul 27;477(7363):171-8.
- Yoo, A.S., Cheng, I., Chung, S., Grenfell, T.Z., Lee,,H., Pack-Chung, E., Handler, M., Shen, J., Xia, W., Tesco, G., Saunders, A.J., Ding, K., Frosch, M.P., Tanzi, R.E., Kim and T.W. Presenilin-mediated modulation of capacitative calcium entry. Neuron. 27: 561-572 (2000).
- Young, K. W., Bampton, E. T., Pinon, L., Bano, D. & Nicotera, P. Mitochondrial Ca^{2+}signalling in hippocampal neurons. Cell Ca^{2+} 43, 296–306 (2008).
- Yu G., Nishimura M., Arawaka S., Levitan D., Zhang L., Tandon A., Song Y.Q., Rogaeva E., Chen F., Kawarai T., Supala A., Levesque L., Yu H., Yang D.S., Holmes E., Milman P., Liang Y., Zhang D.M., Xu D.H., Sato C., Rogaev E., Smith M., Janus C., Zhang Y., Aebersold R., Farrer L.S., Sorbi S., Bruni A., Fraser P., St George-

Hyslop P., Nicastrin modulates presenilin-mediated notch/glp-1 signal transduction and beta-APP processing. Nature, Vol.407, 48–54, 2000

- Yu, J.T., Chang, R.C. and Tan, L. Calcium dysregulation in Alzheimer's disease: from mechanisms to therapeutic opportunities. Prog Neurobiol. 89: 240-255 (2009).
- Zalk R, Clarke OB, des Georges A, Grassucci RA, Reiken S, Mancia F, Hendrickson WA, Frank J, Marks AR Structure of a mammalian ryanodine receptor.Nature. 2015 Jan 1;517(7532):44-9.
- Zampese E., Brunello L., Fasolato C., Pizzo P., Ca^{2+} dysregulation mediated by presenilins in Familial Alzheimer's Disease: Causing or modulating factor? Curr Trends Neurol, Vol.3: 1-9, 2009.
- Zampese E. and Pizzo P., Intracellular organeles in the saga of Ca^{2+} homeostasis: different molecules for different purpose? Cell Mol Life Sci, Vol.69: 1077-1104, 2011.
- Zampese, E. and Pizzo, P. Intracellular organelles in the saga of Ca^{2+} homeostasis: different molecules for different purposes? Cell Mol Life Sci. 69 (7): 1077:1104 (2012).
- Zatti G., Ghidoni R., Barbiero L., Binetti G., Pozzan T., Fasolato C., Pizzo P., The presenilin 2 M239I mutation associated with familial Alzheimer's disease reduces Ca^{2+} release from intracellular stores. Neurobiol Dis, Vol.15: 269-278, 2004.
- Zatti G., Burgo A., Giacomello M., Barbiero L., Ghidoni R., Sinigaglia G., Florean C., Bagnoli S., Binetti G., Sorbi S., Pizzo P., Fasolato C., Presenilin mutations linked to familial Alzheimer's disease reduce endoplasmic reticulum and Golgi apparatus calcium levels. Cell Calcium, Vol.39: 539-50, 2006.
- Zemelman, B. V.; Lee, G. A.; Ng, M.; Miesenböck, G. (2002). "Selective photostimulation of genetically chARGed neurons". Neuron 33 (1): 15–22.
- Zheng H, Koo EH. Biology and pathophysiology of the amyloid precursor protein. Mol Neurodegener. 2011 Apr 28;6(1):27.
- Zhang H., Ma Q., Zhang Y.W., Xu H., Proteolytic processing of Alzheimer's β-amyloid precursor protein. J Neurochem, Vol.120: 9–21, 2012.
- Zhang SL, et al. Genome-wide RNAi screen of Ca^{2+} influx identifies genes that regulate Ca^{2+} release-activated Ca^{2+} channel activity. Proc Natl Acad Sci USA. 2006;103:9357–9362
- Zhang Y.W., Thompson R., Zhang H., Xu H., APP processing in Alzheimer's disease. Mol Brain, Vol.4: 3, 2011
- Zhao Y, Araki S, Wu J, Teramoto T, Chang YF, Nakano M, Abdelfattah AS, Fujiwara M, Ishihara T, Nagai T, Campbell RE. An expanded palette of genetically encoded Ca^{2+} indicators. Science. 2011 Sep 30;333(6051):1888-91.
- Zheng L, Stathopulos PB, Li GY, Ikura M. Biophysical characterization of the EF-hand and SAM domain containing Ca2+ sensory region of STIM1 and STIM2. Biochem Biophys Res Commun. 2008 Apr 25;369(1):240-6.
- Zhou Y, Meraner P, Kwon HT, Machnes D, Oh-hora M, Zimmer J, Huang Y, Stura A, Rao A, Hogan PG. STIM1 gates the store-operated calcium channel ORAI1 *in vitro*. Nat Struct Mol Biol. 2010;17:112–116.
- Zhou Y, Srinivasan P, Razavi S, Seymour S, Meraner P, Gudlur A, Stathopulos PB, Ikura M, Rao A, Hogan PG. Initial activation of STIM1, the regulator of store-operated calcium entry. Nat Struct Mol Biol. 2013 Aug;20(8):973-81.
- Zoccarato F, Nicholls D. The role of phosphate in the regulation of the independent Ca^{2+}-efflux pathway of liver mitochondria. Eur J Biochem 1982;127,333–8.

Acknowledgments

I am grateful to Diana Pendin for performing experiments concerning Cameleon probes modification and generation; to Lorena Zentilin for AAV9 production; to Renato Bozio's group, in particular Ilaria Fortunati and Camilla Ferrante, for performing FLIM experiments; to Israel Sekler's group for the collaboration in Channelrhodopsin generation and characterization.
Of course thanks to all the members of the laboratory and special thanks to my family, in particular Fabio.

Attachments